Investigation of the Activity and Formation of Cold Seep Systems in the SW Barents Sea

vorgelegt von
Diplom-Chemikerin
Julia Christine Nickel
aus Düsseldorf

Von der Fakultät VI - Planen Bauen Umwelt
der Technischen Universität Berlin
zur Erlangung des akademischen Grades

Doktor der Naturwissenschaften
Dr. rer. nat.

genehmigte Dissertation

Promotionsausschuss:

Vorsitzender: Prof. Dr. G. Franz
Gutachter: Prof. Dr. B. Horsfield
Gutachter: Prof. Dr. J. Schwarzbauer
Gutachter: Dr. J. Kallmeyer

Tag der wissenschaftlichen Aussprache: 08.05.2014

Berlin 2014
D83

Fakultät VI - Planen Bauen Umwelt
der Technischen Universität Berlin
Autor: Julia C. Nickel
Die Arbeiten im Rahmen dieser Dissertation wurden am Helmholtz Zentrum Potsdam, Deutsches GeoForschungsZentrum (GFZ) in der Sektion 4.3 Organische Geochemie (Prof. Dr. Brian Horsfield) und an der Universität Potsdam durchgeführt.
Diese Dissertation wurde mit LaTeX unter Verwendung vom MiKTeX 2.9 und TeXnic Center 2.0 erstellt. Sie ist ebenfalls als elektronische Version (PDF) über das digitale Repositorium (System OPUS) der Technischen Universität Berlin erhältlich.
Webadresse: http://opus.kobv.de/tuberlin

Berlin, 2014

Für meine Eltern

"Darin besteht das Wesen der Wissenschaft. Zuerst denkt man an etwas, das wahr sein könnte. Dann sieht man nach, ob es der Fall ist und im Allgemeinen ist es nicht der Fall."

Bertrand Russell (1872-1970)

Statement of Original Authorship

I, Julia C. Nickel, hereby state that the work contained in this thesis or any parts thereof has not previously been submitted to the Fakultät VI - Planen Bauen Umwelt at the Technical University of Berlin or any other institution except where explicitly acknowledged.
To the best of my knowledge and belief, the thesis does not contain any previously published material or any material which has been written by another person except where due reference is made.

Hiermit erkläre ich, Julia C. Nickel, dass diese Arbeit oder darin enthaltene Teile von mir bisher weder an der Fakultät VI - Planen Bauen Umwelt der Technischen Universität Berlin noch einer anderen wissenschaftlichen Einrichtung zum Zwecke der Promotion eingereicht wurde.
Ferner erkläre ich, dass ich diese Arbeit selbständig verfasst und keine anderen als die darin angegebenen Quellen und Hilfsmittel benutzt habe.

Julia Christine Nickel

Acknowledgments

First of all I would like to express my gratitude to my supervisor Dr. Kai Mangelsdorf for his dedication while explaining to me the world of biomarkers and organic/bio-geo*chemistry*. Many inspiring ideas and good discussions and his commitment during the final stages of this thesis contributed to a large extent to this work.
My supervisor Dr. Jens Kallmeyer is thanked for his motivation, for sharing his knowledge in the field of geomicrobiology and marine life communities and his guidance particularly during the first 1.5 years of my PhD project.
My gratitude goes to Prof. Dr. Rolando di Primio for being always willing to help, for the contribution of several ideas and for maintaining the overview at all times.
I would like to thank Prof. Dr. Brian Horsfield for letting me be part of his organic geochemistry group at GFZ Potsdam and for giving me the opportunity to work in a very interesting field of research.

Lundin Petroleum Norway is acknowledged for funding this research project. Special thanks go to Daniel Stoddart and Harald Brunstad for being great cooperation partners who gave me loads of support and were always willing to answer several questions. Further thanks are directed to the other "Norwegians": Jon-Halvard Petersen, Øyvind Hammer, Mauro Pau, Aivo Lepland for shared data and discussions: TUSEN TAKK!

Für ihren außergewöhnlichen Einsatz in diversen Laborlebenslagen möchte ich mich ganz besonders bei Conny Karger, Anke Kaminsky und Axel Kitte bedanken. Weitere Unterstützung im Labor, aber auch beim Lösen diverser technischer Probleme, erhielt ich von Kristin Günther, Alina Koch, Doreen Noack, Ferdinand Perssen, Mirko Rahn, Jessica Stapel und Anika Zabel de-

nen ich an dieser Stelle meinen Dank aussprechen möchte. Ein riesengroßes Dankeschön geht an Claudia Engelhardt, die mir durch das Abnehmen vieler bürokratischer und organisatorischer Aufgaben jede Menge Zeit erspart hat und auch sonst jederzeit mit leckeren Gartenerträgen sowie Rat und Tat zur Hilfe stand.

I would like to thank the members of the Geomicrobiology group from Potsdam University - Rishi, Patrick, Clemens & Micha for the good time when I started my PhD project. Further, I was very lucky to spend my PhD time with my awesome GFZ-colleagues and friends Steffi Pötz, Nick Mahlstedt, Ilya Ostanin, Enmanuel Rodrigues, Annka Scherf, “die” Alex Vetter and “der” Alex Hartwig. I had a great time with you! Many Thanks to Mareike “MK” Noah for the best “Büroklima” ever, for sharing all the good and bad moments and for thousands of personal and scientific discussions.

Sehr dankbar bin ich meinen Eltern, nicht nur dafür, dass sie mich in all den Jahren unterstützt haben wo sie nur konnten, sondern auch für all das Vertrauen welches sie mir immer entgegen brachten. Meiner Oma möchte ich für ihr ganz besonderes Interesse an meiner Arbeit und die stets aufbauenden Worte danken.
Nicht genug danken kann ich Philipp P. Kuhn. Neben der großartigen Hilfe beim Layout und diversen Nachhilfestunden in Geologie hätte ich mir auch sonst keine bessere Unterstützung vorstellen können. Vielen Dank, dass du so toll bist!

Publications

In the scope of this thesis the following articles and conference distributions were published:

Articles:

J. C. Nickel, K. Mangelsdorf, R. di Primio, J. Kallmeyer, B. Horsfield, M. Blumenberg, A. Lepland, D. Stoddart & H. Brunstad, Insights into the activity, formation and origin of cold seep systems on the seafloor of the SW Loppa High in the SW Barents Sea, in preparation.

J. C. Nickel, R. di Primio, J. Kallmeyer, Ø. Hammer, B. Horsfield, D. Stoddart, H. Brunstad & K. Mangelsdorf, 2013, Tracing the origin of thermogenic hydrocarbon signals in pockmarks from the southwestern Barents Sea: Organic Geochemistry, v. 63, p. 73-84.

J. C. Nickel, R. di Primio, K. Mangelsdorf, D. Stoddart & J. Kallmeyer, 2012, Characterization of microbial activity in pockmark fields of the SW-Barents Sea: Marine Geology, v. 332-334, p. 152-162.

Conference distributions:

J. C. Nickel, K. Mangelsdorf, J. Kallmeyer, R. di Primio & D. Stoddart, 2013, Understanding Pockmark Formation in the Southwestern Barents Sea: A biogeochemical Approach: 26^{th} International Meeting on Organic Geochemistry, September 15-20, Tenerife, Spain. (Abstract, Poster)

J. C. Nickel, K. Mangelsdorf, J. Kallmeyer, R. di Primio & D. Stoddart, 2012, Geomicrobiological and Geochemical Study on Pockmarks

in the SW Barents Sea: 22^{nd} V.M. Goldschmidt Conference, June 24-29, Montreal, Canada. (Abstract, Oral)

J. C. Nickel, K. Mangelsdorf, J. Kallmeyer, R. di Primio & D. Stoddart, 2011, Study of microbial activity associated to SW-Barents sea pockmarks: 25^{th} International Meeting on Organic Geochemistry, September 18-23, Interlaken, Switzerland. (Abstract, Poster)

J. C. Nickel, J. Kallmeyer, K. Mangelsdorf, R. di Primio & D. Stoddart, 2011, Pockmarks as indicators for active fluid flow?: European Geosciences Union General Assembly, April 03-08, Vienna, Austria. (Abstract, Poster)

J. C. Nickel, J. Kallmeyer, K. Mangelsdorf, R. di Primio, D. Stoddart & C. Glombitza, 2010, Microbial activity in pockmarks in the southwestern Barents Sea: 12^{th} Norwegian Meeting on Organic Geochemistry, September 08-10, Oslo, Norway. (Abstract, Oral)

Abstract

The Barents Sea is a broad, epicontinental Sea in northern Europe. With an area of about 1.4 million km^2 it extends from Novaya Zemlya (Russia) in the east to the continental slope of the Norwegian-Greenland Sea in the west, and from Svalbard and Franz Josef Land in the north to the coast of Norway and Russia in the south. The southwestern part of the Barents Sea is strongly characterized by its geological history with subsidence and uplift periods and several events of glacial erosion. The last glacial maximum (LGM) is one of the most important and best preserved glacial phases in this area. During the last decades the Barents Sea evolved into an oil and gas prospecting area. Several source rocks have been identified and hydrocarbon discoveries have been made. Additionally, indications for hydrocarbon seepage, so called "cold seeps" have been detected. These include extensive pockmark fields, carbonate crusts bearing areas and fault related gas flares. Leaking hydrocarbons, released by cold seeps, gained increasing attention during the last years for two reasons. First because they are potential indicators for underlying hydrocarbon reservoirs in the subsurface and second because emitted hydrocarbons, particularly methane as a greenhouse gas, are known to significantly affect the global climate when released to the atmosphere.

In this thesis samples from different areas located in the Loppa High region in the southwestern Barents Sea were investigated. Two surface manifestations of cold seep systems such as huge pockmark areas and carbonate crust sites were studied in detail, in order to determine the activity, formation and spatial distribution of the different seepage structures as well as the origin and timing of the seeping hydrocarbon fluids. Therefore, samples, collected during three research cruises, were studied. These include sediment cores from pockmarks, reference sites and carbonate crust areas as well as carbonate crust samples. An interdisciplinary approach, applying organic geochemical, biogeochemical and geomicrobiological methods in combination with a geophysical data set was chosen to answer the key questions mentioned above. In order to determine the abundance of seep-associated microorganisms, the microbial activity was investigated by analyzing sulfate reduction rates (SRRs). Furthermore, the assessment of specific biomarkers was used to characterize the seeping fluids. The detection of petroleum related compounds can, for instance, indicate

the presence of oil in the sediment. The analysis of biomarkers diagnostic for microorganisms, which perform anaerobic oxidation of methane (AOM) in the presence of methane, can indicate the release of gas from the subsurface. Compound specific carbon isotope signatures of microbial biomarkers can offer further indications for seeping hydrocarbon gases, since very negative carbon isotope values indicate the utilization of methane as a carbon source by methanotrophs. Furthermore, the precipitation of carbonates often occurs in consequence of AOM.

The presence of carbonate crust patches in the carbonate crust area together with rising gas bubbles from the sediment are first indications for active methane seepage in this area. Furthermore, diagnostic AOM biomarkers were detected in the sediment samples as well as in the corresponding carbonate crusts. The depth profiles of these biomarkers show a distinct interval of higher concentrations, which points towards a shallow AOM zone in this depth interval. This was further supported by very negative compound specific carbon isotope signatures (δ^{13}C), which suggests the participation of the corresponding organisms in methane consumption processes and, thus, the presence of gas in these study sites.

In the pockmark areas, however, active release of gas from the sediment could not be observed, neither in the data of the gas measurements, nor in the biogeochemical and geomicrobiological data. Throughout the whole depth interval of the sediment cores, both from pockmark and reference cores, unusually low microbial activity was determined. Further, the diagnostic AOM biomarkers were essentially absent. Although the presence of petroleum biomarkers potentially indicates the escape of higher molecular hydrocarbons, it is inferred that their presence is not due to emitted petroleum from the pockmarks. The presence of thermogenic hydrocarbons seems to be ubiquitous in the Loppa High area occurring in pockmark as well as in reference cores. Biomarker depth profiles showed that the mature hydrocarbons show the same variability as the immature background compounds. This implies that the oil related compounds are derived from mature material which has been eroded, mixed with immature organic matter and distributed over the entire area.

Using geophysical data as well as literature data on the geologic and glacial history of the study area and the data obtained during this study, it is sug-

gested that the present pockmark fields are the result of area wide gas hydrate decomposition as a consequence of the retreat of the ice sheet which covered the Barents Sea during the Weichselian. Due to changing temperature and pressure conditions the destabilization and, thus, the decay of gas hydrates which were accumulated under the ice sheet, occurred. This resulted in a massive release of large amounts of gas associated with the formation of the pockmark craters. This scenario explains well the existence of the large areas of inactive pockmarks which are still preserved on the seabed surface. In contrast, the currently active cold seep structures are claimed to be correlated to fault systems in the subsurface as indicated by seismic data. It is known that faults can act as conduits for migrating hydrocarbons. Since numerous faults are present in the carbonate crust areas, and hydrocarbon reservoirs occur in the vicinity, it is well possible that these faults act as migration pathways for hydrocarbon gases from deeper hydrocarbon sources towards the cold seeps.

It can be concluded, that the southwestern Barents Sea contains at least two cold seep systems. Although these systems seem to be morphologically totally different from each other, it is conceivable that these features were related in the past. The gas hydrates which are claimed to be responsible for the formation of the large pockmark areas may have been fed by the same fault system, which today act as conduits for the active cold seeps. Furthermore, it was shown, that by combining geochemical and geomicrobiological tools a good assessment of the current seeping activity of cold seep structures can be achieved which can, thus, be used as a relatively fast and cheap tool to evaluate cold seep systems.

SW Barents Sea, pockmarks, cold seeps, organic geochemistry

Zusammenfassung

Die Barentssee ist ein ausgedehntes Schelfmeer im Norden Europas und umfasst eine Fläche von rund 1.4 Mio km^2. Sie liegt zwischen Spitzbergen (Norwegen) und Franz Josef Land (Russland) im Norden und der Küste Norwegens und Russlands im Süden sowie Novaya Zemlya (Russland) im Osten und dem Europäischen Nordmeer und der Grönlandsee im Westen. Die Morphologie der südwestlichen Barentssee ist geprägt durch die geologische Entstehungsgeschichte mit Phasen von tektonischer Hebung und Senkung sowie durch den Einfluss glazialer Erosionsereignisse insbesondere während der letzten Eiszeit. Durch die Entdeckung diverser Muttergesteine und Kohlenwasserstofflagerstätten hat sich die Barentssee in den letzten Jahrzehnten zu einem aussichtsreichen Ziel für die Öl- und Gasindustrie entwickelt. Darüber hinaus gibt es auf dem Meeresboden eine Reihe Indikatoren, die das natürliche Austreten von Kohlenwasserstoffen aus sogenannten "Cold Seeps" vermuten lassen. Die beobachteten Strukturen umfassen ausgedehnte Felder mit kraterförmigen Strukturen, die als "Pockmarks" bezeichnet werden, sowie Gebiete, in denen entlang von bekannten Störungen Karbonatkrusten und Gasaustritte aufzufinden sind. Cold Seeps haben zunehmend an Bedeutung gewonnen, zum einen weisen Sie auf mögliche Kohlenwasserstoffquellen im Untergrund hin und zum anderen hat der Ausstoß von Kohlenwasserstoffen, insbesondere des Treibhausgases Methan, einen signifikanten Einfluss auf die Klimaentwicklung der Erde, wenn es in die Atmosphäre gelangt.

Im Rahmen der vorliegenden Doktorarbeit wurden Proben aus unterschiedlichen Gebieten innerhalb der Loppa High Region in der südwestlichen Barentssee analysiert. Diese erlauben die Untersuchung von zwei unterschiedlichen Cold Seep Systemen, zum einen Pockmark Felder und zum anderen Gebiete, die Karbonatkrusten aufweisen. Dabei wurde untersucht, inwieweit die Systeme heute noch aktiv sind, durch welche Auslöser sie gebildet wurden und welche die zugrundeliegenden Quellen der Fluide sind. Die Proben wurden im Rahmen von 3 Expeditionen genommen. Diese umfassen Sedimentkerne aus Pockmarkstrukturen und von Referenzstellen außerhalb der Pockmarks, sowie aus Gebieten mit Karbonatkrusten. Des Weiteren wurde Probenmaterial der Karbonatkrusten selbst untersucht. Um die oben genannten Fragestellungen zu beantworten, wurde ein interdisziplinärer Ansatz gewählt, bei dem

organisch geochemische, biogeochemische und geomikrobiologische Methoden angewendet und mit geophysikalischen Daten kombiniert wurden. So wurde beispielsweise die Abundanz der Mikroorganismen, welche im Zusammenhang mit austretenden Fluiden stehen, untersucht. Dies kann durch die Bestimmung der Sulfat Reduktionsraten (SRR) erfolgen, die die mikrobiellen Aktivitäten im Sediment widerspiegeln. Die Analyse spezieller Biomarker liefert darüber hinaus Hinweise über die austretenden Fluide. Spezielle Kohlenwasserstoffverbindungen, z.B. *n*-Alkane oder Hopane, können auf den Eintrag von Öl in das Sediment hinweisen. Charakteristische Biomarker für Mikroorganismen, die an der anaerobe Oxidation von Methan (AOM) beteiligt sind, geben hingegen Hinweise auf den Austritt von Methan aus dem Sediment am Meeresboden. Die Kohlenstoffisotopensignaturen von mikrobiellen Biomarkern können weitere Informationen über den Austritt von Kohlenwasserstoffgasen liefern, da sehr negative Werte die Aufnahme von Methan durch methanotrophe Mikroorganismen anzeigen. Des Weiteren wird im Zuge der AOM häufig die Ausfällung von Karbonaten beobachtet.

Das Vorkommen von Karbonatkrusten in Zusammenhang mit aufsteigenden Gasbläschen in der Wassersäule sind erste deutliche Hinweise für einen derzeit aktiven Methanaustritt aus den Sedimenten in dem durch Karbonatkrusten geprägten Untersuchungsgebiet. Unterstützt werden diese Hinweise durch die Anwesenheit der für AOM spezifischen Biomarker sowohl in den Sedimentkernen, als auch in den dazugehörigen Karbonatkrusten. Im Tiefenprofil des Sedimentkerns weisen diese Biomarker ein ausgeprägtes Intervall erhöhter Konzentrationen auf. In Verbindung mit sehr negativen Kohlenstoffisotopenverhältnissen deutet dies auf eine aktive AOM Zone und somit das Vorhandensein von Methan im Sediment hin.

In den Pockmark Gebieten hingegen können keine Hinweise für den aktiven Austritt von Gas aus dem Sediment gefunden werden, weder durch direkte Messungen der Gaskonzentrationen noch durch biogeochemische und geomikrobiologische Analysen. So können in allen untersuchten Proben, unabhängig von dem Tiefenintervall oder dem Probenahmeort (Pockmarkkerne vs. Referenzkerne), ausschließlich ungewöhnlich niedrige mikrobielle Aktivitäten festgestellt werden. Des Weiteren sind keine spezifischen AOM Biomarker vorhanden. Obwohl spezifische Ölkomponenten im Sediment nachgewiesen

werden können, die potentiell auf den Austritt von Ölkohlenwasserstoffen hinweisen, hat die vorliegende Studie gezeigt, dass deren Anwesenheit vermutlich nicht auf die Freisetzung von Öl aus den Pockmarkstrukturen zurückzuführen ist. In der Loppa High Region scheinen die Ölkomponenten allgegenwärtig zu sein, unabhängig ob es sich um eine Pockmark- oder Referenzlokation handelt. Die Tiefenprofile der Ölkomponenten zeigen sehr ähnliche Variabilität wie die unreifen Komponenten des organischen Hintergrundsignals. Dies legt den Schluss nahe, dass die Erdölbiomarker vielmehr aus erodiertem reifem Material stammen, welches vermischt mit einem unreifen organischen Hintergrundsignal gleichmäßig als allochthoner Eintrag in das Untersuchungsgebiet eingetragen wurde.

Mit Hilfe geophysikalischer sowie publizierter Daten über die geologische und glaziale Geschichte des Untersuchungsgebietes und den in dieser Studie erzielten Ergebnisse können Szenarien über den Ursprung und die Bildung der zwei unterschiedlichen Cold Seep Systeme formuliert werden. So legen die Daten nahe, dass die hier untersuchten Pockmarkfelder auf den Rückgang des aufliegenden Eisschildes im Anschluss des Weichsel-Glazials zurückzuführen sind. Das Abschmelzen der Eisdecke im Zuge des Klimaumschwungs vom letzten Glazial zum Holozän führte, auf Grund sich verändernden Temperatur- und Druckbedingungen, zur Destabilisierung und damit zum Zerfall der unter dem Eispanzer akkumulierten Gashydrate. Dies resultierte in einer Freisetzung immenser Gasmengen, welches zur Entstehung zahlreicher Pockmarkkrater führte. Dieses Szenario liefert eine plausible Erklärung für die Existenz weitreichender Pockmarkfelder die eine hohe Dichte an heutzutage inaktiven Pockmarks auf dem Meeresboden aufweisen. Die aktiven Cold Seep Systeme, die sich hingegen in den Karbonatkrustengebieten befinden, stehen vermutlich in Verbindung mit Störungen im Untergrund, worauf auch seismische Daten hinweisen. Es ist bekannt, dass diese als Migrationspfade für Kohlenwasserstofffluide dienen können. Zahlreiche Störungen im Untergrund der aktiven Karbonatkrustengebiete sowie Gas- und Ölfelder in der näheren Umgebung liefern demnach eine denkbare Erklärung für mögliche Quellen und Migrationspfade für die Versorgung der Cold Seeps in den Karbonatkrustenregionen.

Zusammenfassend kann geschlossen werden, dass es in der südwestlichen Barentssee mindestens zwei verschiedene Cold Seep Systeme gibt. Trotz des

Eindrucks, dass diese Systeme voneinander unabhängig sind, besteht durchaus die Möglichkeit, dass beide Systeme in der Vergangenheit in Verbindung zueinander standen. Die Gashydrate, die als Faktor für die Entstehung der Pockmarkfelder diskutiert werden, können möglicherweise ebenfalls über dieselben Störungen gespeist worden sein, die heutzutage auch die aktiven Cold Seeps in den Karbonatkrustengebieten versorgen. Letztendlich konnte gezeigt werden, dass durch Anwendung geochemischer, biogeochemischer und geomikrobiologischer Techniken eine gute Beurteilung der Gasaustrittsaktivitäten von Cold Seep Systemen erreicht werden kann. Dies liefert eine verhältnismäßig schnelle und kostengünstige Methode zur Beurteilung von Cold Seep Systemen.

SW Barentssee, Pockmarks, Cold Seep, organische Geochemie

Contents

List of Figures

List of Tables

Chapter 1

Introduction

1.1 Objectives and outline

Cold seep systems have widespread implications for their associated environments including the marine water column, the seabed and the subsurface. Active fluid flow from cold seeps strongly affects the seafloor ecosystem, such as microbial communities, and the seafloor morphologies for instance due to the formation of pockmarks or carbonate crusts. Moreover, cold seep systems can provide important information on hydrocarbon systems in the underlying subsurface, they are therefore particularly valuable for the petroleum exploration industry. Furthermore, hydrocarbons emitted from cold seeps, particularly methane, can have significant impact on the global climate and carbon cycle and are, therefore, considered to represent pathways for sedimentary stored carbon and climate-relevant greenhouse gases back to the atmosphere.

In the present thesis different manifestations of cold seep systems from the Loppa High region in the southwestern (SW) Barents Sea have been analyzed using organic geochemical, biogeochemical and microbiological methods. These include widespread fields of pockmarks in high density as well as study sites, which are characterized by patches of carbonate crusts on the seafloor and escaping gas bubbles from the sediment. In order to understand these cold seep systems the main scientific questions addressed within the scope of this thesis were:

- What is the activity of the investigated cold seep systems?

- What is the source and composition of the seeping fluids and how are the seeps related to underlying hydrocarbon sources?
- What caused the formation and spatial distribution of the cold seeps?
- What was the timing of the seeping fluids?
- What is the driving force for the formation of the cold seeps?

Comparison of the results, obtained by the investigation of each area, allows for recognizing characteristic differences or similarities. Furthermore, the data embedded in the general geological framework can offer a consistent understanding of the overall petroleum system in the Loppa High region in the SW Barents Sea.

The following aspects were addressed in three publications forming the Chapters 2, 3 and 4 of this thesis to contribute to the key questions mentioned above:

In **Chapter 2** sediment samples from pockmark fields in the SW Barents Sea were analyzed for their gas content and microbial activity. Several cores in the Loppa High region were investigated to screen the area for locations of elevated gas concentrations. Multibeam bathymetry was used to study the seafloor morphology and to select the target sites in all areas. Gas measurements (adsorbed, occluded and free gas) were conducted in order to obtain information about the presence of gaseous hydrocarbons in the sediment and to pinpoint locations of elevated hydrocarbon concentrations as an indication for active seepage. The analysis of sulfate reduction rates can help to identify areas of elevated microbial activity. In case of increased concentrations of methane in the sediment the presence of specific hydrocarbon-consuming microbial communities can be expected. By tracing the process of sulfate reduction, which goes along with the anaerobic oxidation of methane (AOM) in anoxic sediment, a first indication for sites with elevated gas concentrations can be obtained. The combination of the sulfate reduction rate (SRR) data with depth profiles of pore water sulfate concentration and gas measurements showed that there is currently no active fluid flow. It was hypothesized that the retreat of the ice sheet during the last deglaciation and the gas release due to the related decomposition of gas hydrates caused the formation of the large pockmark fields.

In **Chapter 3** the petroleum biomarker inventory of selected cores of the same study area as described in Chapter 2 was investigated to gain information about the presence of higher molecular hydrocarbons, which may indicate current or past petroleum leakage from a deeper lying hydrocarbon source. In order to identify the presence of oil, the focus was placed on *n*-alkanes and cycloalkanes, which represent the main constituents of petroleum. Additionally, specific lipid biomarkers, ubiquitous in petroleum, such as hopanes and steranes, were analyzed. The abundance of these biomarkers in the study area and their distribution throughout the depth interval should provide new insights on the formation of pockmarks and their relation to petroleum leakage. Various biomarkers, indicating the presence of petroleum hydrocarbons in the sediment could be identified. However, similarities in abundance and level of maturity throughout the depth intervals and between the different cores studied suggested that the presence of thermogenic hydrocarbons is attributed to reworked, eroded material, rather than the result of oil expulsion through the pockmarks.

In **Chapter 4** the inventory of biomarkers diagnostic for AOM was investigated to trace the presence of methane in two different cold seep systems, the pockmark area studied previously (Chapter 2 and 3) and an area with carbonate crusts. Since carbonate crust formation is often the result of AOM, they can be indicative of methane leakage. In order to decipher if the study sites are, or were, affected by methane expulsion, the focus was placed on the analysis of specific AOM-biomarkers. These include methane oxidizing archaea as well as the associated sulfate reducing bacteria. Depth plots of the amounts of these specific biomarkers can, e.g., reveal the existence of a present or past AOM-zone, if elevated concentration of the biomarkers can be found in a certain depth intervals. With this it is possible to trace locations that exhibit active or past expulsion of methane.

The absence of the specific AOM-biomarkers in the pockmark samples supported the results of the previous studies (Chapter 2 and 3). The pockmarks are currently inactive and no present or past release of methane can be identified. In contrast, the cold seep systems in the carbonate crust area show active release of methane at present. Based on the data a link of the cold seep systems to underlying sources and potential plumbing systems was inferred.

Finally, the relation of the two cold seep systems was discussed with respect to the geological context.

1.2 Submarine seeping systems

1.2.1 Cold seeps

The term "submarine seeping systems" is used to describe the flow of fluids (gases and liquids) through the seabed. Such flows of fluid can generally be divided into two groups: "hot vents" and "cold seeps". Hot vents are geothermally or hydrothermally driven systems like volcanoes or black smokers. They are often associated with the formation of new oceanic crust. In contrast to hot vents, cold seeps are not directly linked with thermal anomalies. They are charged by fluids like hydrogen sulfide, methane, groundwater or pore water (Dugan and Flemings, 2000; Taniguchi et al., 2002), and other hydrocarbon-rich fluids rising from the subsurface to the seafloor. This can result in the formation of structures such as pockmarks (seafloor depressions), brine lakes, gas flares or mud volcanoes. Cold seeps have been identified all over the world in a broad range of tectonic settings, on both passive and active continental margins (Levin, 2005; Sibuet and Olu, 1998). Paull et al. (1984) were the first who observed cold seeps as well as the associated faunal communities that could be detected on the seafloor close to the cold seeps (as shown e.g. in Figure 1.1). However, indications for cold seeps have been described long before the term "cold seep" even existed. Most known cold seeps are associated to hydrocarbon (HC) reservoirs or indirectly to gas hydrates. In retrospect, several observations, which were made in the past, can be attributed to the presence of cold seeps. This includes natural oil seeps (Eyer et al., 1977; Link, 1952; Spies and Davis, 1979), tar polluted beaches (Ludwig and Carter, 1961) and oil slicks (Dietz and Lafond, 1950; Kawahara and Ballinger, 1970). Natural occurring bitumen is even mentioned in biblical references. Tar balls have been reported from most of the world's oceans (e.g., Horn et al. 1970; Morris 1971). Sweet Jr. (1974) claimed that hydrocarbon seepage existed throughout most of the geologic history. Today it is assumed that roughly half of the crude oil entering the marine environment is from natural seeps, the residual half is thought to result from leaks and spills caused by anthropogenic utiliza-

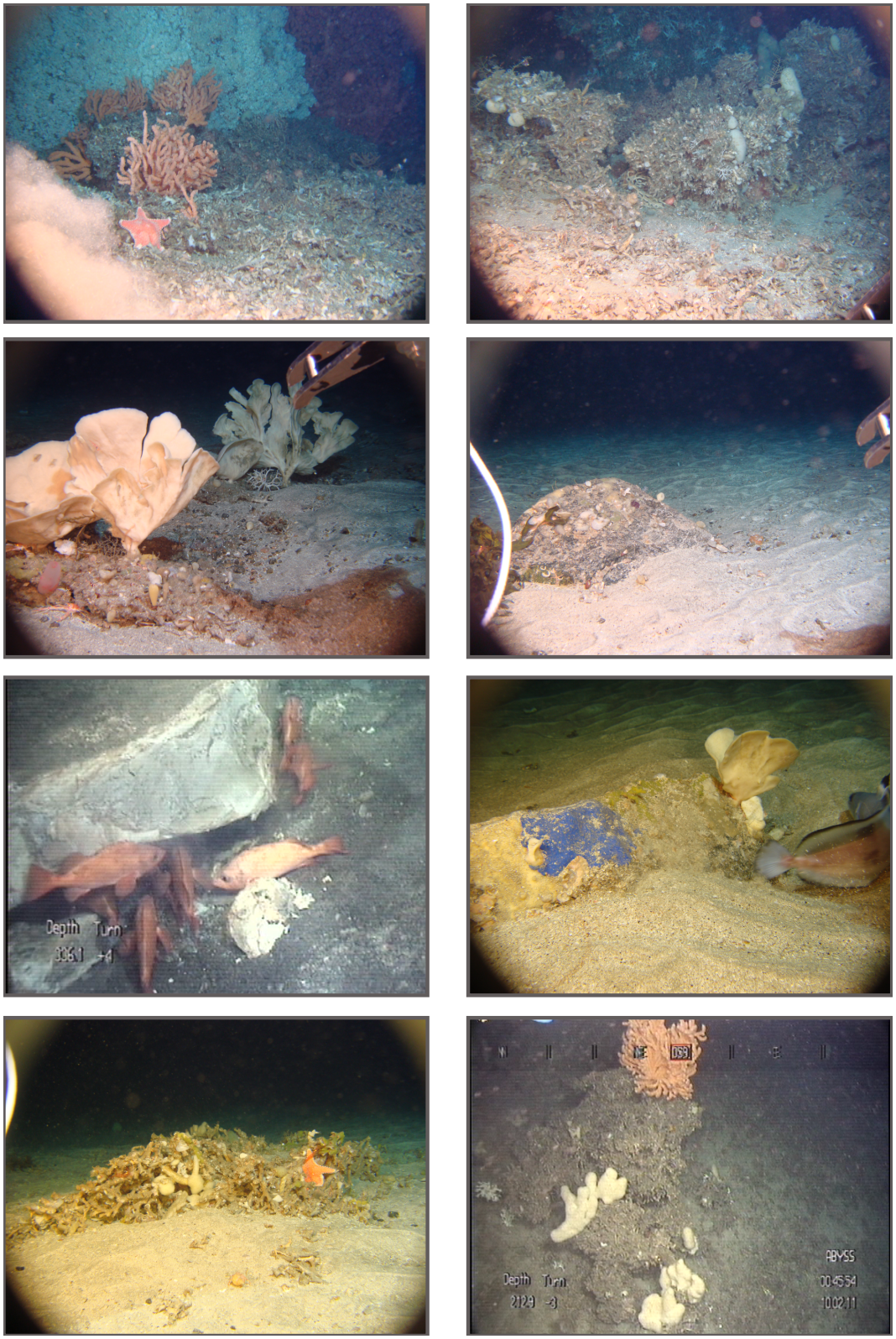

Figure 1.1: Cold seep fauna; pictures were taken during an ROV survey within a research cruise in February 2011.

tion of petroleum including extraction, transportation, refining and storage (Kvenvolden and Cooper, 2003).

1.2.2 Seabed pockmarks

Seabed pockmarks, as one of the topics discussed in this thesis, are features generally classified as cold seeps. They are characterized as craterlike structures that are ubiquitous on the seafloor and in lake sediments. During the late 1960s King and MacLean (1970) were the first to discover pockmarks. They described them as "cone-shaped depressions that occur in large numbers across the La Have clay of the Scotian Shelf" (Nova Scotia, CA) (King and MacLean, 1970).

Pockmarks can exist in many different shapes and sizes. Based on their morphology Hovland et al. (2002) subdivided them into different classes comprising single features e.g., small "unit pockmarks" (diameter 1-10 m) and "normal pockmarks" (diameter 10-700 m) as well as "pockmark cluster" which describes an association of several pockmarks (Hovland and Judd, 1988). Pilcher and Argent (2007) classified two types of pockmarks, the first one being "random pockmarks", an irregular distribution of pockmarks or the occurrences of single craters, the second type designates the "arrangement of pockmarks" such as "strings of pockmarks" and "pockmark clusters". Strings of pockmarks often occur in association to structural features like faults and fractures that are located in the subsurface. Apart from normal pockmarks, larger craters often referred to as "giant pockmarks" or "mega pockmarks", with diameter up to 10 km, have been observed (Bøe et al., 1998; Cole et al., 2000; Davy et al., 2010; Kelley et al., 1994; Maestro et al., 2002).

During the last decades numerous authors have been trying to find explanations for the presence of pockmarks. Scenarios involving the impact of meteorites (Solheim and Elverhøi, 1993), iceberg plunging (e.g., Chand et al. 2012) or even marks from whales (Woodside et al., 2006) have been discussed to account for the crater structures. However, the most widespread and also most reliable theory explains the presence of pockmarks with the expulsion of fluids.

Several models have been developed to explain the mechanisms of pockmark formation due to fluid escape. However, there is no consensus on the detailed

formation mechanism. Hovland and Judd (1988) suggested that fluids from a deeper source in the sediment migrate towards the seabed where accumulation causes doming. Due to the resulting tension, small fractures are formed, leading to small conduits for the migrating gas to "escape" through the sediment to the water column. Thus, a hydraulic connection is built, resulting in a pressure drop which causes a violent burst followed by the formation of a unit pockmark. Clusters of several unit pockmarks can coalesce to a normal pockmark (Hovland and Judd, 1988).

Kelley et al. (1994) propose two very different mechanisms. One describes an ongoing process of continuous gas seepage caused by microbial degradation of organic matter leading to successive excavation of a crater. The second model describes a catastrophic scenario that depends on instantaneous events like tsunamis or earthquakes as a trigger for pockmark formation.

Yet another model of gas induced pockmark formation was described recently by Cathles et al. (2010). They assume that gas is accumulated below a capillary seal in the deeper sediment. Build-up of overpressure causes subsequent seal failure and results in an upward moving gas diapir. At the same time pore waters are displaced, liquefying the near surface sediment which is then removed by ocean bottom currents causing the formation of a pockmark.

Since their first discovery, pockmarks have been detected all over the world in many different environments and geologic settings, e.g., lakes (Chapron et al., 2004), continental slopes, shelves and rises (Vogt et al., 1994), shallow bays (Kelley et al., 1994), fjords (Hammer and Webb, 2010), as well as in the deep sea (Bayon et al., 2009; Judd and Hovland, 2007). Many examples for pockmark sites have been described for the North Atlantic (Kelley et al., 1994), the North Pacific (Paull et al., 2002), the North Sea (Cole et al., 2000), the Norwegian Sea (Mazzini et al., 2006) and the Mediterranean Sea (Acosta et al., 2001; Hasiotis et al., 2002). Also in the Barents Sea, the target area of the present thesis, pockmarks and even extensive pockmark fields have been detected (Chapters 2, 3 and 4; Ostanin et al. 2012; Solheim and Elverhøi 1993; Vadakkepuliyambatta et al. 2013).

Different sources have been taken into account for the formation of the crater structures. In most cases pockmarks are thought to deliver methane of thermogenic or biogenic origin and/or serve as a possible conduit for seeping

oil. However, also gases like CO_2 (De Vittor et al., 2012) or H_2S (Etiope et al., 2006) as well as fluids like pore water (Harrington, 1985), artesian groundwater (Jensen et al., 2002) or combinations of different types of fluids have been discussed to be responsible for the formation of a pockmark crater.

Since hydrocarbons are often the predominant fluids in seeps, pockmarks are considered to be potential indicators for underlying hydrocarbon accumulations. For this reason they have received significant interest from the petroleum industry, because pockmark structures are easy to localize on the seabed and can, therefore, be used as a relatively cheap exploration tool (Heggland, 1998; Hovland, 1981; Hovland and Judd, 1988). Furthermore, the understanding of pockmark systems is important in order to identify, evaluate or avoid potential geologic hazards. Within offshore operations, pockmarks can be valuable indicators of potential gas voids in the subsurface. These gas pockets are stable under high pressure, however, their penetration can lead to failure in the seal, followed by destabilization and eventually resulting in a blowout scenario (Sills and Wheeler, 1992). Furthermore, pockmarks can indicate subsurface hydraulic activity and, thus, the risk of resulting slope failure as well as seabed instability (Hovland et al., 2002). For this reason pockmarks are often targets for diverse geophysical studies to model and understand subsurface fluid flow processes (Cathles et al., 2010), understand seepage dynamics (Hovland, 2003) or visualize the link of the pockmarks to the underlying plumbing systems by seismic interpretation (Chand et al., 2008; Ostanin et al., 2013).

However, pockmarks are not only of considerable interest for the petroleum industry. Due to the seeping fluids pockmarks can build unique habitats for specific microbial communities who use the venting fluids as their sources for nutrients and energy (Kulm et al., 1986; Thauer and Shima, 2008). Therefore, pockmarks often host a wide diversity of organisms, which was documented in several environmental (Hovland et al., 2012; Olu-Le Roy et al., 2007), geomicrobiological and biogeochemical studies (Pimenov et al., 2008; Wegener et al., 2008). Thus, their detailed investigation contributes to the understanding of major microbial and geochemical processes, which take place in the seabed sediment and is, therefore, an important part of the global hydrocarbon cycle.

1.3 The role of methane in the carbon cycle

Methane is the most abundant hydrocarbon in the atmosphere (Reeburgh, 2007) with approximately 3.6 Gt of methane carbon (Whiticar, 1990). After carbon dioxide (CO_2) and water (H_2O), methane is the third most important greenhouse gas (Heimann, 2010). Its global warming potential (GWP), a relative parameter indicating the ability of heat absorption in the atmosphere, is 21 times higher than that of carbon dioxide (Schimel and 75 others, 1996). Thus, enhanced methane concentration in the atmosphere is an important factor that has helped drive recent and past climate changes (e.g., IPCC 2011; Seinfeld and Pandis 2006). Furthermore, changing methane concentrations in the atmosphere considerably affect the carbon cycle, since the equilibrium of chemical reactions, e.g. the photochemical oxidation in the troposphere, is shifted.

Both, natural and anthropogenic sources are known to contribute to the global methane budget. However, the current anthropogenic input (63%) is significantly higher than that from natural sources (EPA, 2010). Enteric fermentation of cattle is the most important anthropogenic source for global methane emission, other human-influenced sources are e.g., fossil fuel mining, landfills, rice agriculture or wastewater decomposition (EPA, 2005; Sheppard et al., 1982; Whiticar, 1990).

With a share of 30% of total methane emissions wetlands, e.g., bogs and swamps, are the dominating natural sources of methane, which is produced by methanogenic microorganisms. Due to an oxygen poor environment and a high level of water saturation these systems provide ideal conditions for fermentation processes. Beside wetlands, also soils, oceans, lakes and rivers, permafrost, and gas hydrates, wildfires, and wild animals contribute to a certain degree to the global methane cycle Figure 1.2 (EPA, 2010; Kvenvolden, 1998; Matthews and Fung, 1987).

Natural methane sources can be divided into biogenic and thermogenic sources, both of which depend on degradation of buried (sedimentary) organic matter (OM). OM is built by photosynthetic processes in which carbohydrates, e.g., glucose, are synthesized from light energy under the uptake and fixation of CO_2. This process is performed by phototrophic organisms, for example

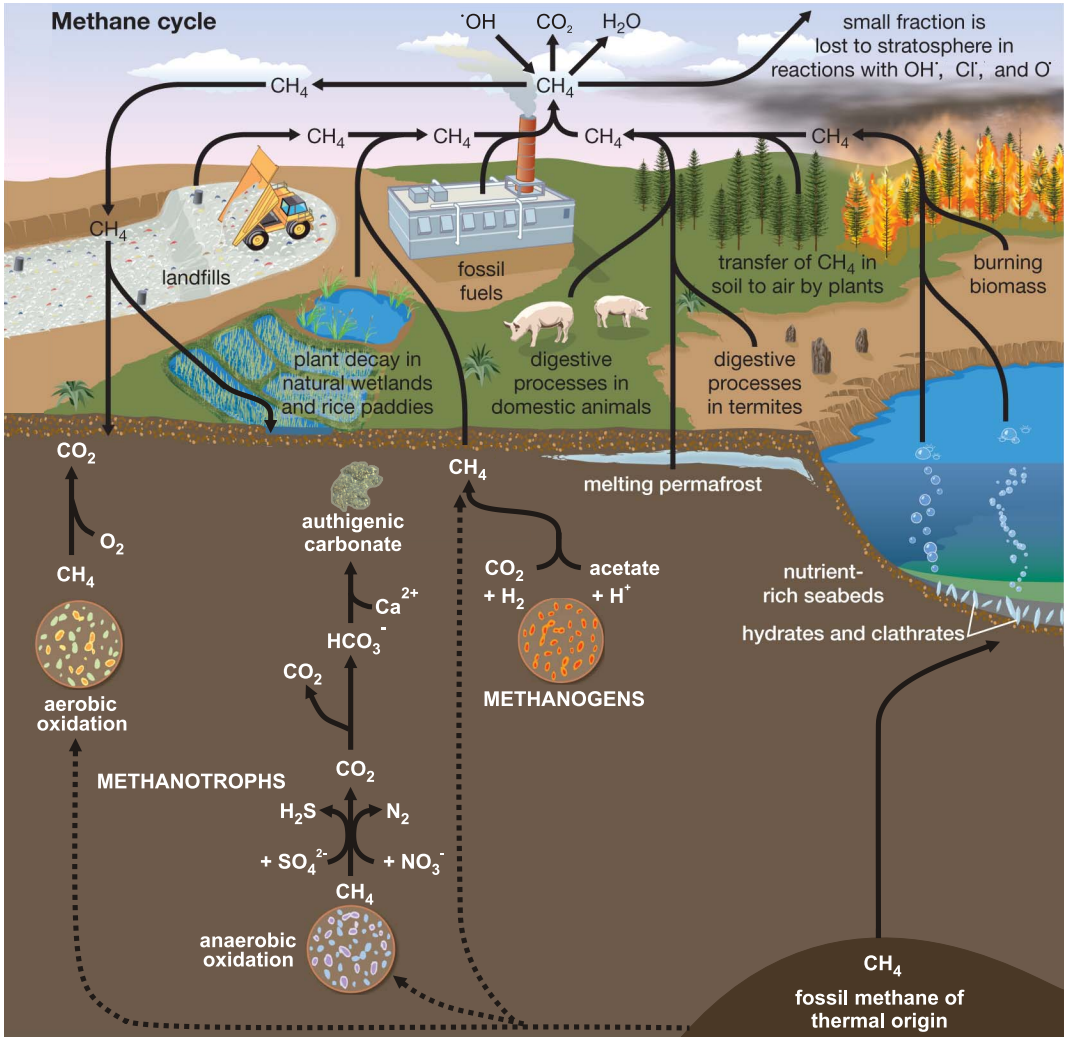

Figure 1.2: Global methane cycle after Encyclopaedia Britannica (2010).

higher plants and phytoplankton. The organic matter formed by photosynthesis can in turn be recycled as part of the nutrient cycle by other organisms or, once the source-organisms die, be brought into the sediment or soil where subsequent decomposition takes place.

The global organic carbon cycle, which integrates the flux of carbon in the lithosphere, biosphere and atmosphere, can be subdivided into the "surface carbon cycle" and the "subsurface carbon cycle". Their common interface is located at the earth surface. However, the residence time of the carbon in either of the two cycles differs by several orders of magnitude. The surface part of the carbon cycle which mainly includes the release of CO_2-carbon back to the atmosphere and hydrosphere has an average duration of days to several

decades (Hunt, 1996; Tissot and Welte, 1984). In contrast, the subsurface carbon cycle, in which geologic processes occur, can last up to millions of years (Horsfield et al., 2006; Tissot and Welte, 1984).

Organic matter available at the sediment surface is mineralized rapidly under aerobic conditions. However, under certain circumstances in both marine as well as terrestrial depositional environments, anoxic conditions promoting organic matter preservation can occur. For example in marine settings the oxic sediment interval is relatively narrow and varies between a few millimeters in coastal areas up to 1 m in pelagic sediment (Jørgensen, 1982). Below this zone, fermentation, denitrification and sulfate reduction processes take place in which anaerobic microorganisms break down OM to obtain energy (Tiedje et al., 1984). As compared to aerobic settings anaerobic environments are characterized by a much slower overall degradation-rate. During the mineralization of organic compounds, such as alcohols and organic acids, CO_2 is formed. Methanogenesis, the process of methane formation, is often the terminal step in the degradation or fermentation of organic matter.

Only approximately 0.1% of the carbon taking part in the surface carbon cycle is sequestered into the geosphere and can lead to the formation of kerogen (Tissot and Welte, 1984). Kerogen is formed by two pathways, either repolymerization and polycondensation processes of organic matter (the "degradation-recondensation" pathway) or by "selective preservation" of resistant biomacromolecules (Tegelaar et al., 1989). The transformation of organic matter during burial can be divided into three stages: diagenesis, catagenesis and metagenesis. Diagenesis, in which mainly polycondensation reactions take place, occurs at relatively low temperatures and pressures, usually at burial depths of a few hundred meters. Biogenic methane is the most important hydrocarbon which is produced during this stage, but also CO_2 is generated (Tissot and Welte, 1984).

Biogenic methane produced by microbial organisms makes up about 20% of the natural gas reserves (Rice and Claypool, 1981). It is generated in anoxic environments at temperatures below 80°C and at burial depths up to 1 km (Rice and Claypool, 1981). Microorganisms of the domain archaea mediate this process by using carbon as an electron acceptor under anaerobic conditions.

The most important pathways of methanogenesis are the reduction of carbon dioxide (Equation 1.1) and acetate (Equation 1.2) to methane (Figure 1.2).

$$CO_2 + 4\,H_2 \longrightarrow CH_4 + 2\,H_2O \tag{1.1}$$

$$CH_3COO^- + H^+ \longrightarrow CH_4 + CO_2 \tag{1.2}$$

Thermogenic methane is generated by thermochemical degradation of higher molecular weight organic matter (mainly kerogen) through cracking and aromatization processes (Tissot and Welte, 1984). This occurs primarily during catagenesis which takes place at burial depths reaching up to several kilometers due to the related increase of subsurface temperature (up to 150°C). At this stage the thermal degradation of kerogen to petroleum (oil and/or gas) controlled by consecutive or parallel bond-cracking reactions occurs.

During metagenesis, at even higher temperature conditions, additional methane along with minor amounts of nonhydrocarbon gases is formed by hydrocarbon cracking processes (Tissot and Welte, 1984). Latest research has shown that also in the transition of catagenesis to metagenesis methane generation can occur, mainly by de-methylation reactions of highly mature kerogen (Mahlstedt and Horsfield, 2012).

The origin of the gas (biogenic vs. thermogenic) can be identified based on its carbon isotopic composition, δ^{13}C (Whiticar, 2000). δ^{13}C values between -52 to -70‰ indicate a biogenic origin, thermogenic methane usually has δ^{13}C values between -25 to -52‰ (Judd, 2000). For details the reader is referred to Chapter 1.4.3.

The majority of the methane generated in the subsurface, biogenic or thermogenic, is controlled and eliminated by microorganisms even before entering the atmosphere. Estimations of methane consumption in marine sediment suggest, that on a global scale, the biogeochemical process of microbial methane oxidation recycles over 90% of the methane flux from sediments (Hinrichs and Boetius, 2002).

Generally there are two pathways of methane oxidation:

1) Aerobic methane oxidation takes place in oxygenated environments. This process is ubiquitous in soil and water and conducted by specific methan-

otrophic bacteria that in most cases belong to the phylum Proteobacteria (Hanson and Hanson, 1996). Under reaction with oxygen methane is oxidized to methanol, formaldehyde, formate, and finally to carbon dioxide.

2) Under oxygen free conditions usually prevailing within centimeters of the sediment-water interface, anaerobic oxidation of methane (AOM) takes place (Boetius et al., 2000). Due to the absence of oxygen another electron acceptor is required to perform methane oxidation. The reduction of sulfate is quantitatively the most important process in AOM in marine sediment (Regnier et al., 2011). Within this process, sulfate functions as an electron acceptor whereas methane, the electron donor, is oxidized (Equation 1.3, see also Chapter 1.3.2).

Net reaction:

$$CH_4 + SO_4^{2-} \longrightarrow HCO_3^- + H_2O + HS^- \tag{1.3}$$

In sulfate-free sediment AOM can also utilize other electron acceptors. In freshwater sediment and enrichment cultures, for instance, denitrification processes occur (Ettwig et al., 2010; Raghoebarsing et al., 2006) in which nitrate assumes the function of the electron acceptor (Equation 1.4).

$$5\,CH_4 + 8\,NO_3^- + 8\,H^+ \longrightarrow 5\,CO_2 + 4\,N_2 + 14\,H_2O \tag{1.4}$$

In marine sediment, however, this process does not seem to play a significant role and has not yet been well proven (Orcutt et al., 2011).

Also metals like manganese and iron have been described to function as potential reducing counterparts in AOM reactions (e.g., Equation 1.5) (Wankel et al., 2012) e.g.,

$$CH_4 + 8\,Fe(OH)_3 + 15\,H^+ \longrightarrow HCO_3^- + 8\,Fe^{2+} + 21\,H_2O \tag{1.5}$$

It was recently shown through incubation experiments, that the processes of metal reduction during AOM may also play a role in lake or marine sediments (Beal et al., 2009; Sivan et al., 2011).

The methane which is not consumed by microorganisms in the sediment or the water column is released to the atmosphere where further reactions occur. In the troposphere, about 85% of the methane are destroyed by photochemical oxidation by radicals. Hydroxyl radicals (OH·) are the most significant reactants, but also smaller fractions of chlorine (Cl·) and atomic oxygen (O·) react

with methane mainly under the formation of water vapor and carbon dioxide (Cicerone and Oremland, 1988; Ehhalt and Schmidt, 1978; Hanson and Hanson, 1996). The remaining 15% of the methane which cannot be retained by the troposphere enter into the stratosphere where it is eventually destroyed (Levy, 1971).

1.3.1 Methane in marine systems

The largest methane reservoir on Earth can be found in marine sediments which contain about 500-10,000 Gt of methane carbon (Kvenvolden, 1988; Whiticar, 1990). Large amounts are stored in gas hydrates which have captured approximately 500-2500 Gt of methane carbon (Milkov, 2004). Earlier estimates even suggested up to 10000 Gt of methane carbon (Knittel and Boetius, 2009; Kvenvolden, 1993; Maslin and Thomas, 2003). The methane can either be of biogenic or thermogenic origin. Methane hydrates, also referred to as clathrates, are rigid water cages that enclose methane molecules in their structure (Kvenvolden, 2002; Sloan, 2003). Their composition mainly depends on the available gas as well as temperature and pressure conditions (Sloan and Koh, 2008). Low temperature and/or high pressure are required to stabilize these structures. Often, these conditions are prevailing on continental margins or in permafrost regions (Kvenvolden et al., 2001).

As long as gas hydrates are present in stable environments, their contribution to the release of methane to the atmosphere is negligible. However, changing environmental conditions, like global warming could result in a tremendous influence on the methane cycle. The destabilization and thus the decomposition of gas hydrates can result in the liberation of large volumes of gas along with the release of methane to the atmosphere. It has been inferred that throughout the geologic history periodic pulses of hydrate-derived methane significantly contributed to increases in global temperatures and changes in global carbon fluxes (e.g., Chappellaz et al. 1993; Dickens 2003; Hesselbo et al. 2000; Kennett et al. 2000; Maslin et al. 2004).

In the subsurface the largest fraction of upward diffusing gas is consumed by microorganisms (Valentine and Reeburgh, 2000). Thus, even though the content of methane in marine sediment is significantly higher, the ocean only accounts for 2 to 5% of the global methane emission to the atmosphere (Judd

et al., 2002; Reeburgh, 2007). Only if the gas concentration exceeds the oxidizing capacity of methanotrophic microorganisms, can methane be discharged to the water column resulting in e.g., microseeps or cold seeps. Globally 0.02 Gt yr^{-1} are estimated to be emitted by cold seeps (Judd, 2004; Kvenvolden et al., 2001). Due to the released hydrocarbons cold seeps are usually colonized by a specific and unique faunal community. Tubeworms, molluscs, crustaceans, bacterial mats and fishes (e.g, Figure 1.1), species often associated to seeping hydrocarbons, can be found at active seeping sites (Foucher et al., 2009; Levin, 2005). The most important faunal community at cold seep sites, however, is the microfauna, which controls the release of large amounts of methane to the surface by the process of anaerobic oxidation of methane (see Chapter 1.3.2).

1.3.2 Anaerobic oxidation of methane (AOM) in marine sediments

The process of AOM along with the presence of sulfate reduction in marine sediments was first inferred in the 1970s (e.g., Barnes and Goldberg 1976; Martens and Berner 1974; Reeburgh 1976). A more detailed hypothesis explaining the functioning of AOM was provided by Hoehler et al. (1994) who proposed the existence of a microbial consortium of methanotrophic archaea and sulfate reducing bacteria (SRB). Approximately 5 years later Hinrichs et al. (1999) and Boetius et al. (2000) provided the first microbiological and biogeochemical evidence for such microbial consortia. They showed that methane oxidizing archaea mediate AOM apparently in syntrophy with SRB (Boetius et al., 2000). Orphan et al. (2002) could finally prove the existence of such a microbial consortium by using coupled isotopic and phylogenetic analyses. In the following years, intensive investigations on this topic have been performed (e.g., Blumenberg et al. 2004; Elvert et al. 2003; Hinrichs and Boetius 2002; Niemann and Elvert 2008; Treude et al. 2005a), but the mechanisms and the participating microbial communities have still not been fully unraveled.

In methane rich sediments AOM with sulfate as the terminal electron acceptor is the dominant biogeochemical process (Hinrichs and Boetius, 2002). Methane is oxidized to bicarbonate and sulfate reduced to sulfide (Equation 1.3). Due to increasing alkalinity and increasing amounts of inorganic carbon, the bicarbonate produced precipitates together with metal ions to form au-

thigenic carbonate (Luff et al., 2004; Valentine, 2002) according Equation 1.6. Net reaction:

$$CH_4 + SO_4^{2-} + Ca^{2+} \longrightarrow CaCO_3 + H_2O + H_2S \tag{1.6}$$

The centimeter to decimeter thick carbonate crusts are predominantly composed of calcium carbonate (aragonite) or magnesium calcite (e.g., Kulm et al. 1986). Typically they are formed at shallow depth in the sediment, however, subsequent erosion or gravitational processes, expose them at the seafloor (Luff et al., 2004). Thus, patches of carbonate crust as well as carbonate reefs can often be found at active seepage sites, building habitats for a diverse faunal marine community (Foucher et al., 2009; Kulm et al., 1986).

Microbiological investigations showed that methanotrophic archaea belong to the three clades of anaerobic methanotrophs (ANME) ANME-1, ANME-2 and ANME-3 within the Euryarchaeota (Knittel and Boetius, 2009). They are distantly or closely related to the orders *Methanomicrobiales* (ANME-1), *Methanosarcinales* (ANME-2 and ANME-1) (Blumenberg et al., 2004), and *Methanococcoides* and *Methanolobus* (ANME-3) (Lösekann et al., 2007; Niemann et al., 2006). All these orders are methanogens, therefore it was claimed that the ANME are also methanogens, but operating with a reverse metabolism (Hallam et al., 2004; Hinrichs et al., 1999). This was further supported by additional microbiological analyses using genomic techniques (e.g., Hallam et al. 2004; Krüger et al. 2003). All three ANME groups can coexist in methane-rich environments, however, ANME-2 is often found to be the dominating clade (e.g., Bertram et al. 2013; Knittel et al. 2005). So far, four subgroups of ANME-2 could be identified, namely ANME-2a, -2b, -2c and -2d (Knittel and Boetius, 2009), but also subgroups of ANME-1 (e.g., ANME-1a and -1b) have been found (Teske et al., 2002). ANMEs often occur in syntrophic association with sulfate reducing bacteria (SRB) (Boetius et al., 2000) belonging to the *Deltaproteobacteria*. These include *Desulfosarcina/Desulfococcus*(for ANME-1, ANME-2) and *Desulfobulbus* (for ANME-3) (e.g., Lösekann et al. 2007; Michaelis et al. 2002; Orphan et al. 2002). However, the possibility has been debated that there are archaea of the group ANME that are capable of methane oxidation even without a syntrophic partner (Milucka et al., 2012; Pernthaler et al., 2008). The sulfate-methane transition zone (SMTZ) forms

the main niche for the AOM microbial ecosystems. It denotes the zone where there is an overlap of dissolved sulfate diffusing into the sediment from above and methane coming from below (Knittel and Boetius, 2009). The depth and width of the SMTZ can vary between a few centimeters up to tens of meters below seafloor, depending on the supply of methane and sulfate and the consumption rates (Knittel and Boetius, 2009).

Dissimilatory sulfate reduction is the quantitatively most important process in the degradation of organic matter (Jørgensen, 1982). Thus, the analysis of sulfate reduction rates, e.g., using a radiotracer technique (Fossing and Jørgensen, 1989; Kallmeyer et al., 2004), can be used to assess microbial activity in general and to trace the interval in which AOM occurs.

Although AOM has been the scientific target of many studies for decades, the underlying mechanisms have not yet been fully understood and cultivation and isolation of the responsible microorganisms has not been successful (Alperin and Hoehler, 2009). Furthermore, there was doubt that this process could support the metabolism of the two syntrophic partners in AOM due to its very low free energy yield of $\Delta G^{0'}$=-25 kJmol^{-1} (Hoehler et al., 1994; Knittel and Boetius, 2009; Valentine and Reeburgh, 2000). Hence, AOM still contains many unsolved questions and deciphering its processes will remain of great significance throughout the upcoming years.

1.4 Biomarkers

Biomarkers, also referred to as geochemical fossils or molecular biological marker compounds, are complex organic molecules derived from formerly living organisms (Wang et al., 2006). During diagenetic and catagenetic processes they lose most of their functional groups, therefore, their basic skeleton is predominantly composed of carbon and hydrogen. However, biomarkers including heteroatoms (mainly N, S and O) are also common. The basic structure of the biomarkers is relatively stable over geological time periods, which means they can even be isolated from very old Precambrian samples (Peters et al., 2005b). Biomarkers can be found in sediments and crude oils and can be extracted from rocks without losing their characteristic features. Many biomarkers are taxonomically specific, which allows assigning them to their specific biological sources. Thus, biomarkers can be used to trace the biological origin of or-

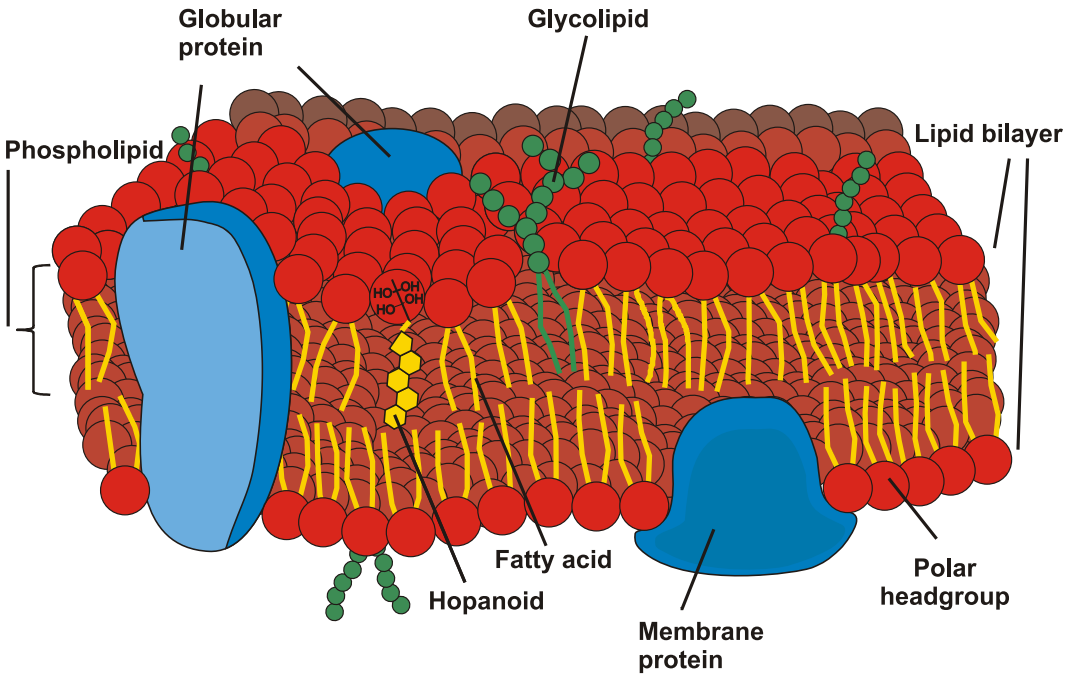

Figure 1.3: Simplified sketch of a cell membrane showing the basic compositional elements (after Ruiz 2007).

ganic matter (Isaksen and Bohacs, 1995), to denote depositional environment (Peters et al., 1986), to unravel past environmental conditions (Seifert and Moldowan, 1981) or to record periods of global climate change (Brassell et al., 1986). Along with the information about the chemical alteration due to diagenetic and catagenetic processes they can also provide insights into thermal maturity of the organic matter (Peters et al., 2005b).

Most biomarkers are derived from lipid components which are parts of cell membranes Figure 1.3. Within the membranes they can assume different functions like the modulation of fluidity of the membranes (e.g., steroids or hopanoids, Chapter 1.4.2). In some organisms they are even responsible for the formation of lipid bilayers (e.g., phospholipids, Chapter 1.4.1) to form cell membranes. These biomarkers can be isolated via chemical extraction and chromatographic separation methods. Archaea, Bacteria and Eukarya, which form the three domains of life, can be distinguished by the molecular structure of their corresponding biomarkers (Peters et al., 2005b). Thus, the structures and the degree of functionalization can provide substantial information on the environment and their associated communities (e.g., Bianchi and Canuel 2011). Additionally, the extent of molecular breakdown can give evidence about the

past environmental conditions such as exposure to higher temperatures and high pressure, anoxic conditions or salinity (Peters et al., 2005b).

The following sub-chapters provide further details on selected biomarkers which are roughly divided into "AOM related biomarkers" and "petroleum biomarker". These cover the biomarkers which were applied and interpreted in the present study. Furthermore, a brief insight into the topic "carbon isotope signature" is provided.

1.4.1 AOM-related biomarkers

The release of methane from the sediment to the water column and/or to the atmosphere is controlled by specific microbial communities which consume most of the methane. Therefore, it is of high importance to understand their metabolism and the occurring processes. Specific biomarkers which are diagnostic for AOM were the subjects of numerous studies described in the literature (e.g., Hinrichs and Boetius 2002; Knittel and Boetius 2009; Orphan et al. 2002; Zhang et al. 2003). From these studies we learned that in most cases AOM is performed and controlled by a consortium which consists of specific archaeal communities in close association to their corresponding bacterial partners capable of performing sulfate reduction. To study the qualitative and quantitative abundance of the archaeal and bacterial communities at cold seep sites, their diagnostic biomarkers can be analyzed. These include e.g., archaeol and hydroxyarchaeol, pentamethylicosane (PMI) and crocetane, specific glycerol dialkyl glycerol tetraethers (GDGTs) as markers for archaea and phospholipid fatty acids (PLFAs) for bacteria. The cell membranes of Archaea consist predominantly of lipids which contain characteristic diether bilayers or tetraether monolayers (De Rosa et al., 1986). These lipids are composed of isoprenoidal alkyl moieties linked by ether bonds to a glycerol backbone (GBB) which is further connected to a polar head group. Tetraethers are composed of two isoprenoid C_{40} moieties which are linked to the GBB at both ends (Figure 1.4).

During the process of diagenesis and the corresponding degradation of the lipid membranes, the polar head groups are lost. In contrast, the relatively stable glycerol dialkyl glycerol tetraether (GDGT) fragments (core lipids) remain well preserved and are, therefore, indicators for fossil archaeal microorganisms.

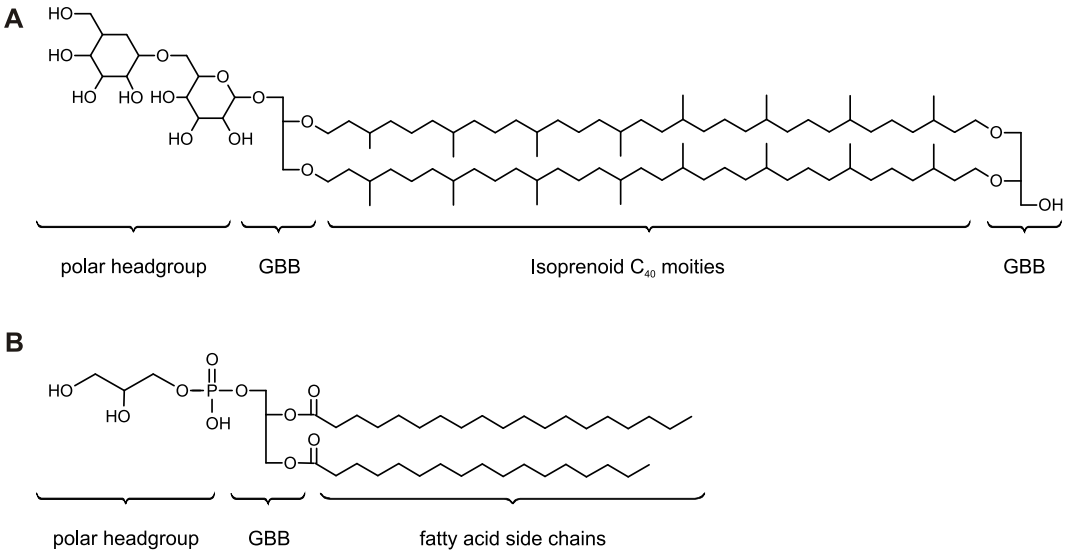

Figure 1.4: Intact polar lipids, (A) archaeal tetraether lipid, (B) bacterial phospholipid, GBB: Glycerol backbone.

The isoprenoidal GDGTs detected in sediments show some variability in their structure. The basic form is GDGT-0 containing only isoprenoid alkyl chains. Additionally, GDGTs can contain between 1 and 4 cyclopentyl rings (GDGT-1 to GDGT-4), while crenarchaeol bears additionally up to 4 cyclopentyl rings one cyclohexyl ring (see Appendix A for GDGT structures).

For years GDGTs have been assigned exclusively to extremophilic archaea (De Rosa and Gambacorta, 1988), however, over the last 10-15 years they have often been detected in mesophilic marine and lacustrine environments with moderate conditions (Schouten et al. 2013 and references therein). GDGTs 0-3, for example, have been shown to derive from mesophilic Euryarchaeota capable of anaerobic oxidation of methane (e.g., Aloisi et al. 2002; Pancost et al. 2001). GDGT-0 is not only related to AOM processes, in fact it is ubiquitous in many different environments. This is the reason why it is often the dominant compound within the GDGTs. Crenarchaeol, which can also be found frequently in sediment samples, is assumed to be derived from Crenarchaeota being the most abundant archaea in marine environments, however, picoplankton coming from the water column can be an additional source (Sinninghe Damsté et al., 2002; Stadnitskaia et al., 2005).

Since they are insufficiently volatile, the identification of entire GDGT-molecules by application of conventional chromatographic methods like gas

chromatography mass spectrometry (GC-MS) has been a challenge for many years. Using GC-MS, only partial structures, subsequent to chemical degradation, could be analyzed (Schouten et al., 2000). Additional attempts for the direct analysis of GDGTs have been made by using high temperature GC-settings (e.g., Nichols et al. 1993). However, insufficient peak resolution as well as technical difficulties in coupling the high temperature GC to an MS unit hindered the major breakthrough (Schouten et al., 2013). With the development of a high performance liquid chromatography (HPLC)-mass spectrometry (MS) method suitable for the analysis of GDGTs a major step forward was achieved, which enabled GDGT structures to be proven and new GDGT compounds to be identified (Bai and Zelles, 1997). This led to, amongst others, the detection of branched GDGTs containing non-isoprenoid alkyl chains that have been assigned to Bacteria or Eukaryotes (Weijers et al., 2006a).

Further information on the structural composition of the ether-bound alkyl chains within the GDGTs can be obtained by hydrolysis experiments to provoke ether cleavage. Different techniques are known to achieve ether cleavage, while the selection of the preferred setup is primarily dependent on the subsequent analysis. Commonly ether cleavage is performed using boron tribromide (BBr_3) or hydroiodic acid (HI) resulting in the respective alkyl halogenides followed by reduction/hydration using lithium aluminium hydride ($LiAlH_4$) or zinc (Zn) (Chappe et al., 1980; Gattinger et al., 2003; Schouten et al., 1998). The analysis of the released alkyl chains via e.g., GC-MS or GC-IR-MS can give additional information on the structure as well as the isotope signature of e.g., carbon (see Chapter 1.4.3).

Bis-O-phytanylglycerolether, also known as archaeol, and its derivatives (e.g., hydroxyarchaeol) are diether compounds which are known to be derived from archaeal organisms. The diacyl-glycerols consist of two alcohol moieties that are ether-bound to a GBB. In contrast to the previously discussed GDGTs which form membrane monolayers, archaeols form lipid bilayers as part of microbial membranes (Lederberg, 2000). The archaeal character is again displayed in the isoprenoid structure of the fatty acids being attached to the glycerol. Archaeol, containing two phytanyl (C_{20}) moieties, is ubiquitous in diverse environments (e.g., Tornabene and Langworthy 1979). Hydroxyarchaeol, containing an additional hydroxyl group on the phytanyl chain either linked

to the second (*sn*2) or third (*sn*3) glycerol carbon, is predominantly found in methanogens (Koga et al., 1998). *Methanosarcina* sp. are believed to be the major producers of *sn*-2-hydroxyarchaeol, whereas *sn*-3-hydroxyarchaeol has been found in *Methanosaeta concilii* (Hinrichs et al., 1999; Sprott et al., 1993). Dihydroxyarchaeol, containing two hydroxyl groups at both phytanyl-chains, has been detected recently and is associated to methanogenic archaea (Birgel et al., 2011; Bradley et al., 2009). Furthermore, Stadnitskaia et al. (2008) described the discovery of extended $C_{20,25}$ *sn*2-hydroxy isoprenoid glycerol diether, inferring that these biomarkers are produced by methanotrophic ANME-2 archaea.

The irregular tail-to-tail linked C_{25} isoprenoid hydrocarbon 2,6,10,15,19-pentamethylicosane (PMI, $C_{25}H_{52}$) is abundant in cold seep samples and attributed to methanogenic and methanotrophic archaea (Elvert, 1999). The analogous C_{20} isoprenoid hydrocarbon crocetane (2,6,11,15-tetramethylhexadecane, $C_{20}H_{42}$) is also known to be derived from methanotrophs (Peters et al., 2005b). The main evidence for their contribution within AOM processes was provided by isotope measurements. Extremely ^{13}C depleted carbon isotope signatures revealed the link of PMI and crocetane to methane consumption (Elvert, 1999; Peters et al., 2005b). While PMI has been ascribed to originate also at least partially from algal sources (Kohnen et al., 1992), the source for crocetane in marine sediments has been assigned exclusively to methanotrophy. PMI has been described to be a free lipid in methanotrophic archaea (Holzer et al., 1979; Rowland, 1990) being particularly abundant in *Methanosarcina barkeri* (Risatti et al., 1984). In addition, the unsaturated counterparts of PMI and crocetane, pentamethylicosenes (Elvert, 1999; Sinninghe Damsté et al., 1997) and crocetenes (Pancost et al., 2000), respectively, have been identified. Their light isotopic composition in seep environments could prove that these biomarkers also participate in methanotrophic processes. Whereas PMI can be easily detected by gas chromatography, the determination of crocetane is difficult due to co-elution with phytane, a specific column setup, however, allows the partial separation of these two compounds (Peters et al., 2005b).

In contrast to archaeal microorganisms characterized by ether-bound isoprenoidal carbon skeletons, bacteria contain ester-linked alkyl-lipids (Woese et al., 1990). Within intact cell membranes of living bacteria they are orga-

nized as intact phospholipid esters (PLs). Intact PLs are usually composed of a polar (hydrophilic) head-group and a non-polar (hydrophobic) tail (Figure 1.4B). The polar head group is linked to a glycerol backbone which is, in turn, ester-linked to one or two fatty acid units representing the hydrophobic part. In a bacterial membrane PLs form lipid bilayers in which the non-polar fatty acid chains are oriented towards each other and the polar head-groups build the inner and outer membrane surface. Intact PLs are known to decompose quickly and can thus be used as "life markers" indicating viable microbial biomass (Harvey et al., 1986; Zink et al., 2003). Direct analysis of intact PLs, however, has been impossible for a long time since the thermally labile molecules are decomposed when analyzed by gas chromatography (Fang and Barcelona, 1998). The development of high performance liquid chromatography coupled to a mass spectrometer (HPLC-MS) in the late 1990s brought tremendous progress in the analysis of intact PLs concerning their qualitative and quantitative assessment (Fang and Barcelona, 1998). The analysis of intact PLs is an important tool to study microbial communities. Based on their structural composition, e.g., diverse head groups and varying fatty acid side chains, the presence of different groups of microorganism can be estimated (Rütters et al., 2002) and adaptation mechanisms of bacteria to varying environmental conditions can be assessed (Mangelsdorf et al., 2009, 2005).

Hydrolysis of intact PLs releases their phospholipid fatty acid (PLFA) side chains. In former times, when HPLC-MS was not yet available, the analysis of PLFAs by GC-MS was the only possibility for quantification of the viable biomass (Vestal and White, 1989). However, PLFAs can also reveal qualitative information on the microbial communities present. With chain lengths between approximately C_{12}-C_{26} they can exhibit a large structural variety including saturated, (poly)unsaturated (enoic) and cyclic (e.g., cyclopropyl) parts. The most abundant PLFAs are the C_{16} and C_{18} saturated fatty acids which are known to occur in the lipids of most living organisms (Rhead et al., 1971a). Dependent on their structure PLFAs can be diagnostic for microorganisms performing specific processes such as sulfate reduction/methane oxidation or differentiate between microbia clades (Zelles, 1999). The diagnostic PLFAs for sulfate reducing bacteria include e.g., *iso*- and *ai*-C_{15}, *iso*- and *ai*-C_{17}, $C_{16:1\omega5}$ as well as cyclo-$C_{17:0}$ (Elvert et al., 2003; Nauhaus et al., 2007; Niemann and

Elvert, 2008). Together with significantly negative isotope signatures (δ^{13}C, see Chapter 1.4.3) they can indicate the presence of SRB involved in the process of AOM.

1.4.2 Petroleum biomarkers

Seepage of gas in cold seeps is often accompanied by petroleum dragged along towards the seabed surface (Hvoslef et al., 1996). Therefore, the presence of petroleum biomarkers can be an indicator for present or past seeping activity.

Petroleum is a complex mixture composed of hydrocarbons (HCs) of various molecular weights. It is formed by deposition and preservation of organic matter due to subsequent burial combined with the impact of high temperature and pressure. The most abundant compounds in petroleum are linear or branched alkanes (paraffins), cycloalkanes (naphthenes) and aromatic hydrocarbons. For the characterization of petroleum, however, the relatively scarce biomarkers are the most frequently utilized compounds. The organic matter of petroleum can basically be divided into 4 classes: aliphatic HCs, aromatic HCs, resins (hetero compounds) and asphaltenes.

Asphaltenes are high molecular weight HCs containing hetero atoms such as sulfur, oxygen and nitrogen. Due to their bulky structure they are not dissolved but dispersed as colloids in petroleum and, in contrast to the remaining petroleum compounds, insoluble in *n*-hexane (e.g., Hirschberg et al. 1984).

Aromatic HCs are cyclic and planar compounds that fulfill Hückel's rule of aromaticity (Hückel, 1937). In petroleum aromatics comprise monoaromatic compounds like benzenes, toluenes, xylenes and polyaromatic compounds like naphthalenes, phenanthrenes, fluorenes and chrysenes as well as their corresponding derivatives (Blumer, 1976).

The polar hetero compound fraction contains hydrocarbons that bear, beside carbon and hydrogen, additional atoms such as nitrogen, sulfur and oxygen and metals. In petroleum, sulfur structures are the most abundant compounds within this class comprising e.g., thiols, disulfides, thioalkanes and thiophenes (Orr and Sinninghe Damsté, 1990). The oxygen compounds comprise, beside alcohols and aliphatic acids, neutral substrates such as furans, dibenzofluranes or fluorenones. Although oxygen and nitrogen containing biomarkers represent only a minor share of the polar hetero compound fraction, they play an

important role in petroleum geochemistry due to their structural complexity and reactivity (Snyder, 1970). The nitrogen compounds resemble the structure of sulfur containing molecules and comprise, beside others, pyrrole, carbazole, pyridine or quinoline and their derivatives. Porphyrins, being tetrapyrrole compounds, are a special class of nitrogen containing biomarkers since they can be regarded as the first biomarkers in the history of geochemistry (Treibs, 1936). Treibs (1936) proposed chlorophyll molecules being the direct precursor of the porphyrins which he detected in oil.

Aliphatic compounds in petroleum mainly include linear and branched alkanes, cycloalkanes, hopanes and steranes. Since the aliphatic petroleum constituents and biomarkers were in the focus of the present thesis they will be discussed in more detail below. Petroleum shows a wide variety in its composition mainly depending on the source and the depositional environment and the subsequent alteration due to e.g., fractionation or degradation. Thus, the qualitative and quantitative analysis of the biomarker inventory plays an important role in the characterization, differentiation, correlation as well as identification of possible sources, the maturity assessment of the organic matter and the interpretation of past or present environmental conditions (Peters et al., 2005a,b). Biomarkers are relatively stable against thermal degradation and show little changes from their parent molecules. However, selective alteration in their molecular structure due to external influences can occur, highlighting the influence of maturation, biodegradation, anoxic/oxic conditions, prevailing temperature or migration processes (Bennett et al., 2006; Brocks et al., 2005; Farrimond et al., 1998; Larter et al., 1996; Weijers et al., 2006b).

In the following the oil-derived biomarkers and petroleum compounds from the aliphatic fraction are discussed in more detail:

Alkanes are the most abundant compounds in crude oils. These include linear *n*-alkanes, branched alkanes as well as isoprenoid alkanes. Their origin can be found in different sources, such as plant material, constituents of lipids from microorganisms or algal material. Alkanes can be easily determined by chromatographic methods, e.g., gas chromatography coupled to a flame ionization detector (GC-FID) or mass spectrometer (GC-MS). Based on the presence of different alkanes and their quantitative abundance to each other they can be used to indicate the source, the maturity as well as the age of the organic

material studied (Peters et al., 2005a,b). An important parameter is the ratio of odd to even carbon numbers. Predominance of odd over even *n*-alkanes is common in many samples derived from lacustrine and marine sources and often represents a contribution of higher-plant epicuticular waxes (Eglinton and Hamilton, 1967). Due to microbial consumption of *n*-alkanes, biodegradation can affect the original distribution of the compounds. Often, biodegradation is reflected by a significant "hump" consisting of an unresolved complex mixture (UCM) of hydrocarbons which increases with the level of biodegradation. The isoprenoid alkanes in particular pristane (Pr) and phytane (Ph) are important compounds within the class of alkanes. Specific ratios between Pr and Ph, also in combination with n-C_{17} and n-C_{18}, can be calculated to estimate the maturity of the organic matter (Alexander et al., 1981), the degree of biodegradation and can be used for petroleum correlation (Peters et al., 2005b).

Hopanes are pentacyclic triterpenes, which originate from cyclisation of the acyclic isoprenoid compound squalene (Rohmer et al., 1984). They consist of four cyclohexyl and one cyclopentyl ring and contain, beside some additional methyl groups, a longer alkyl chain linked to the C21 atom in the cyclopentane ring. Hopanes are indicators for procaryotic organisms since they originate from hopanoic precursors (mainly C_{35} bacteriohopanetetrol), which are main constituents of bacterial cell membranes controlling the fluidity of the membrane (Ourisson et al., 1979). By comparing the terpane fingerprint they are often used to correlate oils and source rocks (Seifert and Moldowan, 1981).

During diagenesis the hydroxyl groups of the bacteriohopanepolyol precursor are rapidly lost and a stepwise degradation of the longer alkyl chain (C_{31} to C_{35}) occurs (Sinninghe Damsté et al., 1995). Additionally, their stereochemistry is changed. Hopanes exhibit a stereocenter at position C17 and C21 which enables the formation of different stereoisomers, α(H)- or β(H)-isomers. The spatial orientation α(H) indicates that the hydrogen is located below the plane of the paper, β(H) signifies that it is above the plane. In the natural precursor usually the 17β(H), 21β(H) (short: $\beta\beta$) configuration exists (see Appendix A for molecular structures). With ongoing diagenesis and catagenesis a systematic change of their configuration to the thermodynamically more stable $\beta\alpha$- and $\alpha\beta$-isomers occurs. $\beta\alpha$-hopanes, also referred

to as moretanes, are thermally less stable than the $\alpha\beta$-hopanes (Peters et al., 2005b). Thus, with increasing maturity the equilibrium is shifted towards the $\alpha\beta$-isomer (Seifert and Moldowan, 1980). By calculating ratios of the different stereoisomers the maturity as well as possible sources of the analyzed material can be estimated. However, the applied ratios have to be evaluated carefully since $\alpha\beta$- and $\beta\alpha$-isomers could also be observed in "immature" sediments and may stem directly from biogenic sources, e.g., $\alpha\beta$-$C_{31}R$- (Thiel et al., 2003), $\beta\alpha$-C_{30}-hopane (Mackenzie, 1984).

The C_{31} to C_{35} homohopanes exhibit an additional stereocenter at the carbon atom C22. In the biologic precursor only the 22R-isomer is present. Since isomerization to the 22S-isomer occurs relatively early, the homohopanes index, a ratio to calculate the isomerization of the homohopanes, can be used to estimate the thermal maturity in the immature to early mature stage (Peters et al., 2005b).

Hopanes being composed of less than 30 C-atoms are referred to as norhopanes. Norhopanes are formed due to the loss of methyl groups, which can occur at different positions. The loss of the methylgroup at C25 leads to the formation of 25-norhopanes and is typically correlated to biodegradation processes (Bennett et al., 2006). Likewise, 30-norhopanes miss a methyl group at position C30. Very prominent examples are the 17α(H)-22,29,30-trisnorhopane (Tm) and the 18α(H-)22,29,30-trisnorhopane (Ts) which are common parameter to determine thermal maturity ratios and sources (Farrimond et al., 1998).

Usually hopanes are analyzed using GC-MS. Identification occurs based on their mass spectra selecting m/z=191 as well as by comparing retention times in the gas chromatograms.

Steranes are tetracyclic triterpenes which consist of three cyclohexyl and one cyclopentyl ring. Beside two methyl groups at position C10 and C13 they contain a hydrocarbon chain of variable length at C17 in the cyclopentane ring (see Appendix A).

The tetracyclic C_{27}- to C_{30}-sterols which occur naturally in plants, animals, and fungi (all belonging to the domain Eukaryota), are source compounds of the homologue steranes (Nes, 1974). Due to their flat fused-ring structure they are important constitutional parts of the cell membranes modulating and refining membrane properties in Eukaryota (Barenholz, 2002).

Sterols and the potentially resulting steranes exhibit several stereocenters leading to different isomers. The biosynthesized sterols reveal only the 8β(H), 9α(H), 10β(CH_3), 13β(CH_3), 14α(H), 17α(H), 20R configuration (Nes, 1974). The steranes built during diagenesis by removal of the OH group, which is attached to C3, and by hydration of the C5 to C6 double bond, first exhibit the configuration which was initially present in the sterols (Dastillung and Albrecht, 1977; Rhead et al., 1971b). However, with progressing diagenesis and catagenesis, isomerization particularly at the C5-, C14-, C17- and C20-atom occurs. Often, a simplified labeling for sterane isomers is applied, e.g., 5α(H), 14α(H), 17α(H), 20R configuration or $\alpha\alpha\alpha R$ (Chapter 3). Within the isomerization process the formation of thermodynamically more stable configurations occurs (Mackenzie et al., 1982). With increasing maturity the formation of the $\alpha\beta\beta$ isomers are favored and isomerisation at the chiral C20 enhances the formation of the 20S isomer (Grantham, 1986; Mackenzie et al., 1982). Thus, beside the biological conformation $\alpha\alpha\alpha R$ three geological sterane configurations are possible: $\alpha\alpha\alpha S$, $\alpha\beta\beta S$ and $\alpha\beta\beta R$. Ratios of these compounds can be used to assess the maturity of the studied sample (Peters et al., 2005b). Additionally, aromatization can occur with progressing diagenesis leading to monoaromatic or triaromatic steranes (Mackenzie et al., 1982).

Diasteranes, also referred to as rearranged steranes do not reveal methyl groups at position C10 and C13 but at C5 and C14. They have no biological precursors, and are most likely a result of diagenetic and catagenetic processes. Since diasteranes are more thermally stable than steranes, their ratio can be used as a maturity parameter (Peters et al., 2005b).

Also steranes are analyzed using GC-MS. Identification is usually based on their mass spectra selecting m/z=217 and by correlation of retention times in the gas chromatograms.

1.4.3 Carbon isotope signature

Isotopes of a given atom contain the same number of protons, but differ in their numbers of neutrons. This results in atoms variable in their atomic mass. Carbon has three naturally occurring isotopes: ^{12}C (6 protons and 6 neutrons), ^{13}C (6 protons and 7 neutrons), and ^{14}C (6 protons and 8 neutrons). ^{12}C and ^{13}C are stable isotopes and occur with a natural abundance of 98.89% and

1.109%, respectively. ^{14}C is produced by thermal neutrons originating from cosmic radiation and can be incorporated by living biomass when entering the lower troposphere. Due to its radioactivity with a half-life time of 5730 years, ^{14}C can be used for radiometric dating (Libby, 1955).

The ratio between the stable ^{12}C and ^{13}C are often used within biomarker approaches and offer important information, such as generic relationships or the origin of a carbon source (Hayes et al., 1990). Values of stable isotope ratios are presented in $\delta^{13}C$ notation and are typically given in per mill (‰) often in relation to the defined standard carbonate rock "Vienna Pee Dee Belemnite" (VPDB), which was assigned to $\delta^{13}C = 0‰$. Negative values indicate that the compound is depleted in the ^{13}C isotope, whereas positive $\delta^{13}C$ values indicate an enrichment of the ^{13}C isotope. The variation within the $\delta^{13}C$ values is caused by isotope fractionation due to preferred incorporation of one isotope, leading to compounds enriched in this isotope and a relative depletion in the respective precursor pool. Isotope fractionation can be influenced by different factors such as isotope exchange reactions (equilibrium processes) or by reaction kinetics e.g., due to different reaction rates. The binding energy between ^{12}C - ^{12}C is slightly weaker than ^{12}C - ^{13}C which leads to preferential cracking (thermogenic and enzymatic/biogenic) of the ^{12}C - ^{12}C bonds in hydrocarbons resulting in ^{12}C enriched light hydrocarbons. However, thermogenic methane generally show values less depleted in ^{13}C compared to biogenic methane. Microorganisms preferentially cleave the bonds of the lighter carbon isotopes (^{12}C) which results in a high isotopic fractionation and, therefore, in low values for the carbon isotopic composition. In contrast, thermogenic gas is usually the result of the impact of high temperatures resulting in less discrimination of higher-energy bonds (Whiticar, 1999). Thus, the origin of gas can be identified based on its carbon isotopic composition. $\delta^{13}C$ values lower than -52‰ indicate a biogenic source, whereas higher $\delta^{13}C$ values (-20 to -52‰) denote a thermogenic origin (Judd, 2000).

Methane shows the largest variation of the $\delta^{13}C$ ratio of any hydrocarbon and typically reveals very "light" values. Incorporation of the very light methane in turn, for example in methane consuming organisms, leads to the enrichment of the light ^{12}C carbon in the microbial biomass resulting in ^{13}C depleted biomarkers (Hoefs, 2004; Peters et al., 2005a).

The $\delta^{13}C$ ratio of samples can be determined by isotope ratio mass spectrometry (IRMS). Additionally it is possible to analyze compound specific (biomarker) isotope signatures by coupling chromatographic methods for example gas chromatography to the IRMS unit (GC-IRMS).

1.5 Geological setting and study area

The Barents Sea is an area which is known for the presence of cold seep systems. Extensive pockmark fields, gas flares in the water column as well as carbonate crust areas exhibiting rising gas bubbles have been detected in several surveys. Additionally, the Barents Sea evolved to an oil and gas prospective area which means that sources are available to potentially feed cold seep systems. Therefore, this area has been chosen as ideal setting for the investigation of cold seep systems. In the following an introduction to the geological setting and the geologic history of the study area is given.

1.5.1 Geological setting

The Barents Sea is located north of Norway and Russia and borders the Norwegian Sea in the southwest, the Arctic Ocean in the north and Novaya Zemlya in the east. The geological evolution has been influenced by several tectonic events since the Early Devonian during which the major structural elements have been established (Gabrielsen et al., 1990). The western part of the Barents Sea has been tectonically active throughout the Mesozoic and Cenozoic, whereas the eastern and northeastern part has been affected by less tectonic activity since the Late Carboniferous. It is proposed, that the structural evolution in the area was always associated to the previously established main structural elements (Gabrielsen, 1984). The erosion and uplift processes that occurred in the Late Pliocene and Pleistocene are believed to be related to glacial events (Eidvin et al., 1993) and will be discusses in more detail in Chapter 1.5.2.

The study areas described in this thesis are located in the southwestern part of the Norwegian Barents Sea. A structural map is provided in Chapter 2, Figure 2.1. Due to the numerous tectonic events in this area it is characterized by several shallow banks, crossed by deep troughs and faults. This led to a complex topographic setting consisting of several basins, highs and platforms,

such as the Loppa High, the Polheim Sub-Platform, the Tromsø Basin or the Hammerfest Basin (Gabrielsen et al., 1990).

The Loppa High, a structural high in the SW Barents Sea, is the main target of the present study. Fault complexes like the Ringvassøy-Loppa Fault Complex (RLFC) and the Bjørnøyrenna Fault Complex (BFC) in the west and the Asterias Fault Complex in the north separate the Loppa High from surrounding basins (Gabrielsen et al., 1990). In the south it borders the Hammerfest Basin, in the western/northwestern part the Bjørnøya Basin. In the eastern/northeastern part it is separated from the Bjarmeland Platform by a monocline (Larssen et al., 2005). The evolution of the Loppa High can be traced back to the Devonian. Subsequently, it passed through several rejuvenation cycles. In its present state the Loppa High is a result of Late Jurassic to Early Cretaceous tectonism (Gabrielsen and Kløvjan, 1997). The Polheim Sub-Platform is a positive, tectonically active element and part of the Loppa High at its western boundary. It was formed during the Late Paleozoic. The western boundary of the Polheim Sub-Platform is defined by the RLFC and BFC, which consist of numerous faults formed during Mid Jurassic to Early Cretaceous and reactivated in the Late Cretaceous (Gabrielsen et al., 1990).

Numerous potential source rock intervals are present in the Barents Sea. In the Norwegian part, the dark, organic rich shales of the Upper Jurassic Hekkingen Formation are described to be the most prolific source (Figure 1.5). Additional source rock potential is described for the underlying Lower Jurassic shales and coals (Tubåen and Nordmela), which are mainly gas prone and the shales of the Upper and Middle Triassic (Kobbe and Snadd Formation). However, the extent of their contribution to the preserved hydrocarbon accumulation in the Barents Sea, especially in the study area, is still under discussion (Doré, 1995). Major hydrocarbon discoveries are located in the Hammerfest Basin including the Albatross, Askeladd and Snøhvit fields, which contain predominantly gas in lower-middle Jurassic sandstones (Doré, 1995). During the last two years the hydrocarbon fields Skrugard and Havis have been discovered. They are located further north, at the northern edge of the Polheim Sub-Platform/Loppa High (Figure 2.1). Each of these fields has been estimated to contain at least 50 million Sm^3 of oil and gas (Maugeri, 2012). Recently, a new oil discovery (well 7120/1-3) was made at the SW edge of the

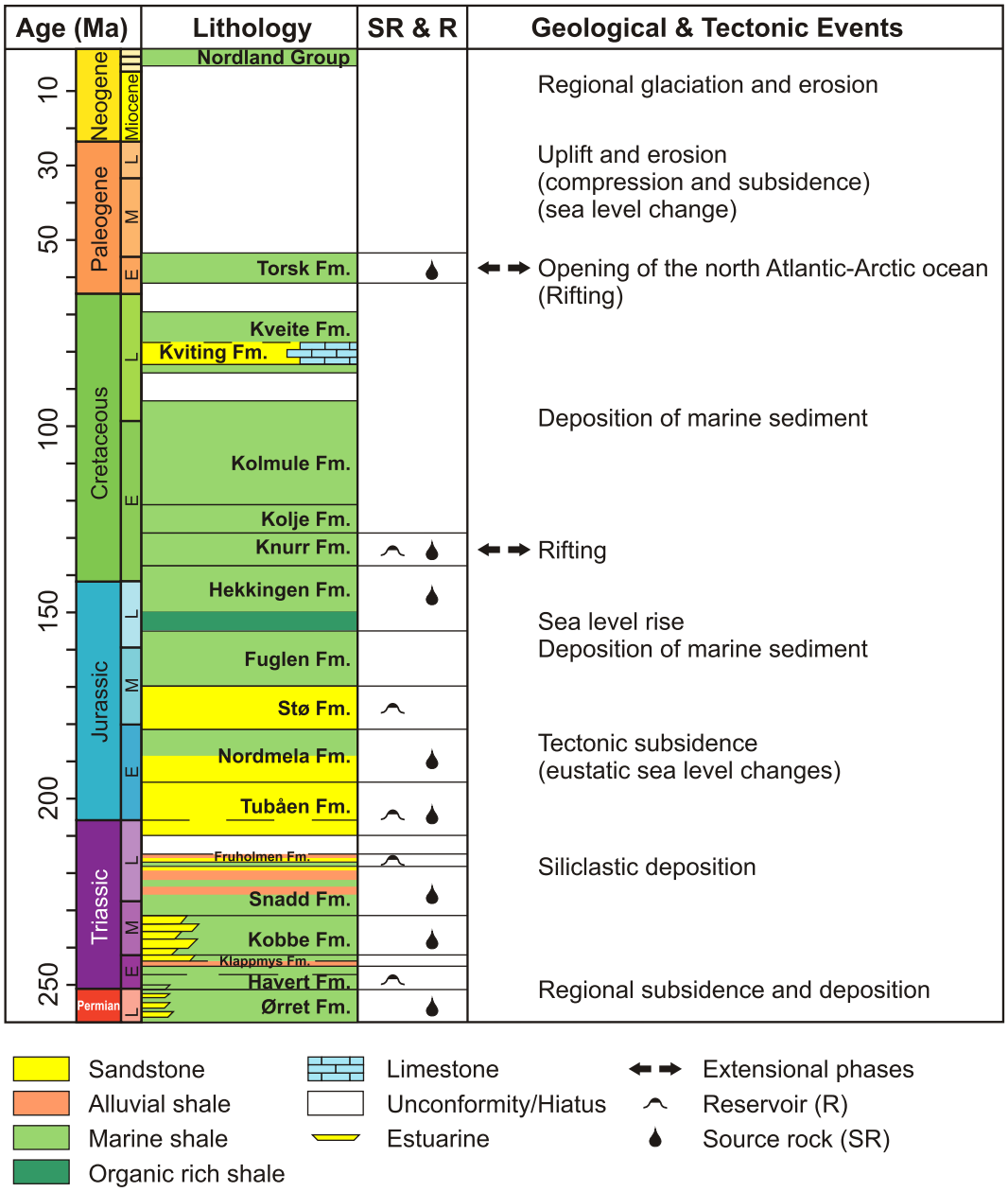

Figure 1.5: Lithostratigraphy of the flanks of the Loppa High and the Hammerfest Basin. Further, the proposed source rocks (SR) and reservoirs (R) as well as the basic elements of the geological and tectonic history of the area are outlined (modified after Rodrigues Duran et al. 2013a).

Loppa High. Preliminary estimations predict 10-23 million Sm^3 of recoverable oil and 8-15 billion Sm^3 of recoverable gas (Norwegian Petroleum Directorate, 2013).

1.5.2 Glacial history

The Barents Sea was affected by many glacial cycles with alternating glaciation and deglaciation. The most important glacial period, however, was the last glacial cycle, the "Weichselian", which lasted from 25 - 13 ka BP. Before this time, during the Arnoya Interstadial about 29 ka BP, most of the southern Barents Sea as well as the coastal areas of northern Norway and Spitsbergen were probably deglaciated (Vorren and Laberg, 1996). During the last glacial maximum (LGM), subsequent to the Arnoya Interstadial, the study area was totally covered by grounded ice (Andreassen et al., 2008; Siegert et al., 2001). During this time the ice sheets reached the shelf break twice (LGM I and LGM II) in the SW Barents Sea. The LGM I occurred at 22 ka BP followed by the Andoya Interstadial (22-19 ka BP) during which large areas of the southern Barents Sea were deglaciated again. The LGM II followed in this area at 20 ka BP (Junttila et al., 2010; Vorren and Laberg, 1996). Ice streams flowing from Bjørnøyrenna and Ingøydjupet were the main contributors to the LGM (Andreassen et al., 2008). A fan-shaped depocenter coming from the accumulation of sediment in front of ice streams can be observed at the trough's mouth in the western part (Vorren and Laberg, 1996). Between 16 and 15 ka BP a warm period caused the thinning of the ice sheets and resulted in deglaciation. A major retreat of the marine-based Barents Sea Ice Sheet took place at about 14.5 ka BP.

Since about 12 ka BP the study area has remained under ice-free conditions. The glacial cycles discussed above are the crucial factors responsible for recent erosion. An additional tectonic event resulted in significant leakage from oil reservoirs during the Oligocene-Miocene (Ohm et al., 2008) whilst the loss of gas can be attributed to glacial erosion events in the recent geologic past (Rodrigues Duran et al., 2013a).

Table 1.1: Numbers of samples and sample types from three different study areas, which were taken during the expedition in November 2009.

	Total	High res PM	High res Ref	Gas anomaly
Area B	150	6	16	-
Area D	16	-	1	2
Area F	47	4	7	-

1.6 Samples and sample processing

1.6.1 Available sample set

In **November 2009** a research and sampling cruise to the Loppa High area, SW Barents Sea was conducted using the R/V HU Sverdrup. The expedition was organized by Lundin Petroleum Norway in cooperation with the Geological Survey of Norway (Norges Geologiske Undersøkelse, NGU), the Norwegian Defense Research Establishment (Forsvarets Forskenings Institutt, FFI), the University of Potsdam and the Helmholtz Centre Potsdam, German Research Centre for Geosciences (GFZ). A Kongsberg Maritime EM710 multibeam echosounder was used to screen the seafloor for seep structures and to create bathymetric maps. Three areas (B, D and F) were sampled during the cruise. Area B and F show pockmark structures on the seabed, area D was of interest due to indications of an underlying gas anomaly which was previously deduced from seismic data (NGU, Lundin).

A total of 213 sediment gravity cores with a maximum length of 2.6 m were taken, both within and outside (as reference) pockmarks. Coring was performed by Fugro N.V.. Gas measurements were conducted on samples from the deepest interval of each core. For high resolution analysis (high res) 36 cores were selected for detailed biogeochemical and geomicrobiological studies. From each high-resolution core ten 10 cm-long whole round cores (WRC), were taken directly on board. The top 50 cm were sampled entirely and the other 5 intervals were spaced over the remaining length of each core. Subsampling was performed by the team of GFZ Potsdam and Potsdam University. Table 1.1 shows the number of cores which were taken in each area.

Table 1.2: Numbers of samples from seven different study sites, which were taken during the expedition in February 2011.

	Total	High res (GFZ)
PM A	6	3
PM B	7	2
PM C	3	1
PM D	3	1
PM F	3	1
Fracture	4	-
Old Well	3	-

In **February 2011** a research and site survey cruise, organized by Lundin Petroleum Norway in cooperation with NGU, FFI and GFZ Potsdam to the Loppa High area, SW Barents Sea was conducted using the R/V HU Sverdrup. Five pockmarks (PM A-D and PM F), 2 reference sites, one location to monitor an old well and samples from a site located above a fracture were taken. In total 33 cores with a maximum length of 1.7 m were gathered. This study was focused only on the pockmark sites. Therefore, 8 pockmark cores were selected for detailed geochemical and geomicrobiological analysis. Again, ten 10 cm-long WRCs were taken directly on board, with the top 50 cm sampled entirely and the other 5 intervals spaced over the remaining length of the core. Subsampling was performed by GFZ staff. Gas measurements were conducted of the deepest interval of each core. Table 1.2 shows the cores which were taken in each area.

The results of the geomicrobiological and organic geochemical analyses are very similar to the data obtained for the samples which were taken during the November 2009 cruise. For this reason they will not be discussed in more detail in this thesis. However, data plots are presented in the Appendix C; tables with the respective data are given in the attached data disc.

In **September 2012** Lundin petroleum Norway conducted a site survey to different areas (PR1-PR5) located in the Loppa High/Polheim Sub-Platform area in the SW Barents Sea on the R/V Fugro Meridian. In total, 12 sediment

Table 1.3: Numbers of samples and sample types from five different study areas, which were taken during the expedition in September 2012.

	Total Cores	Total Crust	Gas samples	High res Cores	Crust GFZ
Area PR1	4	8	3	4	2
Area PR2	only one coral sample				
Area PR3	2	4	/	1	2
Area PR4	4	3	/	3	1
Area PR5	2	4	/	2	/

push cores with a maximum length of 24 cm, 19 carbonate crust samples and 3 gas samples exclusively for gas analysis were taken by a remotely operated vehicle (ROV). Each core was capped, sealed, frozen at -20°C and shipped to GFZ Potsdam for subsampling. Subdivision into 8 intervals was performed on the frozen cores. The frozen cores were entirely sampled into eight depth intervals of two to three cm each. The deepest section of each core was used for gas analysis in the laboratories of Applied Petroleum Technology AS (APT). Table 1.3 shows the samples which were taken in each area.

1.6.2 Applied methods

A wide spectrum of different methods has been applied in the context of the present study to achieve a detailed characterization of the study site and its cold seep systems. In order to give an overview on the interaction of the applied techniques, each method is discussed briefly in this chapter (Figure 1.6). The reader is referred to the method descriptions in the individual papers that constitute separate chapters of this thesis for details.

1. Bathymetry was used to gain a basic understanding of the seabed surface topography and to select the sample targets. A multibeam eco sounder, mounted on the research vessel, transmits a broad acoustic fan shaped pulse was used. According to the shape of the seabed's surface the acoustic beams are reflected. The received data can be used to calculate and create a topographic map of the seabed. Bathymetry maps have been kindly provided by Lundin Petroleum Norway.

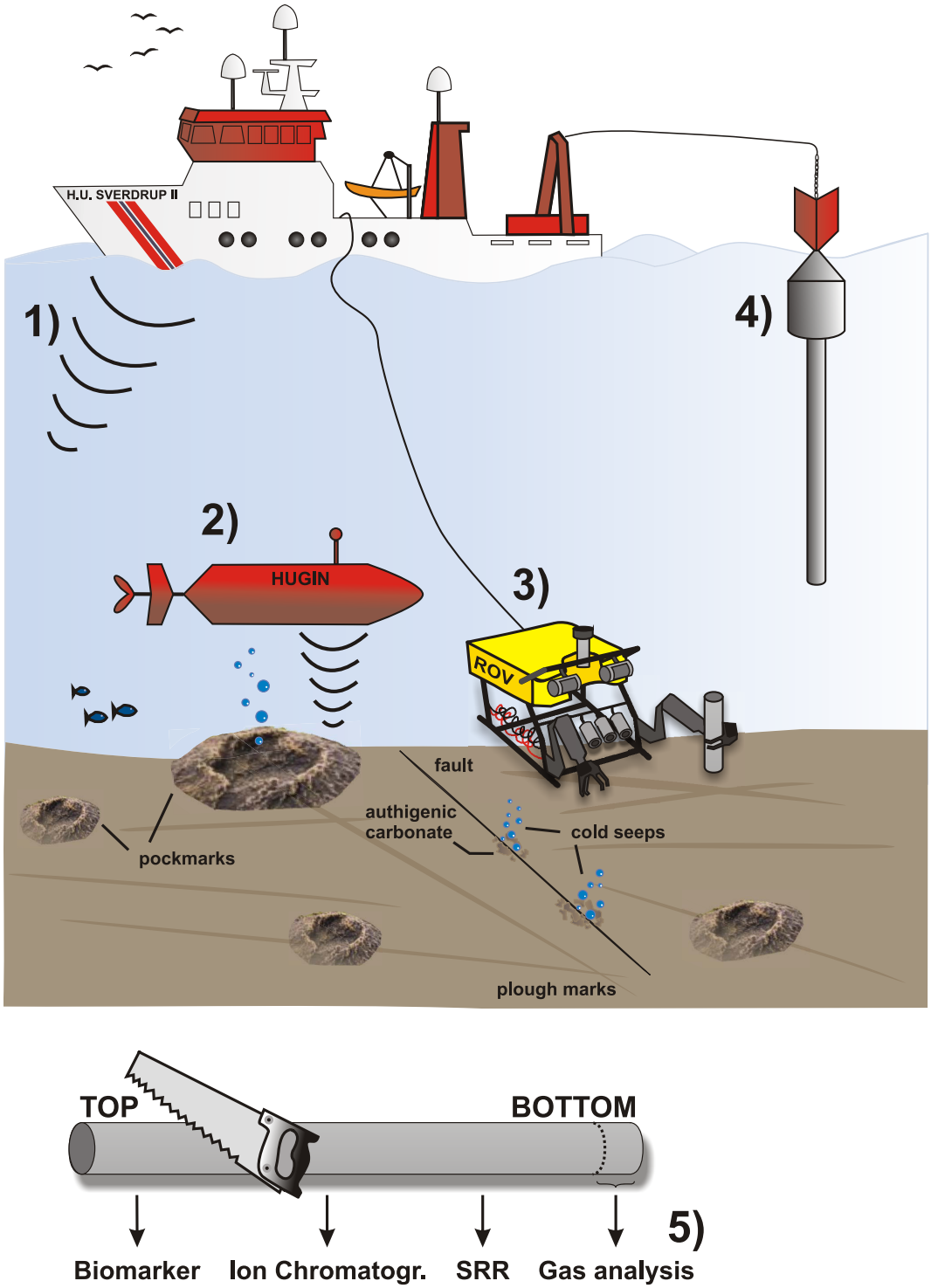

Figure 1.6: Schematic illustration of the methods applied during the different sampling campaigns. The numbers refer to the numeration in Chapter 1.6.2.

2. An autonomous underwater vehicle “Hugin” was used for high-resolution seabed mapping and visual inspection of selected areas. Side scan sonar as well as a still image camera were used. The Hugin was operated by the Norwegian Defense Research Establishment (FFI).

3. A remotely operated vehicle (ROV) was applied at the carbonate crust sites. The installed camera enabled the monitoring of the seep-associated fauna as well as to choose specific sample locations. The remotely operated robotic arm was used for targeted sampling of carbonate crust as well as for taking short push cores. The ROV was operated by Abyss International.

4. Gravity cores of a maximum length of 2.6 m were taken by Fugro and FFI. Sectioning into 10 cm subsamples was done by the teams of GFZ Potsdam, University of Potsdam and Lundin Petroleum Norway immediately after retrieval of the cores.

5. The deepest sample of each core was used for gas analysis of the C_1-C_8 hydrocarbons. The sediment was stored in sealed cans from which the concentration of free, occluded and absorbed gas could be directly determined in the laboratory. Gas measurements were performed by Geolab Nor AS.

6. The subsampling was designed according to the analyses planned within the respective cruise. Generally the core was split into several depth intervals by a regular handsaw. To avoid contamination the outer core material was scraped off. Subsequently, several subsamples were taken, e.g.,

   (a) “Organic geochemistry” samples for biomarker analysis

   (b) “Pore water samples” to analyze the ion inventory as well as sediment density and porosity

   Sampling was performed by the GFZ Potsdam staff.

1.6.3 Additional available background data

Bathymetry data was kindly provided by Lundin Petroleum Norway and was used to identify core locations and assign sample types. Seismic data was available upon request for certain coordinates to explain or support the findings based on geochemical/microbiological work. Since seismic interpretation was not within the scope of this study, the sporadic use of seismic data was limited to information on certain coordinates that were provided by Ilya Ostanin (GFZ Potsdam) or Harald Brunstad (Lundin Petroleum Norway) as part of an internal cooperation. Additionally, the data obtained within this study was brought into the framework of a basin model which was performed by Enmanuel Rodrigues Duran (GFZ Potsdam) in the same study area Rodrigues Duran et al. (2013a,b).

1.6.4 Software

GC-MS analysis and GC-MS data evaluation was performed using the software Xcalibur (Thermo Electron Cooperation). The GC-FID data was analyzed using the software Chem Station (Agilent Technologies) and for GC-IR-MS the program Isodat (Thermo Scientific) was used. Ion chromatography analysis was performed using the software ChromStar (Sykam).

All calculations were performed with Microsoft Excel. Graphs and figures were developed using Microsoft Excel, Grapher 6 and CorelDRAW 14. Chemical structures were designed using the freeware software ChemSketch.

This thesis was layouted with LaTeX using MiKTeX 2.9 and the TeXnicCenter 2.0 editor.

Chapter 2

Characterization of microbial activity in pockmark fields of the SW Barents Sea

2.1 Abstract

Multibeam bathymetry revealed the occurrence of numerous craterlike depressions, so-called pockmarks, on the sea floor of the Hammerfest Basin and the Loppa High, south-western Barents Sea. To investigate whether these pockmarks are related to ongoing gas seepage, microbial processes associated with methane metabolism were analyzed using geochemical, biogeochemical and microbiological techniques. Gravity cores were collected along transects crossing individual pockmarks, allowing a direct comparison between different locations inside (assumed activity center), on the rim, and outside of a pockmark (reference sites). Concentrations of hydrocarbons in the sediment, particularly methane, were measured as headspace (free) gas, and in the occluded and adsorbed gas fraction. Down to a depth of 2.6 m below sea floor (mbsf) sulfate reduction rates were quantified by radiotracer incubations. Concentrations of dissolved sulfate in the porewater were determined as well. Neither the sulfate profiles nor the gas measurements show any evidence of microbial activity or active fluid venting. Methane concentrations and sulfate reduction rates were

This chapter has been published as: J. C. Nickel, R. di Primio, K. Mangelsdorf, D. Stoddart & J. Kallmeyer, 2012, Characterization of microbial activity in pockmark fields of the SW Barents Sea: Marine Geology, v. 332-334, p. 152-162.

extremely low or even below the detection limit. The results show that the observed sediment structures are most likely paleo-pockmarks, their formation probably occurred during the last deglaciation.

2.2 Introduction

Pockmarks are craterlike depressions in the seabed that form due to expulsion of fluids (Hovland and Judd, 1988). Fluids can be aqueous liquids like porewater (Harrington, 1985; Whiticar, 2002) but many published examples indicate formation by seeping hydrocarbons, especially methane, which can be of biogenic (Vaular et al., 2010) or thermogenic origin (Solheim and Elverhøi, 1985; Gay et al., 2006).

Pockmarks were first discovered in the late 1960s in Nova Scotia (King and MacLean, 1970), since then they have been observed globally in many different geologic settings, e.g. lakes, continental slopes, shelves and rises, shallow bays, fjords, as well as in the deep sea (Hovland and Judd, 1988; Judd and Hovland, 2007). They occur in different shapes e.g. as circular craters or as non-circular, elongated forms (Hovland et al., 2002). Sizes generally range from 10 to 200 m with depths up to 35 m, but also giant pockmarks with diameters of up to 1 km or more have been reported (Cole et al., 2000; Ondréas et al., 2005). Pockmarks can appear as single features (Prior et al., 1989) or in aggregations of hundreds of pockmarks, extending over tens of square kilometers (Lammers et al., 1995).

Hovland and Judd (1988) proposed a general model for pockmark evolution. Gas from greater depth migrates upwards through the sediment towards the seabed where it accumulates and causes doming. Stretching of the seabed causes small tensional fractures. Gas migrating along routes towards those fractures establishes a hydraulic connection, which results in a pressure drop followed by a violent burst. A unit pockmark is formed. Clusters of unit pockmarks can coalesce to a normal pockmark. A model by Woolsey et al. (1975) simulating "diatreme emplacements by fluidization" supports this theory. Recently, Cathles et al. (2010) came up with a conceptual model of pockmark and gas chimney formation. They assume that there is a capillary seal which traps the gas in the deeper sediment. Gas accumulation leads to overpressure and seal failure and an upward migrating gas diapir forms. With gas approaching

the seabed, the sediment becomes fluidized and is removed, pockmarks begin to develop.

Pockmark formation is often associated with tectonic or sedimentary features such as faults or buried channels (Chand et al., 2008). It can be controlled by underlying bedrock and lithological boundaries (Forwick et al., 2009), but can also be triggered by extreme events like earthquakes and tsunamis, melting of grounded icebergs or even by human influence (Hovland et al., 2002).

There are only few examples in which active fluid or gas flux could be observed. However, active pockmarks have been found all over the world (Solheim and Elverhøi, 1985; Lammers et al., 1995; Ondréas et al., 2005; Gay et al., 2007) but also inactive, dormant pockmarks (Hovland and Judd, 1988; Ussler et al., 2003; Webb et al., 2009), even entire inactive pockmark fields (Solheim and Elverhøi, 1993; Paull et al., 2002) and buried paleo-pockmarks, discovered by 3D seismic data (Cole et al., 2000; Hartwig et al., 2012), have been described.

Leakage of hydrocarbons through pockmarks infers that there is a gas source in the underlying sediment. As potential indicators for deeper hydrocarbon reservoirs, pockmarks received considerable interest from the hydrocarbon exploration industry (Hovland and Judd, 1988; Hasiotis et al., 2002).

Submarine hydrocarbon seeps, such as pockmarks or mud volcanoes, are habitats for specific microbial communities. Epifaunal and bacterial aggregations like thiotrophic bacterial mats associated with these structures are widely described in the literature (Niemann et al., 2006; Foucher et al., 2009) and provide evidence of ongoing nutrient provision and metabolization. Pockmarks also play an important role in the global methane cycle. Methane coming from a source at greater depth can be released to the overlying ocean and even partly to the atmosphere (Lammers et al., 1995; Reeburgh, 2007; O'Connor et al., 2010), effectively bypassing the zone of anaerobic oxidation of methane, which normally prevents any methane escape from sediments.

In subsurface sediments microbial activity dominates, with dissimilatory sulfate reduction as the quantitatively most important electron acceptor process in the anaerobic degradation of organic matter (Jørgensen, 1982; D'Hondt et al., 2002). Thus, determination of sulfate reduction rates provides a reasonably good estimate of total microbial activity in anoxic marine sediments.

According to the carbon source used, sulfate reduction (SR) can be divided into two main pathways.

Organiclastic sulfate reduction takes place in the upper part of the sediment close to the sediment-water interface. It is fuelled by small organic molecules like fatty acids, derived from the degradation of organic matter. The organic matter is oxidized by dissolved sulfate, which is in turn reduced to hydrogen sulfide (Martens and Berner, 1974; Jørgensen, 1982), according to Equation (2.1).

$$2\,CH_2O + SO_4^{2-} \longrightarrow 2\,HCO_3^- + H_2S \tag{2.1}$$

Methanotrophic SR, also known as anaerobic oxidation of methane (AOM), occurs below the zone of organiclastic sulfate reduction in a narrow band where there is an overlap of dissolved sulfate and methane (Martens and Berner, 1974; Iversen and Jørgensen, 1985), the so-called sulfate-methane transition zone (SMTZ). The reduction of sulfate to sulfide is facilitated by the oxidation of methane to bicarbonate (Equation (2.2)).

$$CH_4 + SO_4^{2-} \longrightarrow HCO_3^- + H_2S + H_2O \tag{2.2}$$

A consortium of archaea and sulfate-reducing bacteria (SRB) has been reported to facilitate the anaerobic oxidation of methane with sulfate as an electron acceptor (Boetius et al., 2000; Orphan et al., 2001b). Recently, other electron acceptors have been identified, e.g. Nitrate (Raghoebarsing et al., 2006).

Below the SMTZ sulfate is usually not detectable in the porewater, some very minor concentrations (single to tens of μM) are usually attributed to reoxidation of hydrogen sulfide during sample processing. However, molecular studies could identify sulfate reducing microbes below the SMTZ (Schippers et al., 2010), even in the zone of active methanogenesis (Leloup et al., 2007).

In this study, three areas in the southwestern Barents Sea were investigated (Figure 2.1). Two of these areas (areas B and F) are part of a large field of many small depressions in the seabed (Figure 2.2), which were identified as pockmarks. The third area (area D) does not contain any pockmark features but was chosen for further investigations due to an assumed underlying gas anomaly, as interpreted from seismic data. Since pockmarks could be valuable

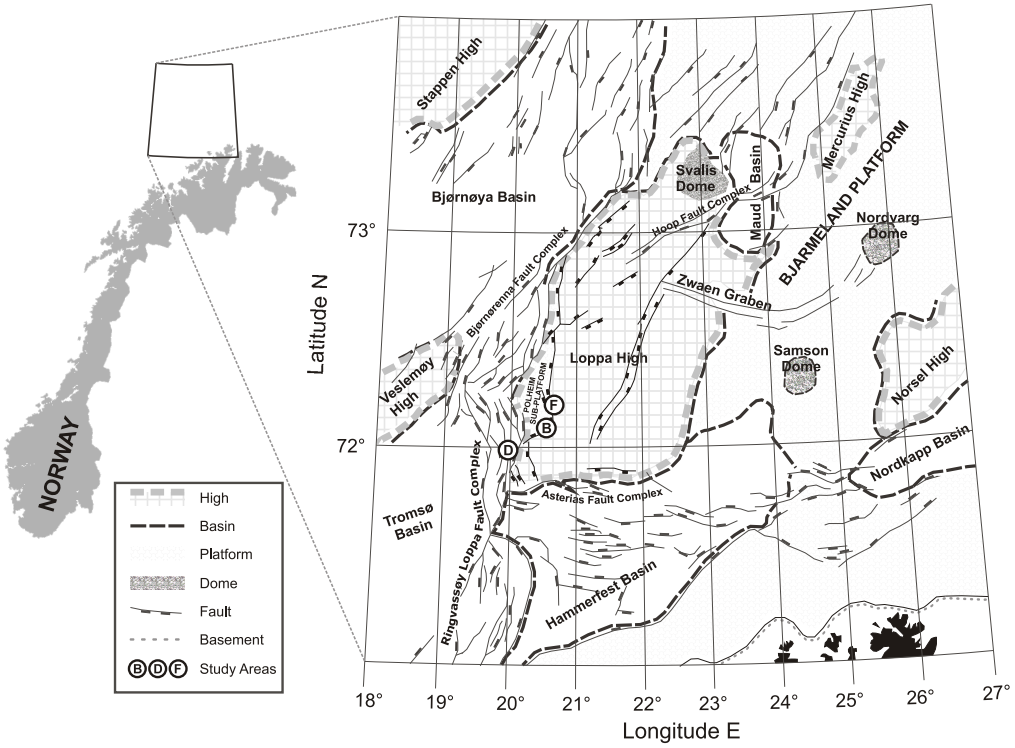

Figure 2.1: Tectonic framework of the sampling areas, southwestern Barents Sea (after Gabrielsen et al. 1990 and Nyland et al. 1992).

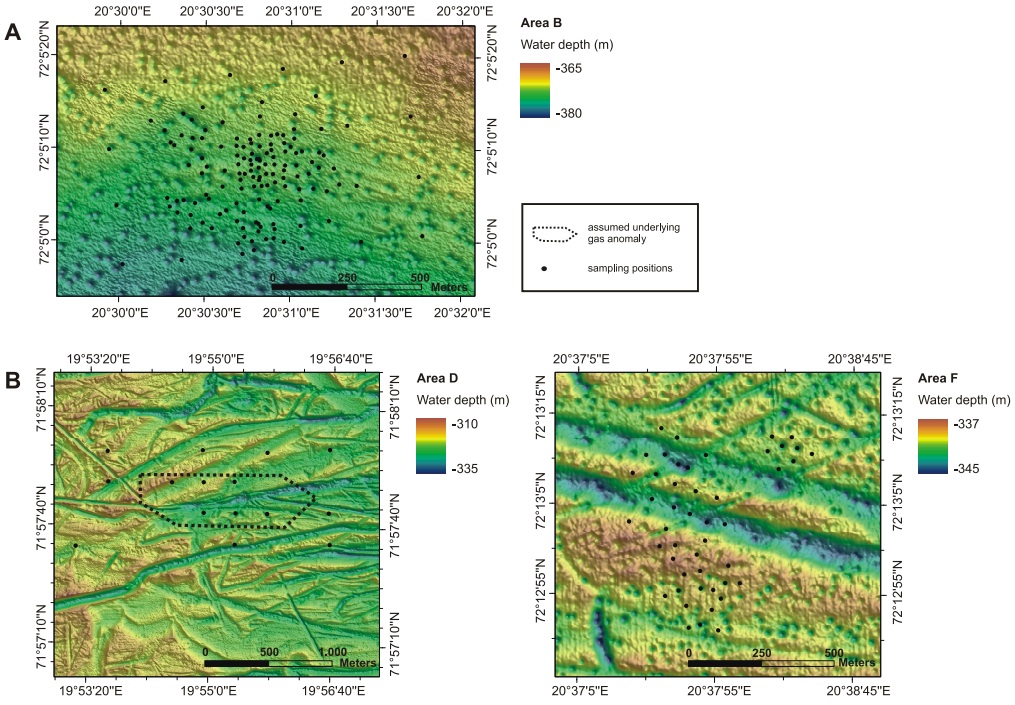

Figure 2.2: Bathymetric map of the three sampling sites in the Loppa High area, southwestern Barents Sea derived from EM 710 echosounder system. The coring positions are indicated by black dots on the map.

indicators for deeper hydrocarbon reservoirs, we investigated whether these pockmarks are related to ongoing gas seepage or if they are manifestations of a past event. About 200 sediment gravity cores were collected and analyzed. A combined study of gas measurements, quantification of geochemical parameters and microbial activity was conducted to obtain a better understanding about ongoing processes in and around the pockmarks and to reveal their formation history.

2.3 Geological setting

The Barents Sea is a deep epicontinental sea, which borders to the Norwegian Sea in the southwest and to the Arctic Ocean in the north. It is characterized by several shallow banks and is crossed by deep troughs and faults (Figure 2.1). The investigated area is located between the southwestern part of the Loppa High, comprising the Polheim Sub-Platform, and the Ringvassøy-Loppa Fault complex and defined by a square with SW and NE coordinates 72°13'N, 20°38'E and 71°57'N, 19°53'E (Figure 2.1).

The Loppa High is a structural high near the south-western margin of the Norwegian Barents Sea. Fault complexes separate the Loppa High from the Hammerfest Basin in the southern and the Bjørnøya Basin in the western part. In the south-east it passes into the Hammerfest Basin and the Bjarmeland Platform, separated by a monocline.

The area has undergone a complex geological history, characterized by several phases of uplift/subsidence and subsequent tilting and erosion (Larssen et al., 2005), whereby the Loppa High is a result of Late Jurassic to Early Cretaceous tectonism (Gabrielsen et al., 1990). According to Eidvin et al. (1993) and Cavanagh et al. (2006) the latest erosion phase is linked to the glacial period.

During the Last Glacial Maximum (LGM) the study area was totally covered by grounded ice (Siegert et al., 2001; Andreassen et al., 2008). During that time the ice sheets reached the shelf break twice (LGM I and LGM II) in the SW Barents Sea. LGM I occurred at 19 ka followed by the Andoya Interstadial which commenced with a high arctic climate after which middle to low arctic climate prevailed. Large areas of the southern Barents Sea were deglaciated again. At 18 ka the LGM II occurred in this area (Vorren and Laberg, 1996;

Junttila et al., 2010). Between 16 and 15 ka a warm spell caused the thinning of the ice sheets, triggering a major deglaciation. A major drawdown of the marine-based Barents Sea Ice Sheet occurred around 14.5 ka. As of roughly 12 ka the study area was totally free of ice.

2.4 Samples and methods

2.4.1 Acoustic survey and sampling

In 2009 the Forsvarets Forskenings Institutt (FFI) conducted a multibeam bathymetric survey of the Hammerfest/Loppa High and the Tromsø Basin/ Ingøydjupet area of the western Barents Sea region, using an EM 710 echo-sounder system, with a medium frequency of 70-100 kHz. During a cruise in November 2009 on R/V HU Sverdrup to the Loppa High about 200 sediment gravity cores with a maximum length of 2.6 m were taken in three different areas (B, D, F).Topographic seafloor maps of the three investigated areas (B, D, F) showing the exact sample locations are given in Figure 2.2. To map the general gas distribution within each area, between 15 and 115 cores were taken for gas analysis. Due to the massive amount of cores for gas analysis, samples were only taken from the deepest part of each core. Two sediment samples of *ca.* 500 cm^3 each were taken and immediately transferred into gas-tight metal cans and stored at -80°C until analysis after the cruise.

A total of 35 cores (exact locations are given in Table 2.1) were selected for detailed microbiological and geochemical studies. Each of these cores was sampled in ten depth intervals directly on board. To avoid contamination from shallower sediment being dragged down during penetration of the core, the exterior of the material was shaved off prior to subsampling.

Sampling for sulfate reduction rate (SRR) incubation experiments was carried out by inserting 5-mL tip-cut plastic syringes into the sediment, thereby retrieving small subcores with an intact sedimentary structure. After retrieval of the subcore, the open end was closed with a butyl rubber stopper and the syringes stored in N_2-flushed gas-tight bags in a refrigerator close to in-situ temperature (+5°C). Usually this type of incubation is carried out in gas-tight glass barrels. Unfortunately our glass barrels got lost during transport, so we had to revert to plastic syringes. Although plastic syringes are less than

Table 2.1: Samples in the SW Barents Sea, investigated in the present study. PM: pockmark.

ID	Area	Type	Latitude	Longitude	Water Depth (m)
LU75	B	reference	72° 5' 2.52" N	20° 30' 42.76" E	375.45
LU76	B	reference	72° 5' 2.66" N	20° 30' 41.96" E	375.34
LU77	B	reference	72° 5' 2.17" N	20° 30' 43.53" E	376.00
LU78	B	reference	72° 5' 10.14" N	20° 30' 45.48" E	374.40
LU81	B	PM rim	72° 5' 10.07" N	20° 30' 40.30" E	374.51
LU84	B	reference	72° 5' 8.93" N	20° 30' 45.01" E	374.40
LU88	B	reference	72° 5' 8.89" N	20° 30' 40.13" E	374.98
LU104	B	reference	72° 5' 7.55" N	20° 30' 43.10" E	374.20
LU105	B	PM rim	72° 5' 10.85" N	20° 30' 43.01" E	375.17
LU111	B	reference	72° 5' 9.72" N	20° 30' 47.82" E	374.98
LU137	B	reference	72° 5' 3.51" N	20° 30' 29.25" E	376.28
LU151	B	reference	72° 5' 5.07" N	20° 30' 57.56" E	375.94
LU175	B	reference	72° 5' 2.58" N	20° 30' 23.19" E	377.00
LU182	B	reference	72° 5' 9.22" N	20° 31' 1.41" E	374.21
LU185	B	PM	72° 5' 6.34" N	20° 31' 1.94" E	374.82
LU294	B	reference	72° 5' 9.56" N	20° 30' 37.53" E	374.16
LU400	B	PM	72° 5' 9.4980" N	20° 30' 42.89" E	374.98
LU401	B	PM	72° 5' 9.4994" N	20° 30' 42.04" E	374.78
LU402	B	PM	72° 5' 9.33" N	20° 30' 43.09" E	374.30
LU420	B	reference	72° 5' 10.82" N	20° 30' 29.46" E	373.57
LU429	B	PM	72° 5' 9.54" N	20° 30' 22.81" E	374.71
LU450	B	PM	72° 5' 9.49" N	20° 30' 42.48" E	374.51
LU252	D	reference	71° 57' 36.41" N	19° 56' 31.95" E	321.78
LU258	D	gas anomaly	71° 57' 44.05" N	19° 55' 14.40" E	322.80
LU266	D	gas anomaly	71° 57' 51.83" N	19° 54' 47.83" E	320.00
LU301	F	reference	72° 13' 11.08" N	20° 37' 45.27" E	342.49
LU302	F	reference	72° 13' 13.00" N	20° 37' 34.77" E	341.42
LU306	F	reference	72° 13' 7.84" N	20° 37' 34.06" E	339.67
LU319	F	reference	72° 12' 58.82" N	20° 37' 53.63" E	338.57
LU320	F	reference	72° 12' 56.88" N	20° 37' 57.82" E	339.57
LU321	F	reference	72° 12' 56.11" N	20° 37' 48.18" E	340.52
LU330	F	PM rim	72° 13' 9.66" N	20° 37' 38.73" E	343.67
LU331	F	PM	72° 13' 10.03" N	20° 37' 35.22" E	343.71
LU332	F	reference	72° 13' 11.11" N	20° 37' 30.34" E	343.42
LU338	F	PM	72° 12' 56.89" N	20° 37' 52.54" E	339.43
LU341	F	PM	72° 12' 55.16" N	20° 37' 50.98" E	339.89

perfect for incubating SRR samples because of their permeability for gasses, in this case the potential bias should be minimal because there is basically no methane in the sample which could potentially be lost. Changes in pH due to loss of CO_2 can also be neglected because the porewater is well-buffered with regard to its carbonate system. An aliquot of the sediment was frozen at -20°C in N_2-flushed gas-tight bags for porewater extraction after the cruise.

2.4.2 Sulfate reduction rates

Sulfate reduction rates were determined using a modification of the whole core $^{35}SO_4^{2-}$ injection method (Jørgensen, 1978) as described by Ferdelman et al. (1999) and Treude et al. (2005b). All incubations were performed in duplicates.

4 μL of carrier-free $^{35}SO_4^{2-}$ (180 kBq/μL) were injected along the longitudinal axis of the subcore. The incubations were conducted for 24 h and terminated by transferring the radiolabeled sediment into 10 mL of 20% (w/v) zinc acetate (ZnAc). Blank samples were prepared by injecting $^{35}SO_4^{2-}$ radiotracer into a sample, followed by immediate transfer into 20% (w/v) zinc acetate. Additionally, tracer blanks were prepared by adding 4 μl of radiotracer directly into ZnAc without any sediment. The total reduced inorganic sulfur (TRIS) compounds (mono- and disulfides, elemental sulfur) were separated using the cold chromium distillation method (Kallmeyer et al., 2004). Radioactivity was quantified using a Perkin Elmer Tri Carb 2800 TR liquid scintillation analyzer and Perkin Elmer Ultima Gold XR Scintillation cocktail. SRRs were calculated using the following equation (Jørgensen, 1978; Kallmeyer et al., 2004):

$$SRR = \frac{\alpha_{TRIS}}{\alpha_{TOT}} \times \frac{[SO_4^{2-}]}{t} \times \rho_{SED} \times 1.06 \times 1000000 \qquad (2.3)$$

where α_{TRIS} and α_{TOT} are the activities of the TRIS compounds and the total activity of the injected $^{35}SO_4^{2-}$, respectively, using the raw counts (given as counts per minute, cpm) from the scintillation counter; t is the incubation time and ρ_{SED} the porosity of the sediment (mL porewater cm^{-3} sediment). SO_4^{2-} is seawater SO_4^{2-} concentration, which was set to 28 mM for all samples, because there was no measurable down-core depletion of porewater SO_4^{2-} concentrations in any of our samples. 1.06 is a correction factor for the expected

isotopic fractionation (Jørgensen and Fenchel, 1974), 1,000,000 is the factor to change units from mmol L^{-1} to pmol cm^{-3}.

2.4.3 Determination of gas concentrations

GeolabNor (Trondheim, Norway) quantified C_1-C_6 hydrocarbons in the headspace (free) and occluded gas fraction as well as C_1-C_8 hydrocarbons in the adsorbed gas fraction, using gas chromatography. Headspace gas was determined by thawing the frozen samples over night with subsequent analysis of the free gas in the headspace of the container. Occluded gas was released mechanically from an aliquot of the sediment using a ball mill under vigorous shaking. Treatment of an aliquot of sediment with orthophosphoric acid led to the detachment of the gas adsorbed to clay minerals. All values are shown in the unit μmol L^{-1} sediment (μM). Interpolated gas distribution maps were generated based on the obtained gas data.

2.4.4 Porewater sulfate concentration

Sediment porewater was obtained by centrifugation and careful decantation followed by filtration through a 0.2 μm membrane. Porewater sulfate concentrations were determined by suppressed ion chromatography using a SYKAM IC-System (injection volume 50 μL, anion exchange column, SYKAM LCA A14; conductivity detector, SYKAM S3115).The elutant was a 6.25 mM sodium carbonate solution with 0.1% (v/v) modifier (1 mL 4-hydroxy-benzonitrile in 50 mL methanol), the flow rate was 1 mL min^{-1}.

2.5 Results

2.5.1 Morphology of seabed

The morphology of the seabed in our study areas is shown in Figure 2.2. Multibeam bathymetry revealed the presence of a multitude of circular seafloor depressions interpreted as pockmarks. Area B and F contain an average density of 100 pockmarks per square kilometer, either randomly distributed or in arrays along iceberg plough marks, which are the result of former iceberg activity, formed primarily during glacial retreat (Solheim, 1991). The up to 15 m deep plough marks can be observed all over the seabed surface.

The circular pockmarks are between 10 and 50 m in diameter with an average depth of about 1-3 m. According to Hovland and Judd (1988); Hovland et al. (2002) these pockmarks can be termed "normal pockmarks". Additionally, some larger, irregular pockmarks with diameters of up to 300 m and depths up to 25 m were observed. As mentioned before, area D does not contain any pockmark features, but, like in area B and F, many plough marks could be seen on the seabed of area D.

2.5.2 Samples

The average water depth in the investigated area was found to be around 350 m with an average water temperature of about 6°C. Sediment composition appeared to be very similar in all three areas, being brown to dark brown in color. Except for the first 10 cm which were softer, porosity averaged around 0.52 throughout the entire length of the core.

In general the cores consisted of very sticky silty clay, occasionally containing some less dense structures like small pieces of siliceous sponges as well as pebbles or fragments of bivalve shells. There was no difference between sediment from within or outside the pockmarks. No hydrogen sulfide smell was noticed in any core nor were there any obvious authigenic carbonate structures.

In area D the penetration depth of the gravity corer was relatively small (average penetration depth of 50 cm). The sediment material above the anomaly structure consisted of very sticky mud preventing a deeper penetration.

2.5.3 Gas concentrations

Concentrations of hydrocarbons (methane and higher *n*-alkanes, cyclic and branched hydrocarbons) in the headspace (free), occluded, and adsorbed gas fraction were determined on samples from the deepest interval of the core (maximum depth 2.6 mbsf). Interpolated gas distribution maps were created to show the distribution of hydrocarbons in the three study areas. All maps show extremely low concentrations and do not reveal any correlation between gas concentration and sampling sites (pockmark or reference site). The following discussion is focused just on adsorbed methane, since this fraction exhibited highest concentrations. In the occluded and free gas fraction only marginal amounts could be found, concentrations of longer chain hydrocarbons were also negligibly low.

Table 2.2: Minimum (Min), maximum (Max) and average (Av.) values of adsorbed and free methane in the three sampling areas. Values are given in μmol L^{-1} (sediment).

Area		**Ads. Methane** μM	**Free Methane** μM
B	Min	0.87	0.047
	Max	**29.08**	**0.200**
	Av. PM	6.19	0.125
	Av. Ref	5.93	0.118
D	Min	2.93	0.072
	Max	**16.84**	**0.145**
	Av.	5.42	0.106
F	Min	1.13	0.054
	Max	**19.18**	**0.202**
	Av. PM	6.63	0.116
	Av. Ref	5.78	0.116

Table 2.2 summarizes some statistic values for the adsorbed methane and free methane fraction of the three study areas. Figure 2.3 shows exemplarily the distribution of adsorbed methane in area B. In area B the highest methane concentration in the adsorbed gas fraction was 29.1 μM. Average values were only 6.19 μM in the pockmark cores and 5.93 μM in reference cores (Table 2.2, Figure 2.3).

In area D the maximum concentration of adsorbed methane was 16.84 μM, with an average value of 5.42 μM. In area F concentrations of adsorbed methane reached a maximum value of 19.18 μM, the average values for the pockmark samples 6.63 μM and for the reference samples 5.78 μM. There are some local maxima in gas concentration in all three areas, but even these anomalies are still very low and they do not generally correlate to pockmarks. Due to the very low gas concentrations no isotope measurements could be carried out. Consequently it remains unknown whether the gas is coming from a biogenic or thermogenic source.

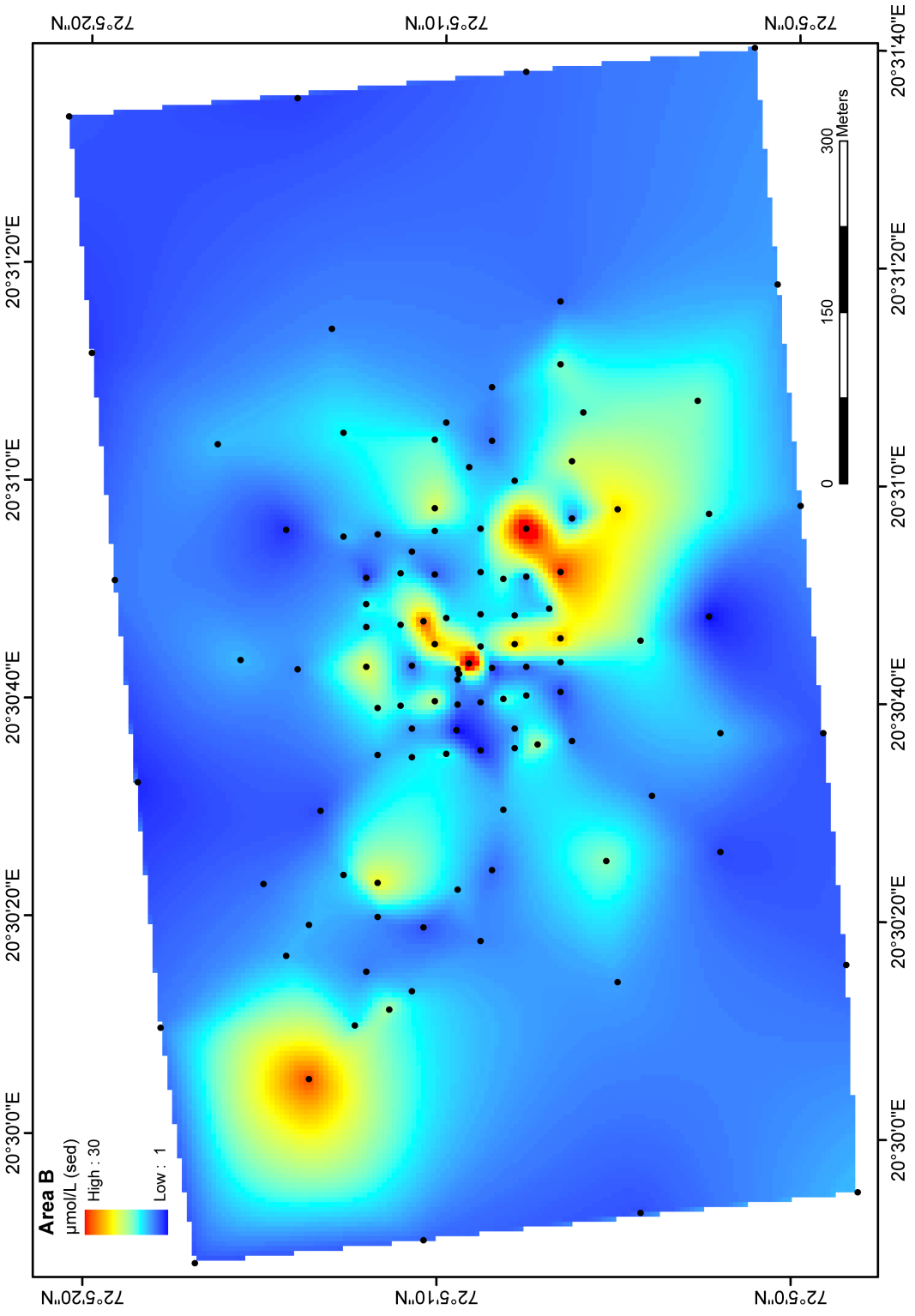

Figure 2.3: Interpolated gas distribution maps of methane (C_1-HCs) for area B, given as an example of the three sampling areas. Sediment samples for gas analysis were taken from the deepest section of the core. The core positions are indicated by black dots on the map. Gas concentrations are extremely low and do not show any correlation with pockmarks.

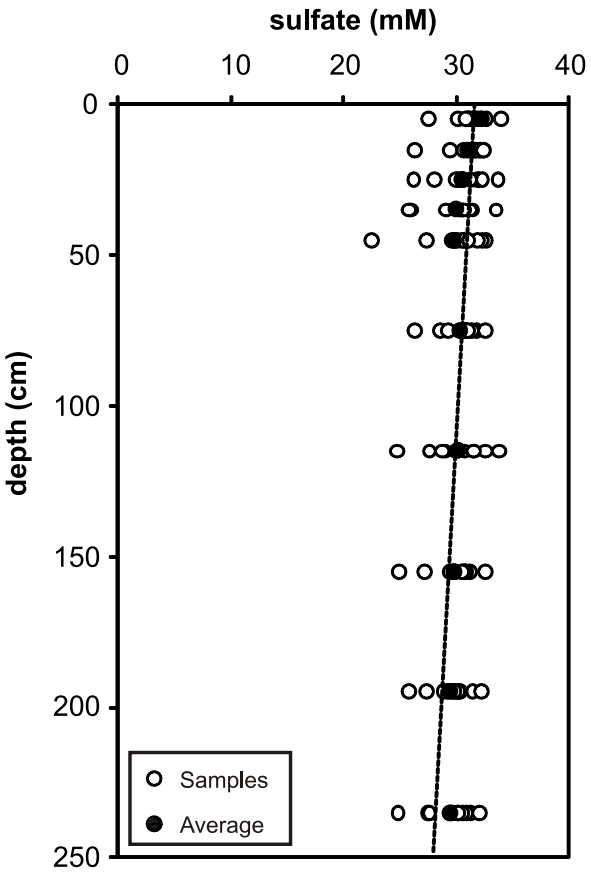

Figure 2.4: Porewater profiles of dissolved sulfate in the upper 240 cmbsf of 12 different sediment cores taken in areas B and F (open symbols). The closed symbols show the average values which were calculated for each depth interval.

2.5.4 Sulfate profiles

On 12 cores porewater sulfate concentrations were determined in 10 depth intervals between 0 and 240 cm. The profiles show very little variation with depth and among each other (Figure 2.4). The almost linear profiles and the only minimal decrease with depth indicate very low net sulfate consumption. When extrapolating linearly, the calculated SO_4^{2-} penetration depth is 37 m, a value that is more common for oligotrophic open ocean sites, not for ocean margins. For gas rich sediments, this value normally ranges between 0.02 and 0.2 m (Luff and Wallmann, 2003; Treude et al., 2005a).

2.5.5 Sulfate reduction rate

Exemplary SRR depth profiles for pockmark and reference sites in area B are presented in Figure 2.5A to D. Irrespective of pockmark or reference site, most of the sulfate reduction activity was restricted to the upper 30 cm of the sediment (Figures 2.5A and B). In this depth interval the highest observed SRR was 600 pmol cm^{-3} d^{-1}. Deeper than 30 cm below the sea floor

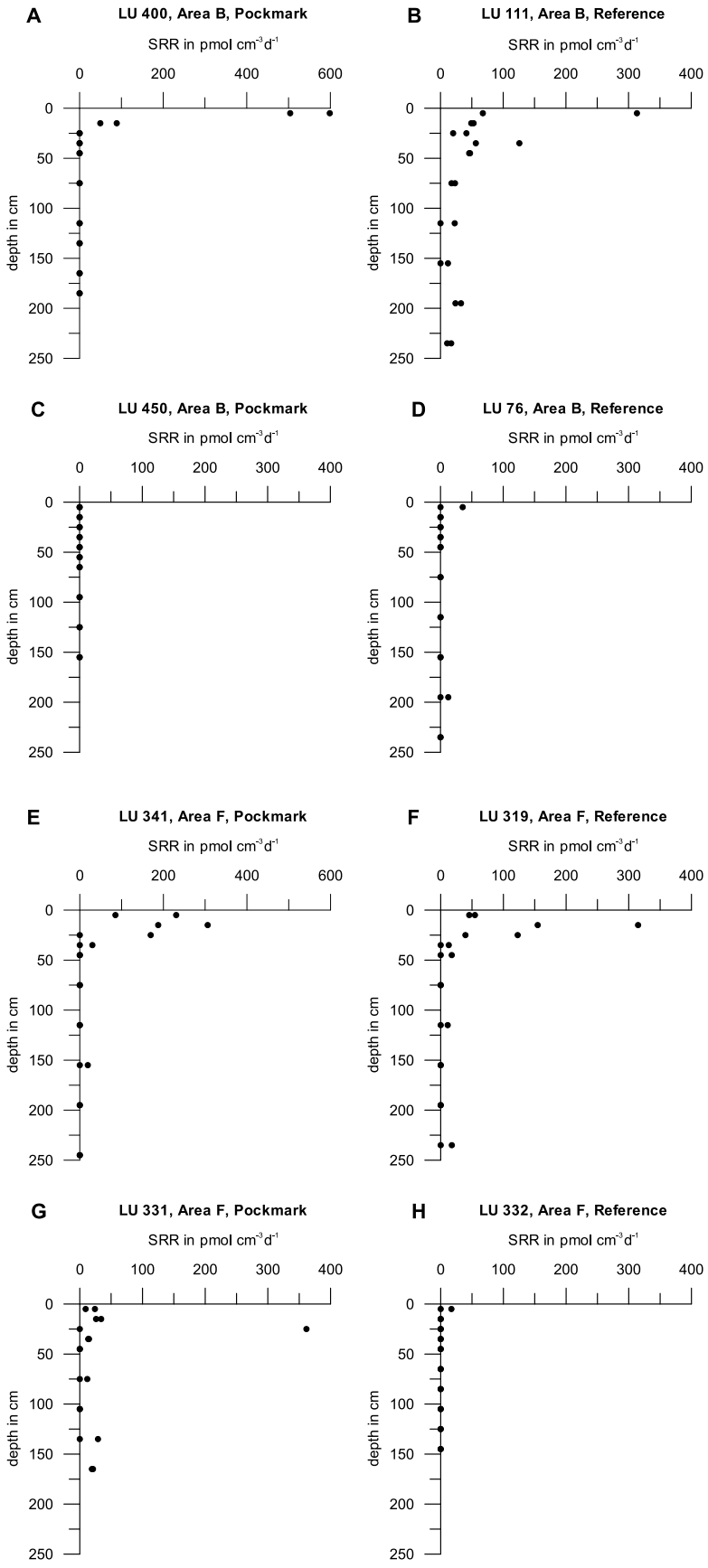

Figure 2.5: Profiles of sulfate reduction rates (SRR) of selected cores from area B and F in the upper 240 cm of the sediments. For each area both profiles from pockmark sites and reference sites are shown for comparison. Irrespective of the location of the core (pockmark or reference site), most of the sulfate reduction activity was restricted to the upper 30 cm of the sediment.

(cmbsf) measurements fell mostly below the minimum detection limit (MDL) of 10 pmol cm^{-3} d^{-1} (Figure 2.5A). Only a few single samples showed higher values of up to 200 pmol cm^{-3} d^{-1} (Figure 2.5B), but even those maximum values are still very low when compared with other sites from literature e.g. active seeps (Boetius et al., 2000; Treude et al., 2003; Pimenov et al., 2010). Even in the permanently cold sediments of Svalbard in the northern part of the Barents Sea, sulfate reduction rates are much higher (around 60 nmol cm^{-3} d^{-1}) (Finke et al., 2007). In some cores all values fell below the MDL, irrespective whether the site was located within or outside of a pockmark (Figures 2.5C and D).

In area F (Figures 2.5E to H), highest SRR was also found in the top layer. For the majority of the samples, sulfate reducing activity was restricted to the upper 30 cm of the sediment, reaching a maximum of up to 370 pmol cm^{-3} d^{-1} (Figure 2.5G). Below this depth interval most values were close or below the MDL (Figures 2.5E and H), slightly higher values could only be detected in very few samples. In several cores from both pockmarks and reference sites, SRR fell continuously below the MDL (Figure 2.5H).

In area D, SRR measurements fell consistently below the minimum detection limit in all samples.

In general, sulfate reduction rates do not show any difference between cores from within or outside of pockmark structures. Profiles with slightly higher values in the upper part as well as profiles showing all values below the MDL have been detected for both pockmark and reference sites. Furthermore all SRR profiles show values close to the detection limit, indicating a generally very low microbial activity in the sediments of the investigated area.

2.6 Discussion

A multi-proxy approach was undertaken to obtain chemical, geomicrobiological and geochemical evidence for active fluid or gas venting. Seafloor seeps that contain methane or hydrogen sulfide can easily be identified by their sediment porewater chemistry, their association with specific microbial communities and high rates of microbial turnover as well as characteristic features in seismic data. However, in our study area there was no evidence for active fluid venting currently occurring from either type of analysis.

During sampling we did not notice any hydrogen sulfide smell, not even on acidified porewater samples, implying that there are neither significant amounts of dissolved H_2S nor any finely precipitated sulfides such as ferrous monosulfide (FeS). Furthermore, no apparent carbonate concretions, being an indicator for active or recent anaerobic oxidation of methane, could be identified (Ferrell and Aharon, 1994; Knittel and Boetius, 2009).

2.6.1 Gas distribution maps

Gas concentrations in sediments of the investigated areas were extremely low. In some single samples, slightly elevated gas concentrations could be detected but no consistent correlation with the occurrence of pockmarks or any other parameter could be established. Headspace gas and occluded gas concentrations were negligibly small, implying that no active seepage is taking place in the pockmark structures. Highest values were always detected in the adsorbed gas fraction, it is therefore reasonable to assume that this gas is derived from previous gas emissions, during which a portion of the gas was adsorbed onto the clay minerals.

There are no significant differences between the concentrations of adsorbed methane in all three areas. Throughout our study site, the average gas content is very low and shows no correlation between sites from within or outside the pockmarks. Very low gas contents in area D demonstrate that there is no connection between the potentially underlying gas anomaly and the surface sediments. Due to the fact that gas concentrations were always below saturation and no bubble formation occurred, any major loss due to degassing during sampling and processing can be ruled out.

2.6.2 Sulfate reduction rate and sulfate profiles

Unlike methane, which can be lost from the sediment during coring due to degassing, porewater sulfate cannot be lost as it does not form a gaseous phase. In sulfidic sediments however, there is the potential for increasing sulfate concentrations due to oxidation of hydrogen sulfide. Because of the lack of hydrogen sulfide, we can rule out this possibility and assume the sulfate profile to represent true in-situ conditions.

The linear decrease in porewater sulfate concentration at all sites indicates that diffusion dominates sulfate transport into the sediment and that there is

no sulfate consumption in this depth interval. As described by Berner (1980) SR activity can be estimated from porewater sulfate profiles. However, direct radiotracer measurements of SRR provide much more reliable results of SR activity, especially if diffusion is not the only means of transport and other processes like advection may replenish the sulfate pool in near-surface sediments (Fossing et al., 2000; Jørgensen et al., 2001; Weber et al., 2001). This is the case in our study because contrary to the linear sulfate profiles, which indicate no net sulfate consumption over the length of the core, direct radiotracer SRR measurements reveal some very low activity in the upper few cm. Much higher rates of sulfate reduction were expected in the pockmark cores, particularly if active fluid venting was taking place. In most cases SR was only measurable in the upper 30-40 cm below sea floor. This also leads to the assumption, that AOM does not occur in the recovered depth interval (2.6 m) and the SR activity can be attributed entirely to organiclastic SR and not to anaerobic oxidation of methane.

The calculated SO_4^{2-} penetration depth of 37 m is quite deep when compared to data of gas-rich sediments. In Eckernförde Bay (German Baltic Sea) for example, Treude et al. (2005a) determined a penetration depth of only 0.32 m. Such a deep sulfate penetration depth as determined here shows that very little sulfate is consumed in the upper part of the seabed. Sulfate reduction rates in our study area are generally very low, with no significant differences between SRR profiles from pockmark cores and reference cores. Additionally, SRR values in area D fall consistently below the minimum detection limit in all samples. This leads to the assumption that the pockmarks do not release any gas at present, which is supported by our findings of very small decreases in porewater sulfate concentration with sediment depth and very low gas concentrations.

2.6.3 Pockmark formation theory

Fluid and gas venting is commonly believed to be the main factor for pockmark generation. While pockmark structures could clearly be detected on the seabed, we did not find any indications for significant concentrations of methane in the sediments of the sampling area. Neither did we find indications for ongoing fluid flow through these features.

Although expulsion of methane is the most frequently reported process leading to the formation of pockmarks, seepage of other fluids has been described as well. However, in most cases only minor quantities of gases like hydrogen sulfide or carbon dioxide are associated with hydrocarbon leakage. The expulsion of porewater through the seabed, so called submarine groundwater discharge (SGD), has been widely described in the literature. In a review Taniguchi et al. (2002) describe different systems showing SGD.

Some examples of pockmarks being formed by porewater discharge, have been reported (Whiticar and Werner, 1981; Harrington, 1985; Webb et al., 2009). However, those few examples are primarily based on assumptions and lacking direct evidence of the processes involved. Moreover, the mechanisms described in these studies are unable to explain the procedure of pockmark formation in detail. Given the enormous area of extensive pockmark occurrence within and beyond our study area and the fact that we have no evidence for past or present SGD, we rule out this mechanism.

Recently the occurrence of unit pockmarks (pockmarks diameter < 5 m) was discussed to be an indicator for active gas seepage (Cathles et al., 2010; Hovland et al., 2010).

Mapping unit pockmarks requires application of high-resolution bathymetry (at least 1 m $\times$ 1 m gridding) (Hovland et al., 2010). The resolution of the bathymetry equipment which was used in this study is too low to locate unit pockmarks. However, due to the very low gas concentrations in the pockmark as well as in the reference sites (Table 2.2) we rule out the existence of seeping hydrocarbons in our study area.

Pockmark structures which are present in the seabed consistently over several years are not necessarily an indicator for active fluid flow (Brothers et al., 2011). Numerical modeling by Hammer et al. (2009) showed that upwelling currents can be a possible mechanism to maintain pockmark structures even if activity has ceased for several years.

This leads us to the more likely hypothesis that the pockmarks in our study area are preserved features from past activity. The present seabed shows many plough marks, derived from iceberg drifting during the last deglaciation. As undisturbed pockmark craters can be found within and outside of the plough

mark structures, the pockmarks must have formed during and after the main phase of iceberg movement.

Considering the glacial history of the Barents Sea as well as the great number of glacial plough marks in the study area, it can be assumed that the whole area was covered by a grounded ice sheet during Last Glacial Maximum (*ca.* 20 ka ago). Gaseous hydrocarbons like methane, derived from a deeper lying source, could have migrated through the porous sediment towards near-seabed sediments. Due to the conditions during the glacial period, including pressure of a thick grounded ice sheet affecting the sediment, combined with the prevailing low temperatures, the necessary conditions for clathrate formation were given (Kvenvolden, 1998; Sloan, 2003). Methane could thus have been trapped as gas hydrate in the shallow sediment.

The uplifted Atlantic margin basins, comprising the Hammerfest Basin and the Loppa High, contain several oil and gas fields commonly occurring in underfilled traps. Corcoran and Doré (2002) suggested that this was caused due to large scale leakage of gas during the Cenozoic exhumation. 2D basin modeling of this area by (Cavanagh et al., 2006) revealed that glacially controlled pressure oscillations provide a mechanism for episodic discharge of methane from the deep petroleum reservoirs and sequestration of methane as gas hydrates near the surface.

Alternatively sub-glacial gas hydrates may have been fed by a biogenic source or a combination of biogenic and thermogenic gases.

About 14 ka ago the climatic conditions of the SW Barents Sea changed within a relatively short time interval (approximately 5 ka, Elverhøi et al. 1995), causing deglaciation, melting of the ice sheet and iceberg calving. Thus, the conditions to preserve hydrate layers no longer persisted, resulting in the rapid decomposition of the gas hydrate as well as the release of potentially accumulated gas. Such an event probably occurred over large areas of the Barents Sea more or less simultaneously, resulting in widespread pockmark structures on the seabed. Similar formation mechanisms have already been described for other areas (Long, 1992; Solheim and Elverhøi, 1993; Long et al., 1998; Mienert et al., 1998; Davy et al., 2010; Sultan et al., 2010; Plaza-Faverola et al., 2012).

Maslin et al. (2004) collected published data from submarine sediment failures and correlated them with climatic changes from the past 45 ka. They found that over 70% of continental slope failures could be dated to the periods between 15-13 ka and 11-8 ka. These dates, as well as the rising sea level and global atmospheric methane records, correlate well with the timing of the last deglaciation. The hypothesis of pockmark formation due to rapid methane release caused by destabilization of gas hydrates during this time is supported by ice-core data (Chappellaz et al., 1993).

From the foregoing discussion we can summarize the following points concerning the proposed scenario on the formation of the Loppa High pockmarks:

1. During LGM a grounded ice sheet existed in the study area. Thermogenic and/or biogenic gas from a source in the Mesozoic bedrock migrated through the sediment and accumulated as gas hydrate, which was stable under the given pressure and temperature conditions (Figure 2.6A).

2. The retreat of the ice sheet during deglaciation caused changes of pressure conditions, which resulted in the decomposition of the hydrate layer and the release of large volumes of gas over a large areal extent, resulting in the formation of seafloor pockmarks (Figure 2.6B).

3. Nowadays the pockmark structures are still preserved despite the seeping activity having ceased several thousand years ago (Figure 2.6C).

The depressions seem to be relatively young features. As many pockmarks are located inside the iceberg plough marks, it can be assumed that the pockmarks were formed postglacially, probably in an early phase after the last deglaciation. Similar observations have also been reported from the northern Barents Sea (Solheim and Elverhøi, 1993) and could be an indication for a large methane release event caused by the decay of the Barents ice sheet during the last deglaciation.

2.7 Conclusions

Deep, craterlike structures, identified as pockmarks were observed by multibeam bathymetry on the seafloor of the SW Loppa High in the SW Barents Sea. Geochemical, biogeochemical and microbiological analyses revealed

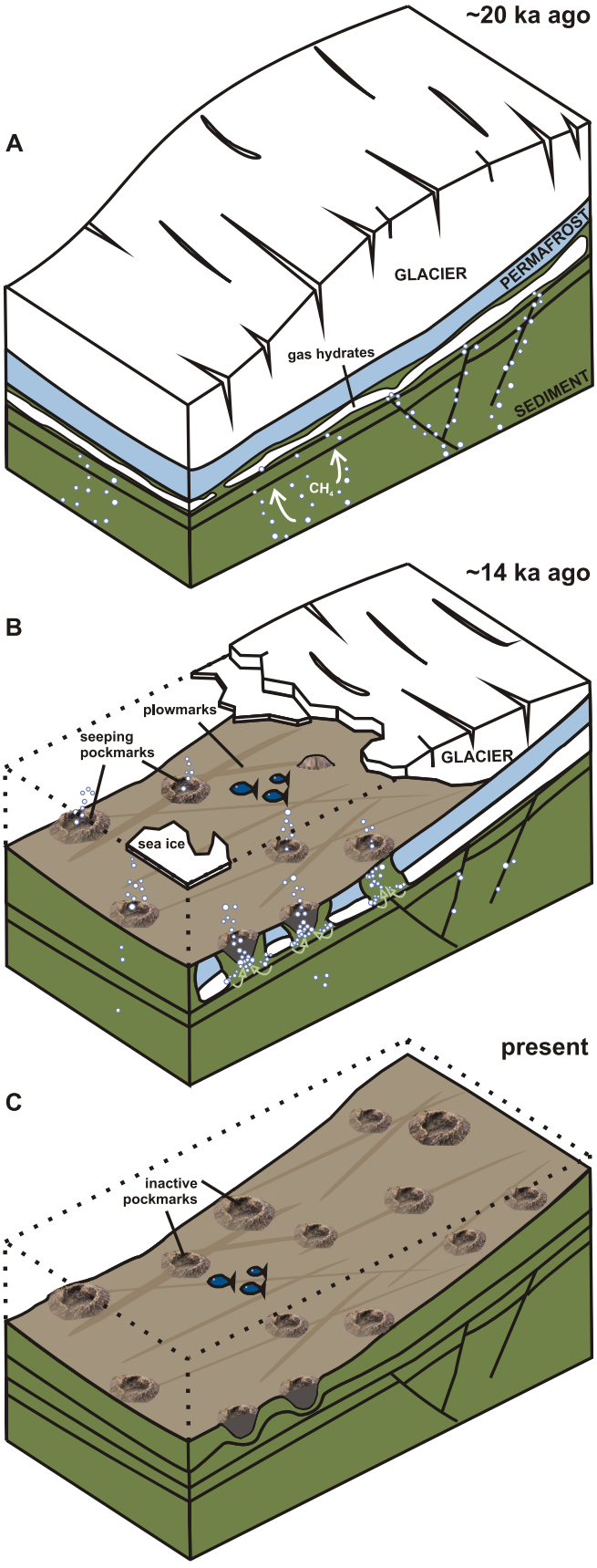

Figure 2.6: (A) During LGM a grounded ice sheet covered the area. Upwards migrating methane accumulated under the ice and formed gas hydrates. (B) During the glacial retreat the gas hydrates decomposed, releasing large volumes of gas, resulting in the formation of pockmarks. (C) Present day situation in the study area. No detectable seeping activity but pockmark structures still preserved.

1. Very low concentrations of hydrocarbons in the sediment.
2. Almost no depletion of porewater sulfate with depth.
3. Low sulfate reduction rates, close to detection limit.
4. Currently no anaerobic oxidation of methane in upper 3 mbsf.
5. No significant and consistent differences in any measured parameter between sites inside and outside of pockmarks.

This indicates astonishingly low microbial activity in the study area, which supports the assumption that currently no active fluid venting is taking place. Based on our own findings and the current literature we hypothesize that the pockmark occurrence and its formation is most likely related to a paleo-event during the last deglaciation.

2.8 Acknowledgments

We would like to thank LUNDIN Petroleum Norway for funding the research project and providing the bathymetric data. GeolabNor AS is acknowledged for providing the gas profile data. We thank the crew and shipboard scientific party of the R/V HU Sverdrup and the shore-based staff of FFI and NGU for excellent support during the expedition and Jan Erik Bjorøy and his crew from Fugro for coring. Ilya Ostanin is thanked for assistance in the preparation of this paper. We acknowledge the two anonymous reviewers and the editor for the constructive comments which helped to improve this manuscript. This work contributed to the Helmholtz Climate Initiative REKLIM.

Chapter 3

Tracing the origin of thermogenic hydrocarbon signals in pockmarks from the southwestern Barents Sea

3.1 Abstract

The glacially influenced southwestern Barents Sea is a promising area for petroleum exploration. The present study area, which is located in the Loppa High region, exhibits extensive pockmark fields covering an area of several square kilometers and containing thousands of pockmarks in high density. To investigate whether the pockmark formation was driven by petroleum leakage to the surface, acting thus as indicators for an active petroleum system, gravity cores from selected pockmark and reference sites were investigated using an organic geochemical approach. Various biomarkers indicative of thermogenic hydrocarbons such as short chain *n*-alkanes with a low carbon preference index, alkylcyclohexanes, $\alpha\beta$-hopanes, steranes and diasteranes mixed with biomarkers representing immature organic matter were detected in the pockmark, but also in reference cores outside of the pockmark and even from a non-pockmark area. The abundance and level of thermal maturity of the

This chapter has been published as: J. C. Nickel, R. di Primio, J. Kallmeyer, Ø. Hammer, B. Horsfield, D. Stoddart, H. Brunstad & K. Mangelsdorf, 2013, Tracing the origin of thermogenic hydrocarbon signals in pockmarks from the southwestern Barents Sea: Organic Geochemistry, v. 63, p. 73-84.

thermogenic hydrocarbons are comparable between the pockmark and reference sites. Additionally, their distribution with depth is quite similar to those of the immature biomarkers. These observations support the conclusion that the thermogenic hydrocarbon signal in the pockmarks is the result of reworked, eroded mature material mixed with immature organic matter distributed across the entire area, rather than the result of seepage events of thermogenic hydrocarbons through the pockmark system. The data show that in the Loppa High region the pure presence of petroleum-derived hydrocarbons in pockmark areas cannot be used to indicate the presence or leakage of deeper petroleum systems.

3.2 Introduction

The Barents Sea is an epicontinental sea, situated between the Norwegian Sea in the southwest and the Arctic Ocean in the north. It consists of several platforms and sedimentary basins, being the result of a complex geological history (for detailed overview see Doré 1995 and Gabrielsen et al. 1990) with several events of tilting, subsidence, uplift and erosion (Larssen et al., 2005).

The study area is located in the southwestern part of the Loppa High (Figure 3.1), a structural high that was formed during Late Jurassic to Early Cretaceous by tectonic movement. To the south, the Loppa High borders to the Hammerfest Basin which is the most promising basin for petroleum exploration in the southwestern (SW) Barents Sea (Doré, 1995). Some hydrocarbon systems also have been recognized in the southwestern part of the Loppa High (Ohm et al., 2008). Source rocks have been identified in all stratigraphic intervals, ranging from the Carboniferous to the Cretaceous (Ohm et al., 2008). The most prolific source rock is the Upper Jurassic Hekkingen shale formation, containing high total organic carbon (TOC) contents with high hydrocarbon potential (S2) and high hydrogen index (HI) values (Ohm et al., 2008). However, most of the discoveries in the SW Barents Sea consist of gas dominated, underfilled traps (Corcoran and Doré 2002; Ohm et al. 2008 and references therein) and it is commonly believed that the lack of oil is due to uplift and leakage caused by several erosion events (Wood et al., 1989; Nyland et al., 1992; Doré and Jensen, 1996; Cavanagh et al., 2006).

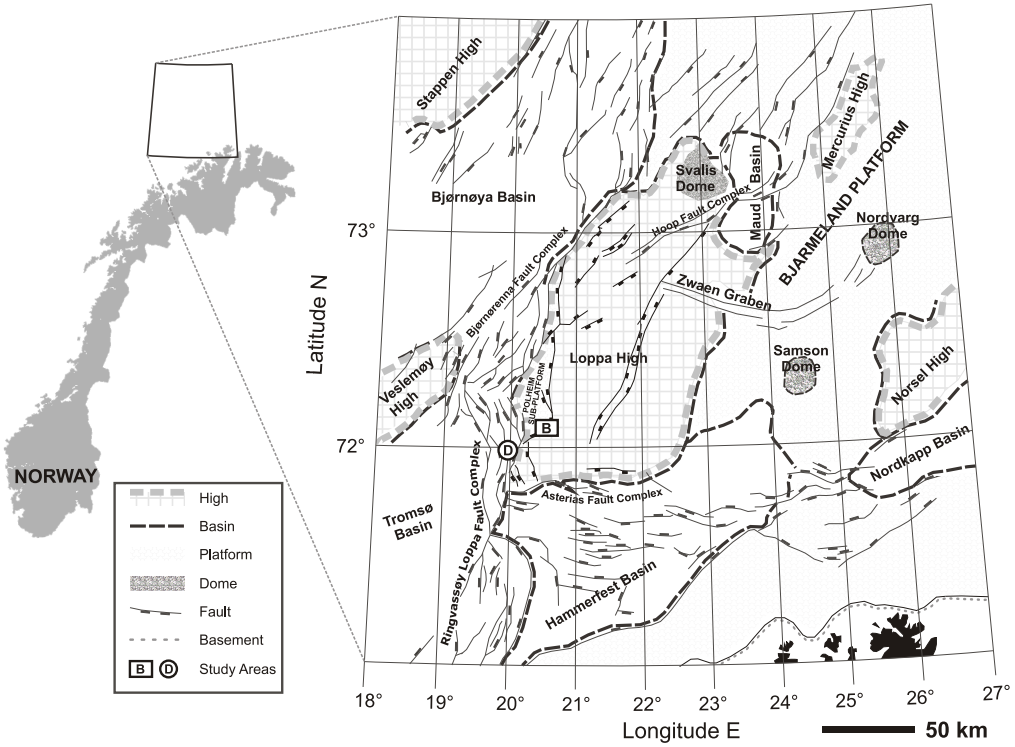

Figure 3.1: Location and tectonic framework of the sampling areas, southwestern Barents Sea (after Nickel et al. 2012). Study areas B and D are indicated.

The Loppa High and its adjacent basins are glacially influenced. During the Last Glacial Maximum (LGM) the entire area was covered at least twice (LGM I: 22 ka and LGM II: *ca.* 19 ka BP) by grounded ice (Siegert et al., 2001; Andreassen et al., 2008), interrupted by an interstadial in which large areas of the SW Barents Sea were deglaciated. According to Eidvin et al. (1993) and Cavanagh et al. (2006) the latest erosional phase in this area took place during the last glacial period. The seabed of the study area still preserves the imprints of the glacial history. Drag marks of drifting icebergs, so called plough marks, are still present all over the seafloor (Solheim, 1991).

A specific feature of the seabed in the study region is that large areas of several square kilometers are covered by a high density of pockmarks (Figure 3.2). Pockmarks are craterlike structures being formed by the seepage of gases or other fluids from deeper sources in the sediments (Hovland and Judd, 1988; Judd and Hovland, 2007). Gas analysis and microbiological investigations in the southwestern Loppa High revealed that the pockmarks in this area are currently inactive (Nickel et al., 2012). Thus, the pockmarks must have

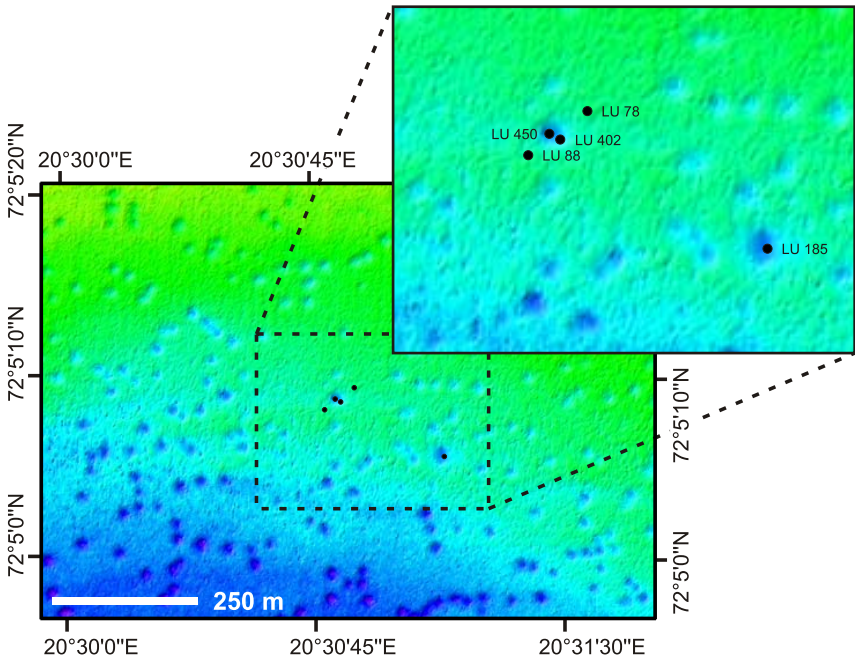

Figure 3.2: Bathymetric map showing a cutout of the larger pockmark field of the sampling area B in the Loppa High region (southwestern Barents Sea) recorded by an EM 710 echo sounder system. The insert shows the positions of the pockmark and reference cores examined in this study.

been formed during seepage events in the near geological past, since their structures are still visible and some of the pockmarks are located within the plough marks. Based on geochemical and microbiological data, Nickel et al. (2012) proposed that pockmark formation in this area may be caused by the decay of gas hydrates during the retreat of the Barents Sea Ice Sheet around 14.5 ka. Similar hypotheses for the SW Barents Sea were reported by Solheim and Elverhøi (1993), analyzing the seabed morphology and Chand et al. (2012) applying seismic stratigraphy and modulation of the methane hydrate stability zone. Based on reconstructions of the pressure and temperature history of the Norwegian Channel Forsberg et al. (2007) described a similar scenario for the North Sea.

Today the gas contents in the studied pockmark sediments are too low to determine the carbon isotopic composition and to assess their origin (Nickel et al., 2012). However, as pockmarks can be indicators for underlying petroleum systems, the sediments might contain oil related hydrocarbons. Together with thermogenic gas, these hydrocarbons might have migrated to the seafloor

(Thrasher et al., 1996; Hood et al., 2002; Logan et al., 2009); thus, forming the pockmark structures (Hvoslef et al., 1996). Boitsov et al. (2011) reported that petroleum leakage pulses might have occurred in pockmarks in the SW Barents Sea. To identify the potential seepage of oil, the pockmark sediments can be analyzed for specific petroleum-derived thermogenically generated biomolecules, such as *n*-alkanes, hopanoids and steranes. The distribution and the degree of structural alteration of these biomarkers can provide strong evidence for the occurrence of petroleum and its thermal maturity (Schumacher and Abrams, 1994; Wenger and Isaksen, 2002).

The aim of the current study is to analyze the sediment of the apparently inactive pockmarks for their organic compound inventory to determine whether seepage of oil can be detected in the pockmarks. The identification of migrating hydrocarbons (macro or micro seeps (Abrams, 1996)) can be an important indicator for underlying petroleum systems (Faber and Stahl, 1984; Hood et al., 2002; Abrams, 2005). Therefore, cores taken within pockmarks were studied for the distribution and composition of petroleum biomarkers and compared to cores taken outside of pockmarks (references cores) or from a non-pockmark area. Furthermore, knowledge on the organic matter (OM) composition of the sediment in the study area might provide insights into the history of pockmark formation.

3.3 Morphology of the seabed in the study area

A typical picture of the seabed morphology in our study area B is shown in Figure 3.2. Multibeam bathymetry revealed the presence of a multitude of circular seafloor depressions that were interpreted as pockmarks. The study area contains an average density of 100 randomly distributed pockmarks per square kilometer. The circular pockmarks are between 10 and 150 m in diameter with an average depth of about 1 to 10 m. According to Hovland and Judd (1988) and Hovland et al. (2002) these pockmarks can be termed “normal pockmarks”. Sampling area D, about 25 km southwest from area B, does not contain any pockmark features, but many plough marks can be observed on the seabed.

The sediment is very similar in all investigated cores at all depths. In general, the cores consisted of sticky silty clay of brown to dark brown color, occasionally containing some less dense structures like small pieces of siliceous sponges as well as pebbles or fragments of bivalve shells. There was no visual difference in the sediment texture between samples from within or from outside the pockmarks in area B or between the samples from different core depth, suggesting that different adsorption effects regarding thermogenic hydrocarbons due to variations in the sedimentary composition (Horvitz, 1985) do not play a significant role in the investigated samples. In area D, the penetration depth of the gravity corer was relatively small (average penetration depth area B: 200 cm, area D: 50 cm) as the very sticky mud prevented a deeper penetration. The average water depth in the investigated areas is around 350 m with an average water temperature of about 6°C.

Seismic data are not directly available from area D. However, several seismic profiles including pockmarks are published from area B and the surrounding areas (Chand et al., 2012).

3.4 Samples and methods

3.4.1 Samples

In November 2009, a research cruise was conducted into the southwestern Barents Sea on the research vessel HU Sverdrup II. The project is a cooperation between the GFZ German Research Centre for Geosciences, the University of Potsdam (Germany), the Swedish oil company Lundin, the Geological Survey of Norway (NGU) and the Norwegian Defense Research Establishment (FFI). During this cruise sample material was recovered from two different sites (area B and D) located in the southwestern Barents Sea (Figure 3.1). In total about 250 gravity cores with a maximum length of 2.6 m were taken from the different sites. Area B is characterized by a large pockmark field (Figure 3.2), area D does not contain any pockmarks, but shows a shallow subsurface seismic anomaly.

From each core 10 whole round core samples of 10 cm length each from different core depths were taken immediately after retrieval of the core. To avoid contamination from shallower sediment being dragged down during penetra-

Table 3.1: Names, sampling areas, types, coring positions and water depth of the investigated cores in the SW Barents Sea.

Core ID	Area	Type	Latitude	Longitude	Water Depth
LU78	B	Reference	72°5'10.14"N	20°30'45.48"E	374 m
LU88	B	Reference	72°5'8.89"N	20°30'40.13"E	375 m
LU185	B	Pockmark	72°5'6.34"N	20°31'1.94"E	375 m
LU402	B	Pockmark	72°5'9.33"N	20°30'43.09"E	374 m
LU450	B	Pockmark	72°5'9.49"N	20°30'42.48"E	375 m
LU266	D	Reference	71°57'51.83"N	19°54'47.83"E	320 m

tion of the gravity corer, the outer core section was removed. The individual whole round core intervals were divided into several subsamples. The sediment samples were immediately frozen at -20°C in N_2 flushed, gas tight bags and transported to GFZ after the cruise in a frozen state.

In the current study, analytical results from three pockmark (PM) cores, two from "pockmark 1"(LU450 in the center, LU402 at the rim) and one from "pockmark 2"(LU185) are presented (Figure 3.2). For comparison two reference (Ref) cores (LU78 and LU88) from area B (Figure 3.2) and one from area D (LU266) were analyzed. The exact locations are given in Table 3.1. Accurate positioning was made possible by a gravity corer equipped with an Ultra Short Baseline (USBL) acoustic GPS transponder allowing the placement of the gravity core above the target site (pockmark or reference site). The sampling positions were selected using high resolution bathymetry data. The deviation from the selected target site was generally less than 3 m.

3.4.2 Biomarker analysis

Samples were freeze dried and ground using a Fritsch *Pulverisette* disk-mill with a stainless steel grinding set. To obtain the total lipid extract, about 70-90 g of the dried sediment were extracted using a flow blending system (Radke et al., 1978) and a modified version of the Bligh and Dyer (1959) extraction method with a mixture of methanol:dichloromethane:ammonium acetate in a volumetric ratio (v:v:v) of 2:1:0.8 (buffered at pH 7.6) for 5 min (for details see Zink and Mangelsdorf 2004). The solvent extract was separated

by centrifugation (3500 rpm) for 10 min at 20°C. The residual sediment was twice re-extracted ultrasonically (for 5 min) using the same extraction mixture. The solvent extracts were combined and collected in a separation funnel. Phase separation was achieved by changing the solvent ratio to 1:1:0.9 (v:v:v). After phase separation the organic phase was separated and the water phase was re-extracted twice with 20 ml dichloromethane (DCM). The organic phases were combined and evaporated to dryness.

Since the sediment material was also intended for biogeochemical investigations, the solvent extract was first separated into different fractions. For this purpose the dissolved extract (1 ml dichloromethane:methanol; 9:1) was separated using two chromatographic columns in sequence. An upper column filled with silica gel (1 g, 63-200 μm) and a lower one with Florisil (1 g, 150-200 μm). Four different fractions of polarity were obtained: a low polar lipid fraction (20 ml chloroform), a free fatty acid fraction (50 ml methylformate +0.025% glacial acetic acid), a glycolipid fraction (20 ml acetone) and a phospholipid fraction (25 ml methanol, only the upper column). Details of the procedure are described in Zink and Mangelsdorf (2004). The biogeochemical analysis of the sample material is not part of this communication.

For the analysis of the petroleum biomarkers, the low polar lipid fraction was separated into aliphatic, aromatic and hetero compound fractions using a medium pressure liquid chromatography (MPLC) system (Radke et al., 1980). Each fraction was concentrated by a TurboVap system, evaporated to dryness via nitrogen stream and stored at -24°C.

Using the methods described above, the volatile hydrocarbons ($< C_{15}$ fraction) might get lost. However, we do not expect to find many of the more volatile components, which are usually only detectable from oils, source rock extracts or fresh oil seepage spots. Volatile hydrocarbons are expected to be lost over the geological past. Headspace gas measurements have shown that there are no C_2-C_8 hydrocarbon gases present in the pockmark sediments (Nickel et al., 2012). For this reason we focused on the C_{15+} *n*-alkane fraction, alkylcyclohexanes, hopanes and steranes in this study.

The aliphatic fraction of the core extracts was analyzed by gas chromatography (GC) and gas chromatography-mass spectrometry (GC-MS). For GC analysis the aliphatic fraction was diluted in *n*-hexane and analyzed on a GC-FID

system (6890, Agilent Technologies, USA) equipped with a 50 m × 0.2 mm × 0.33 μm HP-Ultra 1 capillary column. The injector temperature was set to 40°C and heated with a rate of 11.6°C/s to 300°C held for 3 min. The gas chromatograph oven was programmed from 40°C (2 min isothermal) to a final temperature of 300°C (65 min isothermal) at a heating rate of 5°C/min with a constant helium flow rate of 1 ml/min. The FID was operated at 310°C.

For GC-MS analysis the samples were measured on a DSQ Thermo Finnigan Quadrupole MS coupled to a gas chromatograph. The gas chromatograph was operated in the splitless mode using the following temperature program: initial temperature 50°C (1 min isothermal), heating rate 3°C/min to 310°C (held isothermal for 30 min). The GC was equipped with a Thermo PTV injection system (Thermo Electron Corporation) and a 50 m × 0.22 mm × 0.25 μm BPX5 (SGE) column. Helium was used as carrier gas with a constant flow rate of 1 ml/min. The injector temperature was programmed from 50 to 300°C at a rate of 10°C/s. Full scan mass spectra were recorded from m/z 50 to 600 at a scan rate of 2.5 scans/s.

3.4.3 Foraminiferal analysis

Foraminifera were extracted by wet sieving of *ca.* 100 g of sediment through a 63 micron mesh and identified under a Zeiss stereo microscope.

3.5 Results

To investigate whether petroleum compounds are present in the pockmark sediments, the sediment extracts were analyzed with regard to specific compound classes providing the potential to indicate the presence of migrated oil-derived hydrocarbons such as *n*-alkanes, alkylcyclohexanes, hopanoids and steranes (Simoneit et al., 1992; Rushdi and Simoneit, 2002; Peters et al., 2005b; Logan et al., 2009).

The total organic carbon (TOC) contents in the pockmark and reference sites are quite similar and range between 0.56% and 1.54% with an average value of 1.06%. The TOC profiles do not show any significant trend with depth (Figure 3.3).

A homologous *n*-alkane series is present in all aliphatic fractions of the investigated samples with chain lengths usually between *n*-C_{14} and *n*-C_{35} (Figure

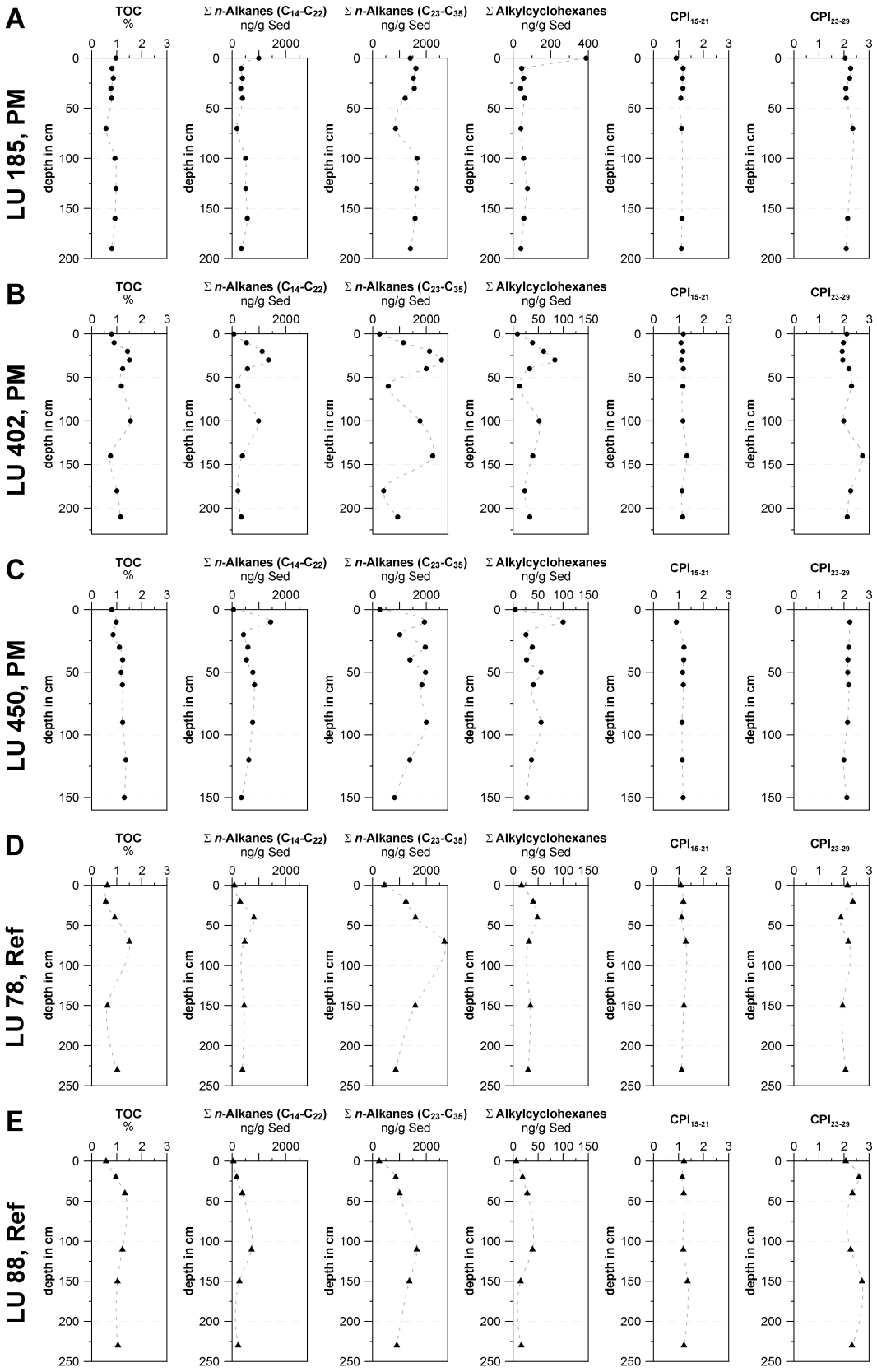
A
LU 185, PM
B
LU 402, PM
C
LU 450, PM
D
LU 78, Ref
E
LU 88, Ref
TOC
%
Σ n-Alkanes (C14-C22)
ng/g Sed
Σ n-Alkanes (C23-C35)
ng/g Sed
Σ Alkylcyclohexanes
ng/g Sed
CPI15-21
CPI23-29
depth in cm

3.4). The *n*-alkane patterns reveal a bimodal distribution for both the pockmark and reference sites (Figure 3.4) with a smaller maximum in the short chain length (*n*-C_{14}-*n*-C_{22}) and a dominating maximum in the long chain range (*n*-C_{23}-*n*-C_{35}). While in the short chain range the difference between odd/even carbon numbers is small, the long chain range is characterized by a stronger odd/even carbon number predominance with the dominating compounds at *n*-C_{25} and *n*-C_{27} (Figure 3.4).

The different distribution of the *n*-alkanes also is reflected in the carbon preference index (CPI). The selected *n*-alkane range and the applied formula for the CPI parameters are presented in the figure caption of Figure 3.3. For the short chain length the average CPI_{15-21} value is 1.14 for the pockmark sites and 1.20 for the reference sites. For the long chain range the average CPI_{23-29} value is higher with 2.15 for the pockmark sites and 2.23 for the reference sites. Depth profiles of the CPI_{15-21} and the CPI_{23-29} values show only minor variability for the pockmark and reference sites (Figure 3.3). The distribution of the sum of all short and long chain *n*-alkanes ($\sum$ *n*-C_{14-22} and $\sum$ *n*-C_{23-35}) with depth for the three pockmark and the two reference cores is shown in Figure 3.3. The amount of short chain *n*-alkanes varies between 50 and 1400 ng/g sediment (Sed) for the pockmark samples and between 50 and 800 ng/g Sed for the reference samples. In the long chain range the values vary between 250 and 2600 ng/g Sed for the pockmark samples and between 250 and 2700 ng/g Sed for the reference samples (Figure 3.3).

The long chain *n*-alkanes as well as the short chain *n*-alkanes reveal a quite similar variability with depth with some occasional deviations. This does not only apply to the pockmark but also to the reference cores (Figure 3.3).

Alkylcyclohexanes are present in all investigated samples, albeit in relatively low abundance. The average amount in all investigated cores is below 50 ng/g Sed with a maximum of up to 400 ng/g Sed (LU185) and 100 ng/g Sed (LU402

Figure 3.3 ***(preceding page)*:** Depth profiles of the TOC values, of the sum of the short and long chained *n*-alkanes, of the CPI_{15-21} for lower molecular weight and the CPI_{23-29} for higher molecular weight *n*-alkanes as well as of the alkylcyclohexanes. (A-C) Pockmark cores, (D-E) reference cores. CPI = Carbon preference index (after Marzi et al., 1993):
$CPI_{15-21} = \frac{1}{2}\left(\frac{nC_{15}+nC_{17}+nC_{19}}{nC_{16}+nC_{18}+nC_{20}} + \frac{nC_{17}+nC_{19}+nC_{21}}{nC_{16}+nC_{18}+nC_{20}}\right)$;
$CPI_{23-29} = \frac{1}{2}\left(\frac{nC_{23}+nC_{25}+nC_{27}}{nC_{24}+nC_{26}+nC_{28}} + \frac{nC_{25}+nC_{27}+nC_{29}}{nC_{24}+nC_{26}+nC_{28}}\right)$

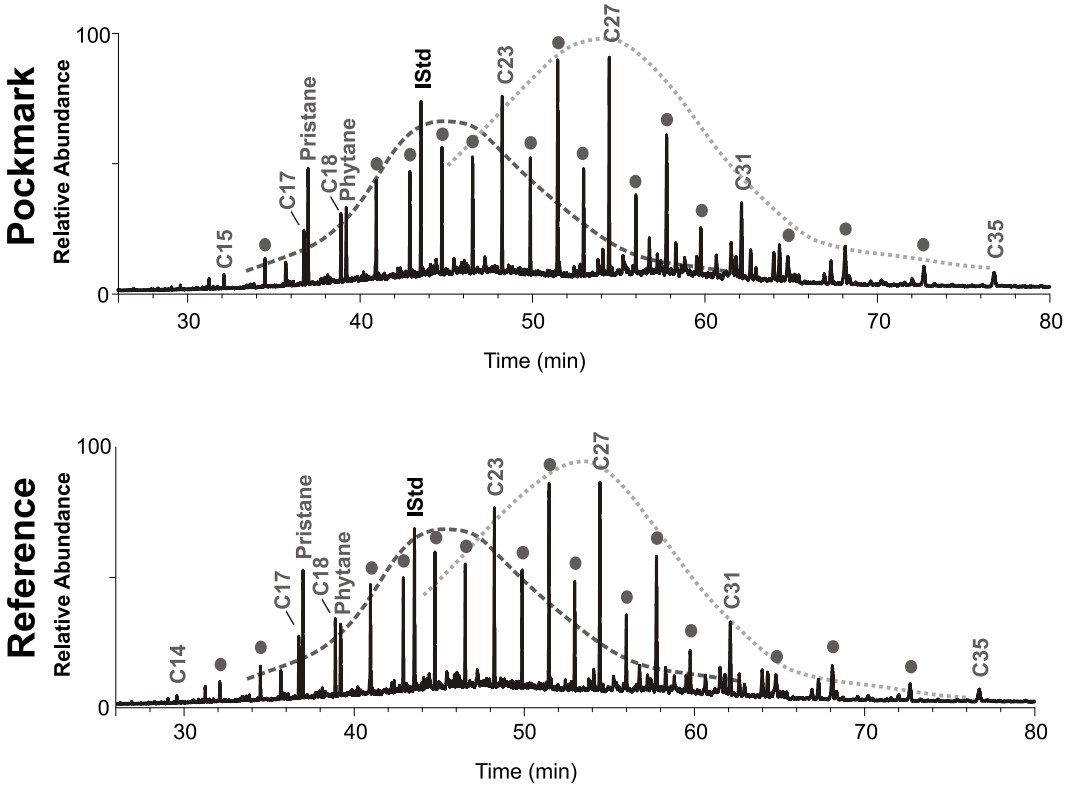

Figure 3.4: Distribution of *n*-alkanes of aliphatic fractions (analyzed by GC-FID) exemplary for (A) a pockmark sample (LU402, 210-220 cm) and (B) a reference sample (LU78, 230-240 cm). IStd: Internal standard 5α-androstane. The *n*-alkanes are indicated by circles. Some *n*-alkanes are marked with their carbon number for orientation.

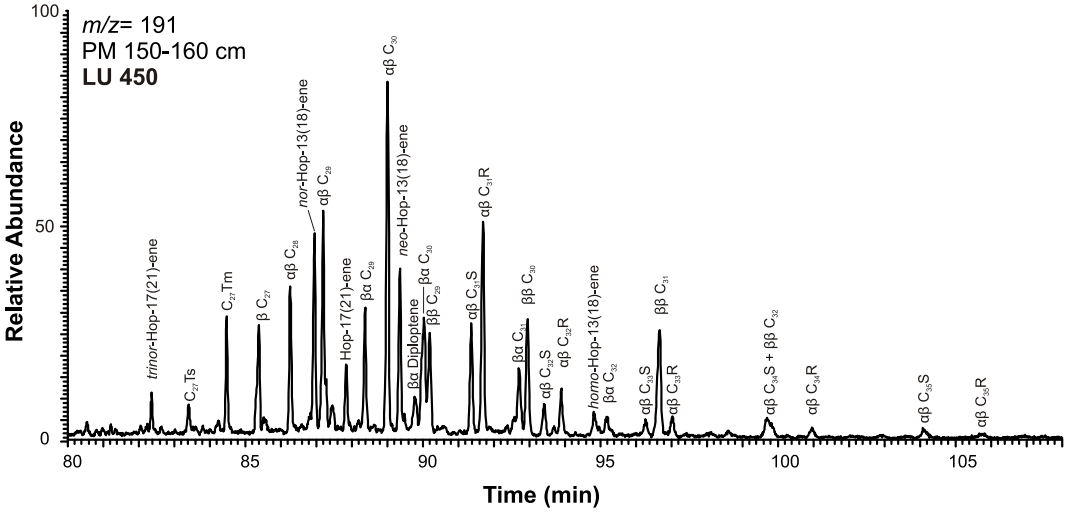

Figure 3.5: Exemplary GC-MS $m/z = 191$ mass trace showing a typical distribution of hopanoids in the studied sediments. The chromatogram represents the deepest interval (150-160 cm) of the pockmark core LU450. Abbreviations see Table 3.2.

and LU450) in the upper part (0-40 cm) of the pockmark cores (Figure 3.3). In the reference cores the values reach a maximum of only 50 ng/g Sed. The alkylcyclohexane depth profiles are similar to those of the short chain *n*-alkanes from the corresponding pockmark or reference cores.

Pentacyclic triterpenoids can be identified in significant amounts based on their mass spectra (selecting $m/z = 191$) and gas chromatographic retention time. Figure 3.5 shows the typical distribution of hopanes in the sediments of the analyzed cores. On average the relative amount of hopanoids ranges from 100-3670 ng/g Sed. The complete homologous series of $\alpha\beta$-hopanes is generally present in the analyzed samples, independent of sample location (PM or Ref) or sediment depth. Overall, the most abundant isomers are the $\alpha\beta$-hopanes. In contrast, the $\beta\alpha$- and $\beta\beta$-hopanes comprise only about one quarter of the total amount of all hopanes. Additionally, a series of hopenes can be found.

No significant trend with depth can be detected in the upper part of the sediment, neither in the PM samples nor in the Ref samples (Figure 3.6). However, in the deepest interval of the two cores taken in pockmark 1 (Figure 3.6B and C), a significant increase in the $\alpha\beta$-hopane concentration can be observed as compared to the reference sites. The distribution of $\alpha\beta$-hopanes shows an analogous trend. The hopane concentration in the sediment of the core from pockmark 2 (Figure 3.6A) does not show an increase in its deeper part. With the exception of a single interval of elevated hopane concentration in pockmark 1, the hopane depth profiles show many similarities to the *n*-alkane and alkylcyclohexane plots in the pockmark as well as in the reference cores. The $22S/(22S + 22R)$ ratio of the C_{31} 17$\alpha\beta$-hopane isomers and the $\alpha\beta/(\alpha\beta + \beta\alpha)$ ratio of the C_{30} hopane isomers are standard geochemical parameters to estimate the sample maturity. Figure 3.6 shows the development of this parameter with depth for the investigated cores. The values range between 0.27-0.35 for the $22S/(22S + 22R)$ ratio and between 0.62-0.70 for the $\alpha\beta/(\alpha\beta + \beta\alpha)$ ratio, respectively. The calculated parameters show no significant change with depth and, the depth profiles of the pockmark and reference cores do not differ significantly from each other.

A wide range of steranes and diasteranes are present in all investigated sediment samples (see Figure 3.7 for an exemplary chromatogram). The 5α,14α,17α(H)-20*R* isomers are clearly the dominating compounds in the m/z

Table 3.2: Hopanoids identified in the *m/z* 191 mass trace of exemplary aliphatic hydrocarbon fractions from pockmark area B and the non-pockmark area D as shown in Figure 3.5 and 3.9.

Abbreviation	Compound
trinor-Hop-17(21)-ene	22,29,30-*trinor*-Hop-17(21)-ene
C_{27} Ts	18α(H)-22,29,30-trinorneohopane
C_{27} Tm	17α(H)-22,29,30-trinorhopane
β C_{27}	17β(H)-22,29,30-trinorhopane
$\alpha\beta$ C_{28}	17α(H), 21β(H)-29, 30-dinorhopane
nor-Hop-13(18)-ene	30-nor-Hop-13(18)-ene
$\alpha\beta$ C_{29}	17α(H), 21β(H)-30-norhopane
Hop-17(21)-ene	Hop-17(21)-ene
$\beta\alpha$ C_{29}	17β(H), 21α(H)-30-normoretane
$\alpha\beta$ C_{30}	17α(H), 21β(H)-hopane
neo-Hop-13(18)-ene	neo-Hop-13(18)-ene
$\beta\alpha$ Diploptene	17β(H), 21α(H)-hop-22(29)-ene
$\beta\alpha$ C_{30}	17β(H), 21α(H)-moretane
$\beta\beta$ C_{29}	17β(H), 21β(H)-30-norhopane
$\alpha\beta$ $C_{31}S$	(22*S*)-17α(H), 21β(H)-29-homohopane
$\alpha\beta$ $C_{31}R$	(22*R*)-17α(H), 21β(H)-29-homohopane
$\beta\alpha$ C_{31}	17β(H), 21α(H)-29-homomoretane
$\beta\beta$ C_{30}	17β(H), 21β(H)-hopane
$\alpha\beta$ $C_{32}S$	(22*S*)-17α(H), 21β(H)-29-dihomohopane
$\alpha\beta$ $C_{32}R$	(22*R*)-17α(H), 21β(H)-29-dihomohopane
homo-Hop-13(18)-ene	homo-Hop-13(18)-ene
$\beta\alpha$ C_{32}	17β(H),21α(H)-29-dihomomoretane
$\alpha\beta$ $C_{32}S$	(22*S*)-17α(H), 21β(H)-29-trihomohopane
$\beta\beta$ C_{31}	17β(H), 21β(H)-29-homohopane
$\alpha\beta$ $C_{33}R$	(22*R*)-17α(H), 21β(H)-29-trihomohopane
$\alpha\beta$ $C_{34}S$ + $\beta\beta$ C_{32}	(22*S*)-17α(H), 21β(H)-29-tetrahomohopane + 17β(H), 21β(H)-29-dihomohopane
$\alpha\beta$ $C_{34}R$	(22*R*)-17α(H), 21β(H)-29-tetrahomohopane
$\alpha\beta$ $C_{35}S$	(22*S*)-17α(H), 21β(H)-29-pentahomohopane
$\alpha\beta$ $C_{35}R$	(22*R*)-17α(H), 21β(H)-29-pentahomohopane

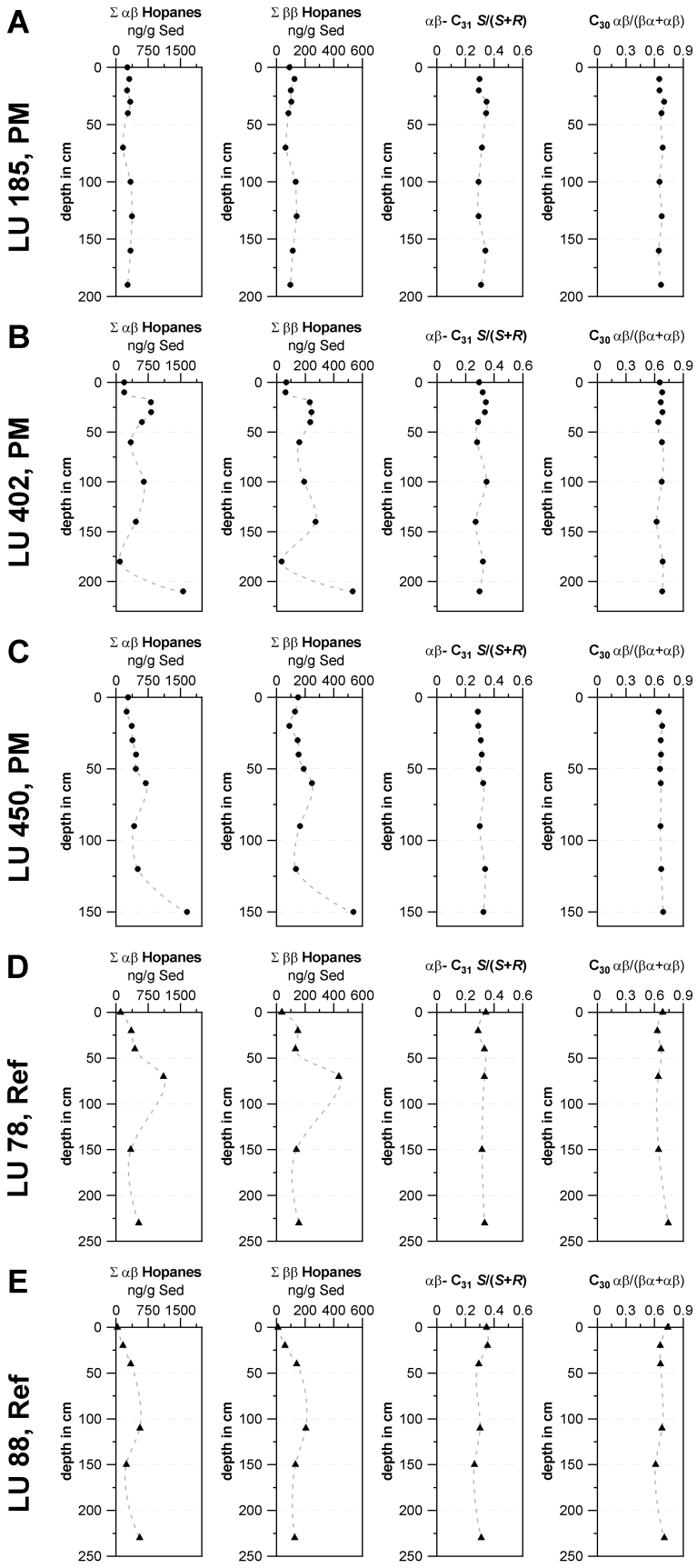

Figure 3.6: Depth profiles of the sum of all 17α(H), 21β(H)-hopanes and 17β(H), 21β(H)- hopanes as well as selected hopane maturity ratios. Abbreviations see Table 3.2. (A-C) Pockmark cores and (D-E) reference cores.

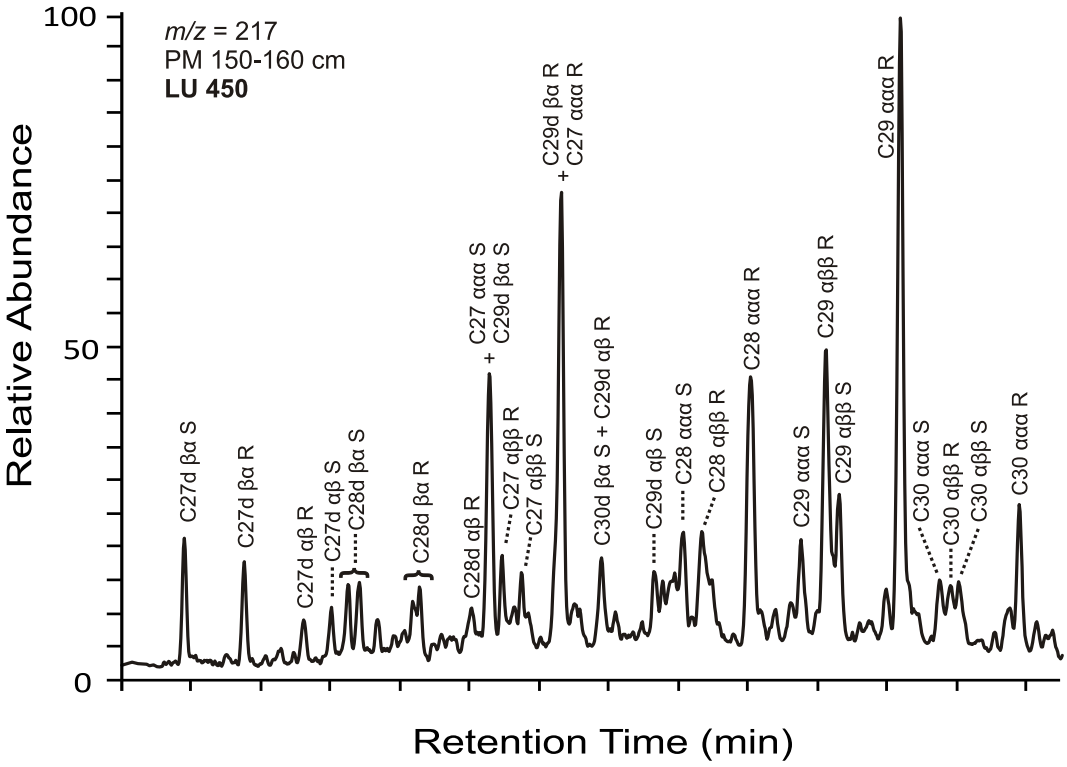

Figure 3.7: Exemplary GC-MS *m/z* 217 mass trace showing a typical distribution of steranes and diasteranes in the studied sediments. The chromatogram represents the deepest interval (150-160 cm) of the pockmark core LU450. Abbreviations see Table 3.3.

217 mass trace (Figure 3.7) within each isomer set of the three regular steranes, cholestane (C_{27}-sterane), 24-methylcholestane (C_{28}-sterane), and 24-ethylcholestane (C_{29}-sterane). Overall the $\alpha\alpha\alpha$-20R-C_{29} isomer is the most abundant sterane. However, some diasteranes occur in significant amounts. The dominating compounds for the rearranged steranes comprise the 14β(H), 17α(H)-20S isomers of diacholestane (C_{27}-diasterane), 24-methyldiacholestane (C_{28}-diasterane) and 24-ethyldiacholestane (C_{29}-diasterane).

The steranes and diasteranes are ubiquitous in all samples investigated although in low amounts ranging between 30-300 ng/g Sed for the steranes and 8-185 ng/g Sed for the diasteranes. The sum of diasteranes as well as the sum of steranes plotted with depth does not show any considerable trend nor is there a significant difference between reference and pockmark cores (Figure 3.8). Again there are many similarities of the sterane and diasterane depth profiles with those of the hopanes, n-alkanes and alkylcyclohexanes. The diasterane/sterane ratio as well as the $\alpha\beta\beta/(\alpha\beta\beta + \alpha\alpha\alpha)$ ratio for the (20R + S)-C_{29} compounds are largely a function of the thermal maturity of the organic matter (Seifert and Moldowan, 1981; Peters et al., 2005b). The analyzed samples show average diasterane/sterane ratios of 0.25 and average $\alpha\beta\beta/(\alpha\beta\beta + \alpha\alpha\alpha)$ ratio values of 0.39. Both ratios do not show significant changes when plotted against depth (Figure 3.8). Additionally, the results obtained from pockmark cores do not differ from those from the reference cores.

For a tentative age assessment of the pockmark sediments foraminiferal assemblages were investigated in selected samples from two cores, LU402 and LU450. In LU402 (pockmark rim), the fauna around 100 cmbsf is completely dominated by *Elphidium* sp., with rare *Cassidulina reniforme* and *Nonionellina labradorica*. At 150 cm, *N. labradorica* dominates, while a somewhat more diverse assemblage with *Elphidium* sp., *C. reniforme*, *N. labradorica* and *Stainforthia* sp. is found at 180-190 cm. Planktonic foraminifera are common below 210 cm. In LU450 (pockmark center), planktonic forms are common already below 100 cm, continuing to the bottom of the core.

Table 3.3: Steranes and diasteranes identified in the *m/z* 217 mass trace of an exemplary aliphatic hydrocarbon fraction from pockmark area B as shown in Figure 3.7.

Abbreviation	Compound
C27d $\beta\alpha S$	20*S*-13β(H), 17α(H)-diacholestane
C27d $\beta\alpha R$	20*R*-13β(H), 17αa(H)-diacholestane
C27d $\alpha\beta R$	20*R*-13α(H), 17β(H)-diacholestane
C27d $\alpha\beta S$	20*S*-13α(H), 17β(H)-diacholestane
C27 $\alpha\alpha\alpha S$	20*S*-5α(H), 14α(H), 17α(H)-cholestane
C27 $\alpha\beta\beta R$	20*R*-5α(H), 14β(H), 17β(H)-cholestane
C27 $\alpha\beta\beta S$	20*S*-5α(H), 14β(H), 17β(H)-cholestane
C27 $\alpha\alpha\alpha R$	20*R*-5α(H), 14α(H), 17α(H)-cholestane
C28d $\beta\alpha S$	20*S*-24-Methyl-13β(H), 17α(H)-diacholestane
C28d $\beta\alpha R$	20*R*-24-Methyl-13β(H), 17α(H)-diacholestane
C28d $\alpha\beta R$	20*R*-24-Methyl-13α(H), 17β(H)-diacholestane
C28d $\alpha\beta S$	20*S*-24-Methyl-13α(H), 17β(H)-diacholestane
C28 $\alpha\alpha\alpha S$	20*S*-24-Methyl-5α(H), 14α(H), 17α(H)-cholestane
C28 $\alpha\beta\beta R$	20*R*-24-Methyl-5α(H), 14β(H), 17β(H)-cholestane
C28 $\alpha\beta\beta S$	20*S*-24-Methyl-5α(H), 14β(H), 17βb(H)-cholestane
C28 $\alpha\alpha\alpha R$	20*R*-24-Methyl-5α(H), 14α(H), 17α(H)-cholestane
C29d $\beta\alpha S$	20*S*-24-Ethyl-13β(H), 17α(H)-diacholestane
C29d $\beta\alpha R$	20*R*-24-Ethyl-13β(H), 17α(H)-diacholestane
C29d $\alpha\beta R$	20*R*-24-Ethyl-13α(H), 17β(H)-diacholestane
C29d $\alpha\beta S$	20*S*-24-Ethyl-13α(H), 17β(H)-diacholestane
C29 $\alpha\alpha\alpha S$	20*S*-24-Ethyl-5α(H), 14α(H), 17α(H)-cholestane
C29 $\alpha\beta\beta R$	20*R*-24-Ethyl-5α(H), 14β(H), 17β(H)-cholestane
C29 $\alpha\beta\beta S$	20*S*-24-Ethyl-5α(H), 14β(H), 17β(H)-cholestane
C29 $\alpha\alpha\alpha R$	20*R*-24-Ethyl-5α(H), 14α(H), 17α(H)-cholestane
C30d $\beta\alpha S$	20*S*-24-Propyl-13β(H), 17α(H)-diacholestane
C30d $\beta\alpha R$	20*R*-24-Propyl-13β(H), 17α(H)-diacholestane
C30d $\alpha\beta R$	20*R*-24-Propyl-13α(H), 17β(H)-diacholestane
C30d $\alpha\beta S$	20*S*-24-Propyl-13α(H), 17β(H)-diacholestane
C30 $\alpha\alpha\alpha S$	20*S*-24-Propyl-5α(H), 14α(H), 17α(H)-cholestane
C30 $\alpha\beta\beta R$	20*R*-24-Propyl-5α(H), 14β(H), 17β(H)-cholestane
C30 $\alpha\beta\beta S$	20*S*-24-Propyl-5α(H), 14β(H), 17β(H)-cholestane
C30 $\alpha\alpha\alpha R$	20*R*-24-Propyl-5α(H), 14α(H), 17α(H)-cholestane

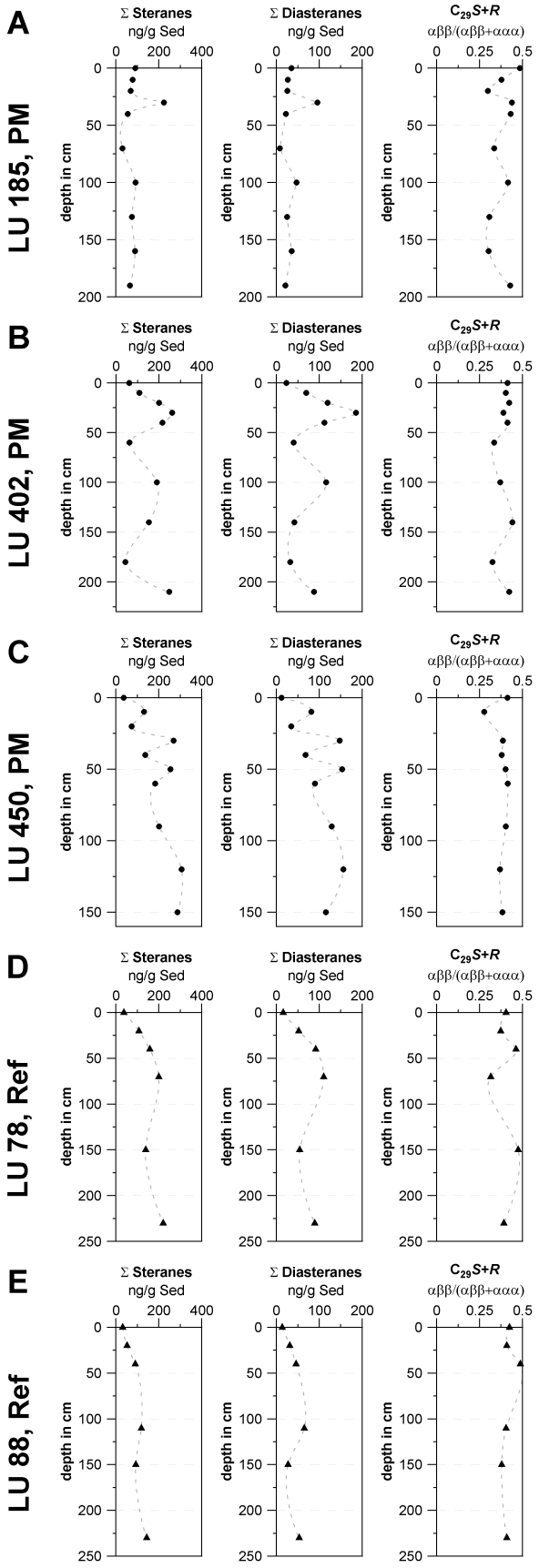

Figure 3.8: Depth profiles of the sum of all steranes and diasteranes and of the C_{29} $(R+S)$ $(\alpha\beta\beta)/(\alpha\beta\beta+\alpha\alpha\alpha)$ ratio. Abbreviations see Table 3.3. (A-C) Pockmark cores and (D-E) reference cores.

3.6 Discussion

3.6.1 Fossil hydrocarbons in the Barents Sea sediments

The bimodal *n*-alkane distribution reveals differences in the odd/even carbon number predominance between the short and the long chain length range as reflected in the CPI. The CPI of *n*-alkanes is an important indicator of the source of the *n*-alkanes and maturity of the organic matter (Bray and Evans, 1961). Values close to unity suggest mature organic matter and petroleum-derived hydrocarbons, whereas higher CPI values in the longer chain length range reflect an input of immature terrestrial higher plant material (Bianchi and Canuel, 2011). In this study the average CPI_{15-21} for the short chain lengths are relatively close to unity for both the pockmark and reference sites, which suggests a contribution of thermogenically derived hydrocarbons to the sediments.

For the long chain *n*-alkanes the average CPI_{23-29} values range around 2.2. This indicates an odd over even carbon number predominance (Figure 3.4), which is characteristic for a terrigenous higher plant signal (Eglinton and Hamilton, 1967; Tissot and Welte, 1984). However, CPI values for hydrocarbons linked to higher plants are usually higher (Bray and Evans, 1961; Marzi et al., 1993). The reason for these intermediate values might be found in a mixture of mature petroleum-derived *n*-alkanes and immature land plant derived *n*-alkanes, whereas the oil-derived hydrocarbons tail into the long chain *n*-alkane signal, reducing the CPI values of the typical land plant signal (Mangelsdorf and Rullkötter, 2003). The immature *n*-alkane signal might also influence the fossil signal in the short chain length range, preventing the values to reach unity. The small variability in the depth profiles of the CPI_{15-21} values for the pockmark and reference sites (Figure 3.3) confirms the thermogenic source of the short chain *n*-alkanes (Bray and Evans, 1965). The variability of the CPI in the long chain range is slightly higher, which might indicate small variations in the composition of the recent source material. Concentrations of short chain *n*-alkanes in the pockmark and reference samples are rather low, however, they fit well with data of other studies that were carried out in the SW Barents Sea (e.g. Boitsov et al. 2011).

Another indication for a supply of thermogenic hydrocarbons into the sediment is the occurrence of alkylated cyclohexanes in all sediments investigated. Alkylated cyclohexanes are compounds ubiquitous in crude oils (Fowler et al., 1986; Kissin, 1990; Hostettler and Kvenvolden, 2002).

Hopanoids, natural pentacyclic compounds, are present in considerable amounts in all samples investigated. They originate from hopanoic precursors (*e.g.*, bacteriohopanepolyols), which occur mainly in cell membranes of aerobic bacteria (Rohmer et al., 1984). However, some anaerobic bacteria are reported to contain hopanoids (Härtner et al., 2005). Their basic structure is relatively stable over geological times; but a systematic change of their configuration at the chiral C17 and C21 positions occurs during late diagenesis/early catagenesis to the beginning of the oil window (Farrimond et al., 1998; Vu et al., 2009). During maturation the biogenic $\beta\beta$-isomers (17β(H), 21β(H)) are replaced by the $\beta\alpha$-isomers (moretanes) and finally by the thermodynamically more stable abisomers. Hence, with increasing maturity the hopanoid composition shifts towards the $\alpha\beta$-isomers, which can be used to assess the maturity of the organic matter (Seifert and Moldowan, 1980).

The dominant presence of a homologous series of $\alpha\beta$-hopanes in the analyzed samples clearly indicates a supply of petroleum hydrocarbons into the sediments of the pockmark and reference sites. However, this petroleum signal is mixed with a series of biogenic $\beta\beta$-hopanes and hopenes and indicates a contribution of recent, immature biomass. These data support the results obtained from the aliphatic hydrocarbon fraction, which suggests that the analyzed organic matter reveals a mixture of thermogenic hydrocarbons and immature organic matter. The hopane maturity parameters do not reach their end points (for $22S/(22S + 22R)$ C_{31} 17$\alpha\beta$-hopanes *ca.* 0.6 and $\alpha\beta/(\alpha\beta + \beta\alpha)$ C_{30} hopanes *ca.* 0.9) yet, indicating a maturity of early catagenesis. However, these parameters might be skewed towards lower maturity by the mixture with immature organic matter. $\alpha\beta$-22R C_{31}-Hopane and $\beta\alpha$-C_{30}-hopane (moretane) are known to derive also from immature sources (Mackenzie, 1984; Mangelsdorf et al., 2011).

The detected steranes also support the presence of thermogenic hydrocarbons. Steranes originate from sterol precursors which are constituents of eukaryotic cell membranes (Mackenzie et al., 1982). They are abundant in oil

and exhibit a complex stereochemistry with a wide variety of stereoisomers. Changes of their chemical configuration during catagenesis can provide important information about the thermal maturity. Changes occur at position C5, C14 and C17 from $\alpha\alpha\alpha$ to $\alpha\beta\beta$ configuration and at C20 from R to S configuration. The presence of $\alpha\beta\beta$ steranes as detected in our samples is an additional indication for the presence of thermogenic hydrocarbons. Besides providing information on the depositional environment (Mello et al., 1988), the diasterane/sterane ratio can be an indicator for thermal maturity of the organic matter, since diasteranes have no biological precursors (Peters et al., 2005b). Significant amounts of diasteranes in our samples are further proof for the presence of oil hydrocarbons. The $\alpha\beta\beta/(\alpha\beta\beta + \alpha\alpha\alpha)$ 20$(R + S)$ C_{29} sterane maturity parameter also does not reach equilibrium yet (endpoint 0.54) indicating a maturity of early catagenesis of the fossil hydrocarbons.

Hopanoid and sterane maturity parameters are very similar (Figure 3.6 and 3.8) independent from the sample depth or the core location (Ref or PM). This implies a similar level of geothermal transformation for the thermogenic hydrocarbons, suggesting a more or less similar source in the whole area over time.

Overall the presented biomarker analysis clearly shows the presence of petroleum hydrocarbons of similar maturity in all sediment samples studied. With the finding of these compounds in the investigated pockmark field the question arises whether these oil-derived hydrocarbons are indicators for underlying petroleum systems being released through the pockmark system to the surface.

3.6.2 Origin of thermogenic hydrocarbons in the Barents Sea sediments

To provide an insight into the origin of the widespread thermogenic hydrocarbon signal, depth profiles of petroleum hydrocarbons are compared to profiles of immature biomarker signals to identify significant differences of these two organic matter sources with depth. Positive deviations of the thermogenic hydrocarbon signal from the trend outlined by the immature biomarkers might demonstrate that both sources are decoupled, indicating intervals of hydrocarbon seepage in the pockmark area on top of a background of a continuous

supply of immature OM into the sediments. In contrast, similar depth distribution patterns might indicate a mixed allochthonous source of mature and immature material being transported into the study area. Since pockmarks can act as conduits for underlying petroleum sources, a particular focus is placed on the pockmark samples.

In the pockmark sites (LU185, LU402 and LU450) the depth profiles of the thermogenic hydrocarbon signal ($\sum$ C_{14}-C_{22} *n*-alkanes and alkylcyclohexanes, Figure 3.3A-C) are, generally, very similar to the profiles of the immature biogenic markers ($\sum$ C_{23}-C_{29} *n*-alkanes, Figure 3.3A-C). The same can be observed when comparing the $\alpha\beta$-hopanes (mature OM, Figure 3.6A-C) with the $\beta\beta$-hopanes (immature OM, Figure 3.6A-C). Generally, the conformity between the different biomarker depth profiles indicates that both OM fractions are somehow related. An exception can be observed in pockmark LU185 (Figure 3.3A) where the uppermost sample shows an increase in fossil hydrocarbons relative to the biogenic organic matter signal, especially within the alkylcyclohexanes. However, this increase is not visible in the respective $\alpha\beta$-hopane profile. The fact that this deviation can only be detected in the uppermost sample seems to indicate a surface contamination rather than seeping oil hydrocarbons coming from below.

If pockmarks are an expression of migration conduits for the oil-derived hydrocarbons, then petroleum hydrocarbons would be expected to be absent or at least much lower in abundance in the reference sites that were taken outside the pockmark structures. However, a comparison (Figure 3.3D-E) shows that fossil hydrocarbons occur in all reference samples and that their abundance is in most cases in the same range. Additionally, the depth profiles of mature and immature markers in the reference samples are very similar. The only difference is a higher proportion of the immature signal (long chain *n*-alkanes, Figure 3.3D) in reference sample LU78 (70 cm depth). Overall, the comparison of the pockmark and reference sites confirms that the contributions of mature and immature OM into the sediments in the pockmark area are similar. These observations contradict a petroleum seepage scenario. A more likely source of the mature hydrocarbons is eroded material from uplifted source rocks, mixed with immature organic matter followed by distribution of this material over the entire area. Such a scenario better explains the similarities in abundance

between the thermogenic hydrocarbon and immature biomarker signals in the sediments. Uplift and erosion occurred several times during the geological history of the study area (Doré et al. 2002; Ohm et al. 2008, see introduction). Yunker et al. (1996) argued that due to the uplift source rocks might be eroded and that the reworked material has been transported and distributed across the entire area. Similar observations were made for other locations in the world. Cole et al. (2001) and Dembicki Jr. (2010) observed a background signal of thermogenic hydrocarbons in some of Gulf of Mexico sample extracts, showing similar distribution patterns as observed in our study. Their samples also revealed a mixture of recent organic matter and signals of reworked material from immature source rocks, indicated by lower molecular weight hydrocarbons (C_{11}-C_{19} *n*-alkanes) as well as a series of mature $\alpha\beta$-hopanes and steranes. Furthermore, Piggott and Abrams (1996) provide an additional example for reworked source rocks for near-surface sediments from the Cretaceous on the Arctic shelf.

Another origin of the oil hydrocarbons might be oil leakage in former geological periods with subsequent erosion and distribution of the respective sediments during modern times. The uplifted Atlantic margin basins, including the Loppa High, enclose under-filled traps containing mainly gas and less oil. The loss of oil is supposed to be a result of Cenozoic uplift and tilting of the basins leading to the leakage of the oil (Doré and Jensen, 1996; Corcoran and Doré, 2002; Ohm et al., 2008). Biodegradation might also be an issue for seeping thermogenic hydrocarbons (Wenger and Isaksen, 2002), however, the chromatograms (Figure 3.4) and the biomarker composition do not provide indication for extensive biodegradation.

An additional argument for the origin of the petroleum hydrocarbons from reworked eroded source rock or eroded material from past oil leakage can be deduced from the biomarker analysis of additional samples taken in the non-pockmarked area D during this study. Figure 3.9 shows an exemplary chromatogram of an aliphatic fraction from core LU266 that is located in area D (see Table 3.1 for exact location). It can be seen, that the general *n*-alkane distribution is very similar to the exemplary chromatogram of the samples in pockmark area B (see Figure 3.4). Furthermore, the *n*-alkanes occur in similar abundance (546 ng/g Sed). The carbon preference index for

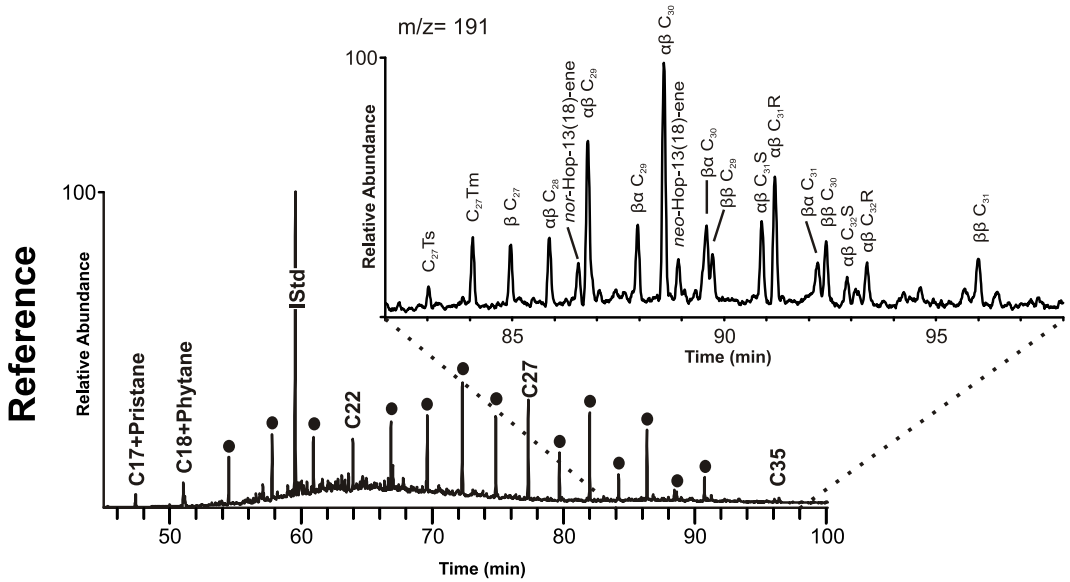

Figure 3.9: Distribution of *n*-alkanes of the aliphatic fraction (analyzed by GC-MS) and the distribution of hopanoids (mass trace m/z = 191) in depth interval 0-10 cm exemplary for sediments in the non-pockmark area D. IStd: Internal standard (5α-Androstane). The *n*-alkanes are indicated by circles. Some *n*-alkanes are marked with their carbon number for orientation.

the short chain *n*-alkanes is close to unity and indicates for the long chain range a predominance of odd chain *n*-alkanes. Additionally, a similar distribution of the hopanoic compounds (see Figure 3.5), especially the homologous series of the $\alpha\beta$-hopanes, can be identified in the m/z trace 191, clearly indicating the presence of thermogenic hydrocarbons in area D sediment. Although area D does not contain any pockmarks, its sediment contains significant amounts of petroleum hydrocarbons, thereby supporting the eroded mature hydrocarbon scenario.

Our conclusions are in contrast to the interpretations of Boitsov et al. (2011), who also investigated a pockmark area in the SW Barents Sea (approximately 50-100 km from our study area). They reported indications for an input of petroleum hydrocarbons to the pockmarks, assuming that these hydrocarbons are a result of migrating fluid pulses from deep strata. However, they only distinguish between samples from a pockmark and a non-pockmark area. Whether sample material was directly from a pockmark is not certain. Also, they do not provide an explanation as to how the migration should have occurred and how the presence of pockmarks could be related to the existence of ubiquitous petroleum hydrocarbons. Such a seepage scenario of thermo-

genic hydrocarbons through the pockmark system cannot be concluded from our data. Nevertheless, the pockmark area investigated by Boitsov et al. (2011) was very close to the Goliat oil field, which might explain the different findings between the two studies.

The assumption that the studied pockmarks do not show active fluid flow is in agreement with geomicrobiological and geochemical data from the same pockmarks in the SW Barents Sea (Nickel et al., 2012). Very low free and adsorbed methane concentrations in the pockmark sediments indicate that seeping activity is not taking place at present. Nickel et al. (2012) concluded that the pockmarks were formed by gas expulsion resulting from the decay of large amounts of gas hydrate during the last deglaciation (about 14 ka ago) due to the pressure release in consequence of the ice shield retreat. This interpretation is in accordance with a scenario presented by Chand et al. (2012). Analyzing seismic data of the Loppa High region as well as modulation of the methane hydrate stability zones they concluded that the present pockmarks are most likely inactive and related to the dissociation of gas hydrates caused by glacial retreat. High resolution sub-bottom profiler images show that the pockmarks cut through the glaciomarine sediments, indicating that their formation occurred during deglaciation. This is supported by the fact that pockmarks are found within plough mark from drifting icebergs. Similar observations were made for the Hammerfest Basin (Figure 3.1) south of the Loppa High. Based on analysis of high resolution 3D seismic data, Ostanin et al. (2013) claimed that gas venting events took place following the Last Glacial Maximum. In contrast, periodic gas venting as well as pore water escape is unlikely, since these scenarios explains more localized phenomena and would not explain the large extend of the observed pockmark fields. All data point to a scenario in which gas from a deeper hydrocarbon source migrated upwards (Floodgate and Judd, 1992; Sassen et al., 2001) and accumulated area-wide as gas hydrates over thousands of years during the last glacial period under the ice shield. During deglaciation the gas hydrates rapidly decay due to the pressure release as a result of the ice shield retreat, releasing huge amounts of hydrocarbon gases forming the large pockmark fields. Thermogenic gas is very likely in an area such as the SW Barents Sea known for underlying hydrocarbon systems (Vorren et al., 1991; Doré, 1995; Doré and Jensen, 1996). The thermogenic

source is supported by gas measurement on methane collected from active gas seeps north of our study area showing a δ^{13}C value of -47‰.

We conclude that the presence of petroleum hydrocarbons in the pockmark sediments in the Loppa High is not an indicator for migrated oil or even active fluid flow. In this context it might be argued that the analysed cores (maximum 2.5 m) are too short to cover the whole history of the pockmarks since their formation during the last deglaciation and that there might have been a period in the past where oil hydrocarbon leakage from the pockmarks was relevant. This was assessed by foraminiferal biostratigraphy, considering the successions in the SW Barents Sea reported by Chistyakova et al. (2010) and Aagaard-Sørensen et al. (2010). The LU402 core, from the pockmark rim, contains a typical ice-marginal fauna at 100-200 cmbsf. The *N. labradorica acme* at 150 cm is typical of the lower part of Zone B in the area, and has been dated to 14-16 ka BP (calibrated) by Chistyakova et al. (2010). The planktonic foraminifera below 210 cm (Zone C) indicate ice-free conditions and could date from the initial end-Weichselian deglaciation phase or even from an older interstadial (*e.g.*, the Eemian, 120 ka BP). The core depths of these bioevents are typical of undisturbed localities in the area. In contrast, the LU450 core contains Zone C fauna in all investigated samples below 100 cm, showing a very thin deglaciation sequence and Holocene cover. This confirms that the core was taken from the centre of a pockmark, and also demonstrates that the sedimentary record of both pockmark rim and centre cores cover an age interval larger than the assumed age of the pockmarks. This observation suggests that seeping oil hydrocarbons never played a significant role in the investigated pockmarks.

3.7 Conclusions

A large pockmark field in the Loppa High area, southwestern Barents Sea, was investigated by organic geochemical approaches to answer the question whether these pockmarks have been conduits for oil-derived hydrocarbons to the surface, thereby indicating deeper petroleum systems. For this purpose sample material from pockmarks and references sites (from outside pockmarks and from a non-pockmark area) were examined with regard to specific oil related biomarkers.

In all pockmark samples the investigated petroleum hydrocarbons are present and mixed with immature organic matter. The presence of thermogenic hydrocarbons is indicated by a series of biomarkers such as short chain *n*-alkanes with almost no odd/even carbon number predominance, alkylcyclohexanes, $\alpha\beta$-hopanes, steranes and diasteranes. Maturity parameters for the investigated samples indicate a similar level of maturity for the thermogenic biomarkers.

However, fossil hydrocarbons with a similar distribution and abundance also were found in the references sites even from a non-pockmark area. Additionally, the depth profiles of the oil-derived biomarkers are very similar to those representing the immature background organic matter. This indicates that the presence of oil-derived hydrocarbons in the pockmarks is rather a signal of eroded material mixed with immature organic matter and distributed across the entire area, than a signal for seeping oil-derived hydrocarbons from deeper petroleum sources through the pockmark system. Age assessment of the pockmark cores suggests that oil hydrocarbons never played a significant role in the pockmark formation scenario. Thus, the data support the conclusion that the pure presence of oil-derived hydrocarbons in pockmark areas in the Loppa High cannot be used to indicate deeper petroleum hydrocarbon systems or at least that care has to be taken while interpreting the mature hydrocarbon signals.

3.8 Acknowledgements

We would like to thank LUNDIN Petroleum Norway for funding the research project and providing the bathymetric data. The crew and shipboard scientific party of the R/V HU Sverdrup and the shore based staff of FFI and NGU is thanked for excellent support during the expedition. We are grateful to Cornelia Karger, Anke Kaminsky and Kristin Günther for their technical and analytical support. We acknowledge Dag Karlsen and the anonymous reviewer for the constructive comments which helped to improve this manuscript. This work contributed to the Helmholtz Climate Initiative REKLIM.

Chapter 4

Insights into the activity, formation and origin of cold seep systems on the seafloor of the SW Loppa High in the SW Barents Sea

4.1 Abstract

The southwestern Loppa High region, located in the SW Barents Sea, is a promising area for oil and gas exploration. The occurrence of numerous fault systems, extensive pockmark (PM) fields, gas hydrates, gas flares and patches of carbonate crusts suggest hydrocarbon seeping in this area. Here, sediment and carbonate crust samples from two different cold seep systems, a PM field and a carbonate crust area, were investigated. To unravel the activity and formation scenarios of the different seep structures as well as the origin and timing of the seeping hydrocarbons a biogeochemical approach was applied. For this purpose the biomarkers of microbial communities being associated to hydrocarbon seeping systems as well as their carbon isotope signatures were examined. In the carbonate crust area archaeal biomarkers diagnostic for the anaerobic oxidation of methane (AOM) such as pentamethylicosane (PMI), crocetane, archaeol and hydroxyarchaeol, highly depleted in ^{13}C, were detected in the sed-

iment as well as in the corresponding carbonate crust. Plotted against depth all biomarkers show a distinct interval of elevated concentrations, indicating the occurrence of a shallow AOM zone. This zone was further confirmed by elevated concentrations of highly ^{13}C depleted phospholipid fatty acids (PLFAs) being specific for sulfate reducing bacteria (SRB) which are known to mediate the AOM in syntrophy with anaerobic methanotrophs (ANMEs). Along with rising gas bubbles, observed during sample recovery, the biomarker data indicate a currently active cold seep system in the carbonate crust area. In contrast the diagnostic AOM biomarkers are absent in the sediment from the PM area which suggests that the PM field is currently inactive. Together with the findings of previous studies performed in this area, it is hypothesized that the large PM fields were formed as a result of the decay of area wide distributed gas hydrates which were destabilized due to the retreat of the thick ice shield during the last deglaciation. In contrast seismic data show that the carbonate crust areas are fault-related active seep structures for hydrocarbon gases presumably from thermogenic origin. During glacial times these seeps might have been the pathway for the hydrocarbon gases leading to an area wide accumulation of gas in form of gas hydrates below the ice shield.

4.2 Introduction

The Barents Sea, a shelf sea located between northern Norway and the European coast of Russia in the south and Svalbard and the Arctic Ocean in the north (Gabrielsen et al., 1990), is a promising area for hydrocarbon exploration. The epicontinental sea consists of many structural platforms and sedimentary basins and reveals several hydrocarbon systems including oil and gas fields (Ohm et al., 2008). The entire region is glacially influenced (e.g. Andreassen et al. 2008; Elverhøi et al. 1993) as the Barents Sea was covered by a thick ice shield during the last glacial period, and its retreat is still visible on the seafloor in form of drag marks (plough marks) from drifting icebergs.

The Loppa High, a structural high in the southwestern part of the Barents Sea, is characterized by extensive pockmark fields on the seabed (Hovland, 1992; Nickel et al., 2012). Pockmarks are craterlike seafloor structures resulting from fluid expulsion. They can be conduits for hydrocarbon gases such as methane being released from deeper formations to the seafloor (Hovland

et al., 2005). Thus, in a hydrocarbon prospective area such as the Barents Sea, pockmarks may serve as indicators for underlying hydrocarbon systems, making such areas an attractive target for hydrocarbon exploration as already demonstrated by the finding of the Skrugard, Havis and Lundin 7120 oil fields (Figure 4.1).

Additionally, multibeam ecosounder monitoring detected active gas seepage in form of gas flares in the water column in certain parts of the SW Loppa High (Chand et al., 2012). Patches of carbonate crusts on the seafloor, known to be often associated with methane seeping (e.g. Naehr et al. 2007; Peckmann and Thiel 2004), were visible on high resolution interferometric synthetic aperture sonar (HISAS) images and seafloor photos.

Methane is one of the most important greenhouse gases in the atmosphere (Heimann, 2010). Fluid flow processes, like hydrocarbon leakage through pockmarks, have been estimated to contribute up to 2% of global methane emissions (Judd et al., 2002). Therefore, methane formation and migration dynamics are of considerable interest regarding the global carbon and climate cycle.

Hydrocarbon seeps form a particular habitat for microbial communities which use methane as a carbon and energy source (Foucher et al., 2009; Watkinson and Morgan, 1991). In anoxic subsurface sediments methane is consumed by microorganisms performing the anaerobic oxidation of methane (AOM), which effectively controls the release of methane from the sediment to the ocean and finally to the atmosphere (Knittel and Boetius, 2009). AOM is mediated by anaerobic methanotrophic archaea (ANME) reversing methanogenesis and living primarily in syntrophy with sulfate reducing bacteria (SRB) (Boetius et al., 2000; Hinrichs et al., 1999; Orphan et al., 2001a). Three involved archaeal clades, ANME-1, ANME-2 and ANME-3, all belonging to the Euryarchaeota, are known (Niemann et al., 2006; Orphan et al., 2001a). SRB comprise the groups Desulfosarcina/Desulfococcus for ANME-1 and ANME-2 and Desulfobulbus for ANME-3 (Knittel et al., 2005; Lösekann et al., 2007; Orphan et al., 2002). During AOM the electron acceptor (sulfate) is reduced to sulfide and methane as the electron donor is oxidized to bicarbonate (Iversen and Jørgensen, 1985; Reeburgh, 2007). Due to reaction of bicarbonate with dissolved cations (e.g. calcium or potassium), the precipitation of authigenic

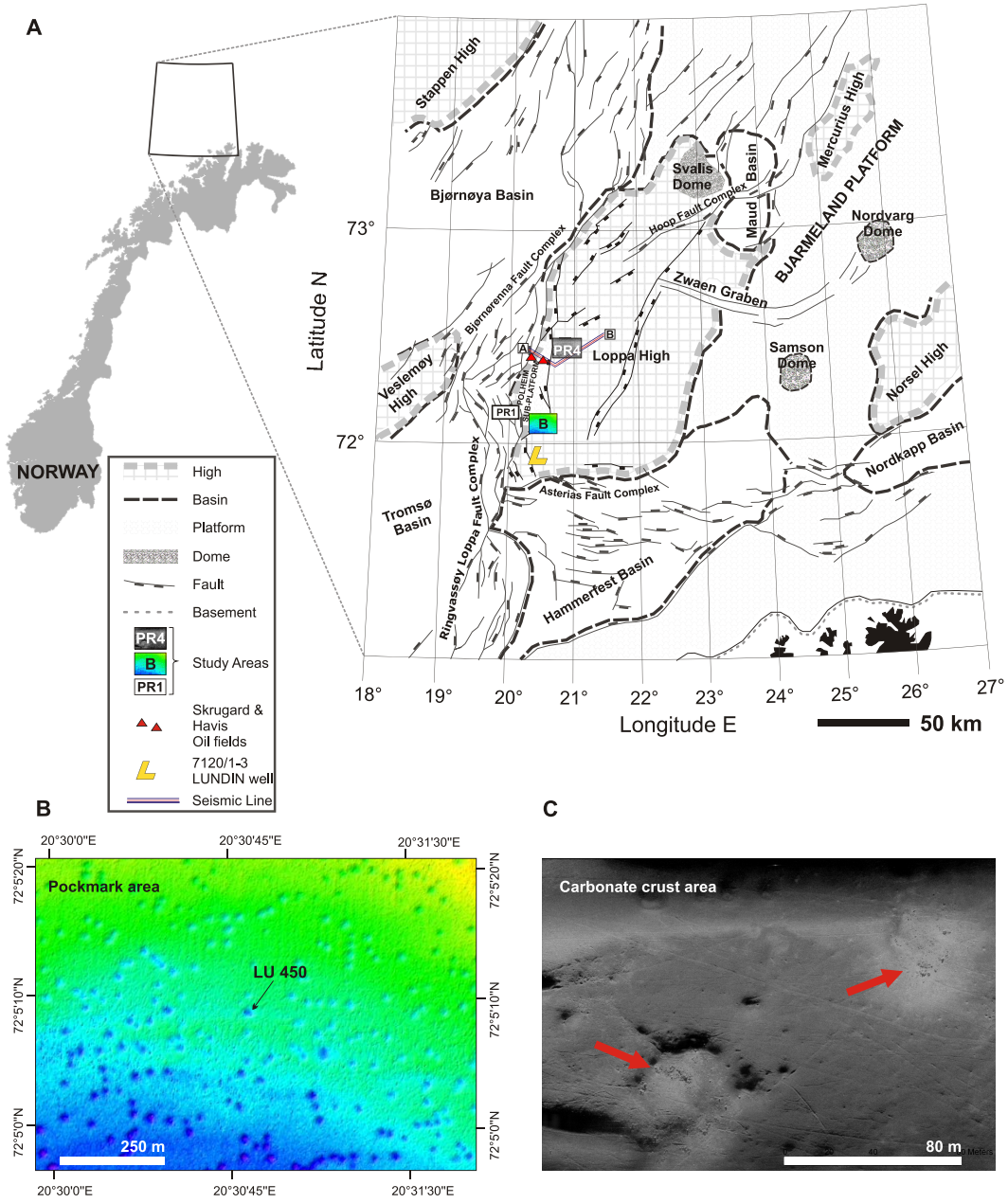

Figure 4.1: (A) Location and tectonic framework of the sampling areas in the southwestern Barents Sea (after Nickel et al. 2012). Study areas B, PR 4 and PR1 are indicated. Red triangles: oil fields Skrugard and Havis, yellow L: Lundin discovery. The position of the seismic line (Figure 4.9) is shown. (B) Bathymetry of the pockmark area B indicating the location of core LU450. (C) High-resolution interferometric synthetic aperture sonar (HISAS) image obtained by autonomous underwater vehicle (AUV) of the carbonate crust area PR4. The carbonate crusts occur in the upper right and lower left parts of the image as dm- to m-scale mounds (red arrows).

carbonates can occur, leading to the formation of carbonate crusts associated with the seeps (Aloisi et al., 2002; Ritger et al., 1987).

Since part of the isotopically very negative methane carbon is incorporated into the biomass of the microorganisms participating in AOM, the carbon isotope signal of characteristic molecular markers (biomarkers) for these microorganisms can be used to track seeping processes (e.g. Blumenberg et al. 2004; Elvert et al. 2003; Hinrichs et al. 1999; Orphan et al. 2002). Common biomarkers used to trace archaea are e.g. archaeol, hydroxyarchaeol (Hinrichs et al., 1999; Koga et al., 1998) 2,6,10,15,19-pentamethylicosane (PMI), 2,6,11,15-tetramethylhexadecane (crocetane) (e.g. Boetius et al. 2000; Elvert et al. 2000; Thiel et al. 2001) and glycerol dialkyl glycerol tetraethers (GDGTs) (Schouten et al., 2001; Wakeham et al., 2004; Weijers et al., 2011). For SRB, specific phospholipid fatty acids (PLFAs) can be used, for instance *iso*- and *anteiso*-C_{15} fatty acids etc. (Blumenberg et al., 2004; Boetius et al., 2000; Niemann and Elvert, 2008; Zhang et al., 2002).

Studies of geomicrobiological and organic geochemical gas and oil biomarker analyses of cores taken from a large pockmark field in the SW part of the Loppa High suggested that most of the pockmarks are presently inactive. There are neither indications for high microbial activity nor for current gas or oil release from the pockmarks (Nickel et al., 2012, 2013).

In the present paper we extended our previous work (Nickel et al., 2012, 2013) by biogeochemical investigations on sediment cores as well as a carbonate crust samples taken from the different seep structures (pockmark and carbonate crust areas) in the SW Loppa High region. A focus was laid on polar molecular markers characteristic for microbial communities associated to methane seeps. Together with the compound-specific carbon isotope signals ($\delta^{13}C$) of these biomarkers, the data offer a deep insight into the activity and formation of the different seepage structures and the origin and timing of the seeping hydrocarbon fluids.

4.3 Samples and methods

4.3.1 Samples

Lundin Petroleum Norway AS, the Norwegian Defense Research Establishment (Forsvarets Forskenings Institutt, FFI) and the Geological Survey of Norway (Norges Geologiske Undersøkelse, NGU) conducted an extensive survey program to identify potential hydrocarbon leakage structures such as pockmarks, gas flares and carbonate crusts on the seafloor in the SW Loppa High region.

A Kongsberg Maritime EM710 multibeam echosounder with seafloor reflection (backscatter) capability was used to screen the seafloor for seep structures and the water column for gas flares (Chand et al., 2012). Promising areas were further inspected using the autonomous underwater vehicle (AUV) "Hugin" equipped with high-resolution interferometric synthetic aperture sonar (HISAS). Acquired sonar images and photos of the seafloor allowed to identify carbonate crust areas.

The sample material for the current study was recovered from two different sampling areas (labeled areas B and PR4) in the southwestern Barents Sea (Figure 4.1A). Area B is located at the southwestern edge of the Loppa High and shows an extensive field of pockmarks of different sizes (between 10 and 50 m in diameter), which are randomly distributed on the seafloor (Figure 4.1B). Area PR4 is located at the northern edge of the Polheim Sub-Platform towards the Loppa High and is characterized by patches of carbonate crust (Figure 4.1C). Furthermore, area PR4 reveals several iceberg plough marks.

In November 2009 a series of sediment gravity cores with a maximum length of 2.6 m were collected in area B both within and outside (as reference) pockmarks. The cruise was initiated and conducted by Lundin Petroleum Norway in cooperation with the NGU, FFI, University of Potsdam and GFZ Potsdam using the R/V HU Sverdrup. Gas measurements were conducted on samples from the deepest interval of each core. For detailed geochemical and geomicrobiological studies, several cores were selected. From each core ten 10 cm-long whole round cores (WRC), spaced over the entire length of each core, were taken directly on board, whereas the top 50 cm were always sampled entirely. To avoid contamination from shallower sediment, the exterior of the core material was removed prior to subsampling for the diverse biogeochemical and

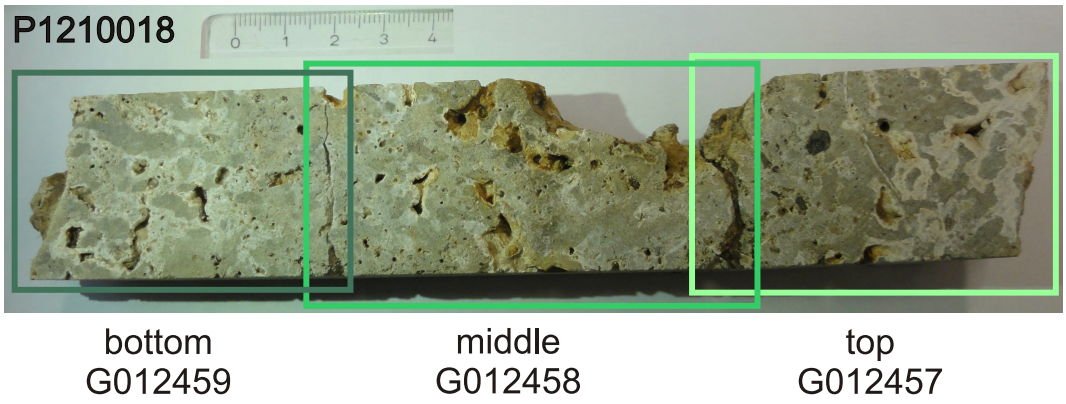

Figure 4.2: Carbonate Crust sample P1210018, taken in PR4. The sample was divided into three parts: top, middle and bottom to investigate the variation over the entire crust.

microbiological analyses. For detailed biogeochemical analyses in the home laboratory an aliquot of each sediment sample was stored in N_2-flushed gas-tight bags and stored frozen at -20°C until analysis. Since the results of the pockmark cores are quite similar, in the current paper we present the results of one pockmark core (LU450) as an example of the pockmarks in area B. For more information on cores from the pockmark areas see also Nickel et al. (2013) and Nickel et al. (2012).

In September 2012 Lundin Petroleum Norway AS conducted a ROV survey in four carbonate crust areas using the R/V Fugro Meridian. In total, 12 sediment push cores with a maximum length of 24 cm and 18 carbonate crust samples were taken. Each core was capped, sealed, frozen at -20°C, shipped to GFZ Potsdam and subsectioned while still frozen. The deepest section of each core was used for gas analysis. Again, the outer core material was removed to avoid possible contamination from shallower sediment.

For this paper we focus on sediment push core P1210020 (divided into 8 depth intervals) and carbonate crust sample P1210018 (divided into 3 parts: top, middle and bottom, Figure 4.2), both from the carbonate crust area PR4. The reported push core was split into 2 cm intervals for the upper 10 cm and 3 cm for the lower part (10-19 cm depth). The exact locations of the investigated sample material from areas B and PR4 are presented in Table 4.1.

Table 4.1: Sample IDs, sampling areas as well as types and coring positions of the investigated samples in the SW Barents Sea.

Sample ID	Area	Area Type	Sample	Latitude	Longitude
P1210018	PR4	Crust	Carbonate Crust	72°34'02.19"N	20°52'09.26"E
P1210020	PR4	Crust	Sediment	72°34'02.07"N	20°52'05.96"E
P1210031	PR1	Crust	Gas	72°09'28.07"N	19°43'37.72"E
LU450	B	Pockmark	Sediment	72°05'09.49"N	20°30'42.48"E

4.3.2 Sample preparation, extraction and chromatographic separation

Each sample was homogenized prior to any processing. The frozen sediment samples were freeze dried, ground, extracted and divided into a low polar fraction including glycerol dialkyl glycerol tetraethers (GDGTs), a free fatty acid fraction, a glycolipid fraction and an intact phospholipid (PL) fraction using a chromatographic method (Zink and Mangelsdorf, 2004).

Half of the low polar fraction was analyzed by high performance liquid chromatography - mass spectrometry (HPLC-MS) for GDGT analysis (see section 4.3.5). After measurement selected samples from specific depth intervals and from the carbonate crust were exposed to ether cleavage to determine the $\delta^{13}C$ values of the detected GDGTs. As described by Gattinger et al. (2003) the GDGT samples were treated with 2 mL hydriodic acid (57%, v/v), sealed and kept for 18 h at 100°C to cleave the ether bonds and to produce the corresponding alkyl diiodides. 4 mL water was added to stop the reaction followed by three times extraction with 10 mL *n*-hexane. The combined organic phases were washed in succession with 10 mL water, sodium carbonate solution (10%, w/v) and sodium thiosulfate solution (50% w/v). The dried samples of the resulting alkyl diiodides were reduced to the corresponding hydrocarbons using 300 mg zinc powder in 3 mL glacial acetic acid at 100°C for 18 h. After cooling, the reaction mixture was neutralized by adding 5 mL sodium carbonate solution (0.1 M), and extracted three times with 7 mL *n*-hexane. The combined organic phases were washed with 10 mL of sodium carbonate solution (0.1 M) and twice with 10 mL of water followed by evaporation to dryness.

The other half of the low polar fraction was separated into an aliphatic compound, aromatic compound and hetero compound (NSO) fraction using medium pressure liquid chromatography (MPLC). The NSO fractions containing the glycerol diethers were derivatized prior to analysis. Trimethylsilylation was performed using *N*-methyl-*N*-(trimethylsilyl) trifluoroacetamide (MSTFA) for 1h at 75°C. For analytical details see Nickel et al. (2013).

Half of the PL fraction was used for mild alkaline hydrolysis to obtain the phospholipid fatty acids (PLFA) fraction via ester cleavage. Following the method of Müller et al. (1990), the aliquot was dissolved in 500 μL dichloromethane/methanol (9:1 v/v). 500 μL trimethylsulfonium hydroxide (TMSH) was added and kept at 70°C for 2 h. After cooling, the reaction mixture was dried under a stream of nitrogen and re-dissolved in dichloromethane for GC-MS analysis.

4.3.3 Gas measurements

Gas compositional and isotopic measurements were performed by APT (Applied Petroleum Technology AS, Norway) following NIGOGA (Weiss et al., 2000) analytical recommendations.

4.3.4 GC-MS analysis

The aliphatic, NSO and PLFA fractions of the core extracts were analyzed by gas chromatography-mass spectrometry (GC-MS). For GC-MS analysis, the samples were measured on a DSQ Thermo Finnigan Quadrupole MS coupled to a gas chromatograph (Trace GC Ultra, Thermo Electron Corporation). The gas chromatograph was operated in the splitless mode using the following temperature programs. For the NSO fraction the initial temperature was 50°C (1 min isothermal), heating rate 3°C/min to 350°C (held isothermal for 25 min). For the aliphatic and PLFA fraction the initial temperature was 50°C (1 min isothermal), heating rate 3°C/min to 310°C (held isothermal for 30 min). The GC was equipped with a Thermo PTV injection system (Thermo Electron Corporation) and a 50 m × 0.22 mm × 0.25 μm BPX5 (SGE) column. Helium was used as carrier gas with a constant flow rate of 1 mL/min. The injector temperature was programmed from 50 to 300°C at a rate of 10°C/s. Full scan mass spectra for NSO and aliphatic fractions were recorded from m/z 50 to 650 u or m/z 50 to 600 u, respectively, at a scan rate of 2.5 scans/s.

4.3.5 High Performance Liquid Chromatography - Atmospheric Pressure Chemical Ionization - Mass Spectrometry (HPLC-APCI-MS)

Glycerol dialkyl glycerol tetraethers (GDGTs) were analyzed by HPLC-APCI-MS using a Shimadzu LC10AD HPLC coupled to a Finningan MAT TSQ 7000 mass spectrometer. Compounds were separated at 30°C using a Prevail Cyano column (2.1 × 150 mm, 3 μm; Alltech) equipped with a precolumn filter. Tetraethers were eluted isocratically with 99% *n*-hexane and 1% *iso*-propanol for 5 min, followed by a linear gradient to 1.8% *iso*-propanol in 40 min. The gradient was changed within 1 min to 10% *iso*-propanol and maintained for 5 min to clean the column and set back to initial conditions and kept for 16 min until equilibrium was reached. Flow rate was set to 200 μL/min.

Atmospheric pressure chemical ionization (APCI) was used to detect the compounds in the eluent, applying a corona current of 5 mA (5 kV), a vaporizer temperature of 350°C, a capillary temperature of 200°C and nitrogen sheath gas at 60 psi without auxiliary gas. Positive ion mass spectra were generated by selected ion monitoring (SIM) using the following masses for isoprenoid GDGTs 1302, 1300, 1298, 1296, 1294 and 1292 for branched GDGTs 1049, 1047, 1045, 1035, 1033, 1031, 1021, 1019 and 1017 and for archaeol 654. Absolute quantification of GDGTs is not possible without appropriate response factors of the different GDGTs (Huguet et al., 2006). However, to enable the comparison of GDGTs from different samples within our sample set, we quantified the GDGTs relative to archaeol used as external standard. Thus, the GDGT concentrations can only be considered as semi-quantitative.

4.3.6 Gas Chromatography - Isotope Ratio Mass Spectrometry (GC-IRMS)

The carbon isotope composition of selected biomarkers was either determined at the GFZ in Potsdam or at the University Göttingen, Germany.

The GC-IRMS system in Potsdam consisted of a GC unit (7890, Agilent Technology, USA) connected to a GC-C/TC III combustion device coupled via open split to a Delta V Plus isotope mass spectrometer (ThermoFisher Scientific, Germany). The organic substances of the GC effluent stream were

oxidized to CO_2 in the combustion furnace held at 940°C on a CuO/Ni/Pt catalyst. CO_2 was transferred on line to the mass spectrometer to determine carbon isotope ratios. 3 μL of the aliphatic fraction were injected to the programmable temperature vaporization inlet (PTV, Agilent Technology, USA). The injector was held at a split ratio of 1:2 and an initial temperature of 230°C. Upon injection, the injector was heated to 300°C with a heating rate of 700°C/min and held at this temperature for the rest of the analysis time. The aliphatic fractions were separated on a fused silica capillary column (HP Ultra 1, 50 m × 0.2 mm ID, 0.33 μm FT, Agilent Technology, Germany) with a temperature program starting at 40°C, increased with a rate of 4°C/min to 300°C held for 45 min. For the ether cleavage products the initial temperature was set to 50°C and increased to 310°C at a heating rate of 3°C/min and was held isothermal for 45 min. Helium, set to a flow rate of 1.0 mL/min, was used as carrier gas. All aliphatic hydrocarbon fractions were measured in triplicate with a usual standard deviation of ≤0.5‰. The quality of the carbon isotope measurements was checked regularly by measuring *n*-alkane standards (*n*-C_{15}, *n*-C_{20}, *n*-C_{25}) with known isotopic composition (provided by Campro Scientific, Germany).

$\delta^{13}C$ values of selected biomarkers in the derivatized polar fraction (BSTFA) were repeatedly determined in Göttingen using a Trace GC, equipped with an SGE BPX5 column (30 m, 0.32 mm inner diameter, 0.25 μm film thickness) and coupled to a Delta Plus IRMS (both ThermoFisher Scientific). Helium was the carrier gas (flow 2.0 mL/min) and the GC temperature program was 80°C (3 min) to 310°C (held 35 min) at 6°C/min. Samples were injected splitless into a split-splitless injector held at 300°C (splitless for 0.8 min). The combustion reactor was similar to the one described above. GC-C-IRMS precision in Göttingen (usually ≤0.5‰) and linearity were routinely checked by using an external *n*-alkane isotopic standard provided by A. Schimmelmann (Indiana University).

4.3.7 Stable isotope composition $\delta^{13}C$ of the carbonate crusts

The stable isotope composition $\delta^{13}C$ of the carbonate crust was determined using a Finningan GasBench II with carbonate option coupled to a DELTA-

plusXL mass spectrometer, following the analytical procedure described by (Spötl and Vennemann, 2003).

4.4 Results

4.4.1 First indications for active seeping

Indications for gas seepage were obvious from the detection of visible gas bubbles in the carbonate crust areas using the ROV camera. Gas bubbles emanated when the core liner was pushed into the sediment, indicating that the sediment was supersaturated with gas. In one of the carbonate crust areas (PR1), from which no carbonate crusts were sampled, bubbling gas was collected. Subsequent gas measurements revealed that the gas was almost pure methane (>99%) with a δ^{13}C value of -47.8‰. Cores from the carbonate crust area PR4 (e.g. P1210020) emitted a strong H_2S smell upon opening. When the cores were pushed out of the liner for subsampling small expanding gas voids could be observed on the core exterior indicating the release of gas. Gas measurements of the deepest interval of the core revealed the presence of significant amounts of methane, whereas higher hydrocarbon gases (e.g. ethane, propane) were below the detection limit. The carbonate crust had a δ^{13}C signal of -36‰.

4.4.2 Characteristic biomarkers for archaeal communities

In the following result chapters biomarker concentrations are provided in ng/g Sed (sediment) or ng/g CC (carbonate crust). Since total organic carbon (TOC) values of the studied sediment samples show almost no variation with depth (data not shown), TOC has no influence on the depth trends of the biomarker profiles presented. Partial chromatograms highlighting the biomarkers archaeol, hydroxyarchaeol, dihydroxyarchaeol, crocetane, pentamethylicosane (PMI) and GDGTs (see Appendix A for molecular structures) being characteristic for archaeal communities are shown in Figure 4.3 for the three sample types investigated (carbonate crust samples, sediment from carbonate crust area and sediment from pockmark area).

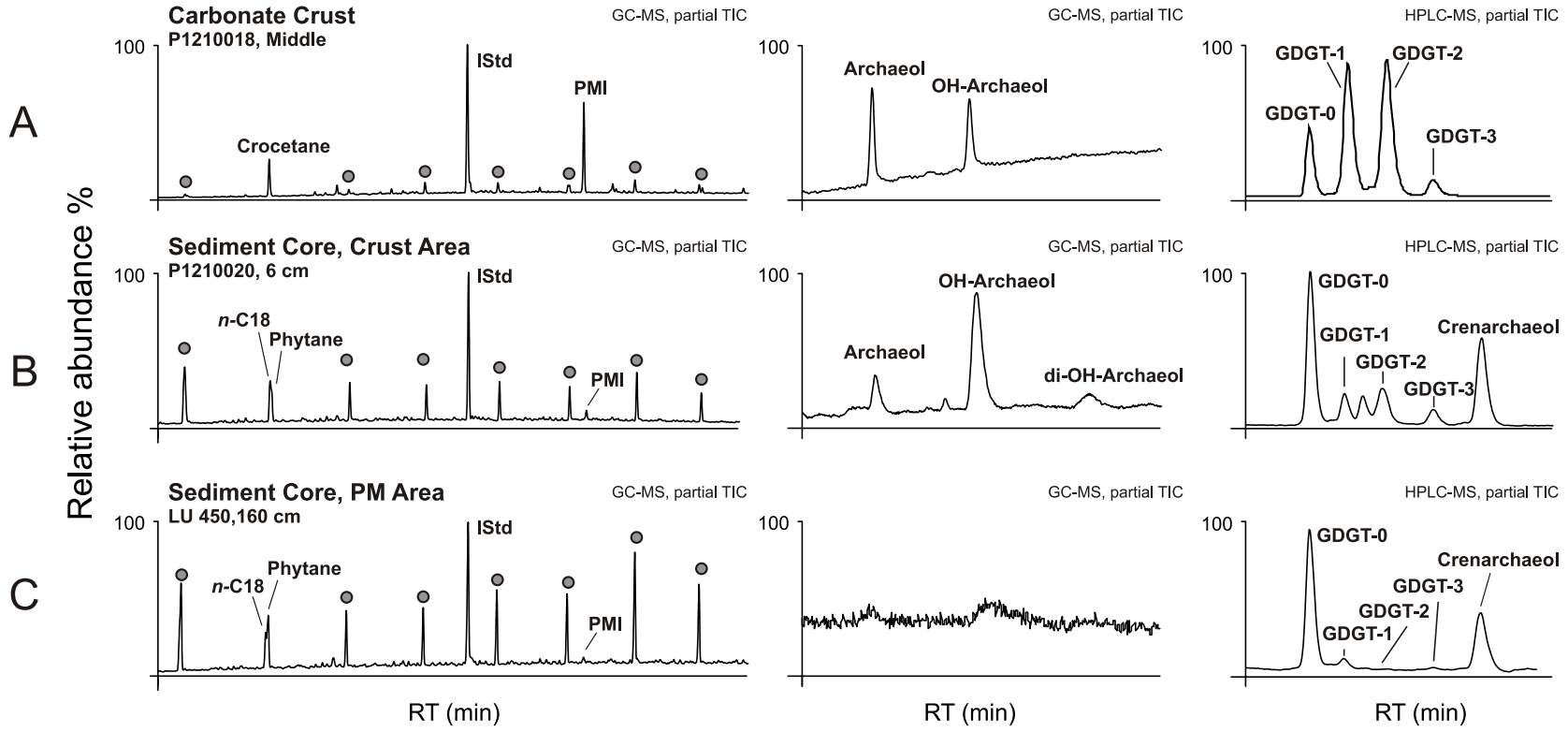

Figure 4.3: Exemplary chromatograms showing characteristic archaeal biomarkers such as archaeol, hydroxyarchaeol, dihydroxyarchaeol, crocetane, pentamethylicosane (PMI) and glycerol dialkyl glycerol tetraethers (GDGTs) for the three sample types investigated: Carbonate crust and sediment core both from carbonate crust area PR4 and sediment core LU450 from pockmark area B. IStd: internal standard. TIC: Total ion chromatogram.

Table 4.2: Concentration of selected microbial biomarkers in the carbonate crust sample (P1210018) from area PR4. PMI = pentamethylicosane; OH-archaeol = hydroxyarchaeol; GDGT = glycerol dialkyl glycerol tetraether; PLFA = phospholipid fatty acids; CC: carbonate crust.

	P1210018		
Compounds	top (ng/g CC)	middle (ng/g CC)	bottom (ng/g CC)
Crocetane	86.3	53.5	74.9
PMI	136.5	109.0	218.0
Archaeol	2383	2088	3597
OH-archaeol	4591	1795	2496
Σ GDGTs	1471	5566	11433
Σ PLFAs	452	581	573

Carbonate crust (CC) samples

In the carbonate crust (CC) samples (top, middle, bottom part of P1210018; Figure 4.2) from area PR4, archaeol and hydroxyarchaeol was present in high amounts (archaeol: 2088-3597 ng/g CC and hydroxyarchaeol: 1795-4591 ng/g CC; Table 4.2). The relative proportions of archaeol and hydroxyarchaeol varied within the crust. For example, in the top part of the crust hydroxyarchaeol was more abundant than archaeol, whereas in the middle and bottom intervals archaeol was slightly more abundant than hydroxyarchaeol. The $\delta^{13}C$ values determined exemplarily for the bottom sample from the carbonate crust were 110.7‰ for archaeol and 112.7‰ and 113.5‰ for hydroxyarchaeol as di- and mono trimethylsilylated (TMS) derivatives, respectively (Table 4.3). PMI and crocetane were the dominant compounds in the aliphatic fractions of the crust samples. Generally, crocetane (75-86 ng/g CC) was less abundant than PMI (109-218 ng/g CC) (Figure 4.3A, Table 4.2). Both compounds were significantly depleted in ^{13}C with $\delta^{13}C$ values ranging between 100.5‰ and 108.5‰ for crocetane and 111.3‰ and 113.2‰ for PMI (Table 4.3). Additionally, minor amounts of the unsaturated homologues (like crocetenes and pentamethylicosenes) could be traced, but not quantified.

High amounts of GDGTs ranging between 1471-11433 ng/g CC were found (Table 4.2). All three parts showed a similar isoprenoidal GDGT composition

Table 4.3: δ^{13}C signal given in ‰ of selected archaeal biomarkers in the carbonate crust sample (P1210018) and the sediment core (P1210020) both from the carbonate crust area PR4. PMI: pentamethylicosane, EL: etherlipid, n.d.: not determinable, n.a.: not analyzed, TMS: trimethylsilyl.

	δ^{13}C (‰)				
Sample Type	**Carbonate Crust Core**		**Carbonate Crust**		
Interval	2 cm	6 cm	top	middle	bottom
Crocetane	n.d.	n.d.	-107.5	-100.5	-108.5
PMI	n.d.	n.d.	-111.5	-111.3	-113.2
Archaeol	-115.0	-102.0	n.a.	n.a.	-110.7
Hydroxyarchaeol (monoTMS)	/	/	n.a.	n.a.	-113.5
Hydroxyarchaeol (diTMS)	-111.7	-111.8	n.a.	n.a.	-112.7
Dihydroxyarchaeol	-108.5	-116.3	n.a.	n.a.	/
EL-0	n.d.	n.d.	-106.3	-112.4	-111.4
EL-1	n.d.	n.d.	-106.4	-112.5	-112.0
EL-2	n.d.	n.d.	n.d.	-113.2	-113.2

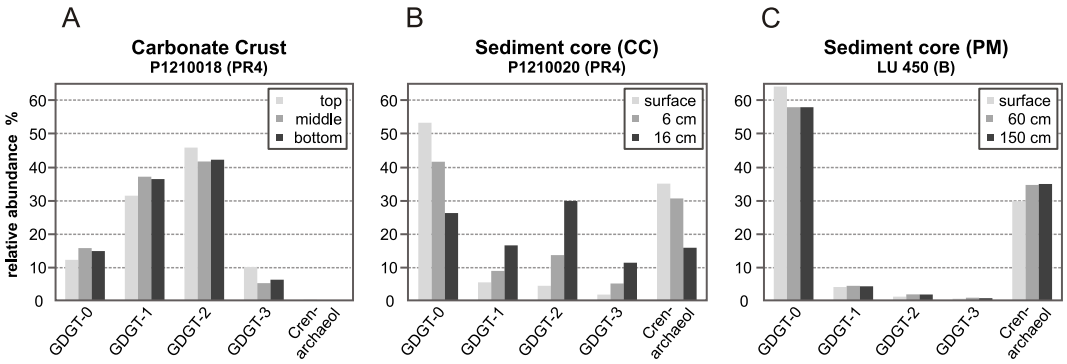

Figure 4.4: Relative abundance of isoprenoid GDGTs within different intervals for A) the top, middle and bottom part of the carbonate crust sample P1210018 from the carbonate crust area PR4 B) the surface, 6 and 16 cm intervals of the sediment core P1210020 from the carbonate crust (CC) area PR4 and C) the surface, 60 and 150 cm intervals of the sediment core from pockmark (PM) LU450 from the pockmark area B.

with GDGT-1 (31-37%) and GDGT-2 (41-46%) being the dominating compounds followed by GDGT-0 (12-16%) and GDGT-3 (5-10%) (Figure 4.4A). Crenarchaeol was only present in traces of less than 0.5% (Figures 4.3A and 4.4A). Cleavage of the ether bonds in GDGTs resulted in the formation of acyclic- (EL-0) monopentacyclic (EL-1) and dipentacyclic (EL-2) biphytane molecules (Appendix A). The acyclic biphytane can be released from GDGT-0, -1 or -2, the monopentacyclic biphytane from GDGT-1, -2 and -3. The δ^{13}C values of the three biphytanes (EL-0, EL,-1, EL-2) are highly depleted in ^{13}C ranging from 106.3 to -113.2‰ (Table 4.3).

Sediment from the carbonate crust area

In the sediment from the carbonate crust area (PR4) archaeol and hydroxyarchaeol were present within the entire depth interval of the analyzed core P1210020 (Figure 4.5A). Additionally and in contrast to the carbonate crust, small amounts of dihydroxyarchaeol could be traced in the depth intervals between 2 and 8 cm (Figure 4.5A). Archaeol was present in amounts ranging between 107-376 ng/g Sed and was generally less abundant than hydroxyarchaeol ranging between 193-1544 ng/g Sed. Dihydroxyarchaeol accounted for 63 to 293 ng/g Sed. Plotted against depth, the concentration of all archaeol derivatives showed increased values between 3 and 9 cm with a maximum at a depth of 6 cm (Figure 4.5A). The δ^{13}C values determined for selected intervals of the core (2 and 6 cm depth) ranged between -102 and -115‰ for

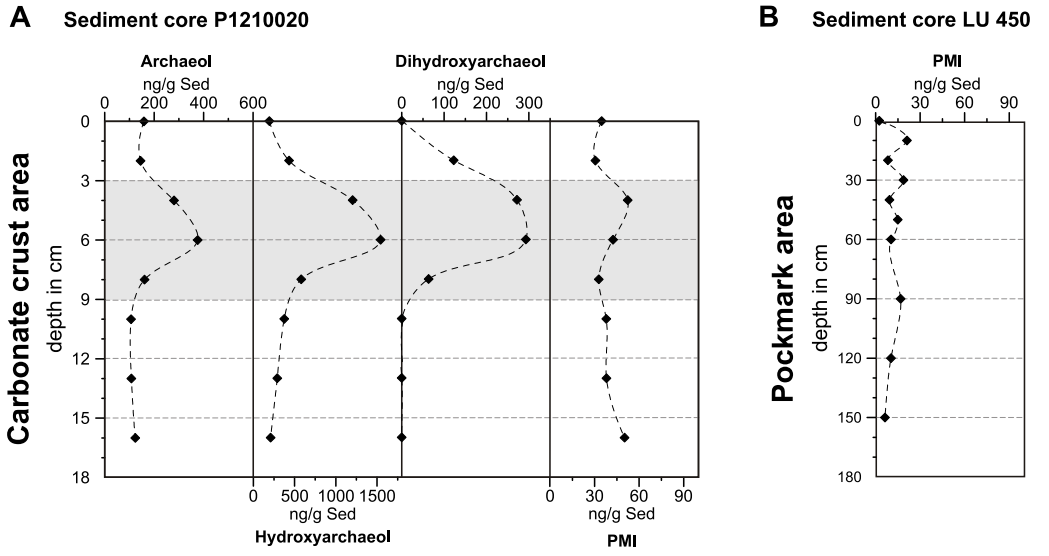

Figure 4.5: Diagrams showing the depth profiles of A) archaeol, hydroxyarchaeol, dihydroxyarchaeol and pentamethylicosane (PMI) for the sediment core in the carbonate crust area PR4 and B) PMI for the pockmark core from the pockmark area B. The shaded area indicates the presumed AOM (anaerobic oxidation of methane) zone.

archaeol, -111.7 and -111.8‰ for hydroxyarchaeol and -108.5 and -116.3‰ for dihydroxyarchaeol (Table 4.3).

Pentamethylicosane (PMI) was also present in all depth intervals, although in much lower amounts than the isoprenoidal diethers. The concentrations generally ranged between 31-52 ng/g Sed. A small maximum was also obvious between 3 and 9 cm (Figure 4.5A). For δ^{13}C analyses the compound concentrations were too low. Crocetane could be detected in traces. However, with the GC-column used reliable quantification was impossible due to co-elution with phytane and n-C_{18} alkane.

Archaeal GDGTs were present in significant concentrations. The total concentration ranged between 128 and 291 ng/g Sed. The absolute amounts of the archaeal GDGTs were generally 20 times lower than in the carbonate crust from the same area. A small maximum at 6 cm depth was observed, which is mainly derived from slightly increased concentrations of GDGT-0, GDGT-1, GDGT-2 and crenarchaeol. Below 8 cm an increasing trend with depth in the total GDGT concentration was found, which arises from an increase of mainly GDGT-1 and GDGT-2 as well as slightly of GDGT-0 and GDGT-3 (Figure 4.6). In contrast, crenarchaeol remains relatively constant or even decreases

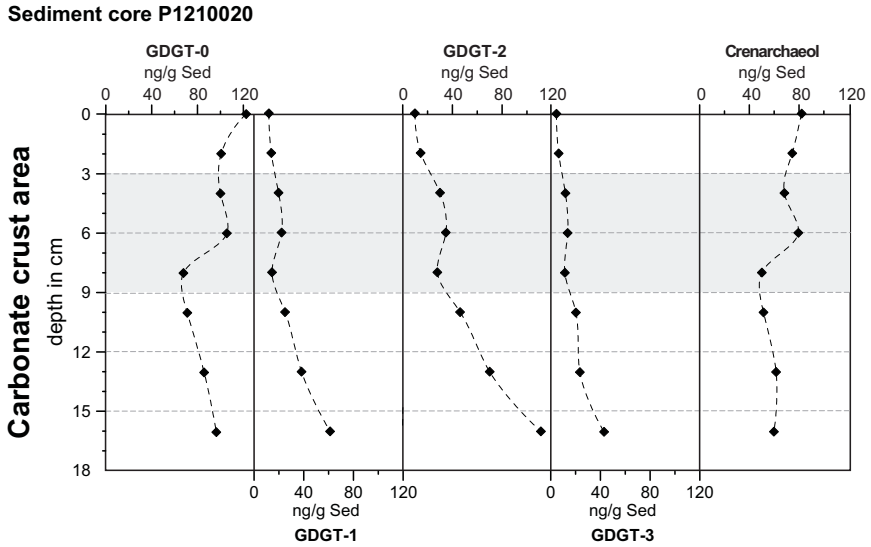

Figure 4.6: Diagrams showing the depth profiles of the glycerol dialkyl glycerol tetraethers (GDGTs) with 0, 1, 2, and 3 cyclopentyl rings and crenarchaeol for the sediment core P1210020 taken in the carbonate crust area PR4. The shaded area indicates the presumed AOM (anaerobic oxidation of methane) zone.

slightly (Figure 4.6). This trend becomes more obvious when comparing the relative GDGT-compositions of the surface, 6 cm and deepest sample. In the surface sample, GDGT-0 and crenarchaeol dominated with 53% and 35%, respectively. In the 6 cm sample, GDGT-0 (42%) and crenarchaeol (31%) decreased, while GDGT-1, GDGT-3 and mainly GDGT-2 (14%) increase (Figure 4.4B). This trend continued in the deepest samples, where GDGT-2 became the dominant component (30%).

Sediment from the pockmark area

In the pockmark (PM) core (LU450) from area B archaeol and hydroxyarchaeol were absent (Figure 4.3C). The mass spectra of the small peaks in Figure 4.3C could neither be assigned to archaeol nor hydroxyarchaeol. Crocetane was also absent in the sediment samples of the PM core. PMI was present only in marginal amounts ranging between 2.4-21.1 ng/g Sed (Figure 4.5B).

GDGT-0 and crenarchaeol were by far the most prominent compounds of all archaeal GDGTs. Their relative abundance comprised up to 64% and 37%, respectively. GDGT-1 to -3 were present only in minor amounts (Figure 4.4C). A comparison between samples from the surface, from 60 cm and 150 cm shows

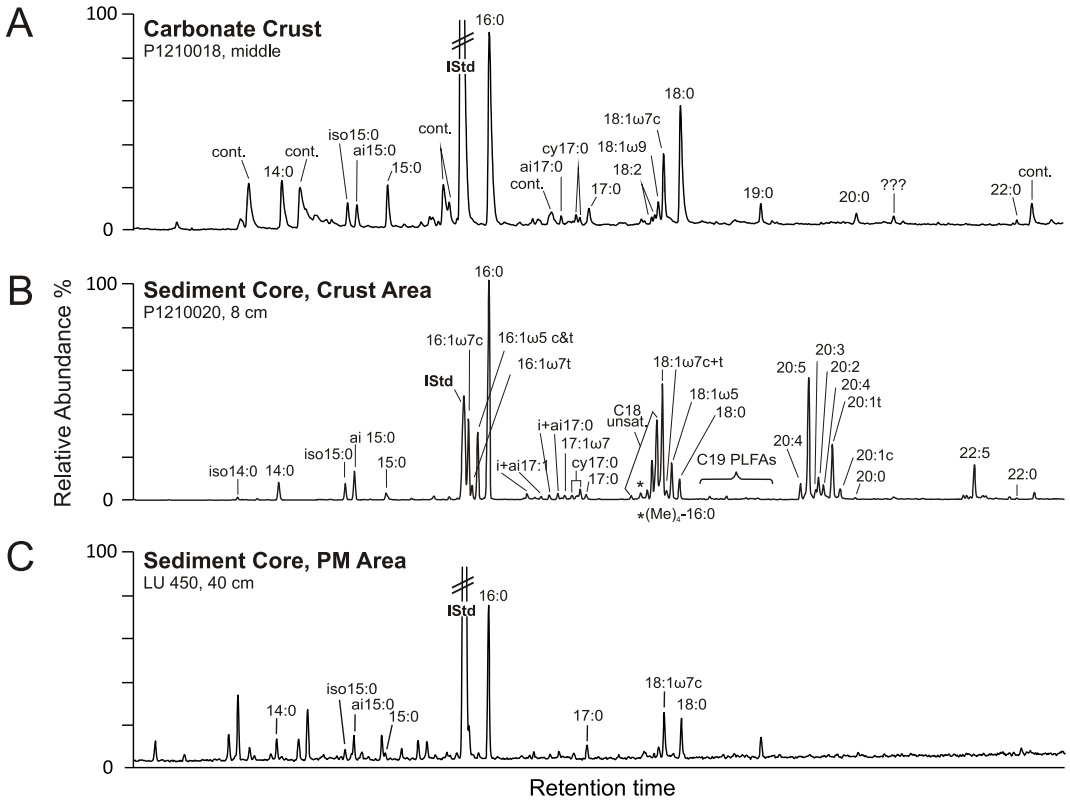

Figure 4.7: Exemplary chromatograms for the characteristic bacterial biomarkers (phospholipid fatty acids, PLFA) for the three sample types investigated: Carbonate crust and sediment core both from carbonate crust area PR4 and sediment core from pockmark LU450 from pockmark (PM) area B.

that the relative proportions of the GDGTs does not change significantly with depth. The total archaeal GDGTs concentration (41-438 ng/g Sed), however, was similar to the amounts of GDGTs detected in the sediment core from the carbonate crust area.

4.4.3 Characteristic biomarkers for bacterial communities

Exemplary partial total ion chromatograms for the analyzed biomarkers characteristic for bacterial communities (phospholipid fatty acids, PLFA) are shown in Figure 4.7.

Carbonate crust samples

The carbonate crust revealed a series of saturated- ($C_{14:0}$ to $C_{20:0}$), branched- (*iso/anteiso*-$C_{15:0}$, *iso/ai*-$C_{17:0}$) unsaturated- ($C_{18:1\omega7c}$ and $C_{17:1\omega8}$) PLFAs as

Table 4.4: δ^{13}C signal given in ‰ of selected phospholipid fatty acids (PLFAs) in the sediment core (P1210020) from the carbonate crust area PR4. n.d.: not determinable.

	δ^{13}C (‰) in Carbonate Crust Core			
Interval	0 cm	2 cm	4 cm	6 cm
ai-$C_{15:0}$	n.d.	-72.0	-76.2	-87.5
$C_{16:1\omega5}$ *cis* + *trans*	-56.2	-69.8	-65.3	-65.8
$C_{20:5}$	-39.2	-52.0	-42.2	n.d.
$C_{22:5}$	-43.0	-55.0	-42.3	-40.4

well as the cyclopropyl-$C_{17:0}$ fatty acid. The most prominent compounds were $C_{16:0}$, $C_{18:0}$ and $C_{18:1\omega7c}$ PLFAs. The concentration of the total PLFAs, with 452-581 ng/gCC, did not vary much within the top, middle and bottom sample (Table 4.2).

Sediment from the carbonate crust area

In contrast to the PLFA composition in the carbonate crust, the sediment from the crust area revealed a broader range of different PLFAs. Especially, a higher diversity in mono- and polyunsaturated PLFAs with 16, 18 and 20 carbon atoms was observed. Additional PLFAs were *iso*-$C_{14:0}$, *cis*- and *trans*-$C_{16:1\omega7}$, *cis*- and *trans*-$C_{16:1\omega5}$, *iso*- and *anteiso* $C_{17:1}$, polyunsaturated C_{18} PLFAs, *cis*- and *trans*-$C_{18:1\omega7}$, $C_{18:1\omega5}$, $C_{19:1\omega9}$, a range of mono- to polyunsaturated C_{20} compounds and $C_{22:5}$ fatty acid (Figure 4.7B). The total concentration of PLFA was higher than in the carbonate crust samples. The depth profile of the total PLFA-signal in general decreases from the surface sediment (17938 ng/g Sed) to the 16 cm sample (503 ng/gSed). However, the data reveal an intermediate increase between 2 and 8 cm with values up to 12028 ng/gSed. The same trend was observed for selected PLFAs such as the *iso*-, *ai*-$C_{15:0}$, *cis*- and *trans*-$C_{16:1\omega5}$, $C_{20:5}$ and $C_{22:5}$ fatty acids (Figure 4.8A). δ^{13}C measurements of selected samples demonstrated relatively negative values for the *ai*-$C_{15:0}$ ranging between -72 and -87.5‰ and for the *cis*- and *trans*-$C_{16:1\omega5}$ ranging between -56.2 and -69.8‰. Additionally, also $C_{20:5}$ and $C_{22:5}$ showed ^{13}C depleted values between -39.2 and -55.0‰ (Table 4.4).

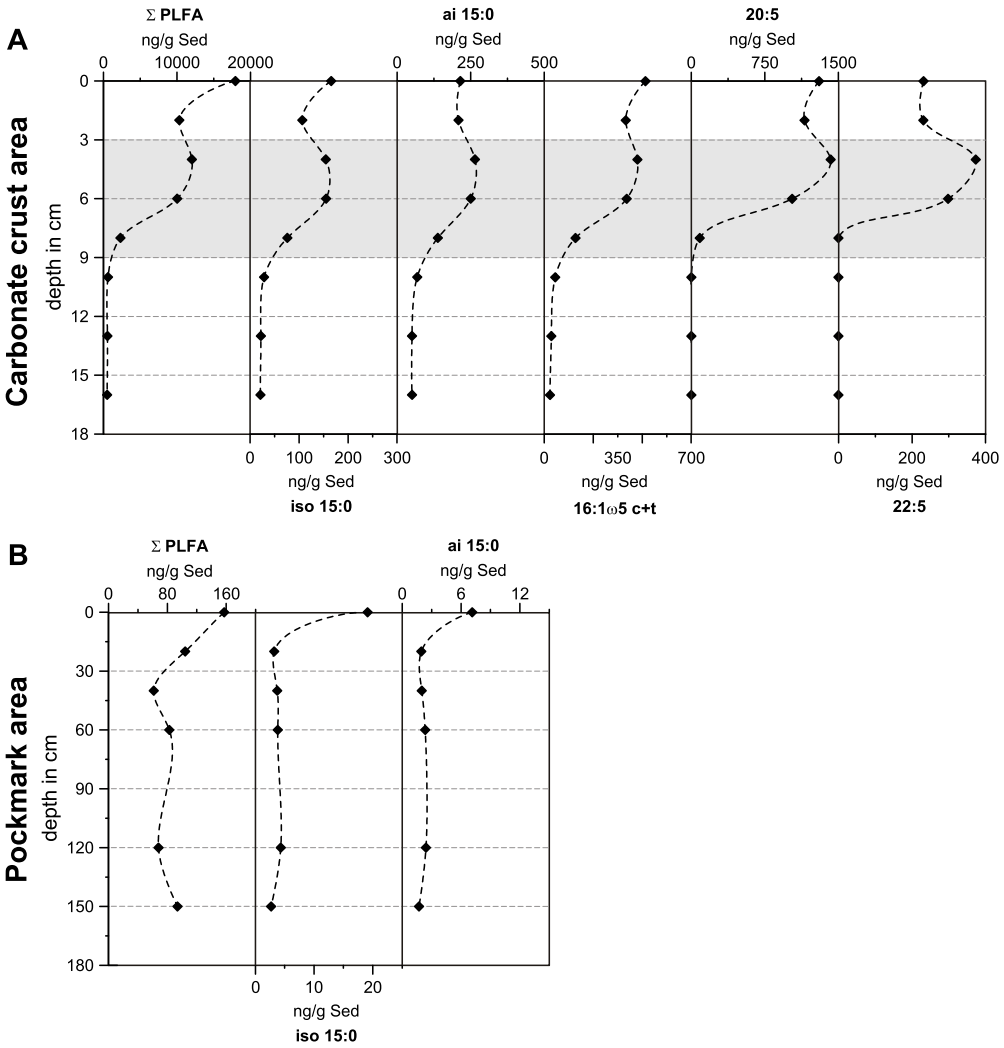

Figure 4.8: Depth profiles showing the abundance of total phospholipid fatty acids (Σ PLFAs) as well as selected PLFAs for A) the sediment core P1210020 taken in the crust area PR4 and B) the sediment core LU450 taken in the pockmark area B. The shaded area indicates the presumed AOM (anaerobic oxidation of methane) zone.

Sediment from the pockmark area

In the sediment of the pockmark area, the PLFA composition was characterized by the abundance of $C_{16:0}$, $C_{18:0}$ and $C_{18:1\omega7c}$ compounds, which is similar to the carbonate crust sample. Although present in only low concentrations, other PLFAs include $C_{14:0}$, *iso*/*ai*-$C_{15:0}$ and $C_{15:0}$. The total PLFA concentrations were lower than in the carbonate crust ranging from 61 to 157 ng/gSed. Highest total PLFA concentrations were observed for the surface sample followed by a significant decrease in the upper 30 cm. Further downcore, the concentration remained relatively constant (Figure 4.8B). Similar trends were recognized for the *iso*/*ai*-$C_{15:0}$ fatty acids (Figure 4.8B).

4.5 Discussion

4.5.1 Archaeal and bacterial biomarkers in a carbonate crust and sediments from the SW Barents Sea

Carbonate crust (CC)

The carbonate crust material from area PR4 contained significant amounts of specific archaeal biomarkers like archaeol, hydroxyarchaeol, pentamethylicosane (PMI) and crocetane (Figure 4.3). Their carbon isotope signatures revealed a strong depletion in ^{13}C (Table 4.3), indicating that the corresponding archaea are involved in the process of anaerobic oxidation of methane (AOM, Blumenberg et al. 2004; Hinrichs et al. 1999; Pape et al. 2005), utilizing methane as a carbon and energy source (Hayes et al., 1990; Whiticar, 1999).

Isoprenoid GDGTs, indicative for archaea, were also found in high concentrations in the crust material. The high relative abundance of GDGT-1 and -2 compared to GDGT-0 and crenarchaeol (Figure 4.3A and 4A) seems to be a feature for archaeal communities involved in AOM. This has been inferred by several authors who described elevated concentrations of GDGT-1 and -2 in sediment from cold seeps (Pancost et al., 2001; Zhang et al., 2011), sediment characterized by diffusive methane flux (Weijers et al., 2011) as well as in carbonate crusts samples (Bouloubassi et al., 2006). The strongly negative carbon isotope signatures of the biphytanes with 0 to 2 cyclopentyl rings (Table 4.3)

that were obtained after ether cleavage of the GDGTs confirm that the producing archaea participated in the AOM process (Aloisi et al., 2002; Schouten et al., 1998; Thiel et al., 2001). The variability in the relative proportions of the archaeal biomarkers (PMI vs. crocetane; archaeol vs. hydroxyarchaeol; GDGT and/or biphytane abundance) between the top, middle and bottom part of the crust (Table 4.2) might reflect variations in the composition of ANME (Blumenberg et al., 2004; Niemann and Elvert, 2008).

In contrast to the high abundance of archaeal AOM related biomarkers, only relatively low amounts of bacteria-derived phospholipid fatty acids (PLFAs) were detected. Biomarkers specific for sulfate reducing bacteria (SRB) such as *iso* , *ai*-C_{15}; *iso*-, *ai*-C_{17}; $C_{16:1\omega5}$ cyclo-$C_{17:0}$ (Elvert et al., 2003; Nauhaus et al., 2007; Niemann and Elvert, 2008), were found only in relatively low concentrations. This observation is most likely due to the fact that the crust represents an ancient AOM setting, now exposed to the seafloor as a consequence of an exhumation process (Naehr et al., 2007). Intact phospholipids might already be partly degraded since they are considered to be indicators for living bacteria (life markers) due to rapid degradation after cell death (White et al., 1979; Zink and Mangelsdorf, 2004; Zink et al., 2003).

Overall, the presence of the archaeal and bacterial biomarkers, together with the highly negative $\delta^{13}C$ signatures of the archaeal compounds and the carbonate itself (-36‰) indicate that the crust was formed as a result of AOM (Crémière et al., 2011; Peckmann and Thiel, 2004).

Sediment core from carbonate crust area

In the sediment core from the crust area PR4 specific ^{13}C-depleted archaeal biomarkers like archaeol, hydroxyarchaeol and dihydoxyarchaeol as well as PMI were abundant (Table 4.3). Crocetane was present only in traces. The depth profiles of these biomarkers show an increased concentration between 2 and 9 cm depth with a maximum at about 6 cm (Figure 4.5A). Together, our data point at an AOM zone (2 and 9 cm) in the sediment from the carbonate crust area.

The presence of an AOM zone in this interval is supported by depth profiles of GDGT 0, 1 and 2 (Figure 4.6), which show slightly elevated values around 6 cm depth. However, also crenarchaeol shows a small increase at the same depth. Relative abundance of archaeal GDGTs changes with depth. In the

uppermost sample a typical marine GDGT pattern (Sinninghe Damsté et al., 2002; Wakeham et al., 2003; Wuchter et al., 2003) dominated by GDGT-0 and crenarchaeol is observed. At 6 cm depth this pattern changes to less GDGT-0 and and enhanced GDGT 1 and 2 abundances (Figures 4.4B and 4.6). As mentioned above, a relative increase of GDGT 1 and 2 to GDGT 0 and crenarchaeol is typically observed in AOM areas. However, the relative increase of GDGT 1 and GDGT 2 continues further down core (Figure 4.4B) until, in the deepest sample of the core (16 cm), GDGT 2 is the dominating compound (Figures 4.4B and 4.6). This continuous increase of GDGT 1 and 2, which is considered to be indicative for AOM, is remarkable, since none of the other lipid biomarkers diagnostic for AOM show this increase with depth, except for their local maximum at 6 cm. It is still unclear how the increase of GDGT 1 and 2 in the crust core can be interpreted.

PLFAs were also detected in high abundance (Figure 4.8A), indicating an intensive bacterial life in the upper 10 cm of the investigated core from the carbonate crust area. Bacterial PLFAs including those fatty acids being diagnostic for SRB like iso $C_{15:0}$, *ai*-$C_{15:0}$, cyclo-$C_{17:0}$ and $C_{16:1\omega5}$ (Elvert et al., 2003; Nauhaus et al., 2007; Niemann and Elvert, 2008) were detected in varying patterns (Figure 4.7). The high abundance of PLFA at the sediment surface (Figure 4.8A) is explainable by contributions of fresh material and a wide variety of living bacterial organisms on the seafloor. However, a maximum in PLFA concentration was also found in the interval between 2 and 8 cm depth, overlapping with the maximum of archaeal biomarkers denoting the zone where AOM seems to take place. This is also confirmed by the pronounced maxima of specific fatty acids being common in SRBs within this interval (Figure 4.8A) as well as their ^{13}C-depleted isotope signatures (Table 4.4). The ^{13}C depletions were most pronounced for *ai*-$C_{15:0}$ as well as *cis*- and *trans*-$C_{16:1\omega5}$ PLFAs. Additionally, also $C_{20:5}$ and $C_{22:5}$ reveal maximum concentrations in the presumed AOM zone. Formerly highly polyunsaturated fatty acids like $C_{20:5}$ and $C_{22:5}$ were considered to be exclusively attributed to eukaryotic algae (Volkman et al., 1998). However, more recent studies showed that these compounds can also be derived from bacteria (e.g. Freese et al. 2009; Metz et al. 2001). Fang et al. (2006) described the presence of $C_{20:5}$ PLFAs in cold seep sediment, however, they did not assign their occurrence to the presence

of SRB. A significant rise in concentration of these polyunsaturated PLFAs in the presumed AOM zone along with their negative $\delta^{13}C$ values might imply the involvement of the source organism in AOM or feeding on ^{13}C-depleted biomass.

Overall the depth profiles of the bacterial and archaeal biomarkers in the sediment core from the crust area indicate the presence of a consortium of SRB and archaea mediating the process of AOM at a depth interval between 2 and 8 cm. Since the PLFAs are the result of the hydrolysis of intact phospholipids, being indicators for living bacteria, their depth profiles, especially of those being indicative for SRB, point towards a currently active AOM zone. The depth of this AOM zone is remarkably shallow. However, Niemann et al. (2006) also observed AOM activity close to the seabed (2-4 cm) in the sediment of the Haakon Moosby Mud Volcano. Furthermore, in upper slope sediments from the Chilean continental margin Treude et al. (2005b) reported about methane oxidation close to the surface significantly above the sulfate methane transition zone (SMTZ). It is conceivable, that something comparable is also observed in the carbonate crust area PR4 and that the actual SMTZ is located in the deeper part of the sediment not recovered by the 19 cm long push core.

Sediment core from the pockmark area B

In contrast to the carbonate crust area, specific archaeal biomarkers excluding PMI, which was traced only in small amounts, are absent in the pockmark sediment (Figure 4.5B). The absence or low abundance of AOM related archaeal biomarkers suggest that AOM does not play a significant role in the pockmark sediment recovered.

Total PLFAs are also a hundred-fold lower, indicating much lower microbial life in the pockmark core than in the sediment core from the crust area. Also the *iso*- and *ai*-$C_{15:0}$ fatty acid concentrations are much lower suggesting only low rates of sulfate reduction. This is in accordance with the findings of Nickel et al. (2012) who described the absence of seepage gas in the investigated pockmark cores from area B as well as extremely low sulfate reduction rates.

Biomarkers indicative for archaea were recognized mainly by the presence of GDGTs in similar concentrations as in the sediment from the carbonate crust area. However, GDGT-0 and crenarchaeol are the dominant compounds throughout the entire core material representing the typical marine sedimen-

tary GDGT record from marine water columns (Sinninghe Damsté et al., 2002; Wakeham et al., 2003; Wuchter et al., 2003). A distinct shift to more GDGT-1 and -2 as seen in the crust area was not observed in the pockmark sediment. Hence, from the GDGT distribution pattern in the investigated pockmark sediment, the presence of an AOM zone cannot be inferred.

These biomarker findings hold also true for other PM (2 cores) and reference cores (2 cores) taken in area B (data not shown), which show similar qualitative and quantitative biomarkers distributions.

It might be argued that due to the lower sample resolution of the pockmark core (first meter of the core was split into ten 10 cm subintervals) as compared to the core from the carbonate crust area (first 10 cm were subdivided into five 2 cm intervals), an AOM zone as in the crust area might be overlooked (Figure 4.8) since the extent of the AOM zone can be limited to a range of a few centimeters (e.g. Niemann et al. 2006; Pohlman et al. 2011). However, in a 10 cm section containing an AOM zone of several centimeters, the typical markers diagnostic for AOM processes should be detectable, which was not the case in any of the pockmark cores investigated from area B neither in the surface samples nor in deeper sedimentary intervals. Carbonate crust pieces were also never found in the recovered pockmark material. Additional evidence for the absence of an AOM zone is given by the study conducted by Nickel et al. (2012) who determined the corresponding sulfate profiles of several cores in area B. Despite a small decrease with depth, which could be attributed exclusively to diffusion, there was no significant change in sulfate concentration. The lack of an AOM zone in the studied Barents Sea pockmark (area B) is in accordance with measurements on the pockmark material, showing no free gas and only very small amounts of adsorbed and occluded gas (Nickel et al., 2012).

4.5.2 Origin and formation of different seeping structures in the SW Barents Sea

The findings of the current study imply that there are at least two different seeping systems on the seafloor of the investigated area of the SW Loppa High, an active and an inactive system. The active seeps are characterized by carbonate crusts, the occurrence of diagnostic AOM biomarkers, microbial life

markers (intact phospholipids) and relatively high gas concentrations in the sediment. In contrast, the extensive pockmark fields appear to be inactive at present, considering the absence of diagnostic AOM biomarkers, extremely low gas concentrations and generally low microbial activity (Nickel et al., 2012).

The presence of these active and inactive seeping systems in close vicinity is an intriguing feature. In a gas and oil prospective area such as the SW Barents Sea, the feeding of these systems by an underlying thermogenic hydrocarbon source is likely. At least in the crust area, this is supported by the observation of seeping gas with a $\delta^{13}C$ value of -47.8‰ in crust area PR1, most likely an analogue to area PR4. However, the different activity of the seeping systems implies different geological histories and formation scenarios.

Crust area PR4 is located in the western part of the Loppa High at the northern edge of the Polheim Sub-Platform. It is situated close to the newly discovered oil fields Skrugard and Havis (Figure 4.1), which have been estimated to contain at least 300 million barrels of oil and gas each (Maugeri, 2012). Within that area, gas anomalies (Andreassen and Hansen, 1995) as well as bottom simulating reflectors (BSR) have been observed, indicating the presence of gas hydrates in the subsurface (Shipley et al., 1979). Chand et al. (2012) supported the presence of gas in the subsurface by seismic interpretation and disclosed the presence of gas flares connected to faults in the subsurface. Generally, the whole area surrounding the Polheim Sub-Platform is known for numerous faults of varying sizes (Gabrielsen et al., 1990). As shown in seismic data (Figure 4.9), area PR4 is also the surface manifestation of an underlying fault system. It is conceivable that this active seep structure is related to thermogenic gases migrating upwards along fault systems in the subsurface from hydrocarbon reservoirs such as the Skrugard field (Figure 4.9).

In contrast to the carbonate crust area PR4, all data obtained from the current study and from Nickel et al. (2012) point to presently inactive pockmark structures in area B indicating that their formation is dated back to former times. The existence, the wide distribution and the high number of the pockmarks require a more complex formation scenario.

Using high resolution SBP (sub-bottom profiler) images of PMs, Chand et al. (2012) were able to show that the present pockmarks were formed during the last deglaciation period, since the pockmarks cut through the glaciomarine

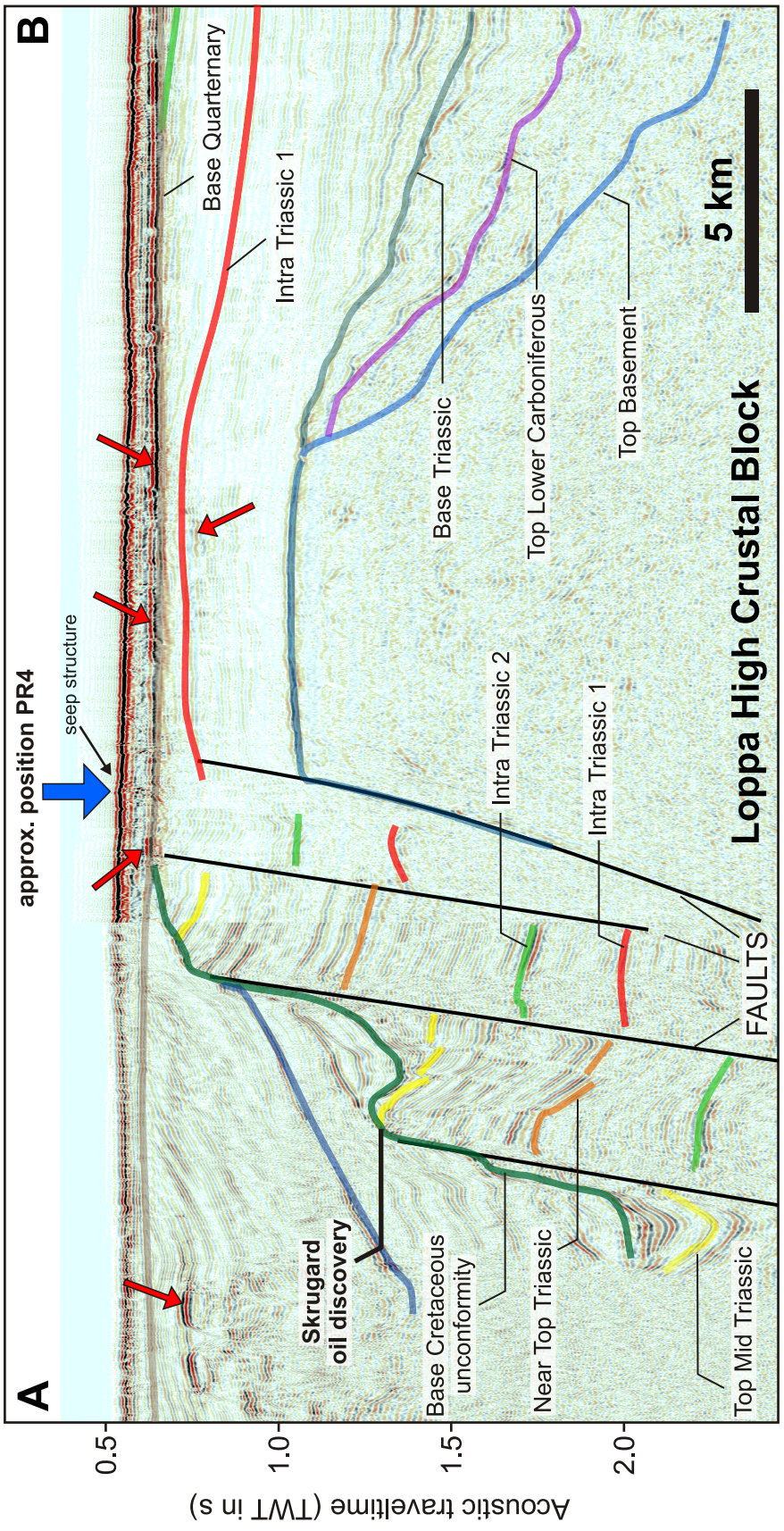

Figure 4.9: Seismic line (see Figure 4.1 for position) showing the regional position of PR4 in relation to the Skrugard oil discovery. Colored lines represent interpreted seismic horizons, black lines mark faults. Gas anomalies in the shallow sediments are marked by red arrows. Shallow gas anomalies in the western area are partly sealed by gas hydrates.

deposits. This is also supported by the observation of pockmarks occurring within plough marks of drifting icebergs (Nickel et al., 2012). It is known that during the Last Glacial Maximum the entire area was covered by a thick ice shield (e.g. Andreassen et al. 2008; Siegert et al. 2001). Hydrocarbon gases from reservoirs present in the deeper subsurface might have migrated upwards through the sediment towards the surface and accumulated under the ice shield. Due to prevailing pressure and temperature these gases were trapped as gas hydrates in the sediment below the ice. With the retreat of the glaciers about 14 ka ago (Elverhøi et al., 1995) these gas hydrates might have decomposed, resulting in a massive release of large volumes of gas over a huge area which formed the pockmark fields (Nickel et al., 2012). Since there is no gas left from this event today (Nickel et al., 2012) the source of the migrating hydrocarbon gases (e.g. thermogenic vs. biogenic gases) cannot be determined. However, several oil and gas fields in the SW Barents Sea (e.g. Snøhvit) are known to occur in underfilled traps (Corcoran and Doré, 2002), indicating past leakage of thermogenic gas which might have sourced the gas hydrates.

Even though migration of gas often occurs along with oil migration (Hvoslef et al., 1996), indications for simultaneous or subsequent migration of oil could not be detected in the pockmark cores of area B (Nickel et al., 2013). It might be also argued that the formation of the pockmark fields is a result of, for instance, episodic gas release or the escape of porewater. However, such scenarios are more localized phenomena and cannot explain these large pockmark fields.

Due to the absence of indications for gas, neither for present day activity nor for the dissociation of gas hydrates in the sediment of the studied pockmarks of area B, it might be claimed that the cores with a maximum length of 2.5 m are too short and have never reached the interface of pockmark formation. However, foraminiferal age assessment of selected intervals from the pockmark core LU450 from pockmark area B showed that the sedimentary record of the investigated pockmark core covers an age interval larger than the assumed age of the pockmarks (Nickel et al., 2013). Thus, the fact that no AOM related biomarker signals could be observed in the pockmarks might point to a very rapid process of gas release preventing an extensive establishment of associated microbial communities. Indications for a massive or maybe explosive gas

release are provided by Pau and Hammer (pers. comm.) who observed the loss of sedimentary layers in a pockmark core from the Loppa High area when comparing it to a reference core.

The current results show that even in areas located at short distances to each other, different gas discharge scenarios can develop. Moreover, the close vicinity of the seep and seep structures is supportive for the hypothesis that these structures are related. The fault systems in this area are numerous (Chand et al., 2012) forming conduits for migrating gas from deeper hydrocarbon systems. Still active gas seeps in areas PR4 and PR1 might be examples of this process. During glacial times a thick ice shield prevented the release of migrating gas by sealing the sediment surface. In consequence the gas accumulated over thousands of years below the ice and might have migrated laterally into specific areas such as area B where it was trapped as gas hydrates. During deglaciation the gas hydrates rapidly decayed leaving behind a large field of currently inactive pockmarks.

4.6 Conlusions

Different seep structures from two study areas on the seafloor of the SW Loppa High in the SW Barents Sea were investigated using organic biogeochemical analyses. One area is characterized by a large field of pockmarks (area B), and the other area by patchy carbonate crusts (PR4) located further to the north at the western edge of the Loppa High. To gain information on the activity and formation of the different seepage structures sediment cores from the pockmark and the carbonate crust area, as well as carbonate crust material were analyzed with the focus on AOM diagnostic biomarkers.

The sediment from the carbonate crust area contained bacterial and archaeal AOM biomarkers with a maximum abundance within the same depth interval between 3-8 cm. δ^{13}C values of these biomarkers showed strong depletion in ^{13}C, demonstrating the participation of the source microorganisms in the process of AOM. Visual observation of gas escape during sampling and the presence of life markers (fatty acids from intact phospholipids) with highly negative δ^{13}C values further point towards an active gas seepage site. Similar AOM biomarkers with low δ^{13}C values were also found in an authigenic carbonate crust indicating the formation of the crust as a result of AOM.

In contrast, in sediment cores retrieved from the pockmark field AOM biomarkers were essentially absent, indicating that AOM related processes did not play an important role neither at present day nor in the past. This different extent and activity suggests different formation scenarios for the described seeping systems. The seeps in the carbonate crust area seem to be the surface phenomenon of thermogenic gas migrating upwards from deeper hydrocarbon sources along faults to the surface. In contrast, the pockmarks in area B are speculated to be attributed to large volumes of gas accumulated over a large area as gas hydrates under the ice shield covering the Barents Sea during the last glacial period, which rapidly decomposed upon the pressure release due to the retreating ice shield during the last deglaciation. It is conceivable that the faults, nowadays still active, were the conduits for the migrating gas which sourced widespread gas hydrates in area B.

4.7 Acknowledgements

We would like to thank LUNDIN Petroleum Norway for funding the research project. The crew and shipboard scientific party of the R/V HU Sverdrup and the shore based staff of FFI and NGU is thanked for excellent support during the expedition. Alina Koch and Birgit Plessen are acknowledged for analytical support. M. B. thanks the Deutsche Forschungsgemeinschaft for financial support (grant BL 971/1-3).

Chapter 5

Summary and Outlook

5.1 Summary

Hydrocarbon seeps provide a wealth of information on energy and mass fluxes in sedimentary basins. For the petroleum industry they increasingly gain significance as potential indicators for hydrocarbon reservoirs located deeper in the sedimentary column. In addition, they can be used to estimate the seafloor stability, which is important for offshore operations since cold seeps potentially point to the presence of underlying overpressured gas pockets or slope instabilities. Thus, they can raise awareness to prevent operational hazards like blow out scenarios.

Furthermore, it has been proposed that the release of hydrocarbons in the form of cold seeps affects the global carbon cycle, since significant amounts of carbon (e.g., methane and CO_2) can be released to the atmosphere. Thus, formation, migration and degradation of seeping hydrocarbons and their subsequent release from the sediment into the water column and/or atmosphere are key processes which should be considered when evaluating, reconstructing or predicting climate conditions.

The basic approach to understand the fluid flow processes, however, is a detailed assessment of the object's current state. In this context, the following key questions play an important role:

- In which areas does hydrocarbon seepage occur?
- When did the cold seep systems form?

- What is the activity and spatial distribution of the cold seep systems?
- Which sources and triggers caused the presence of hydrocarbon seeps?

The goal of this thesis is to contribute to the understanding of the complex dynamics of cold seeps, their association with underlying sources and their role in the global carbon cycle. Detailed investigations of cold seep systems, with emphasis on their fluid flow activity, should provide an insight into current processes. The southwestern Barents Sea represents a perfect setting for such investigations. Within the last decades the area has developed into a promising region for hydrocarbon exploration due to the discovery of numerous reservoirs (e.g., Hammerfest Basin). The Barents Sea, located in polar latitudes, was strongly influenced by glacial cycles and the resulting dynamics of grounded ice sheets that underwent several periods of buildup and destabilization. Glacier induced erosional phases and severe uplifts are believed to be responsible for leakage events, which caused partial drainage of local reservoirs and the predominance of gas over oil. Due to several tectonic events a complex fault system developed (e.g. Ohm et al. 2008). Thus, the southwestern Barents Sea provides the main preconditions for hydrocarbon leakage to the seafloor, in particular the presence of hydrocarbon sources and the existence of potential migration pathways. Furthermore, huge pockmark fields as well as carbonate crust aggregations as seen in the Loppa High and extensively studied in the present thesis, point to hydrocarbon leakage activity in this area.

Determination of the gas content is a direct approach to trace gas seepage as a consequence of sediment saturated with gas. However, the analysis of the gas concentration alone is insufficient to evaluate a cold seep system. In order to investigate the current processes in a cold seep it is of great use to identify the response of the microbial community to the available hydrocarbons. Since some microorganisms use oil or gas as their carbon and energy source (Foucher et al., 2009) it is possible to identify these specific hydrocarbon-degrading communities if hydrocarbons are present. Different approaches can be used to assess the microbial community, e.g., by determination of microbial activity, pore water geochemistry and the analysis of specific biomarkers in the sediment. These methods provide appropriate tools for the evaluation of the present day situation in the shallow sediment as well as of processes which may

have occurred in the past. Thus, this multidisciplinary approach was chosen to address the key questions mentioned above.

Within this project different study areas have been investigated, all located in the Loppa High. Generally they can be divided into pockmark and carbonate crust areas. The pockmark areas are extensive fields which contain thousands of pockmarks with an average density of 100 pockmarks per square kilometer. Furthermore, they are characterized by many iceberg plough marks that reveal the glacial history of the area. The carbonate crust sites cover much smaller areas. However, due to the carbonate crust patches on the seafloor and gas bubbles emitted from the sediment, these study site are of high interest since these observations provide direct evidence for the presence of gas.

A screening of the pockmark areas was achieved by detailed analysis of several sediment cores from within and outside the pockmark structures combining different geomicrobiological, organic geochemical and geophysical methods.

The analysis of gas in the sediment reveals that only low amounts of adsorbed and very low amounts of free gas are present in all studied cores (Chapter 2). Extremely low microbial activity, as inferred from the quantification of sulfate reduction rates, shows that the microbial community, which is expected to be on site in the presence of methane, is essentially absent. These are first indications for extremely low methane concentrations (Chapter 2). This observation is further supported by the corresponding sulfate profiles which show almost no depletion with depth (Chapter 2). In case of methane oxidation, which is driven by sulfate reduction, a consumption of sulfate and significant sulfate depletion should occur. Additionally, the microbial lipid biomarkers diagnostic for AOM are absent, which supports the previous hypothesis that methane and thus, a corresponding AOM zone, are absent in the depth intervals studied (Chapter 4). In contrast, the analysis of petroleum biomarkers, shows elevated concentrations of petroleum compounds in the investigated sediment samples. This could imply that thermogenic hydrocarbons from deeper sources migrating towards the seabed are responsible for the formation of the pockmark structures. Extensive analysis showed, however, that petroleum compounds are also present in the reference samples which were taken outside of the pockmarks. Even sediment samples from areas that do not contain any pockmark structures show very similar compositions and amounts of petroleum

compounds. It was further shown that the depth profiles of the oil-derived biomarkers exhibit very similar trends compared to the compounds which display the input of immature organic background material. This led to the conclusion that the petroleum hydrocarbons detected are most likely derived from eroded material mixed with immature organic matter and distributed across a wide area in the SW Barents Sea rather than indications for seeping oil (Chapter 3). Generally, and independent of the compounds studied or the core location, it is striking that all sedimentary depth profiles in the pockmark areas are very similar to each other. The integrated results suggest that the investigated pockmark areas are not related to present day seepage activity. They neither revealed indications for present day hydrocarbon expulsion, nor for past/paleo seepage activity, neither for oil (Chapter 3) nor gas (Chapter 2, Chapter 4).

In contrast, the carbonate crust areas reveal obvious indications for methane seeping activity. The presence of carbonate crust patches on the seafloor as well as rising gas bubbles from the seafloor to the water column suggest that the sediment is supersaturated with gas. This assumption is supported by subsequent sediment analysis, in particular from area PR4, which reveals the presence of the typical AOM biomarkers. These diagnostic AOM biomarkers denote a distinct zone of elevated concentrations, which probably displays an active AOM zone in the sediment (Chapter 4). All studied biomarkers that are known to be associated to the process of AOM show elevated concentrations in this interval, which includes biomarkers of archaeal as well as bacterial origin. Furthermore, the compound-specific carbon isotope signature reveals very negative values which indicate methane consumption by the source organisms of the respective biomarkers.

It is intriguing that the two studied cold seep systems, even though they are located in relatively close proximity, are at the same time very different concerning their fluid leakage behavior. Even though the areas are believed to have undergone the same geological and glacial histories, two apparently independent cold seep systems are found. On the one hand there are the huge, currently “inactive” pockmark areas, on the other hand there are the carbonate crust sites that show active fluid flow.

To identify the origin and formation processes of these cold seep structures it is necessary to embed the findings into a geological context.

The active carbonate crust site PR4 is located at the northern edge of the Polheim Sub-platform in the western part of the Loppa High. Generally this area contains several indications for the presence of oil. Beside the detection of shallow gas, gas anomalies and bottom simulating reflectors (BSRs), which indicate the presence of gas hydrates in the subsurface, also the oil fields Skrugard and Havis are located close to the carbonate crust site. Additionally, gas flares which are connected to faults (Chand et al., 2012) have been described to occur in this area. The edges of the Polheim Sub-platform comprise many faults of varying sizes. Hence, the localized seeps of the carbonate crust area are likely related to a thermogenic source in the subsurface, which releases the fluids by focused migration along fault systems to the sediment surface. For the study site PR4 this is supported by seismic data (Chapter 4).

In contrast, the existence and formation of extensive fields of presently inactive pockmarks cannot be explained by distinct events of fluid migration along faults. The present pockmarks are not necessarily related to structural features in the subsurface. Additionally, the influence of fluids others than hydrocarbons (e.g., pore water, CO_2 or H_2S) can be excluded since these sources are not suitable to explain the wide distribution of the pockmarks in such high density. Therefore, an alternative formation model is required. Due to the observation that the pockmarks cut through the glaciomarine deposits (Chand et al., 2012) and the pockmarks occur within plough marks of drifting icebergs (Chapter 2) it was concluded that the present pockmarks were formed during the last deglaciation period. Several authors (e.g., Andreassen et al. 2008; Siegert et al. 2001) estimated that the entire area was covered by a thick ice sheet during the Last Glacial Maximum. This ice sheet, acting as a seal, trapped all hydrocarbon gases that possibly migrated from biogenic sources or from reservoirs in the deeper subsurface towards the surface. Accumulation under the ice shield occurred in the form of gas hydrates since appropriate pressure and temperature conditions were present to support clathrate formation. Large volumes of gas might have led to a lateral distribution of gas along with the formation of gas hydrates in the entire area. The retreat of the glaciers occurred about 14 ka ago (Elverhøi et al., 1995). Decomposition of gas hydrates might have been induced in a rapid process when the ice burden on the sediment was released for instance due to an upfloating event of

the melting ice sheet which caused a very rapid change of temperature and pressure conditions. This resulted in a release of large volumes of gas which formed the pockmark craters. Such a rapid event may also explain the absence of biomarkers diagnostic for the presence of methane in the upper meters of the sediment. The sudden expulsion of large volumes of gas did not leave the microbial community enough time to adjust to these conditions. It is further imaginable that large parts of the sediment have been removed due to the explosive character of pockmark formation. This may have also removed the signals (biomarkers) of the microbial communities (Chapter 2, Chapter 4).

The amounts of gas released from the sediment within such methane venting events are too large to be consumed by methanotrophic microbes. Thus, rapid large-scale methane venting scenarios during deglaciation periods may have a tremendous effect on the flux of large amounts of methane to the atmosphere and the global climate. Such a scenario is also supported by the work of Maslin et al. (2004) who linked slope failure to climatic changes and showed, that there is a good correlation between deglaciation events with global atmospheric methane records.

The results of this study show that even in areas located in close proximity to each other, different seepage systems can develop. However, it is conceivable, that pockmarks were formed by decaying gas hydrates, which were sourced through the same fault systems that still feed the active seeps today.

This thesis has proven that the SW Barents Sea contains cold seep systems, which are related to natural occurring seepage. Additionally, it shows that pockmarks are not necessarily indicators for active fluid expulsion. Thus, it is always essential to have a more detailed look at the entire system by applying different methods. In this context, geochemical methods proved to be useful tools to screen the sediment for hydrocarbons as they can provide further evidence for potential sources in the subsurface and the fluid expulsion activity of cold seep structures.

5.2 Outlook

For this study several sediment cores were taken in the SW Barents Sea. Detailed analysis of the samples with focus on geochemical and geomicrobiological methods showed that both, inactive and active cold seep systems, are present

in the SW Barents Sea. Hypotheses for potential formation scenarios of the investigated cold seep structures were developed. However, additional research could be conducted to further constrain the results of the present work and to enhance the understanding of the hydrocarbon systems in the Barents Sea.

Within the framework of this project, interdisciplinary techniques, e.g., analysis of seismic data, age assessment of the sediment and microbiological methods, have been applied. However, due to time constrains and limitations on the available infrastructure not all methods could be used on the entire sample set. The integration of the gathered data with other disciplines would be of great advantage to understand the processes in the area and the broader context. Age analysis of every interval of the studied sediment core could establish a direct link to the geologic history. Based on this, it is possible to relate certain events, which are proven and well documented in the literature (e.g., phases of glaciation or deglaciation), to distinct intervals and the corresponding data. Additional high resolution seismic data of cold seep sites could be useful to identify further possible migration pathways, e.g., underlying faults, which feed into the seep structure. Additionally, the seismic data could help to identify deeper lying reservoirs, shallow gas accumulation or gas hydrates, as potential sources of the seeping hydrocarbons.

The integration of the results in a basin model could be used to test the developed theory in a broader geological context. Based on the predicted volumes of hydrocarbons generated from the potential source rocks and in comparison to the volumes potentially retained in the fields of the southwestern Barents Sea, a mass balance could be derived to calculate the volume of hydrocarbons available as a feed to cold seeps. Combined with a detailed migration model and considering the available fault systems, preferred locations for active cold seeps could be predicted.

For active seep systems, such as the carbonate crust sites of the present study, the application and integration of geomicrobiological methods would add great value. Quantitative assessment of the microbial community could be achieved for example by determination of total cell abundance. The analysis of sulfate reduction rate and rates of methane oxidation could provide additional evidence for the presence of an AOM zone. Qualitative evaluation of the microbial inventory could be achieved using microbial ecology methods, e.g.,

fluorescent in situ hybridization (FISH). With this it is possible to classify the composition of different species (e.g., methanotrophic archaea) within the microbial community in order to draw conclusions on occurring processes.

The analysis of the seep-associated macrofauna could be used to determine whether the seeping fluids form the base of the trophic cycle.

During the examination of the short push cores from the carbonate crust site questions arose concerning a deeper located AOM zone in depth intervals which were not reached by the cores. The retrieval of longer cores could further verify this hypothesis.

Sampling of smaller intervals of the core would lead to data in higher resolution, which could improve the ability to capture subtle changes within the sediment and to better resolve small zones e.g., the sulfate methane transition zone (SMTZ).

Although seepage has always been described as expulsion of hydrocarbon fluids in this study, only indications for seeping methane could be found. The present oil biomarkers in the sediment are proposed to be derived from eroded material which was distributed across the entire study area. The investigation of sediment, which is obviously affected by leaking oil/oil slicks, could display a typical fingerprint of petroleum compounds in the sediment in case of oil leakage.

As part of a global perspective it would be of interest to transfer and correlate the data of the current study with settings which exhibit similar conditions. Appropriate settings are regions which are also exposed to arctic conditions e.g., the North Shelf of Alaska (Beaufort Strait or the Mackenzie Delta), the Kara Sea (West Siberian Basin) or the West Spitsbergen continental margin. Glacial retreat induced events of hydrocarbon venting, similar to those described for the southwestern Barents Sea, may have also occurred in these arctic regions.

List of Abbreviations

ai	anteiso
ANME	anaerobic methanotroph
AOM	anaerobic oxidation of methane
APCI	atmospheric pressure chemical ionization
BP	before present
bsf	below sea floor
CC	carbonate crust
cmbsf	cm below the sea floor
CPI	carbon preference index
δ^{13}C	carbon isotope ratio
$\Delta G^{0'}$	standard free energy change
DCM	dichloromethane
eq.	equation
FFI	Forsvarets Forskenings Institutt
	(Norwegian Defense Research Establishment)
FID	flame ionization detector
GC	gas chromatography
GC-MS	gas chromatography-mass spectrometry
GBB	glycerol backbone
GDGT	glycerol dialkyl glycerol tetraether
GPS	Global positioning system
Gt	gigatons
GWP	global warming potential
HC	hydrocarbon
HISAS	high resolution interferometric synthetic aperture sonar
HPLC	high performance liquid chromatography

IRMS	isotope ratio mass spectrometry
IStd	internal standard
ka	thousand years
LGM	Last Glacial Maximum
NGU	Geological Survey of Norway
MDL	minimum detection limit
MPLC	medium pressure liquid chromatography
MS	mass spectrometry
m/z	mass/charge
OM	organic matter
Ph	phytane
PL	phospholipid
PLFA	phospholipid fatty acid
PM	pockmark
PMI	pentamethylicosane
Pr	pristane
Ref	reference
ROV	remotely operated vehicle
Sed	sediment
SGD	submarine groundwater discharge
Sm^3	standard cubic meter
SMTZ	sulfate-methane transition zone
sp.	species
SR	sulfate reduction
SRB	sulfate reducing bacteria
SRR	sulfate reduction rate
SW	southwest(ern)
TIC	total ion chromatogram
TMS	trimethylsilyl
TOC	total organic carbon
TRIS	total reduced inorganic sulfur
UCM	unresolved complex mixture
USBL	Ultra Short Baseline
yr	year

References

Aagaard-Sørensen, S., Husum, K., Hald, M., and Knies, J. (2010). Paleoceanographic development in the SW Barents Sea during the Late Weichselian-Early Holocene transition. *Quaternary Science Reviews*, 29:3442–3456.

Abrams, M. A. (1996). Distribution of subsurface hydrocarbon seepage in near-surface marine sediments. In Schumacher, D. and Abrams, M. A., editors, *Hydrocarbon migration and its near-surface expression*, pages 1–14. The American Association of Petroleum Geologists.

Abrams, M. A. (2005). Significance of hydrocarbon seepage relative to petroleum generation and entrapment. *Marine and Petroleum Geology*, 22(4):457–477.

Acosta, J. A., Muñoz, A. M. n., Herranz, P. H., Palomo, C. P., Ballesteros, M. B., Vaquero, M. V., and Uchupi, E. U. (2001). Pockmarks in the Ibiza Channel and western end of the Balearic Promontory (western Mediterranean) revealed by multibeam mapping. *Geo-Marine Letters*, 21(3):123–130.

Alexander, R., Kagi, R. I., and Woodhouse, G. W. (1981). Geochemical correlation of Windalia oil and extracts of Winning Group (Cretaceous) potential source rocks, Barrow subbasin, Western Australia. *AAPG Bulletin*, 65:235–250.

Aloisi, G., Bouloubassi, I., Heijs, S. K., Pancost, R. D., Pierre, C., Sinninghe Damsté, J. S., Gottschal, J. C., Forney, L. J., and Rouchy, J.-M. (2002). CH_4-consuming microorganisms and the formation of carbonate crusts at cold seeps. *Earth and Planetary Science Letters*, 203(1):195–203.

Alperin, M. J. and Hoehler, T. M. (2009). Anaerobic methane oxidation by archaea/sulfate-reducing bacteria aggregates: 1. Thermodynamic and physical constraints. *American Journal of Science*, 309(10):869–957.

Andreassen, K. and Hansen, T. (1995). Inferred gas hydrates offshore Norway and Svalbard. *Norsk Geologisk Tidskrift*, 45:10–34.

Andreassen, K., Laberg, J. S., and Vorren, T. O. (2008). Seafloor geomorphology of the SW Barents Sea and its glaci-dynamic implications. *Geomorphology*, 97(1-2):157–177.

Bai, Q. Y. and Zelles, L. (1997). A method for determination of archaeal ether-linked glycerolipids by high performance liquid chromatography with fluorescence detection as their 9-anthroyl derivatives. *Chemosphere*, 35:263–274.

Barenholz, Y. (2002). Cholesterol and other membrane active sterols: from membrane evolution to "rafts". *Progress in Lipid Research*, 41(1):1–5.

Barnes, R. O. and Goldberg, E. D. (1976). Methane production and consumption in anoxic marine sediments. *Geology*, 4(5):297–300.

Bayon, G., Loncke, L., Dupré, S., Caprais, J. C., Ducassou, E., Duperron, S., Etoubleau, J., Foucher, J. P., Fouquet, Y., Gontharet, S., Henderson, G. M., Huguen, C., Klaucke, I., Mascle, J., Migeon, S., Olu-Le Roy, K., Ondréas, H., Pierre, C., Sibuet, M., Stadnitskaia, A., and Woodside, J. (2009). Multidisciplinary investigation of fluid seepage on an unstable margin: The case of the Central Nile deep sea fan. *Marine Geology*, 261:92–104.

Beal, E. J., House, C. H., and Orphan, V. J. (2009). Manganese- and iron-dependent marine methane oxidation. *Science*, 325(5937):184–187.

Bennett, B., Fustic, M., Farrimond, P., Huang, H., and Larter, S. R. (2006). 25-Norhopanes: Formation during biodegradation of petroleum in the subsurface. *Organic Geochemistry*, 37(7):787–797.

Berner, R. A. (1980). *Early Diagenesis: A Theoretical Approach.* Princeton University Press, New Jersey, US.

Bertram, S., Blumenberg, M., Michaelis, W., Siegert, M., Krüger, M., and Seifert, R. (2013). Methanogenic capabilities of ANME-archaea deduced from ^{13}C-labeling approaches. *Environmental Microbiology*, pages 2384–2393.

Bianchi, T. S. and Canuel, E. A. (2011). *Chemical Biomarkers in Aquatic Ecosystems*. Princeton Univ Press, Princeton, New Jersey, US.

Birgel, D., Feng, D., Roberts, H. H., and Peckmann, J. (2011). Changing redox conditions at cold seeps as revealed by authigenic carbonates from Alaminos Canyon, northern Gulf of Mexico. *Chemical Geology*, 285(1-4):82–96.

Bligh, E. G. and Dyer, W. J. (1959). A rapid method of total lipid extraction and purification. *Canadian Journal of Biochemistry and Physiology*, 37(8):911–917.

Blumenberg, M., Seifert, R., Reitner, J., Pape, T., and Michaelis, W. (2004). Membrane lipid patterns typify distinct anaerobic methanotrophic consortia. *Proceedings of the National Academy of Sciences of the United States of America*, 101(30):11111–11116.

Blumer, M. (1976). Polycyclic aromatic compounds in nature. *Scientific American*, 234(3):35–45.

Bøe, R., Rise, L., and Ottesen, D. (1998). Elongate depressions on the southern slope of the Norwegian Trench (Skagerrak): morphology and evolution. *Marine Geology*, 146:191–203.

Boetius, A., Ravenschlag, K., Schubert, C. J., Rickert, D., Widdel, F., Gieseke, A., Amann, R., Jorgensen, B. B., Witte, U., and Pfannkuche, O. (2000). A marine microbial consortium apparently mediating anaerobic oxidation of methane. *Nature*, 407(6804):623–626.

Boitsov, S., Petrova, V., Jensen, H. K. B., Kursheva, A., Litvinenko, I., Chen, Y., and Klungsøyr, J. (2011). Petroleum-related hydrocarbons in deep and subsurface sediments from south-western Barents Sea. *Marine Environmental Research*, 71(5):357–368.

Bouloubassi, I., Aloisi, G., Pancost, R. D., Hopmans, E., Pierre, C., and Sinninghe Damsté, J. S. (2006). Archaeal and bacterial lipids in authigenic carbonate crusts from eastern Mediterranean mud volcanoes. *Organic Geochemistry*, 37(4):484–500.

Bradley, A. S., Hayes, J. M., and Summons, R. E. (2009). Extraordinary ^{13}C enrichment of diether lipids at the Lost City Hydrothermal Field indicates a carbon-limited ecosystem. *Geochimica et Cosmochimica Acta*, 73(1):102–118.

Brassell, S. C., Eglinton, G., Marlowe, I. T., Pflaumann, U., and Sarnthein, M. (1986). Molecular stratigraphy: a new tool for climatic assessment. *Nature*, 320(6058):129–133.

Bray, E. E. and Evans, E. D. (1961). Distribution of *n*-paraffins as a clue to recognition of source beds. *Geochimica et Cosmochimica Acta*, 22(1):2–15.

Bray, E. E. and Evans, E. D. (1965). Hydrocarbons in non-reservoir-rock source beds. *AAPG Bulletin*, 49(3):248–257.

Brocks, J. J., Love, G. D., Summons, R. E., Knoll, A. H., Logan, G. A., and Bowden, S. A. (2005). Biomarker evidence for green and purple sulphur bacteria in a stratified Palaeoproterozoic sea. *Nature*, 437(7060):866–870.

Brothers, L., Kelley, J., Belknap, D., Barnhardt, W., Andrews, B., and Maynard, M. (2011). More than a century of bathymetric observations and present-day shallow sediment characterization in Belfast Bay, Maine, USA: Implications for pockmark field longevity. *Geo-Marine Letters*, 31(4):237–248.

Cathles, L. M., Su, Z., and Chen, D. (2010). The physics of gas chimney and pockmark formation, with implications for assessment of seafloor hazards and gas sequestration. *Marine and Petroleum Geology*, 27(1):82–91.

Cavanagh, A. J., Di Primio, R., Scheck-Wenderoth, M., and Horsfield, B. (2006). Severity and timing of Cenozoic exhumation in the southwestern Barents Sea. *Journal of the Geological Society*, 163(5):761–774.

Chand, S., Mienert, J., Andreassen, K., Knies, J., Plassen, L., and Fotland, B. (2008). Gas hydrate stability zone modelling in areas of salt tectonics and pockmarks of the Barents Sea suggests an active hydrocarbon venting system. *Marine and Petroleum Geology*, 25(7):625–636.

Chand, S., Thorsnes, T., Rise, L., Brunstad, H., Stoddart, D., Bøe, R., Lågstad, P., and Svolsbru, T. (2012). Multiple episodes of fluid flow in the SW Barents Sea (Loppa High) evidenced by gas flares, pockmarks and gas hydrate accumulation. *Earth and Planetary Science Letters*, 331-332(0):305–314.

Chappe, B., Michaelis, W., and Albrecht, P. (1980). Molecular fossils of Archaebacteria as selective degradation products of kerogen. *Physics and Chemistry of The Earth*, 12(0):265–274.

Chappellaz, J., Bluniert, T., Raynaud, D., Barnola, J. M., Schwander, J., and Stauffert, B. (1993). Synchronous changes in atmospheric CH_4 and greenland climate between 40 and 8 kyr bp. *Nature*, 366(6454):443–445.

Chapron, E., Van Rensbergen, P., De Batist, M., Beck, C., and Henriet, J. P. (2004). Fluid-escape features as a precursor of a large sublacustrine sediment slide in Lake Le Bourget, NW Alps, France. *Terra Nova*, 16:305–311.

Chistyakova, N., Ivanova, E., Risebrobakken, B., Ovsepyan, E., and Ovsepyan, Y. (2010). Reconstruction of the postglacial environments in the southwestern Barents Sea based on foraminiferal assemblages. *Oceanology*, 50(4):573–581.

Cicerone, R. J. and Oremland, R. S. (1988). Biogeochemical aspects of atmospheric methane. *Global Biogeochemical Cycles*, 2(4):299–327.

Cole, D., Stewart, S. A., and Cartwright, J. A. (2000). Giant irregular pockmark craters in the Palaeogene of the Outer Moray Firth Basin, UK North Sea. *Marine and Petroleum Geology*, 17(5):563–577.

Cole, G., Requejo, R., DeVay, J., Yu, A., Peel, F., Taylor, C., Brooks, J., Bernard, B., Zumberge, J., and Brown, S. (2001). *The Deepwater GoM Petroleum System: Insights from Piston Coring, Defining Seepage, Anomalies, and Background*. GCS-SEPM Foundation.

Corcoran, D. V. and Doré, A. G. (2002). Depressurization of hydrocarbon-bearing reservoirs in exhumed basin settings: Evidence from Atlantic margin and borderland basins. *Geological Society, London, Special Publications*, 196(1):457–483.

Crémière, A., Pierre, C., Aloisi, G., Blanc-Valleron, M.-M., Henry, P., Zitter, T., and Çağatay, N. (2011). Authigenic carbonates related to thermogenic gas hydrates in the sea of Marmara (Turkey). *Proceedings of the 7th International Conference on Gas Hydrates (ICGH 2011)*.

Dastillung, M. and Albrecht, P. (1977). D2-Sterenes as diagenetic intermediates in sediments. *Nature*, 269(5630):678–679.

Davy, B., Pecher, I., Wood, R., Carter, L., and Gohl, K. (2010). Gas escape features off New Zealand: Evidence of massive release of methane from hydrates. *Geophysical Research Letters*, 37(21):L21309.

De Rosa, M. and Gambacorta, A. (1988). The lipids of archaebacteria. *Progress in Lipid Research*, 27(3):153–175.

De Rosa, M., Gambacorta, A., and Gliozzi, A. (1986). Structure, biosynthesis, and physicochemical properties of archaebacterial lipids. *Microbiol Rev.*, 50(1):70–80.

De Vittor, C., Beaubien, S., and Karuza, A. (2012). Cruise report ECO2-4 (Panarea Island, Italy). Technical report, Istituto Nazionale di Oceanografia e Geofisica Sperimentale, Trieste, Italy / Università di Roma La Sapienza, Roma, Italy.

Dembicki Jr., H. (2010). Recognizing and compensating for interference from the sediment's background organic matter and biodegradation during interpretation of biomarker data from seafloor hydrocarbon seeps: An example from the Marco Polo area seeps, Gulf of Mexico, USA. *Marine and Petroleum Geology*, 27(9):1936–1951.

D'Hondt, S., Rutherford, S., and Spivack, A. J. (2002). Metabolic activity of subsurface life in deep-sea sediments. *Science*, 295(5562):2067–2070.

Dickens, G. R. (2003). Rethinking the global carbon cycle with a large, dynamic and microbially mediated gas hydrate capacitor. *Earth and Planetary Science Letters*, 213:169–183.

Dietz, R. S. and Lafond, E. C. (1950). Natural slicks on the ocean. *Journal of Marine Research*, 9:69–76.

Doré, A. (1995). Barents Sea geology, petroleum resources and commercial potential. *Arctic*, 48(3):207–221.

Doré, A. G., Corcoran, D. V., and Scotchman, I. C. (2002). Prediction of the hydrocarbon system in exhumed basins, and application to the NW European margin. In Dore, A. G., Cartwright, J. A., Stoker, M. S., Turner, J. P., and White, N. J., editors, *Exhumation of the North Atlantic Margin: Timing, Mechanisms and Implications for Petroleum Exploration*, volume 196, pages 401–429. Geological Society (London) Special Publications, London.

Doré, A. G. and Jensen, L. N. (1996). The impact of late Cenozoic uplift and erosion on hydrocarbon exploration: Offshore Norway and some other uplifted basins. *Global and Planetary Change*, 12(1-4):415–436.

Dugan, B. and Flemings, P. B. (2000). The New Jersey margin: compaction and fluid flow. *Journal of Geochemical Exploration*, 69-70(0):477–481.

Eglinton, G. and Hamilton, R. J. (1967). Leaf Epicuticular Waxes. *Science*, 156(3780):1322–1335.

Ehhalt, D. H. and Schmidt, U. (1978). Sources and sinks of atmospheric methane. *Pure and Applied Geophysics*, 116(2-3):452–464.

Eidvin, T., Jansen, E., and Riis, F. (1993). Chronology of Tertiary fan deposits off the western Barents Sea: Implications for the uplift and erosion history of the Barents Shelf. *Marine Geology*, 112(1-4):109–131.

Elverhøi, A., Andersen, E. S., Dokken, T., Hebbeln, D., Spielhagen, R., Svendsen, J. I., Sørflaten, M., Rørnes, A., Hald, M., and Forsberg, C. F. (1995). The growth and decay of the Late Weichselian ice sheet in western Svalbard and adjacent areas based on provenance studies of marine sediments. *Quaternary Research*, 44(3):303–316.

Elverhøi, A., Fjeldskaar, W., Solheim, A., Nyland-Berg, M., and Russwurm, L. (1993). The Barents Sea ice sheet - A model of its growth and decay during the last ice maximum. *Quaternary Science Reviews*, 12(10):863–873.

Elvert, M. (1999). Anaerobic methane oxidation associated with marine gas hydrates: superlight C-isotopes from saturated and unsaturated C_{20} and C_{25} irregular isoprenoids. *Naturwissenschaften*, 86:295–300.

Elvert, M., Boetius, A., Knittel, K., and Jørgensen, B. B. (2003). Characterization of specific membrane fatty acids as chemotaxonomic markers for sulfate-reducing bacteria involved in anaerobic oxidation of methane. *Geomicrobiology Journal*, 20(4):403–419.

Elvert, M., Suess, E., Greinert, J., and Whiticar, M. J. (2000). Archaea mediating anaerobic methane oxidation in deep-sea sediments at cold seeps of the eastern Aleutian subduction zone. *Organic Geochemistry*, 31(11):1175–1187.

Encyclopaedia Britannica, I. (2010). http://www.britannica.com/ebchecked/media/141533.

EPA (2005). Global anthropogenic emissions of non-CO_2 greenhouse gases: 1990-2020. Technical report, U.S. Environmental Protection Agency, Washington DC, USA.

EPA (2010). Methane and nitrous oxide emissions from natural sources. *U.S. Environmental Protection Agency, Washington, DC, USA.*

Etiope, G., Papatheodorou, G., Christodoulou, D. P., Ferentinos, G., Sokos, E., and Favali, P. (2006). Methane and hydrogen sulfide seepage in the northwest Peloponnesus petroliferous basin (Greece): Origin and geohazard. *AAPG Bulletin*, 90(5):701–713.

Ettwig, K. F., Butler, M. K., Le Paslier, D., Pelletier, E., Mangenot, S., Kuypers, M. M. M., Schreiber, F., Dutilh, B. E., Zedelius, J., de Beer, D., Gloerich, J., Wessels, H. J. C. T., van Alen, T., Luesken, F., Wu, M. L., van de Pas-Schoonen, K. T., Op den Camp, H. J. M., Janssen-Megens, E. M., Francoijs, K.-J., Stunnenberg, H., Weissenbach, J., Jetten, M. S. M., and Strous, M. (2010). Nitrite-driven anaerobic methane oxidation by oxygenic bacteria. *Nature*, 464(7288):543–548.

Eyer, J. A., Foreman, J. E., and Raney, G. L. (1977). Natural oil seep detection in marine environments. In *Offshore Technology Conference*. Offshore Technology Conference.

Faber, E. and Stahl, W. (1984). Geochemical surface exploration for hydrocarbons in North Sea. *AAPG Bulletin*, 68(3):363–386.

Fang, J. and Barcelona, M. J. (1998). Structural determination and quantitative analysis of bacterial phospholipids using liquid chromatography/electrospray ionization/mass spectrometry. *Journal of Microbiological Methods*, 33(1):23–35.

Fang, J., Shizuka, A., Kato, C., and Schouten, S. (2006). Microbial diversity of cold-seep sediments in Sagami Bay, Japan, as determined by 16S rRNA gene and lipid analyses. *FEMS Microbiology Ecology*, 57(3):429–441.

Farrimond, P., Taylor, A., and Telnæs, N. (1998). Biomarker maturity parameters: The role of generation and thermal degradation. *Organic Geochemistry*, 29(5-7):1181–1197.

Ferdelman, T. G., Fossing, H., Neumann, K., and Schulz, H. D. (1999). Sulfate reduction in surface sediments of the southeast Atlantic continental margin between 15° 38's and 27° 57's (Angola and Namibia). *Limnology and Oceanography*, 44(3):650–661.

Ferrell, R. E. and Aharon, P. (1994). Mineral assemblages occurring around hydrocarbon vents in the northern Gulf of Mexico. *Geo-Marine Letters*, 14(2):74–80.

Finke, N., Vandieken, V., and Jørgensen, B. B. (2007). Acetate, lactate, propionate, and isobutyrate as electron donors for iron and sulfate reduction in Arctic marine sediments, Svalbard. *FEMS Microbiology Ecology*, 59:10–22.

Floodgate, G. D. and Judd, A. G. (1992). The origins of shallow gas. *Continental Shelf Research*, 12(10):1145–1156.

Forsberg, C. F., Planke, S., Tjelta, T. I., Svanø, G., Strout, J. M., and Svensen, H. (2007). Formation of pockmarks in the Norwegian Channel. *Proceedings*

of the 6th International Offshore Site Investigation and Geotechnics Conference: Confronting New Challenges and Sharing Knowledge, 11-13 September 2007, London, UK, pages 221–230.

Forwick, M., Baeten, N. J., and Vorren, T. O. (2009). Pockmarks in Spitsbergen fjords. *Norwegian Journal of Geology*, 89:65–77.

Fossing, H., Ferdelman, T., and Berg, P. (2000). Sulfate reduction and methane oxidation in continental margin sediments influenced by irrigation (southeast Atlantic off Namibia). *Geochimica et Cosmochimica Acta*, 64(5):897–910.

Fossing, H. and Jørgensen, B. B. (1989). Measurement of bacterial sulfate reduction in sediments: Evaluation of a single-step chromium reduction method. *Biogeochemistry*, 8(3):205–222.

Foucher, J.-P., Westbrook, G. K., Boetius, A., Ceramicola, S., Dupre, S., Mascle, J., Mienert, J., Pfannkuche, O., Pierre, C., and Praeg, D. (2009). Structure and Drivers of Cold Seep Ecosystems. *Oceanography*, 22(1):92–109.

Fowler, M. G., Abolins, P., and Douglas, A. G. (1986). Monocyclic alkanes in Ordovician organic matter. *Organic Geochemistry*, 10(4-6):815–823.

Freese, E., Rütters, H., Köster, J., Rullkötter, J., and Sass, H. (2009). Gammaproteobacteria as a possible source of eicosapentaenoic acid in anoxic intertidal sediments. *Microbial Ecology*, 57(3):444–454.

Gabrielsen, R. H. (1984). Long-lived fault zones and their influence on the tectonic development of the southwestern Barents Sea. *Journal of the Geological Society*, 141(4):651–662.

Gabrielsen, R. H., Færseth, R. B., Jensen, L., Kalheim, J., and Riis, F. (1990). Structural elements of the Norwegian continental shelf, Part I: The Barents Sea Region. *NPD-Bulletin*, No. 6:1–33.

Gabrielsen, R. H. and Kløvjan, O. S. (1997). Late jurassic - early Cretaceous caprocks of the southwestern Barents Sea: fracture systems and rock

mechanical properties. *Norwegian Petroleum Society Special Publications*, 7:73–89.

Gattinger, A., Günthner, A., Schloter, M., and Munch, J. C. (2003). Characterisation of archaea in soils by polar lipid analysis. *Acta Biotechnologica*, 23(1):21–28.

Gay, A., Lopez, M., Berndt, C., and Séranne, M. (2007). Geological controls on focused fluid flow associated with seafloor seeps in the Lower Congo Basin. *Marine Geology*, 244(1-4):68–92.

Gay, A., Lopez, M., Cochonat, P., Levaché, D., Sermondadaz, G., and Seranne, M. (2006). Evidences of early to late fluid migration from an upper Miocene turbiditic channel revealed by 3D seismic coupled to geochemical sampling within seafloor pockmarks, Lower Congo Basin. *Marine and Petroleum Geology*, 23(3):387–399.

Grantham, P. J. (1986). Sterane isomerisation and moretane/hopane ratios in crude oils derived from Tertiary source rocks. *Organic Geochemistry*, 9(6):293–304.

Hallam, S. J., Putnam, N., Preston, C. M., Detter, J. C., Rokhsar, D., Richardson, P. M., and DeLong, E. F. (2004). Reverse methanogenesis: Testing the hypothesis with environmental genomics. *Science*, 305(5689):1457–1462.

Hammer, Ø., Webb, K., and Depreiter, D. (2009). Numerical simulation of upwelling currents in pockmarks, and data from the Inner Oslofjord, Norway. *Geo-Marine Letters*, 29(4):269–275.

Hammer, Ø. and Webb, K. E. (2010). Piston coring of Inner Oslofjord pockmarks, Norway: constraints on age and mechanism. *Norwegian Journal of Geology*, 90:79–91.

Hanson, R. S. and Hanson, T. E. (1996). Methanotrophic bacteria. *Microbiological Reviews*, 60(2):439–71.

Harrington, P. (1985). Formation of pockmarks by pore-water escape. *Geo-Marine Letters*, 5(3):193–197.

Härtner, T., Straub, K. L., and Kannenberg, E. (2005). Occurrence of hopanoid lipids in anaerobic geobacter species. *FEMS Microbiology Letters*, 243(1):59–64.

Hartwig, A., Anka, Z., and di Primio, R. (2012). Evidence of a widespread paleo-pockmarked field in the Orange Basin: An indication of an early Eocene massive fluid escape event offshore South Africa. *Marine Geology*, 332-334(0):222–234.

Harvey, H. R., Fallon, R. D., and Patton, J. S. (1986). The effect of organic matter and oxygen on the degradation of bacterial membrane lipids in marine sediments. *Geochimica et Cosmochimica Acta*, 50(5):795–804.

Hasiotis, T., Papatheodorou, G., and Ferentinos, G. (2002). A string of large and deep gas-induced depressions (pockmarks) offshore Killini peninsula, western Greece. *Geo-Marine Letters*, 22(3):142–149.

Hayes, J. M., Freeman, K. H., Popp, B. N., and Hoham, C. H. (1990). Compound-specific isotopic analyses: A novel tool for reconstruction of ancient biogeochemical processes. *Organic Geochemistry*, 16:1115–1128.

Heggland, R. (1998). Gas seepage as an indicator of deeper prospective reservoirs. A study based on exploration 3D seismic data. *Marine and Petroleum Geology*, 15(1):1–9.

Heimann, M. (2010). How stable is the methane cycle? *Science*, 327(5970):1211–1212.

Hesselbo, S. P., Gröcke, D. R., Jenkyns, H. C., Bjerrum, C. J., Farrimond, P., Morgans Bell, H. S., and Green, O. R. (2000). Massive dissociation of gas hydrate during a Jurassic oceanic anoxic event. *Nature*, 406(6794):392–395.

Hinrichs, K.-U. and Boetius, A. (2002). The anaerobic oxidation of methane: New insights in microbial ecology and biogeochemistry. In Wefer, G., Billett, D., Hebbeln, D., Jørgensen, B. B., Schlüter, M., and van Weering, T., editors, *Ocean Margin Systems*, pages 457–477, Berlin Heidelberg. Springer-Verlag.

Hinrichs, K.-U., Hayes, J. M., Sylva, S. P., Brewer, P. G., and DeLong, E. F. (1999). Methane-consuming archaebacteria in marine sediments. *Nature*, 398(6730):802–805.

Hirschberg, A., deJong, L., Schipper, B., and Meijer, J. (1984). Influence of temperature and pressure on asphaltene flocculation. *Society of Petroleum Engineers Journal*, pages 283–293.

Hoefs, J. (2004). *Stable Isotope Geochemistry*. Springer-Verlag, 5th edition.

Hoehler, T. M., Alperin, M. J., Albert, D. B., and Martens, C. S. (1994). Field and laboratory studies of methane oxidation in an anoxic marine sediment: Evidence for a methanogen-sulfate reducer consortium. *Global Biogeochemical Cycles*, 8(4):451–463.

Holzer, G., Oró, J., and Tornabene, T. G. (1979). Gas chromatographic-mass spectrometric analysis of neutral lipids from methanogenic and thermoacidophilic bacteria. *Journal of Chromatography A*, 186(0):795–809.

Hood, K. C., Wenger, L. M., Gross, O. P., and Harrison, S. (2002). Hydrocarbon systems analysis of the northern Gulf of Mexico: Delineation of hydrocarbon migration pathways using seeps and seismic imaging. In Schumacher, D. and LeSchack, L. A., editors, *Surface exploration case histories: Applications of geochemistry, magnetics, and remote sensing*, pages 25–40. AAPG Studies in Geology.

Horn, M. H., Teal, J. M., and Backus, R. H. (1970). Petroleum lumps on the surface of the sea. *Science*, 168(3928):245–246.

Horsfield, B., Schenk, H. J., Zink, K., Ondrak, R., Dieckmann, V., Kallmeyer, J., Mangelsdorf, K., di Primio, R., Wilkes, H., Parkes, R. J., Fry, J., and Cragg, B. (2006). Living microbial ecosystems within the active zone of catagenesis: Implications for feeding the deep biosphere. *Earth and Planetary Science Letters*, 246(1-2):55–69.

Horvitz, L. (1985). Geochemical exploration for petroleum. *Science*, 229(4716):821–827.

Hostettler, F. D. and Kvenvolden, K. A. (2002). Alkylcyclohexanes in environmental geochemistry. *Environmental Forensics*, 3(3-4):293–301.

Hovland, M. (1981). Characteristics of pockmarks in the Norwegian Trench. *Marine Geology*, 39(1-2):103–117.

Hovland, M. (1992). Hydrocarbon seeps in northern marine waters: Their occurrence and effects. *PALAIOS*, 7(4):376–382.

Hovland, M. (2003). Geomorphological, geophysical, and geochemical evidence of fluid flow through the seabed. *Journal of Geochemical Exploration*, 78-79:287–291.

Hovland, M., Gardner, J. V., and Judd, A. G. (2002). The significance of pockmarks to understanding fluid flow processes and geohazards. *Geofluids*, 2(2):127–136.

Hovland, M., Heggland, R., De Vries, M. H., and Tjelta, T. I. (2010). Unit-pockmarks and their potential significance for predicting fluid flow. *Marine and Petroleum Geology*, 27(6):1190–1199.

Hovland, M., Jensen, S., and Fichler, C. (2012). Methane and minor oil macroseep systems - Their complexity and environmental significance. *Marine Geology*, 332-334:163–173.

Hovland, M. and Judd, A. (1988). *Seabed Pockmarks and Seepages. Impact on Geology, Biology and the Marine Environment.* Graham and Trotman, London.

Hovland, M., Svensen, H., Forsberg, C. F., Johansen, H., Fichler, C., Fosså, J. H., Jonsson, R., and Rueslåtten, H. (2005). Complex pockmarks with carbonate-ridges off mid-Norway: Products of sediment degassing. *Marine Geology*, 218(1-4):191–206.

Hückel, E. (1937). Grundzüge der Theorie ungesättigter und aromatischer Verbindungen. *Zeitschrift für Elektrochemie und angewandte physikalische Chemie*, 43(9):752–788.

Huguet, C., Hopmans, E. C., Febo-Ayala, W., Thompson, D. H., Sinninghe Damsté, J. S., and Schouten, S. (2006). An improved method to determine the absolute abundance of glycerol dibiphytanyl glycerol tetraether lipids. *Organic Geochemistry*, 37(9):1036–1041.

Hunt, J. (1996). *Petroleum Geochemistry and Geology*. W. H. Freeman and Company, New York, USA.

Hvoslef, S., Christie, O. H. J., Sassen, R., Kennicutt II, M. C., Requejo, A. G., and Brooks, J. M. (1996). Test of a new surface geochemistry tool for resource prediction in frontier areas. *Marine and Petroleum Geology*, 13(1):107–124.

IPCC (2011). *Climate change 2001. The scientific basis*. Cambrigde University Press, Cambrigde, UK.

Isaksen, G. H. and Bohacs, K. M. (1995). Geological Controls of Source Rock Geochemistry Through Relative Sea Level; Triassic, Barents Sea. In Katz, B. J., editor, *Petroleum Source Rocks*, pages 25–50, Berlin Heidelberg. Springer-Verlag.

Iversen, N. and Jørgensen, B. B. (1985). Anaerobic methane oxidation rates at the sulfate-methane transition in marine sediments from Kattegat and Skagerrak (Denmark). *Limnology and Oceanography*, 30(5):944–955.

Jensen, J. B., Kuijpers, A., Bennike, O., Laier, T., and Werner, F. (2002). New geological aspects for freshwater seepage and formation in Eckernförde Bay, western Baltic. *Continental Shelf Research*, 22(15):2159–2173.

Jørgensen, B. B. (1978). A comparison of methods for the quantification of bacterial sulfate reduction in coastal marine sediments I. Measurement with radiotracer techniques. *Geomicrobiology Journal*, 1(1):11–26.

Jørgensen, B. B. (1982). Mineralization of organic matter in the sea bed - the role of sulphate reduction. *Nature*, 296(5858):643–645.

Jørgensen, B. B. and Fenchel, T. (1974). The sulfur cycle of a marine sediment model system. *Marine Biology*, 24(3):189–201.

Jørgensen, B. B., Weber, A., and Zopfi, J. (2001). Sulfate reduction and anaerobic methane oxidation in Black Sea sediments. *Deep Sea Research 1*, 48:2097–2120.

Judd, A. and Hovland, M. (2007). *Seabed Fluid Flow. The Impact on Geology, Biology, and the Marine Environment.* Cambridge University Press, New York, US.

Judd, A. G. (2000). Geological sources of methane. In Khalil, M. A. K., editor, *Atmospheric Methane*, pages 280–303, Berlin, Germany. Springer.

Judd, A. G. (2004). Natural seabed gas seeps as sources of atmospheric methane. *Environmental Geology*, 46(8):988–996.

Judd, A. G., Hovland, M., Dimitrov, L. I., García Gil, S., and Jukes, V. (2002). The geological methane budget at continental margins and its influence on climate change. *Geofluids*, 2(2):109–126.

Junttila, J., Aagaard-Sørensen, S., Husum, K., and Hald, M. (2010). Late Glacial-Holocene clay minerals elucidating glacial history in the SW Barents Sea. *Marine Geology*, 276(1-4):71–85.

Kallmeyer, J., Ferdelman, T. G., Weber, A., Fossing, H., and Jørgensen, B. B. (2004). A cold chromium distillation procedure for radiolabeled sulfide applied to sulfate reduction measurements. *Limnology and Oceanography: Methods*, 2:171–180.

Kawahara, F. K. and Ballinger, D. G. (1970). Characterization of oil slicks on surface waters. *Product R&D*, 9(4):553–558.

Kelley, J. T., Dickson, S. M., Belknap, D. F., Barnhardt, W. A., and Henderson, M. (1994). Giant sea-bed pockmarks: Evidence for gas escape from Belfast Bay, Maine. *Geology*, 22(1):59–62.

Kennett, J. P., Cannariato, K. G., Hendy, I. L., and Behl, R. J. (2000). Carbon isotopic evidence for methane hydrate instability during Quaternary interstadials. *Science*, 288(5463):128–133.

King, L. H. and MacLean, B. (1970). Pockmarks on the Scotian Shelf. *Geological Society of America Bulletin*, 81(10):3141–3148.

Kissin, Y. V. (1990). Catagenesis of light cycloalkanes in petroleum. *Organic Geochemistry*, 15(6):575–594.

Knittel, K. and Boetius, A. (2009). Anaerobic oxidation of methane: Progress with an unknown process. *Annual Review of Microbiology*, 63:311–334.

Knittel, K., Losekann, T., Boetius, A., Kort, R., and Amann, R. (2005). Diversity and distribution of methanotrophic archaea at cold seeps. *Applied and Environmental Microbiology*, 71(1):467–479.

Koga, Y., Morii, H., Akagawa-Matsushita, M., and Ohga, M. (1998). Correlation of polar lipid composition with 16S rRNA phylogeny in methanogens. Further analysis of lipid component parts. *Bioscience, Biotechnology, and Biochemistry*, 62(2):230–236.

Kohnen, M. E. L., Schouten, S., Sinninghe Damsté, J. S., de Leeuw, J. W., Merritt, D. A., and Hayes, J. M. (1992). Recognition of paleobiochemicals by a combined molecular sulfur and isotope geochemical approach. *Science*, 256(5055):358–362.

Krüger, M., Meyerdierks, A., Glöckner, F. O., Amann, R., Widdel, F., Kube, M., Reinhardt, R., Kahnt, J., Böcher, R., Thauer, R. K., and Shima, S. (2003). A conspicuous nickel protein in microbial mats that oxidize methane anaerobically. *Nature*, 426(6968):878–881.

Kulm, L. D., Suess, E., Moore, J. C., Carson, B., Lewis, B. T., Ritger, S. D., Kadko, D. C., Thornburg, T. M., Embley, R. W., Rugh, W. D., Massoth, G. J., Langseth, M. G., Cochrane, G. R., and Scamman, R. L. (1986). Oregon subduction zone: Venting, fauna, and carbonates. *Science*, 231(4738):561–566.

Kvenvolden, K. A. (1988). Methane hydrate - A major reservoir of carbon in the shallow geosphere? *Chemical Geology*, 71:41–51.

Kvenvolden, K. A. (1993). Gas hydrates - geological perspective and global change. *Reviews of Geophysics*, 31(2):173–187.

Kvenvolden, K. A. (1998). A primer on the geological occurrence of gas hydrate. *Geological Society, London, Special Publications*, 137(1):9–30.

Kvenvolden, K. A. (2002). Methane hydrate in the global organic carbon cycle. *Terra Nova*, 14(5):302–306.

Kvenvolden, K. A. and Cooper, C. K. (2003). Natural seepage of crude oil into the marine environment. *Geo-Marine Letters*, 23(3-4):140–146.

Kvenvolden, K. A., Lorenson, T. D., and Reeburgh, W. S. (2001). Attention turns to naturally occurring methane seepage. *Eos, Transactions American Geophysical Union*, 82(40):457–457.

Lammers, S., Suess, E., and Hovland, M. (1995). A large methane plume east of Bear Island (Barents Sea): Implications for the marine methane cycle. *Geologische Rundschau*, 84(1):59–66.

Larssen, G. B., Elvebakk, G., B., H. L., Kristensen, S.-E., Nilsson, I., Samuelsberg, T., Svånå, T. A., Stemmerik, L., and Worsely, D. (2005). *Upper Palaeozoic lithostratigraphy of the southern Norwegian Barents Sea*. Geological Survey of Norway, Trondheim.

Larter, S. R., Bowler, B. F. J., Li, M., Chen, M., Brincat, D., Bennett, B., Noke, K., Donohoe, P., Simmons, D., Kohnen, M., Allan, J., Telnaes, N., and Horstad, I. (1996). Molecular indicators of secondary oil migration distances. *Nature*, 383(6601):593–597.

Lederberg, J. (2000). *Encyclopedia of Microbiology*, volume 1, A-Hi. Academic Press, New York, USA, 2nd edition.

Leloup, J., Loy, A., Knab, N. J., Borowski, C., Wagner, M., and Jørgensen, B. B. (2007). Diversity and abundance of sulfate-reducing microorganisms in the sulfate and methane zones of a marine sediment, Black Sea. *Environmental Microbiology*, 9(1):131–142.

Levin, L. A. (2005). Ecology of cold seep sediments: Interactions of fauna with flow, chemistry and microbes. *Oceanography and Marine Biology, An Annual Review*, 43.

Levy, H. (1971). Normal atmosphere: Large radical and formaldehyde concentrations predicted. *Science*, 173(3992):141–143.

Libby, W. F. (1955). *Radiocarbon Dating*. Chicago Univ. Press, Chicago, USA.

Link, W. K. (1952). Significance of oil and gas seeps in world oil exploration. *AAPG Bulletin*, 36(8):1505–1540.

Logan, G. A., Abrams, M. A., Dahdah, N. F., and Grosjean, E. (2009). Laboratory methods for evaluating migrated high molecular weight hydrocarbons in marine sediments at naturally occurring oil seeps. *Organic Geochemistry*, 40(3):365–375.

Long, D. (1992). Devensian late-glacial gas escape in the central North Sea. *Continental Shelf Research*, 12(10):1097–1110.

Long, D., Lammers, S., and Linke, P. (1998). Possible hydrate mounds within large sea-floor craters in the Barents Sea. *Geological Society, London, Special Publications*, 137(1):223–237.

Lösekann, T., Knittel, K., Nadalig, T., Fuchs, B., Niemann, H., Boetius, A., and Rudolf, A. (2007). Diversity and abundance of aerobic and anaerobic methane oxidizers at the Haakon Mosby Mud Volcano, Barents Sea. *Applied and Environmental Microbiology*, 73(10):3348–3362.

Ludwig, H. F. and Carter, R. (1961). Analytical characteristics of oil-tar materials on southern California beaches. *Journal (Water Pollution Control Federation)*, 33(11):1123–1139.

Luff, R. and Wallmann, K. (2003). Fluid flow, methane fluxes, carbonate precipitation and biogeochemical turnover in gas hydrate-bearing sediments at Hydrate Ridge, Cascadia Margin: Numerical modeling and mass balances. *Geochimica et Cosmochimica Acta*, 67(18):3403–3421.

Luff, R., Wallmann, K., and Aloisi, G. (2004). Numerical modeling of carbonate crust formation at cold vent sites: Significance for fluid and methane budgets and chemosynthetic biological communities. *Earth and Planetary Science Letters*, 221(1-4):337–353.

Mackenzie, A. S. (1984). Applications of biomarkers in petroleum geochemistry. In Brooks, J. and Welte, D. H., editors, *Advances in Petroleum Geochemistry*, volume 1, pages 115–214. Academic Press, London, UK.

Mackenzie, A. S., Brassell, S. C., Eglinton, G., and Maxwell, J. R. (1982). Chemical fossils: The geological fate of steroids. *Science*, 217(4559):491–504.

Maestro, A., Barnolas, A., Somoza, L., Lowrie, A., and Lawton, T. (2002). Geometry and structure associated to gas-charged sediments and recent growth faults in the Ebro Delta (Spain). *Marine Geology*, 186(3-4):351–368.

Mahlstedt, N. and Horsfield, B. (2012). Metagenetic methane generation in gas shales I. screening protocols using immature samples. *Marine and Petroleum Geology*, 31:27–42.

Mangelsdorf, K., Finsel, E., Liebner, S., and Wagner, D. (2009). Temperature adaptation of microbial communities in different horizons of Siberian permafrost-affected soils from the Lena Delta. *Chemie der Erde - Geochemistry*, 69:169–182.

Mangelsdorf, K. and Rullkötter, J. (2003). Natural supply of oil-derived hydrocarbons into marine sediments along the California continental margin during the late Quaternary. *Organic Geochemistry*, 34(8):1145–1159.

Mangelsdorf, K., Zink, K.-G., Birrien, J.-L., and Toffin, L. (2005). A quantitative assessment of pressure dependent adaptive changes in the membrane lipids of a piezosensitive deep sub-seafloor bacterium. *Organic Geochemistry*, 36:1459–1479.

Mangelsdorf, K., Zink, K.-G., di Primio, R., and Horsfield, B. (2011). Microbial lipid markers within and adjacent to Challenger Mound in the Belgica carbonate mound province, Porcupine Basin, offshore Ireland (IODP Expedition 307). *Marine Geology*, 282(1-2):91–101.

Martens, C. S. and Berner, R. A. (1974). Methane production in the interstitial waters of sulfate-depleted marine sediments. *Science*, 185(4157):1167–1169.

Marzi, R., Torkelson, B. E., and Olson, R. K. (1993). A revised carbon preference index. *Organic Geochemistry*, 20(8):1303–1306.

Maslin, M., Owen, M., Day, S., and Long, D. (2004). Linking continental-slope failures and climate change: Testing the clathrate gun hypothesis. *Geology*, 32(1):53–56.

Maslin, M. A. and Thomas, E. (2003). Balancing the deglacial global carbon budget: The hydrate factor. *Quaternary Science Reviews*, 22(15-17):1729–1736.

Matthews, E. and Fung, I. (1987). Methane emission from natural wetlands: Global distribution, area, and environmental characteristics of sources. *Global Biogeochemical Cycles*, 1(1):61–86.

Maugeri, L. (2012). Oil: The next revolution. *Discussion Paper 2012-10*, pages 1–86.

Mazzini, A., Svensen, H., Hovland, M., and Planke, S. (2006). Comparison and implications from strikingly different authigenic carbonates in a Nyegga complex pockmark, G11, Norwegian Sea. *Marine Geology*, 231(1-4):89–102.

Mello, M. R., Telnæs, N., Gaglianone, P. C., Chicarelli, M. I., Brassell, S. C., and Maxwell, J. R. (1988). Organic geochemical characterisation of depositional palaeoenvironments of source rocks and oils in Brazilian marginal basins. *Organic Geochemistry*, 13(1-3):31–45.

Metz, J. G., Roessler, P., Facciotti, D., Levering, C., Dittrich, F., Lassner, M., Valentine, R., Lardizabal, K., Domergue, F., Yamada, A., Yazawa, K., Knauf, V., and Browse, J. (2001). Production of polyunsaturated fatty acids by polyketide synthases in both prokaryotes and eukaryotes. *Science*, 293(5528):290–293.

Michaelis, W., Seifert, R., Nauhaus, K., Treude, T., Thiel, V., Blumenberg, M., Knittel, K., Gieseke, A., Peterknecht, K., Pape, T., Boetius, A., Amann, R., Jørgensen, B. B., Widdel, F., Peckmann, J., Pimenov, N. V., and Gulin, M. B. (2002). Microbial reefs in the Black Sea fueled by anaerobic oxidation of methane. *Science*, 297(5583):1013–1015.

Mienert, J., Posewang, J., and Baumann, M. (1998). Gas hydrates along the northeastern Atlantic margin: Possible hydrate-bound margin instabilities

and possible release of methane. *Geological Society, London, Special Publications*, 137(1):275–291.

Milkov, A. V. (2004). Global estimates of hydrate-bound gas in marine sediments: How much is really out there? *Earth-Science Reviews*, 66(3-4):183–197.

Milucka, J., Ferdelman, T. G., Polerecky, L., Franzke, D., Wegener, G., Schmid, M., Lieberwirth, I., Wagner, M., Widdel, F., and Kuypers, M. M. M. (2012). Zero-valent sulphur is a key intermediate in marine methane oxidation. *Nature*, 491(7425):541–546.

Morris, B. F. (1971). Petroleum: Tar quantities floating in the northwestern Atlantic taken with a new quantitative neuston net. *Science*, 173(3995):430–432.

Müller, K. D., Husmann, H., and Nalik, H. P. (1990). A new and rapid method for the assay of bacterial fatty acids using high resolution capillary gas chromatography and trimethylsulfonium hydroxide. *Zentralblatt für Bakteriologie: International journal of medical microbiology*, 274(2):174–182.

Naehr, T. H., Eichhubl, P., Orphan, V. J., Hovland, M., Paull, C. K., Ussler III, W., Lorenson, T. D., and Greene, H. G. (2007). Authigenic carbonate formation at hydrocarbon seeps in continental margin sediments: A comparative study. *Deep Sea Research Part II: Topical Studies in Oceanography*, 54(11-13):1268–1291.

Nauhaus, K., Albrecht, M., Elvert, M., Boetius, A., and Widdel, F. (2007). In vitro cell growth of marine archaeal-bacterial consortia during anaerobic oxidation of methane with sulfate. *Environmental Microbiology*, 9(1):187–196.

Nes, W. R. (1974). Role of sterols in membranes. *Lipids*, 9(8):596–612.

Nichols, P. D., Shaw, P. M., Mancuso, C. A., and Franzmann, P. D. (1993). Analysis of archaeal phospholipid-derived di- and tetraether lipids by high temperature capillary gas chromatography. *Journal of Microbiological Methods*, 18(1):1–9.

Nickel, J. C., di Primio, R., Kallmeyer, J., Hammer, O., Horsfield, B., Stoddart, D., Brunstad, H., and Mangelsdorf, K. (2013). Tracing the origin of thermogenic hydrocarbon signals in pockmarks from the southwestern Barents Sea. *Organic Geochemistry*, 63(0):73–84.

Nickel, J. C., di Primio, R., Mangelsdorf, K., Stoddart, D., and Kallmeyer, J. (2012). Characterization of microbial activity in pockmark fields of the SW-Barents Sea. *Marine Geology*, 332-334(0):152–162.

Niemann, H. and Elvert, M. (2008). Diagnostic lipid biomarker and stable carbon isotope signatures of microbial communities mediating the anaerobic oxidation of methane with sulphate. *Organic Geochemistry*, 39(12):1668–1677.

Niemann, H., Lösekann, T., de Beer, D., Elvert, M., Nadalig, T., Knittel, K., Amann, R., Sauter, E. J., Schlüter, M., Klages, M., Foucher, J. P., and Boetius, A. (2006). Novel microbial communities of the Haakon Mosby mud volcano and their role as a methane sink. *Nature*, 443(7113):854–858. 10.1038/nature05227.

Norwegian Petroleum Directorate (2013). Oil discovery northwest of the Snøhvit field in the Barents Sea - 7120/1-3. *http://www.npd.no/en/news/Exploration-drilling-results/2013/71201-3/*.

Nyland, B., Jensen, L. N., Skagen, J., Skarpnes, O., and Vorren, T. O. (1992). Tertiary uplift and erosion in the Barents Sea: Magnitude, timing and consequences. In Larsen, R., Brekke, H., Larsen, B., and Talleraas, E., editors, *Structural and Tectonic Modelling and its Application to Petroleum Geology*, volume Special Publication 1., pages 153–162. Norwegian Petroleum Society, Amsterdam.

O'Connor, F. M., Boucher, O., Gedney, N., Jones, C. D., Folberth, G. A., Coppell, R., Friedlingstein, P., Collins, W. J., Chappellaz, J., Ridley, J., and Johnson, C. E. (2010). Possible role of wetlands, permafrost, and methane hydrates in the methane cycle under future climate change: A review. *Reviews of Geophysics*, 48(4):RG4005.

Ohm, S. E., Karlsen, D. A., and Austin, T. J. F. (2008). Geochemically driven exploration models in uplifted areas: Examples from the Norwegian Barents Sea. *AAPG Bulletin*, 92(9):1191–1223.

Olu-Le Roy, K., Caprais, J. C., Fifis, A., Fabri, M. C., Galéron, J., Budzinsky, H., Le Ménach, K., Khripounoff, A., Ondréas, H., and Sibuet, M. (2007). Cold-seep assemblages on a giant pockmark off West Africa: Spatial patterns and environmental control. *Marine Ecology*, 28(1):115–130.

Ondréas, H., Olu, K., Fouquet, Y., Charlou, J., Gay, A., Dennielou, B., Donval, J., Fifis, A., Nadalig, T., Cochonat, P., Cauquil, E., Bourillet, J., Moigne, M., and Sibuet, M. (2005). ROV study of a giant pockmark on the Gabon continental margin. *Geo-Marine Letters*, 25(5):281–292.

Orcutt, B. N., Sylvan, J. B., Knab, N. J., and Edwards, K. J. (2011). Microbial ecology of the dark ocean above, at, and below the seafloor. *Microbiology and Molecular Biology Reviews*, 75(2):361–422.

Orphan, V. J., Hinrichs, K. U., Ussler, W., r., Paull, C. K., Taylor, L. T., Sylva, S. P., Hayes, J. M., and Delong, E. F. (2001a). Comparative analysis of methane-oxidizing archaea and sulfate-reducing bacteria in anoxic marine sediments. *Applied and Environmental Microbiology*, 67(4):1922–34. Orphan, V J Hinrichs, K U Ussler, W 3rd Paull, C K Taylor, L T Sylva, S P Hayes, J M Delong, E F Appl Environ Microbiol. 2001 Apr;67(4):1922-34.

Orphan, V. J., House, C. H., Hinrichs, K.-U., McKeegan, K. D., and DeLong, E. F. (2001b). Methane-consuming archaea revealed by directly coupled isotopic and phylogenetic analysis. *Science*, 293(5529):484–487.

Orphan, V. J., House, C. H., Hinrichs, K.-U., McKeegan, K. D., and DeLong, E. F. (2002). Multiple archaeal groups mediate methane oxidation in anoxic cold seep sediments. *Proceedings of the National Academy of Sciences*, 99(11):7663–7668.

Orr, W. L. and Sinninghe Damsté, J. S. (1990). Geochemistry of sulfur in petroleum systems. In Orr, W. and White, C., editors, *Geochemistry of Sulfur in Fossil Fuels*, pages 2–29. ACS Symposium Series.

Ostanin, I., Anka, Z., di Primio, R., and Bernal, A. (2012). Identification of a large Upper Cretaceous polygonal fault network in the Hammerfest basin: Implications on the reactivation of regional faulting and gas leakage dynamics, SW Barents Sea. *Marine Geology*, 332-334(0):109–125.

Ostanin, I., Anka, Z., di Primio, R., and Bernal, A. (2013). Hydrocarbon plumbing systems above the Snøhvit gas field: Structural control and implications for thermogenic methane leakage in the Hammerfest Basin, SW Barents Sea. *Marine and Petroleum Geology*, 43(0):127–146.

Ourisson, G., Albrecht, P., and Rohmer, M. (1979). The hopanoids: Palaeochemistry and biochemistry of a group of natural products. *Pure and Applied Chemistry*, 51(4):709–729.

Pancost, R. D., Hopmans, E. C., and Sinninghe Damsté, J. S. (2001). Archaeal lipids in Mediterranean cold seeps: Molecular proxies for anaerobic methane oxidation. *Geochimica et Cosmochimica Acta*, 65(10):1611–1627.

Pancost, R. D., Sinninghe Damsté, J. S., de Lint, S., van der Maarel, M. J. E. C., Gottschal, J. C., and The Medinaut Shipboard Scientific Party (2000). Biomarker evidence for widespread anaerobic methane oxidation in mediterranean sediments by a consortium of methanogenic archaea and bacteria. *Applied and Environmental Microbiology*, 66(3):1126–1132.

Pape, T., Blumenberg, M., Seifert, R., Egorov, V. N., Gulin, S. B., and Michaelis, W. (2005). Lipid geochemistry of methane-seep-related Black Sea carbonates. *Palaeogeography, Palaeoclimatology, Palaeoecology*, 227:31–47.

Paull, C., Ussler, W., Maher, N., Greene, H. G., Rehder, G., Lorenson, T., and Lee, H. (2002). Pockmarks off Big Sur, California. *Marine Geology*, 181(4):323–335.

Paull, C. K., Hecker, B., Commeau, R., Freeman-Lynde, R. P., Neumann, C., Corso, W. P., Golubic, S., Hook, J. E., Sikes, E., and Curray, J. (1984). Biological communities at the Florida escarpment resemble hydrothermal vent taxa. *Science*, 226(4677):965–967.

Peckmann, J. and Thiel, V. (2004). Carbon cycling at ancient methane-seeps. *Chemical Geology*, 205(3-4):443–467.

Pernthaler, A., Dekas, A. E., Brown, C. T., Goffredi, S. K., Embaye, T., and Orphan, V. J. (2008). Diverse syntrophic partnerships from deep-sea methane vents revealed by direct cell capture and metagenomics. *Proceedings of the National Academy of Sciences*, 105(19):7052–7057.

Peters, K. E., Moldowan, J. M., Schoell, M., and Hempkins, W. B. (1986). Petroleum isotopic and biomarker composition related to source rock organic matter and depositional environment. *Organic Geochemistry*, 10(1-3):17–27.

Peters, K. E., Walters, C. C., and Moldowan, J. M. (2005a). *The Biomarker Guide: Volume 1, Biomarkers and Isotopes in the Environment and Human History*. Cambridge University Press, Cambridge, second edition.

Peters, K. E., Walters, C. C., and Moldowan, J. M. (2005b). *The Biomarker Guide: Volume 2, Biomarkers and Isotopes in Petroleum Systems and Earth History*. Cambridge University Press, Cambridge, second edition.

Piggott, N. and Abrams, M. A. (1996). Near-surface coring in the Beaufort and Chukchi Seas, northern Alaska. In Schumacher, D. and Abrams, M. A., editors, *Hydrocarbon Migration and Its Near-surface Expression.*, volume 66, pages 385–399. AAPG Memoir.

Pilcher, R. and Argent, J. (2007). Mega-pockmarks and linear pockmark trains on the West African continental margin. *Marine Geology*, 244(1-4):15–32.

Pimenov, N., Ul'yanova, M., Kanapatskii, T., Sivkov, V., and Ivanov, M. (2008). Microbiological and biogeochemical processes in a pockmark of the Gdansk depression, Baltic Sea. *Microbiology*, 77:579–586.

Pimenov, N., Ul'yanova, M., Kanapatsky, T., Veslopolova, E., Sigalevich, P., and Sivkov, V. (2010). Microbially mediated methane and sulfur cycling in pockmark sediments of the Gdansk Basin, Baltic Sea. *Geo-Marine Letters*, 30(3):439–448.

Plaza-Faverola, A., Bünz, S., and Mienert, J. (2012). The free gas zone beneath gas hydrate bearing sediments and its link to fluid flow: 3-D seismic imaging offshore mid-Norway. *Marine Geology*, 291-294(0):211–226.

Pohlman, J. W., Bauer, J. E., Waite, W. F., Osburn, C. L., and Chapman, N. R. (2011). Methane hydrate-bearing seeps as a source of aged dissolved organic carbon to the oceans. *Nature Geoscience*, 4(1):37–41.

Prior, D. B., Doyle, E. H., and Kaluza, M. J. (1989). Evidence for sediment eruption on deep sea floor, Gulf of Mexico. *Science*, 243(4890):517–519.

Radke, M., Sittardt, H. G., and Welte, D. H. (1978). Removal of soluble organic matter from rock samples with a flow-through extraction cell. *Analytical Chemistry*, 50(4):663–665.

Radke, M., Willsch, H., and Welte, D. H. (1980). Preparative hydrocarbon group type determination by automated medium pressure liquid chromatography. *Analytical Chemistry*, 52(3):406–411.

Raghoebarsing, A. A., Pol, A., van de Pas-Schoonen, K. T., Smolders, A. J. P., Ettwig, K. F., Rijpstra, W. I. C., Schouten, S., Sinninghe Damsté, J. S., Op den Camp, H. J. M., Jetten, M. S. M., and Strous, M. (2006). A microbial consortium couples anaerobic methane oxidation to denitrification. *Nature*, 440(7086):918–921.

Reeburgh, W. S. (1976). Methane consumption in Cariaco Trench waters and sediments. *Earth and Planetary Science Letters*, 28(3):337–344.

Reeburgh, W. S. (2007). Oceanic methane biogeochemistry. *Chemical Reviews*, 107(2):486–513.

Regnier, P., Dale, A. W., Arndt, S., LaRowe, D. E., Mogollón, J., and Van Cappellen, P. (2011). Quantitative analysis of anaerobic oxidation of methane (AOM) in marine sediments: A modeling perspective. *Earth-Science Reviews*, 106(1-2):105–130.

Rhead, M., Eglinton, G., Draffan, G., and England, P. (1971a). Conversion of oleic acid to saturated fatty acids in severn estuary sediments. *Nature*, 232:327–330.

Rhead, M. M., Eglinton, G., and Draffan, G. H. (1971b). Hydrocarbons produced by the thermal alteration of cholesterol under conditions simulating the maturation of sediments. *Chemical Geology*, 8(4):277–297.

Rice, D. D. and Claypool, G. E. (1981). Generation, accumulation, and resource potential of biogenic gas. *AAPG Bulletin*, 65(1):5–25.

Risatti, J. B., Rowland, S. J., Yon, D. A., and Maxwell, J. R. (1984). Stereochemical studies of acyclic isoprenoids-XII. Lipids of methanogenic bacteria and possible contributions to sediments. *Organic Geochemistry*, 6(0):93–104.

Ritger, S., Carson, B., and Suess, E. (1987). Methane-derived authigenic carbonates formed by subduction-induced pore-water expulsion along the Oregon/Washington margin. *Geological Society of America Bulletin*, 98(2):147–156.

Rodrigues Duran, E., di Primio, R., Anka, Z., Stoddart, D., and Horsfield, B. (2013a). 3D-basin modelling of the Hammerfest Basin (southwestern Barents Sea): A quantitative assessment of petroleum generation, migration and leakage. *Marine and Petroleum Geology*, 45(0):281–303.

Rodrigues Duran, E., di Primio, R., Anka, Z., Stoddart, D., and Horsfield, B. (2013b). Petroleum system analysis of the Hammerfest Basin (southwestern Barents Sea): Comparison of basin modelling and geochemical data. *Organic Geochemistry*, 63(0):105–121.

Rohmer, M., Bouvier-Nave, P., and Ourisson, G. (1984). Distribution of hopanoid triterpenes in prokaryotes. *Journal of General Microbiology*, 130(5):1137–1150.

Rowland, S. J. (1990). Production of acyclic isoprenoid hydrocarbons by laboratory maturation of methanogenic bacteria. *Organic Geochemistry*, 15(1):9–16.

Ruiz, M. (2007). http://commons.wikimedia.org/wiki/File:Cell_membrane_detailed_diagram_en.svg.

Rushdi, A. I. and Simoneit, B. R. T. (2002). Hydrothermal alteration of organic matter in sediments of the northeastern Pacific Ocean: Part 1. Middle Valley, Juan de Fuca Ridge. *Applied Geochemistry*, 17(11):1401–1428.

Rütters, H., Sass, H., Cypionka, H., and Rullkötter, J. (2002). Phospholipid analysis as a tool to study complex microbial communities in marine sediments. *Journal of Microbiological Methods*, 48(2-3):149–160.

Sassen, R., Losh, S. L., Cathles III, L., Roberts, H. H., Whelan, J. K., Milkov, A. V., Sweet, S. T., and DeFreitas, D. A. (2001). Massive vein-filling gas hydrate: Relation to ongoing gas migration from the deep subsurface in the Gulf of Mexico. *Marine and Petroleum Geology*, 18(5):551–560.

Schimel, D. and 75 others (1996). Radiative forcing of climate change. In Houghton, J., Meira Filho, L., Callander, B., Harris, N., Kattenberg, A., and Maskell, K., editors, *Climate change 1995: the science of climate change*, pages 65–131, Cambridge, UK. Cambridge University Press.

Schippers, A., Köweker, G., Höft, C., and Teichert, B. M. A. (2010). Quantification of microbial communities in forearc sediment basins off Sumatra. *Geomicrobiology Journal*, 27(2):170–182.

Schouten, S., Hoefs, M. J. L., Koopmans, M. P., Bosch, H.-J., and Sinninghe Damsté, J. S. (1998). Structural characterization, occurrence and fate of archaeal ether-bound acyclic and cyclic biphytanes and corresponding diols in sediments. *Organic Geochemistry*, 29(5-7):1305–1319.

Schouten, S., Hopmans, E. C., Pancost, R. D., and Damsté, J. S. S. (2000). Widespread occurrence of structurally diverse tetraether membrane lipids: Evidence for the ubiquitous presence of low-temperature relatives of hyperthermophiles. *Proceedings of the National Academy of Sciences*, 97(26):14421–14426.

Schouten, S., Hopmans, E. C., and Sinninghe Damsté, J. S. (2013). The organic geochemistry of glycerol dialkyl glycerol tetraether lipids: A review. *Organic Geochemistry*, 54(0):19–61.

Schouten, S., Wakeham, S. G., and Damsté, J. S. S. (2001). Evidence for anaerobic methane oxidation by archaea in euxinic waters of the Black Sea. *Organic Geochemistry*, 32(10):1277–1281.

Schumacher, D. and Abrams, M. A. (1994). *Hydrocarbon Migration and its Near-Surface Expression*, volume 66. American Association of Petroleum Geologists Memoir 66, Tulsa, Oklahoma, US.

Seifert, W. K. and Moldowan, J. M. (1980). The effect of thermal stress on source-rock quality as measured by hopane stereochemistry. *Physics and Chemistry of The Earth*, 12(0):229–237.

Seifert, W. K. and Moldowan, J. M. (1981). Paleoreconstruction by biological markers. *Geochimica et Cosmochimica Acta*, 45(6):783–794.

Seinfeld, J. H. and Pandis, S. N. (2006). *Atmospheric Chemistry and Physics: From Air Pollution to Climate Change*, volume 2. John Wiley & Sons, Hoboken, New Jersey.

Sheppard, J. C., Westberg, H., Hopper, J. F., Ganesan, K., and Zimmerman, P. (1982). Inventory of global methane sources and their production rates. *Journal of Geophysical Research: Oceans*, 87(C2):1305–1312.

Shipley, T., Houston, M., Buffler, R., Shaub, F., McMillen, K., Ladd, J., and Worzel, J. (1979). Seismic evidence for widespread possible gas hydrate horizons on continental slopes and rises. *American Association of Petroleum Geologists Bulletin*, 63(12):2204–2213.

Sibuet, M. and Olu, K. (1998). Biogeography, biodiversity and fluid dependence of deep-sea cold-seep communities at active and passive margins. *Deep Sea Research Part II: Topical Studies in Oceanography*, 45(1-3):517–567.

Siegert, M. J., Dowdeswell, J. A., Hald, M., and Svendsen, J.-I. (2001). Modelling the eurasian ice sheet through a full (Weichselian) glacial cycle. *Global and Planetary Change*, 31(1-4):367–385.

Sills, G. C. and Wheeler, S. J. (1992). The significance of gas for offshore operations. *Continental Shelf Research*, 12(10):1239–1250.

Simoneit, B. R. T., Leif, R. N., Sturz, A. A., Sturdivant, A. E., and Gieskes, J. M. (1992). Geochemistry of shallow sediments in Guaymas Basin, Gulf of California: Hydrothermal gas and oil migration and effects of mineralogy. *Organic Geochemistry*, 18(6):765–784.

Sinninghe Damsté, J. S., Schouten, S., Hopmans, E. C., van Duin, A. C. T., and Geenevasen, J. A. J. (2002). Crenarchaeol: The characteristic core glycerol dibiphytanyl glycerol tetraether membrane lipid of cosmopolitan pelagic crenarchaeota. *Journal of Lipid Research*, 43(10):1641–1651.

Sinninghe Damsté, J. S., Schouten, S., van Vliet, N. H., Huber, R., and Geenevasen, J. A. J. (1997). A polyunsaturated irregular acyclic C_{25} isoprenoid in a methanogenic archaeon. *Tetrahedron Letters*, 38(39):6881–6884.

Sinninghe Damsté, J. S., Van Duin, A. C. T., Hollander, D., Kohnen, M. E. L., and De Leeuw, J. W. (1995). Early diagenesis of bacteriohopanepolyol derivatives: Formation of fossil homohopanoids. *Geochimica et Cosmochimica Acta*, 59(24):5141–5157.

Sivan, O., Adler, M., Pearson, A., Gelman, F., Bar-Or, I., John, S. G., and Eckerte, W. (2011). Geochemical evidence for iron-mediated anaerobic oxidation of methane. *Limnology and Oceanography*, 56(4):1536–1544.

Sloan, E. D. (2003). Fundamental principles and applications of natural gas hydrates. *Nature*, 426(6964):353–363.

Sloan, E. D. and Koh, C. A. (2008). *Clathrate Hydrates of Natural Gases*. CRC Press, Boca Raton, FL, 3rd edition.

Snyder, L. R. (1970). Petroleum nitrogen compounds and oxygen compounds. *Accounts of Chemical Research*, 3(9):290–299.

Solheim, A. (1991). The depositional environment of surging sub-polar tidewater glaciers: A case study of the morphology, sedimentation and sediment properties in a surge affected marine basin outside Nordaustlandet, Northern Barents Sea. *Norsk Polarinstitutt Skrifter*, 194:97.

Solheim, A. and Elverhøi, A. (1985). A pockmark field in the central Barents Sea; gas from a petrogenic source? *Polar Research*, 3(1):11–19.

Solheim, A. and Elverhøi, A. (1993). Gas-related sea floor craters in the Barents Sea. *Geo-Marine Letters*, 13(4):235–243.

Spies, R. B. and Davis, P. H. (1979). The infaunal benthos of a natural oil seep in the Santa Barbara channel. *Marine Biology*, 50(3):227–237.

Spötl, C. and Vennemann, T. W. (2003). Continuous-flow isotope ratio mass spectrometric analysis of carbonate minerals. *Rapid Communications in Mass Spectrometry*, 17(9):1004–1006.

Sprott, G. D., Dicaire, C. J., Choquet, C. G., Patel, G. B., and Ekiel, I. (1993). Hydroxydiether lipid structures in Methanosarcina spp. and Methanococcus voltae. *Applied and Environmental Microbiology*, 59(3):912–914.

Stadnitskaia, A., Bouloubassi, I., Elvert, M., Hinrichs, K. U., and Sinninghe Damsté, J. S. (2008). Extended hydroxyarchaeol, a novel lipid biomarker for anaerobic methanotrophy in cold seepage habitats. *Organic Geochemistry*, 39(8):1007–1014.

Stadnitskaia, A., Muyzer, G., Abbas, B., Coolen, M. J. L., Hopmans, E. C., Baas, M., van Weering, T. C. E., Ivanov, M. K., Poludetkina, E., and Sinninghe Damsté, J. S. (2005). Biomarker and 16S rDNA evidence for anaerobic oxidation of methane and related carbonate precipitation in deep-sea mud volcanoes of the Sorokin Trough, Black Sea. *Marine Geology*, 217(1-2):67–96.

Sultan, N., Marsset, B., Ker, S., Marsset, T., Voisset, M., Vernant, A. M., Bayon, G., Cauquil, E., Adamy, J., Colliat, J. L., and Drapeau, D. (2010). Hydrate dissolution as a potential mechanism for pockmark formation in the Niger Delta. *Journal of Geophysical Research*, 115(B8):B08101.

Sweet Jr., W. E. (1974). Tar balls in the sea: A new source concept.

Taniguchi, M., Burnett, W. C., Cable, J. E., and Turner, J. V. (2002). Investigation of submarine groundwater discharge. *Hydrological Processes*, 16:2115–2129.

Tegelaar, E. W., de Leeuw, J. W., Derenne, S., and Largeau, C. (1989). A reappraisal of kerogen formation. *Geochimica et Cosmochimica Acta*, 53:3103–3106.

Teske, A., Hinrichs, K.-U., Edgcomb, V., de Vera Gomez, A., Kysela, D., Sylva, S. P., Sogin, M. L., and Jannasch, H. W. (2002). Microbial diversity

of hydrothermal sediments in the Guaymas Basin: Evidence for anaerobic methanotrophic communities. *Applied and Environmental Microbiology*, 68(4):1994–2007.

Thauer, R. K. and Shima, S. (2008). Methane as fuel for anaerobic microorganisms. *Annals of the New York Academy of Sciences*, 1125(1):158–170.

Thiel, V., Blumenberg, M., Pape, T., Seifert, R., and Michaelis, W. (2003). Unexpected occurrence of hopanoids at gas seeps in the Black Sea. *Organic Geochemistry*, 34:81–87.

Thiel, V., Peckmann, J., Richnow, H. H., Luth, U., Reitner, J., and Michaelis, W. (2001). Molecular signals for anaerobic methane oxidation in Black Sea seep carbonates and a microbial mat. *Marine Chemistry*, 73(2):97–112.

Thrasher, J., Strait, D., and Lugo, R. (1996). Surface geochemistry as an exploration tool in the south Caribbean. In Schumacher, D. and Abrams, M., editors, *Hydrocarbon Migration and its Near-surface Expression*, volume 66, pages 373–384. American Association of Petroleum Geologists Memoir.

Tiedje, J. M., Sexstone, A. J., Parkin, T. B., and Revsbech, N. P. (1984). Anaerobic processes in soil. *Plant and Soil*, 76:197–212.

Tissot, B. P. and Welte, D. H. (1984). *Petroleum Formation and Occurrence*. Springer Verlag, Heidelberg, 2nd edition.

Tornabene, T. and Langworthy, T. (1979). Diphytanyl and dibiphytanyl glycerol ether lipids of methanogenic archaebacteria. *Science*, 203(4375):51–53.

Treibs, A. (1936). Chlorophyll- und Häminderivate in organischen Mineralstoffen. *Angewandte Chemie*, 49(38):682–686.

Treude, T., Boetius, A., Knittel, K., Wallmann, K., and Jørgensen, B. B. (2003). Anaerobic oxidation of methane above gas hydrates at Hydrate Ridge, NE Pacific Ocean. *Marine Ecology Progress Series*, 264:1–14.

Treude, T., Krüger, M., Boetius, A., and Jørgensen, B. B. (2005a). Environmental control on anaerobic oxidation of methane in the gassy sediments of Eckernförde Bay (German Baltic). *Limnology and Oceanography*, 50(6):1771–1786.

Treude, T., Niggemann, J., Kallmeyer, J., Wintersteller, P., Schubert, C. J., Boetius, A., and Jørgensen, B. B. (2005b). Anaerobic oxidation of methane and sulfate reduction along the Chilean continental margin. *Geochimica et Cosmochimica Acta*, 69(11):2767–2779.

Ussler, W., Paull, C. K., Boucher, J., Friederich, G. E., and Thomas, D. J. (2003). Submarine pockmarks: A case study from Belfast Bay, Maine. *Marine Geology*, 202(3-4):175–192.

Vadakkepuliyambatta, S., Bünz, S., Mienert, J., and Chand, S. (2013). Distribution of subsurface fluid-flow systems in the SW Barents Sea. *Marine and Petroleum Geology*, 43(0):208–221.

Valentine, D. L. (2002). Biogeochemistry and microbial ecology of methane oxidation in anoxic environments: A review. *Antonie van Leeuwenhoek*, 81:271–282.

Valentine, D. L. and Reeburgh, W. S. (2000). New perspectives on anaerobic methane oxidation. *Environmental Microbiology*, 2(5):477–484.

Vaular, E. N., Barth, T., and Haflidason, H. (2010). The geochemical characteristics of the hydrate-bound gases from the Nyegga pockmark field, Norwegian Sea. *Organic Geochemistry*, 41(5):437–444.

Vestal, J. R. and White, D. C. (1989). Lipid analysis in microbial ecology. *BioScience*, 39(8):535–541.

Vogt, P. R., Crane, K., Sundvor, E., Max, M. D., and Pfirman, S. L. (1994). Methane-generated (?) pockmarks on young, thickly sedimented oceanic crust in the Arctic: Vestnesa ridge, Fram strait. *Geology*, 22(3):255–258.

Volkman, J. K., Barrett, S. M., Blackburn, S. I., Mansour, M. P., Sikes, E. L., and Gelin, F. (1998). Microalgal biomarkers: A review of recent research developments. *Organic Geochemistry*, 29(5-7):1163–1179.

Vorren, T. O. and Laberg, J. S. (1996). Late glacial air temperature, oceanographic and ice sheet interactions in the southern Barents Sea region. *Geological Society, London, Special Publications*, 111(1):303–321.

Vorren, T. O., Richardsen, G., Knutsen, S.-M., and Henriksen, E. (1991). Cenozoic erosion and sedimentation in the western Barents Sea. *Marine and Petroleum Geology*, 8(3):317–340.

Vu, T. T. A., Zink, K. G., Mangelsdorf, K., Sykes, R., Wilkes, H., and Horsfield, B. (2009). Changes in bulk properties and molecular compositions within New Zealand Coal Band solvent extracts from early diagenetic to catagenetic maturity levels. *Organic Geochemistry*, 40(9):963–977.

Wakeham, S. G., Hopmans, E. C., Schouten, S., and Sinninghe Damsté, J. S. (2004). Archaeal lipids and anaerobic oxidation of methane in euxinic water columns: A comparative study of the Black Sea and Cariaco Basin. *Chemical Geology*, 205:427–442.

Wakeham, S. G., Lewis, C. M., Hopmans, E. C., Schouten, S., and Sinninghe Damsté, J. S. (2003). Archaea mediate anaerobic oxidation of methane in deep euxinic waters of the Black Sea. *Geochimica et Cosmochimica Acta*, 67(7):1359–1374.

Wang, Z., Stout, S. A., and Fingas, M. (2006). Forensic fingerprinting of biomarkers for oil spill characterization and source identification. *Environmental Forensics*, 7(2):105–146.

Wankel, S. D., Adams, M. M., Johnston, D. T., Hansel, C. M., Joye, S. B., and Girguis, P. R. (2012). Anaerobic methane oxidation in metalliferous hydrothermal sediments: Influence on carbon flux and decoupling from sulfate reduction. *Environmental Microbiology*, 14(10):2726–2740.

Watkinson, R. J. and Morgan, P. (1991). Physiology of aliphatic hydrocarbon-degrading microorganisms. In Ratledge, C., editor, *Physiology of Biodegradative Microorganisms*, pages 79–92, Netherlands. Springer.

Webb, K., Hammer, Ø., Lepland, A., and Gray, J. (2009). Pockmarks in the inner Oslofjord, Norway. *Geo-Marine Letters*, 29(2):111–124.

Weber, A., Riess, W., Wenzhoefer, F., and Jørgensen, B. B. (2001). Sulfate reduction in Black Sea sediments: in situ and laboratory radiotracer measurements from the shelf to 2000 m depth. *Deep Sea Research Part I: Oceanographic Research Papers*, 48(9):2073–2096.

Wegener, G., Shovitri, M., Knittel, K., Niemann, H., Hovland, M., and Boetius, A. (2008). Biogeochemical processes and microbial diversity of the Gullfaks and Tommeliten methane seeps (Northern North Sea). *Biogeosciences*, 5:1127–1144.

Weijers, J. W. H., Lim, K. L. H., Aquilina, A., Sinninghe Damsté, J. S., and Pancost, R. D. (2011). Biogeochemical controls on glycerol dialkyl glycerol tetraether lipid distributions in sediments characterized by diffusive methane flux. *Geochemistry, Geophysics, Geosystems*, 12(10):Q10010.

Weijers, J. W. H., Schouten, S., Hopmans, E. C., Geenevasen, J. A. J., David, O. R. P., Coleman, J. M., Pancost, R. D., and Sinninghe Damsté, J. S. (2006a). Membrane lipids of mesophilic anaerobic bacteria thriving in peats have typical archaeal traits. *Environmental Microbiology*, 8(4):648–657.

Weijers, J. W. H., Schouten, S., Spaargaren, O. C., and Sinninghe Damsté, J. S. (2006b). Occurrence and distribution of tetraether membrane lipids in soils: Implications for the use of the TEX_{86} proxy and the bit index. *Organic Geochemistry*, 37(12):1680–1693.

Weiss, H., Wilhelms, A., Mills, N., Scotchmer, J., Hall, P., Lind, K., and Brekke, T. (2000). *NIGOGA - The Norwegian industry guide to organic geochemical analyses*. Norsk Hydro, Statoil, Geolab Nor, SINTEF Petroleum Research, Norwegian Petroleum Directorate, 4^{th} edition.

Wenger, L. M. and Isaksen, G. H. (2002). Control of hydrocarbon seepage intensity on level of biodegradation in sea bottom sediments. *Organic Geochemistry*, 33(12):1277–1292.

White, D. C., Davis, W. M., Nickels, J. S., King, J. D., and Bobbie, R. J. (1979). Determination of the sedimentary microbial biomass by extractible lipid phosphate. *Oecologia*, 40(1):51–62.

Whiticar, M. and Werner, F. (1981). Pockmarks: Submarine vents of natural gas or freshwater seeps? *Geo-Marine Letters*, 1(3):193–199.

Whiticar, M. J. (1990). A geochemial perspective of natural gas and atmospheric methane. *Organic Geochemistry*, 16(1-3):531–547.

Whiticar, M. J. (1999). Carbon and hydrogen isotope systematics of bacterial formation and oxidation of methane. *Chemical Geology*, 161(1-3):291–314.

Whiticar, M. J. (2000). Can stable isotopes and global budgets be used to constrain atmospheric methane budgets? In Khalil, M. A. K., editor, *Atmospheric Methane*, pages 63–85, Berlin Heidelberg. Springer-Verlag.

Whiticar, M. J. (2002). Diagenetic relationships of methanogenesis, nutrients, acoustic turbidity, pockmarks and freshwater seepages in Eckernförde Bay. *Marine Geology*, 182(1-2):29–53.

Woese, C. R., Kandler, O., and Wheelis, M. L. (1990). Towards a natural system of organisms: Proposal for the domains archaea, bacteria, and eucarya. *Proceedings of the National Academy of Sciences*, 87(12):4576–4579.

Wood, R. J., Edrich, S., and Hutchison, I. (1989). Influence of North Atlantic tectonics on the large scale uplift of Stappen High and Loppa High, western Barents Shelf. In Tankard, A. and Balkwill, H., editors, *Extensional Tectonics and Stratigraphy of the North Atlantic Margins*, volume 46, pages 559–566. American Association of Petroleum Geologists Memoir 46.

Woodside, J. M., David, L., Frantzis, A., and Hooker, S. K. (2006). Gouge marks on deep-sea mud volcanoes in the eastern Mediterranean: Caused by Cuvier's beaked whales? *Deep Sea Research Part I: Oceanographic Research Papers*, 53(11):1762–1771.

Woolsey, T. S., McCallum, M. E., and Schumm, S. A. (1975). Modeling of diatreme emplacement by fluidization. *Physics and Chemistry of The Earth*, 9(0):29–42.

Wuchter, C., Schouten, S., Boschker, H. T. S., and Sinninghe Damsté, J. S. (2003). Bicarbonate uptake by marine Crenarchaeota. *FEMS Microbiology Letters*, 219(2):203–207.

Yunker, M. B., Snowdon, L. R., Macdonald, R. W., Smith, J. N., Fowler, M. G., Skibo, D. N., McLaughlin, F. A., Danyushevskaya, A. I., Petrova, V. I., and Ivanov, G. I. (1996). Polycyclic aromatic hydrocarbon composition and potential sources for sediment samples from the Beaufort and Barents seas. *Environmental Science & Technology*, 30(4):1310–1320.

Zelles, L. (1999). Fatty acid patterns of phospholipids and lipopolysaccharides in the characterisation of microbial communities in soil: A review. *Biology and Fertility of Soils*, 29(2):111–129.

Zhang, C. L., Li, Y., Wall, J. D., Larsen, L., Sassen, R., Huang, Y., Wang, Y., Peacock, A., White, D. C., Horita, J., and Cole, D. R. (2002). Lipid and carbon isotopic evidence of methane-oxidizing and sulfate-reducing bacteria in association with gas hydrates from the Gulf of Mexico. *Geology*, 30(3):239–242.

Zhang, C. L., Pancost, R. D., Sassen, R., Qian, Y., and Macko, S. A. (2003). Archaeal lipid biomarkers and isotopic evidence of anaerobic methane oxidation associated with gas hydrates in the Gulf of Mexico. *Organic Geochemistry*, 34(6):827–836.

Zhang, Y. G., Zhang, C. L., Liu, X.-L., Li, L., Hinrichs, K.-U., and Noakes, J. E. (2011). Methane Index: A tetraether archaeal lipid biomarker indicator for detecting the instability of marine gas hydrates. *Earth and Planetary Science Letters*, 307(3-4):525–534.

Zink, K.-G. and Mangelsdorf, K. (2004). Efficient and rapid method for extraction of intact phospholipids from sediments combined with molecular structure elucidation using LC-ESI-MS-MS analysis. *Analytical and Bioanalytical Chemistry*, 380(5):798–812.

Zink, K. G., Wilkes, H., Disko, U., Elvert, M., and Horsfield, B. (2003). Intact phospholipids-microbial "life markers" in marine deep subsurface sediments. *Organic Geochemistry*, 34(6):755–769.

Appendix A

Molecular Structures

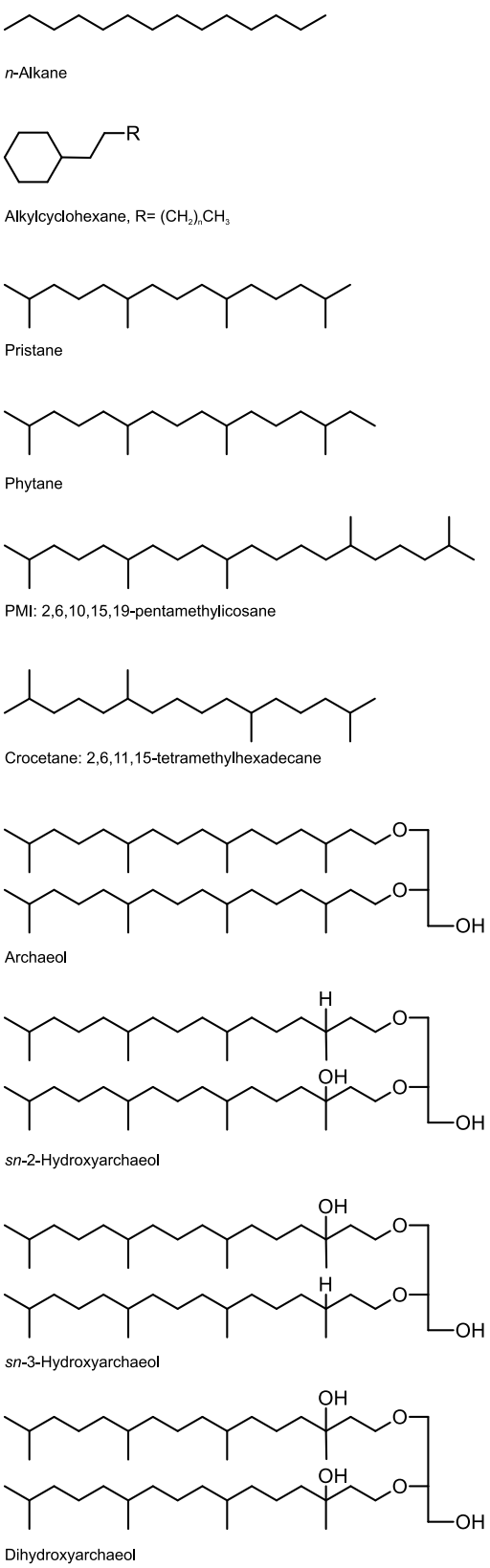

Figure A.1: Archaeols and saturated alkanes

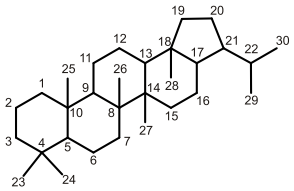

General structure

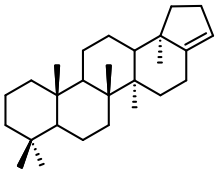

22,29,30-Trinorhop-17(21)-ene

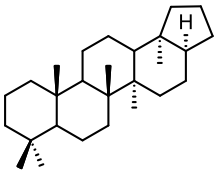

Tm: 17α(H)-22,29,30-Trinorhopane

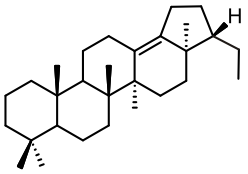

30-Norneohop-13(18)-ene

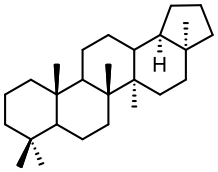

Ts: 18α(H)-22,29,30-Trinorneohopane

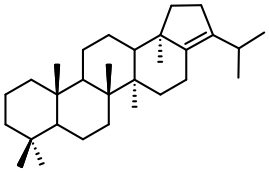

Hop-17(21)-ene

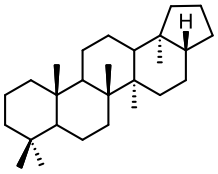

17β(H)-22,29,30-Trinorhopane

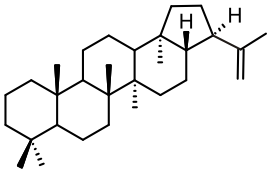

17β(H),21α(H)-Hop-22(29)ene (diploptene)

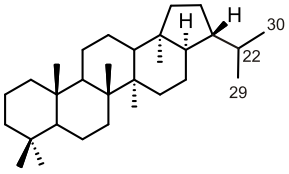

17α(H),21β(H)-Hopanes (C_{28}-C_{30})

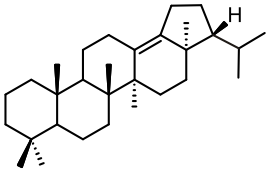

Neohop-13(18)-ene

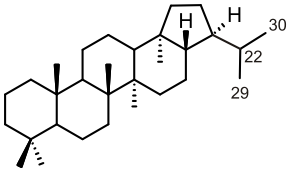

17β(H),21α(H)-Hopanes (C_{28}-C_{30})

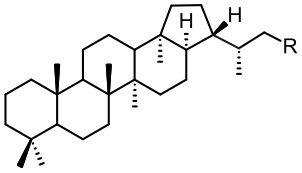

(22S)-17α(H),21β(H)-Hopanes (C_{31}-C_{35})

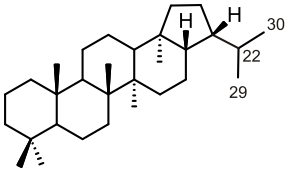

17β(H),21β(H)-Hopanes (C_{28}-C_{30})

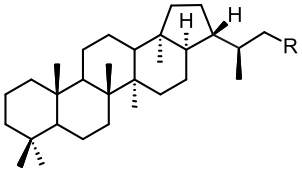

(22R)-17α(H),21β(H)-Hopanes (C_{31}-C_{35})

Figure A.2: Pentacyclic triterpanes

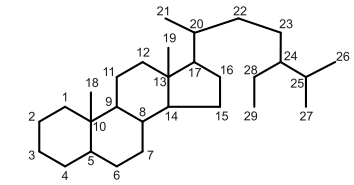

General structure R= H, C_1- C_3

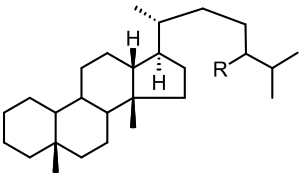

20*R*-13β(H),17α(H)-Diacholestanes (C_{27}-C_{30})

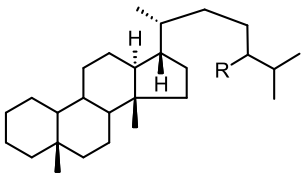

20*R*-13α(H),17β(H)-Diacholestanes (C_{27}-C_{30})

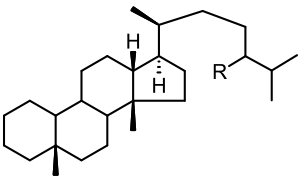

20S-13β(H),17α(H)-Diacholestanes (C_{27}-C_{30})

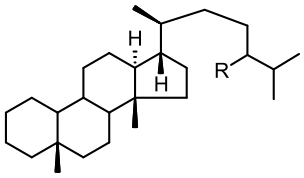

20S-13α(H),17β(H)-Diacholestanes (C_{27}-C_{30})

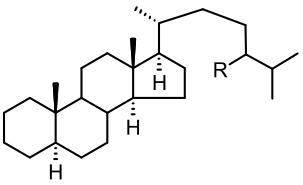

20*R*-5α(H),14α(H),17α(H)-Cholestanes (C_{27}-C_{30})

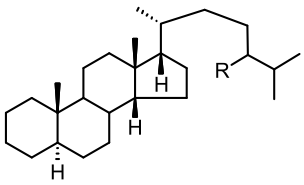

20*R*-5α(H),14β(H),17β(H)-Cholestanes (C_{27}-C_{30})

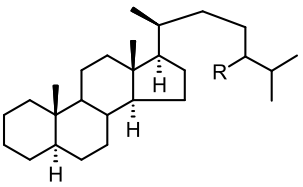

20*S*-5α(H),14α(H),17α(H)-Cholestanes (C_{27}-C_{30})

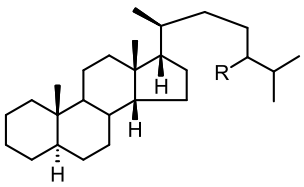

20*S*-5α(H),14β(H),17β(H)-Cholestanes (C_{27}-C_{30})

Figure A.3: Steranes and diasteranes

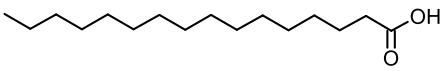

Saturated fatty acid, e.g. 16:0-FA

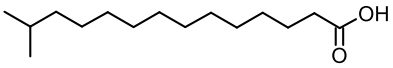

iso-Methyl-branched fatty acid, e.g. *iso*-15:0-FA

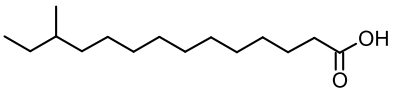

anteiso-Methyl-branched fatty acid, e.g. *ai*-15:0-FA

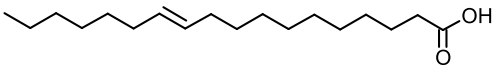

Unsaturated fatty acid (trans), e.g. 18:1ω7t-FA

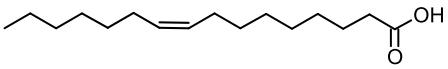

Unsaturated fatty acid (cis), e.g. 16:1ω7c-FA

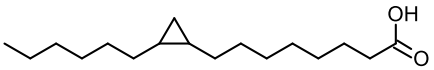

Cyclopropyl fatty acid, e.g. cy17:0-FA

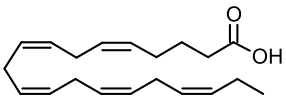

Polyunsaturated fatty acid, e.g. 22:5-FA

Figure A.4: Phospholipid fatty acids (PLFAs)

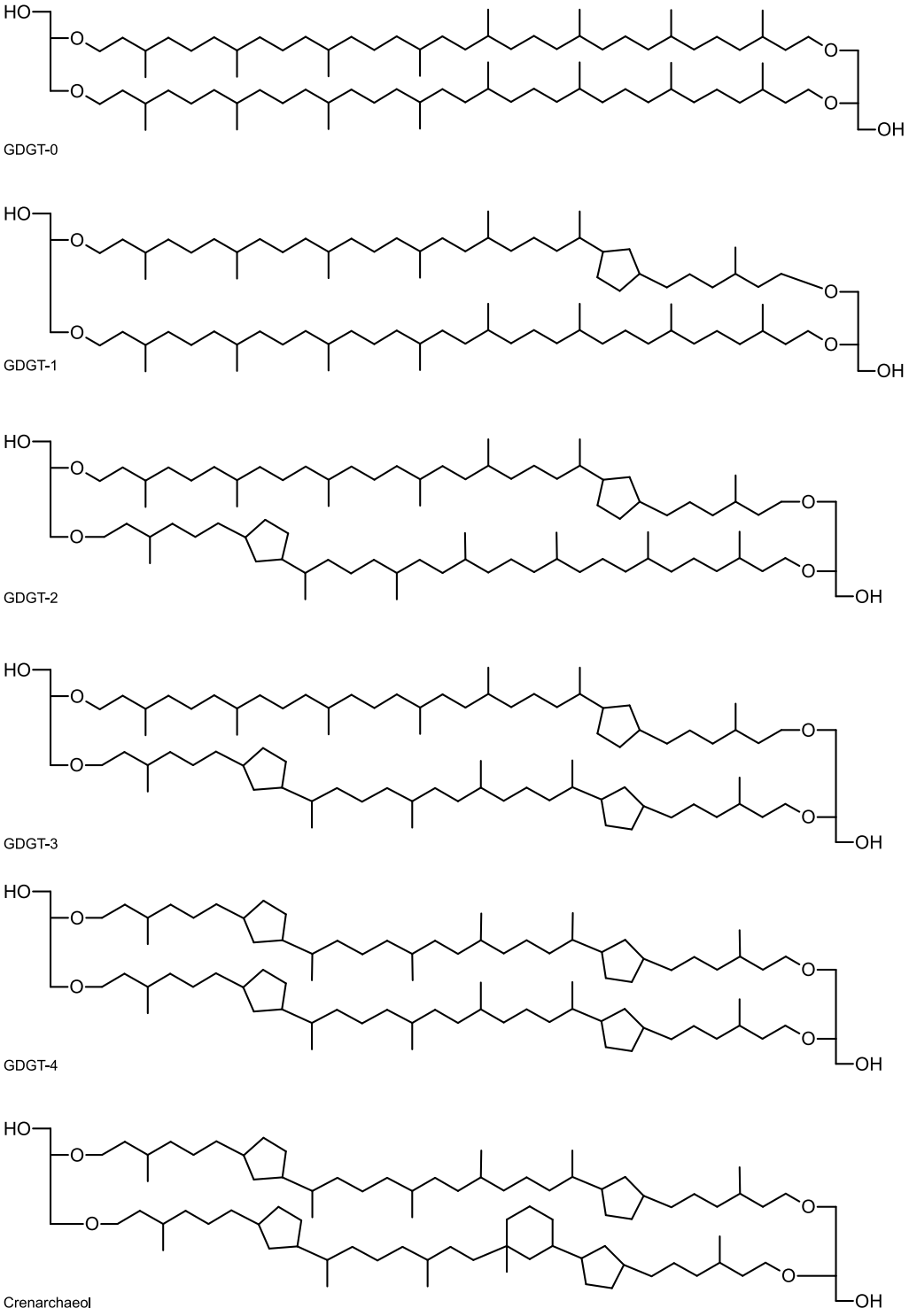

Figure A.5: Glycerol dialkyl glycerol tetraethers (GDGTs)

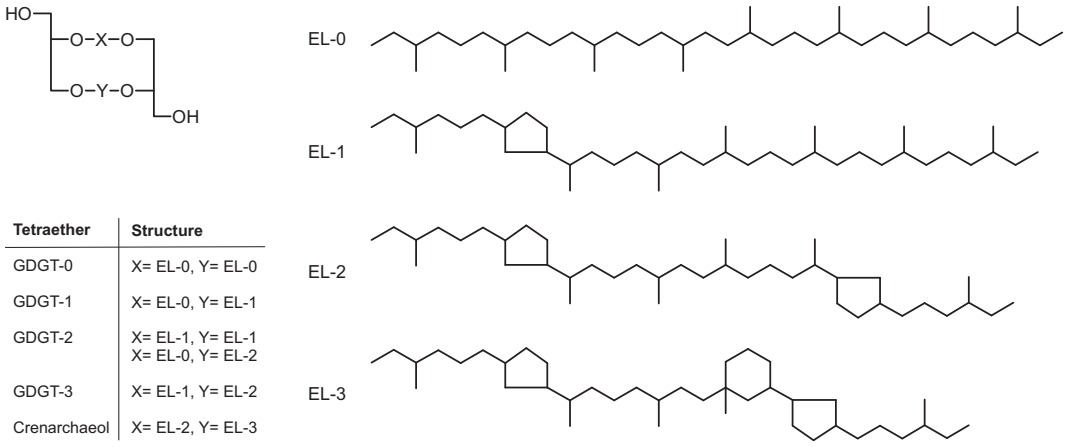

Tetraether	Structure
GDGT-0	X= EL-0, Y= EL-0
GDGT-1	X= EL-0, Y= EL-1
GDGT-2	X= EL-1, Y= EL-1 X= EL-0, Y= EL-2
GDGT-3	X= EL-1, Y= EL-2
Crenarchaeol	X= EL-2, Y= EL-3

Figure A.6: Ether cleavage products of GDGTs

Appendix B

Publication Data

Table B.1: Data of Figure 2.3.

Sample	**Adsorbed Gas, Area B**	**Coordinates**	
	Methane	WGS84, Zone 34	
	μmol/L Sediment	Longitude (E)	Latitude (N)
LU 078	16.67	20.51263	72.08615
LU 081	11.37	20.51119	72.08613
LU 084	7.97	20.51250	72.08581
LU 088	3.70	20.51115	72.08580
LU 091	6.63	20.50968	72.08636
LU 093	1.43	20.50987	72.08581
LU 094	6.16	20.51000	72.08553
LU 095	4.44	20.51020	72.08508
LU 096	8.72	20.51101	72.08656
LU 097	8.01	20.51112	72.08644
LU 098	3.80	20.51105	72.08594
LU 099	8.74	20.51111	72.08562
LU 104	3.32	20.51197	72.08543
LU 105	3.28	20.51195	72.08635
LU 106	6.48	20.51216	72.08516
LU 108	16.79	20.51272	72.08519
LU 109	6.26	20.51304	72.08668
LU 110	19.68	20.51308	72.08625
LU 111	7.42	20.51328	72.08603
LU 113	6.22	20.51347	72.08527
LU 114	8.83	20.51433	72.08564
LU 115	2.15	20.51423	72.08669
LU 116	3.24	20.51444	72.08620
LU 117	7.23	20.51434	72.08646
LU 118	6.48	20.51444	72.08579
LU 119	20.38	20.51445	72.08516
LU 120	5.96	20.51528	72.08688
LU 121	4.87	20.51531	72.08659

continued on next page

Table B.1 – continued

Sample	**Adsorbed Gas, Area B**	**Coordinates**	
	Methane	WGS84, Zone 34	
	μmol/L Sediment	Longitude (E)	Latitude (N)
LU 122	6.49	20.51550	72.08616
LU 123	6.30	20.51553	72.08579
LU 124	2.77	20.49680	72.08801
LU 125	3.55	20.49727	72.08623
LU 126	2.84	20.49803	72.08455
LU 127	5.82	20.49866	72.08279
LU 128	4.12	20.50268	72.08828
LU 130	5.03	20.50394	72.08470
LU 131	3.33	20.50442	72.08292
LU 133	13.81	20.50632	72.08659
LU 134	3.52	20.50680	72.08573
LU 135	9.48	20.50703	72.08477
LU 136	2.68	20.50733	72.08388
LU 139	5.66	20.50855	72.08561
LU 140	4.48	20.50873	72.08442
LU 141	1.73	20.50901	72.08849
LU 142	2.91	20.51034	72.08312
LU 143	5.92	20.51039	72.08390
LU 145	5.69	20.51213	72.08768
LU 146	8.83	20.51276	72.08455
LU 147	1.17	20.51334	72.08402
LU 148	4.07	20.51414	72.08868
LU 149	1.92	20.51538	72.08733
LU 150	8.22	20.51598	72.08398
LU 151	14.83	20.51599	72.08474
LU 152	4.86	20.51616	72.08330
LU 153	5.81	20.51738	72.08788
LU 154	7.61	20.51794	72.08689
LU 155	5.57	20.51819	72.08610

continued on next page

Table B.1 – continued

Sample	**Adsorbed Gas, Area B**	**Coordinates**	
	Methane	WGS84, Zone 34	
	μmol/L Sediment	Longitude (E)	Latitude (N)
LU 156	8.54	20.5185	72.08502
LU 157	9.14	20.5188	72.08413
LU 158	2.25	20.5199	72.08890
LU 159	4.48	20.5205	72.08699
LU 160	3.71	20.5214	72.08519
LU 161	5.06	20.5219	72.08351
LU 162	3.03	20.5260	72.08910
LU 163	2.42	20.5266	72.08728
LU 164	3.60	20.5275	72.08547
LU 165	4.45	20.5279	72.08370
LU 167	5.54	20.5053	72.08714
LU 168	5.61	20.5045	72.08731
LU 170	19.17	20.5013	72.08710
LU 177	4.14	20.5158	72.08508
LU 178	24.61	20.5156	72.08546
LU 179	4.77	20.5150	72.08635
LU 180	12.59	20.5161	72.08621
LU 181	8.20	20.5177	72.08618
LU 182	5.86	20.5171	72.08590
LU 183	6.38	20.5167	72.08554
LU 184	3.84	20.5177	72.08573
LU 185	11.59	20.5172	72.08509
LU 186	9.05	20.5197	72.08523
LU 187	4.47	20.5192	72.08571
LU 294	0.97	20.5104	72.08600
LU 400	4.41	20.5119	72.08597
LU 401	4.56	20.5117	72.08597
LU 402	32.64	20.5120	72.08593
LU 403	7.66	20.5130	72.08641

continued on next page

Table B.1 – continued

Sample	**Adsorbed Gas, Area B**	**Coordinates**	
	Methane	WGS84, Zone 34	
	μmol/L Sediment	Longitude (E)	Latitude (N)
LU 404	8.13	20.5136	72.08672
LU 405	4.65	20.5104	72.08633
LU 406	5.46	20.5097	72.08658
LU 407	6.64	20.5133	72.08552
LU 408	4.65	20.5143	72.08541
LU 409	5.33	20.5105	72.08553
LU 410	10.73	20.5101	72.08535
LU 411	8.25	20.5098	72.08607
LU 412	7.19	20.5113	72.08543
LU 413	2.51	20.5114	72.08515
LU 414	1.60	20.5119	72.08571
LU 415	12.85	20.5119	72.08670
LU 416	16.49	20.5126	72.08553
LU 417	6.68	20.5134	72.08581
LU 418	10.48	20.5033	72.08645
LU 419	3.79	20.5064	72.08751
LU 421	2.77	20.5083	72.08706
LU 422	4.46	20.5119	72.08725
LU 423	6.22	20.5066	72.08683
LU 424	7.37	20.5027	72.08681
LU 425	4.26	20.5043	72.08666
LU 426	6.00	20.5036	72.08637
LU 427	4.68	20.5054	72.08659
LU 428	2.87	20.5053	72.08624
LU 429	6.82	20.5063	72.08598
LU 430	4.40	20.5050	72.08577
LU 450	4.15	20.5118	72.08597

Table B.2: Data of Figure 2.4.

Core	Depth Interval	c (SO_4^{2-})	c (SO_4^{2-})
	cm	mg/L	mmol/L
LU 137	0-10	3056.771	31.84
LU 137	10-20	3085.295	32.14
LU 137	20-30	3063.856	31.92
LU 137	30-40	2901.33	30.22
LU 137	40-50	3132.462	32.63
LU 137	70-80	2742.146	28.56
LU 137	110-120	2784.795	29.01
LU 137	150-160	2821.718	29.39
LU 137	190-200	2620.381	27.3
LU 137	230-240	2631.055	27.41
LU 420	0-10	2996.704	31.22
LU 420	10-20	3039.004	31.66
LU 420	20-30	3074.447	32.03
LU 420	30-40	3017.755	31.43
LU 420	40-50	2924.519	30.46
LU 420	70-80	2948.655	30.72
LU 420	110-120	2948.644	30.72
LU 420	150-160	2949.536	30.72
LU 420	190-200	2797.668	29.14
LU 420	230-240	2893.529	30.14
LU 78	0-10	3259.384	33.95
LU 78	10-20	3080.193	32.09
LU 78	20-30	3101.248	32.3
LU 78	30-40	3218.387	33.52
LU 78	40-50	3102.947	32.32
LU 78	70-80	3049.522	31.77
LU 78	110-120	3244.507	33.8
LU 78	150-160	2992.211	31.17

continued on next page

Table B.2 – continued

Core	**Depth Interval**	**c (SO_4^{2-})**	**c (SO_4^{2-})**
	cm	mg/L	mmol/L
LU 78	190-200	3014.845	31.4
LU 78	230-240	3001.541	31.27
LU 88	0-10	2889.155	30.1
LU 88	10-20	2827.366	29.45
LU 88	20-30	2893.882	30.14
LU 88	30-40	2933.262	30.55
LU 88	40-50	3063.354	31.91
LU 88	70-80	2961.385	30.85
LU 88	110-120	3025.74	31.52
LU 88	150-160	2959.803	30.83
LU 88	190-200	2907.299	30.28
LU 88	230-240	2826.895	29.45
LU 175	0-10	6893	71.8
LU 175	10-20	2428	25.29
LU 175	20-30	2470	25.73
LU 175	30-40	2426	25.27
LU 175	40-50	2370	24.69
LU 175	70-80	2737	28.51
LU 175	110-120	2841	29.6
LU 175	150-160	2516	26.2
LU 175	190-200	2451	25.53
LU 175	230-240	2428	25.29
LU 151	0-10	3132.49	32.63
LU 151	10-20	3007.473	31.33
LU 151	20-30	3234.658	33.69
LU 151	30-40	2790.087	29.06
LU 151	40-50	2883.157	30.03
LU 151	70-80	2806.154	29.23
LU 151	110-120	2647.542	27.58

continued on next page

Table B.2 – continued

Core	**Depth Interval** cm	**c (SO_4^{2-})** mg/L	**c (SO_4^{2-})** mmol/L
LU 151	150-160	2608.968	27.18
LU 151	190-200	2769.323	28.85
LU 151	230-240	2647.44	27.58
LU 84	0-10	2638.671	27.49
LU 84	10-20	2525.322	26.31
LU 84	20-30	2515.831	26.21
LU 84	30-40	2488.87	25.93
LU 84	40-50	2625.277	27.35
LU 84	70-80	2524.908	26.3
LU 84	110-120	2374.264	24.73
LU 84	150-160	2385.799	24.85
LU 84	190-200	2469.561	25.72
LU 84	230-240	2379.826	24.79
LU 175	0-10	4329.827	45.1
LU 175	10-20	3044.138	31.71
LU 175	20-30	3000.154	31.25
LU 175	30-40	2928.502	30.51
LU 175	40-50	2844.246	29.63
LU 175	70-80	2958.571	30.82
LU 175	110-120	3125.351	32.56
LU 175	150-160	3123.815	32.54
LU 175	190-200	3091.035	32.2
LU 175	230-240	3071.183	31.99
LU 151	0-10	2973.25	30.97
LU 151	10-20	2941.084	30.64
LU 151	20-30	2932.097	30.54
LU 151	30-40	2919.726	30.41
LU 151	40-50	2864.939	29.84
LU 111	70-80	2947.592	30.7

continued on next page

Table B.2 – continued

Core	**Depth Interval**	**c (SO_4^{2-})**	**c (SO_4^{2-})**
	cm	mg/L	mmol/L
LU 111	110-120	2868.702	29.88
LU 111	150-160	2849.111	29.68
LU 111	190-200	2852.813	29.72
LU 111	230-240	2840.173	29.59
LU 338	0-10	2982.118	31.06
LU 338	10-20	3112.455	32.42
LU 338	20-30	2688.661	28.01
LU 338	30-40	2474.574	25.78
LU 338	40-50	2157.191	22.47
LU 338	70-80	3124.162	32.54
LU 338	110-120	3031.287	31.58
LU 338	150-160	2938.956	30.61
LU 338	190-200	2888.648	30.09
LU 338	230-240	2966.3	30.9
LU 77	0-10	3028.455	31.55
LU 77	10-20	3113.835	32.44
LU 77	20-30	2878.861	29.99
LU 77	30-40	2997.556	31.22
LU 77	40-50	2942.637	30.65
LU 77	70-80	3011.02	31.36
LU 77	110-120	2896.122	30.17
LU 77	150-160	2920.572	30.42
LU 77	190-200	2891.985	30.12
LU 77	230-240	2933.967	30.56
LU 76	0-10	2963.352	30.87
LU 76	10-20	3001.979	31.27
LU 76	20-30	2934.432	30.57
LU 76	30-40	2943.901	30.67
LU 76	40-50	2982.857	31.07

continued on next page

Table B.2 – continued

Core	**Depth Interval**	**c (SO_4^{2-})**	**c (SO_4^{2-})**
	cm	mg/L	mmol/L
LU 76	70-80	2975.286	30.99
LU 76	110-120	2760.167	28.75
LU 76	150-160	2868.684	29.88
LU 76	190-200	2867.031	29.86
LU 76	230-240	2896.43	30.17

Table B.3: Data of Figure 2.5.

Core	Depth Interval cm	SRR pmol/cc/d
LU 400	0-10 A	598.61
LU 400	0-10 B	503.92
LU 400	10-20 A	88.80
LU 400	10-20 B	49.54
LU 400	20-30 A	0.00
LU 400	20-30 B	0.00
LU 400	30-40 A	0.00
LU 400	30-40 B	0.00
LU 400	40-50 A	0.00
LU 400	40-50 B	0.00
LU 400	70-80 A	0.00
LU 400	70-80 B	0.00
LU 400	110-120 A	0.00
LU 400	110-120 B	0.00
LU 400	130-140 A	0.00
LU 400	130-140 B	0.00
LU 400	160-170 A	0.00
LU 400	160-170 B	0.00
LU 400	180-190 A	0.00
LU 400	180-190 B	0.00
LU 450	0-10 A	0.00
LU 450	0-10 B	0.00
LU 450	10-20 A	0.00
LU 450	10-20 B	0.00
LU 450	20-30 A	0.00
LU 450	20-30 B	0.00
LU 450	30-40 A	0.00
LU 450	30-40 B	0.00
LU 450	40-50 A	0.00

continued on next page

Table B.3 – continued

Core	Depth Interval cm	SRR pmol/cc/d
LU 450	40-50 B	0.00
LU 450	50-60 A	0.00
LU 450	50-60 B	0.00
LU 450	60-70 A	0.00
LU 450	60-70 B	0.00
LU 450	90-100 A	0.00
LU 450	90-100 B	0.00
LU 450	120-130 A	0.00
LU 450	120-130 B	0.00
LU 450	150-160 A	0.00
LU 450	150-160 B	0.00
LU 341	0-10 A	85.28
LU 341	0-10 B	230.66
LU 341	10-20 A	187.60
LU 341	10-20 B	306.03
LU 341	20-30 A	0.00
LU 341	20-30 B	169.68
LU 341	30-40 A	30.09
LU 341	30-40 B	0.00
LU 341	40-50 A	0.00
LU 341	40-50 B	0.00
LU 341	70-80 A	0.00
LU 341	70-80 B	0.00
LU 341	110-120 A	0.00
LU 341	110-120 B	0.00
LU 341	150-160 A	0.00
LU 341	150-160 B	19.16
LU 341	190-200 A	0.00
LU 341	190-200 B	0.00

continued on next page

Table B.3 – continued

Core	Depth Interval cm	SRR pmol/cc/d
LU 341	240-250 A	0.00
LU 341	240-250 B	0.00
LU 331	0-10 A	9.32
LU 331	0-10 B	24.15
LU 331	10-20 A	25.96
LU 331	10-20 B	34.08
LU 331	20-30 A	0.00
LU 331	20-30 B	361.53
LU 331	30-40 A	14.63
LU 331	30-40 B	13.42
LU 331	40-50 A	0.00
LU 331	40-50 B	0.00
LU 331	70-80 A	11.94
LU 331	70-80 B	0.00
LU 331	100-110 A	0.00
LU 331	100-110 B	0.00
LU 331	130-140 A	29.00
LU 331	130-140 B	0.00
LU 331	160-170 A	21.02
LU 331	160-170 B	19.29
LU 111	0-10 A	313.35
LU 111	0-10 B	67.54
LU 111	10-20 A	52.79
LU 111	10-20 B	49.09
LU 111	20-30 A	41.35
LU 111	20-30 B	20.18
LU 111	30-40 A	56.35
LU 111	30-40 B	125.81
LU 111	40-50 A	47.08

continued on next page

Table B.3 – continued

Core	Depth Interval cm	SRR pmol/cc/d
LU 111	40-50 B	45.81
LU 111	70-80 A	17.61
LU 111	70-80 B	23.10
LU 111	110-120 A	22.65
LU 111	110-120 B	0.00
LU 111	150-160 A	11.89
LU 111	150-160 B	0.00
LU 111	190-200 A	32.72
LU 111	190-200 B	23.88
LU 111	230-240 A	17.04
LU 111	230-240 B	10.61
LU 76	0-10 A	35.36
LU 76	0-10 B	0.00
LU 76	10-20 A	0.00
LU 76	10-20 B	0.00
LU 76	20-30 A	0.00
LU 76	20-30 B	0.00
LU 76	30-40 A	0.00
LU 76	30-40 B	0.00
LU 76	40-50 A	0.00
LU 76	40-50 B	0.00
LU 76	70-80 A	0.00
LU 76	70-80 B	0.00
LU 76	110-120 A	0.00
LU 76	110-120 B	0.00
LU 76	150-160 A	0.00
LU 76	150-160 B	0.00
LU 76	190-200 A	0.00
LU 76	190-200 B	12.39

continued on next page

Table B.3 – continued

Core	Depth Interval cm	SRR pmol/cc/d
LU 76	230-240 A	0.00
LU 76	230-240 B	0.00
LU 319	0-10 A	54.62
LU 319	0-10 B	45.52
LU 319	10-20 A	314.88
LU 319	10-20 B	154.76
LU 319	20-30 A	39.47
LU 319	20-30 B	122.81
LU 319	30-40 A	0.00
LU 319	30-40 B	12.91
LU 319	40-50 A	17.63
LU 319	40-50 B	0.00
LU 319	70-80 A	0.00
LU 319	70-80 B	0.00
LU 319	110-120 A	0.00
LU 319	110-120 B	11.18
LU 319	150-160 A	0.00
LU 319	150-160 B	0.00
LU 319	190-200 A	0.00
LU 319	190-200 B	0.00
LU 319	230-240 A	17.73
LU 319	230-240 B	0.00
LU 332	0-10 A	0.00
LU 332	0-10 B	17.06
LU 332	10-20 A	0.00
LU 332	10-20 B	0.00
LU 332	20-30 A	0.00
LU 332	20-30 B	0.00
LU 332	30-40 A	0.00

continued on next page

Table B.3 – continued

Core	**Depth Interval** cm	**SRR** pmol/cc/d
LU 332	30-40 B	0.00
LU 332	40-50 A	0.00
LU 332	40-50 B	0.00
LU 332	60-70 A	0.00
LU 332	60-70 B	0.00
LU 332	80-90 A	0.00
LU 332	80-90 B	0.00
LU 332	100-110 A	0.00
LU 332	100-110 B	0.00
LU 332	120-130 A	0.00
LU 332	120-130 B	0.00
LU 332	140-150 A	0.00
LU 332	140-150 B	0.00

Table B.4: Data of Figure 3.3.

Core	Core Type	GFZ Sample Number	Depth	TOC	$\Sigma n C_{14}$-$n C_{22}$	$\Sigma n C_{23}$-$n C_{35}$	Alkylcyclo-hexanes	CPI 15-21	CPI 23-29
			cm	%	ng/gSed	ng/gSed	ng/gSed	Whole Oil Analysis	
LU 78	Ref	G008880	0	0.62	82.2	430.7	16.5	1.09	2.14
LU 78	Ref	G008882	20	0.56	295.7	1238.8	39.9	1.19	2.34
LU 78	Ref	G008884	40	0.92	805.8	1592.4	48.3	1.12	1.87
LU 78	Ref	G008886	70	1.5	469	2672.5	31.3	1.28	2.17
LU 78	Ref	G008887	150	0.63	446.9	1582.8	34.3	1.22	1.94
LU 78	Ref	G008889	230	1.02	385.6	857.8	29.8	1.12	2.06
LU88	Ref	G008910	0	0.57	50.3	247.3	5.9	1.22	2.06
LU88	Ref	G008912	20	0.96	166.6	865.3	18.6	1.15	2.59
LU88	Ref	G008914	40	1.32	372.7	1002.2	28.3	1.2	2.33
LU88	Ref	G008915	110	1.22	722.1	1645	38.6	1.19	2.26
LU88	Ref	G008917	150	1.03	271.8	1366.3	14.9	1.36	2.71
LU88	Ref	G008919	230	1.04	222.5	900.2	15.9	1.21	2.31
LU 402	PM	G009165	0	0.79	62.3	255.8	8.2	1.18	2.1
LU 402	PM	G009166	10	0.89	527.1	1137.6	38.4	1.09	1.97

continued on next page

Table B.4 – continued

Core	Core Type	GFZ Sample Number	Depth	TOC	$\Sigma n C_{14}$-$n C_{22}$	$\Sigma n C_{23}$-$n C_{35}$	Alkylcyclo-hexanes	CPI 15-21	CPI 23-29
			cm	%	ng/gSed	ng/gSed	ng/gSed	Whole Oil Analysis	
LU 402	PM	G009167	20	1.42	1109.7	2115.5	60.5	1.17	1.92
LU 402	PM	G009168	30	1.5	1346.8	2560.7	82.9	1.1	1.94
LU 402	PM	G009169	40	1.23	563.4	1997.8	32.7	1.18	2.19
LU 402	PM	G009170	60	1.18	209.9	577.6	12.7	1.16	2.29
LU 402	PM	G009171	100	1.54	976.3	1759.4	51.5	1.16	1.98
LU 402	PM	G009172	140	0.74	373.7	2237.4	38.8	1.33	2.73
LU 402	PM	G009173	180	1	210.7	404.1	22.5	1.13	2.26
LU 402	PM	G009174	210	1.14	326.4	924.3	32.9	1.16	2.12
LU450	PM	G009195	0	0.8	47.6	264.7	4.4	/	/
LU450	PM	G009196	10	0.98	1434.3	1927.5	100	0.91	2.23
LU450	PM	G009197	20	0.85	420.6	1008.5	25.8	/	/
LU450	PM	G009198	30	1.11	586.4	1957.7	38.5	1.21	2.19
LU450	PM	G009199	40	1.23	534.6	1392.1	26.7	1.2	2.15
LU450	PM	G009200	50	1.17	767.9	1968.6	55.3	1.16	2.14
LU450	PM	G009201	60	1.22	836.5	1831.7	40.2	1.19	2.18

continued on next page

Table B.4 – continued

Core	Core Type	GFZ Sample Number	Depth	TOC	$\Sigma n\mathrm{C}_{14}$-$n\mathrm{C}_{22}$	$\Sigma n\mathrm{C}_{23}$-$n\mathrm{C}_{35}$	Alkylcyclo-hexanes	CPI 15-21	CPI 23-29
			cm	%	ng/gSed	ng/gSed	ng/gSed	Whole Oil Analysis	
LU450	PM	G009202	90	1.23	761.5	2004.4	55.6	1.14	2.14
LU450	PM	G009203	120	1.36	615.4	1380.7	36.4	1.15	1.99
LU450	PM	G009204	150	1.3	348.3	816.1	27.5	1.18	2.1
LU185	PM	G008990	0	0.96	992.4	1398.2	388	0.9	2.05
LU185	PM	G008991	10	0.81	334.3	1610.1	45.2	1.18	2.26
LU185	PM	G008992	20	0.86	382.1	1514.4	55.3	1.15	2.22
LU185	PM	G008993	30	0.77	323.5	1551.1	39	1.17	2.07
LU185	PM	G008994	40	0.79	381	1207.3	60	1.08	2.08
LU185	PM	G008995	70	0.57	181.8	853.4	40.8	1.12	2.35
LU185	PM	G008996	100	0.93	496.8	1651.2	55.3	/	/
LU185	PM	G008997	130	0.97	508.6	1635.3	76	/	/
LU185	PM	G008998	160	0.93	563.4	1578.7	57	1.13	2.14
LU185	PM	G008999	190	0.8	342.8	1406.6	41.3	1.11	2.08

Table B.5: Data of Figure 3.6.

Core	Core Type	GFZ Sample Number	Depth	$\Sigma\alpha\beta$ Hopanes	$\Sigma\beta\beta$ Hopanes	α,β-C_{31} S/(S+R)	C_{30} $\alpha\beta/(\beta\alpha+\alpha\beta)$
			cm	ng/gSed	ng/gSed		
LU 78	Reference	G008880	0	107.6	37.9	0.34	0.68
LU 78	Reference	G008882	20	351.3	149.9	0.29	0.63
LU 78	Reference	G008884	40	436.8	132.4	0.33	0.67
LU 78	Reference	G008886	70	1107.2	435.1	0.33	0.64
LU 78	Reference	G008887	150	347.2	139.4	0.32	0.64
LU 78	Reference	G008889	230	528.3	156.8	0.33	0.74
LU88	Reference	G008910	0	31.9	9.9	0.35	0.74
LU88	Reference	G008912	20	163.8	59.3	0.35	0.66
LU88	Reference	G008914	40	346.5	141.8	0.29	0.66
LU88	Reference	G008915	110	554.4	204.8	0.30	0.68
LU88	Reference	G008917	150	239.2	132.3	0.26	0.61
LU88	Reference	G008919	230	551.9	127.1	0.31	0.70
LU 402	Pockmark	G009165	0	185.4	66.4	0.29	0.65
LU 402	Pockmark	G009166	10	189.2	61.0	0.32	0.68

continued on next page

Table B.5 – continued

Core	**Core Type**	**GFZ Sample Number**	**Depth**	**$\Sigma\alpha\beta$ Hopanes**	**$\Sigma\beta\beta$ Hopanes**	**α,β-C_{31} S/(S+R)**	**C_{30} $\alpha\beta/(\beta\alpha+\alpha\beta)$**
			cm	ng/gSed	ng/gSed		
LU 402	Pockmark	G009167	20	805.9	232.2	0.34	0.66
LU 402	Pockmark	G009168	30	814.1	243.4	0.33	0.68
LU 402	Pockmark	G009169	40	600.4	235.1	0.29	0.64
LU 402	Pockmark	G009170	60	341.8	157.7	0.28	0.68
LU 402	Pockmark	G009171	100	647.9	192.6	0.35	0.67
LU 402	Pockmark	G009172	140	456.9	271.8	0.27	0.62
LU 402	Pockmark	G009173	180	86.9	34.9	0.32	0.68
LU 402	Pockmark	G009174	210	1560.4	530.5	0.3	0.68
LU450	Pockmark	G009195	0	280.7	150.6	0.28	0.68
LU450	Pockmark	G009196	10	247.8	127.9	0.29	0.64
LU450	Pockmark	G009197	20	366.5	90.0	0.29	0.68
LU450	Pockmark	G009198	30	384.1	147.2	0.31	0.67
LU450	Pockmark	G009199	40	467.9	153.8	0.31	0.67
LU450	Pockmark	G009200	50	459.4	188.8	0.29	0.66
LU450	Pockmark	G009201	60	693.4	248	0.32	0.66

continued on next page

Table B.5 – continued

Core	**Core Type**	**GFZ Sample Number**	**Depth**	**$\Sigma\alpha\beta$ Hopanes**	**$\Sigma\beta\beta$ Hopanes**	**α,β-C_{31} S/(S+R)**	**C_{30} $\alpha\beta/(\beta\alpha+\alpha\beta)$**
			cm	ng/gSed	ng/gSed		
LU450	Pockmark	G009202	90	422.2	163.8	0.30	0.66
LU450	Pockmark	G009203	120	506.9	135.8	0.34	0.67
LU450	Pockmark	G009204	150	1653.2	537.3	0.33	0.69
LU185	Pockmark	G008990	0	265.4	89.9		
LU185	Pockmark	G008991	10	307.3	126.3	0.30	0.65
LU185	Pockmark	G008992	20	261.4	99.9	0.29	0.65
LU185	Pockmark	G008993	30	331.6	103.1	0.35	0.70
LU185	Pockmark	G008994	40	276.7	82.2	0.35	0.67
LU185	Pockmark	G008995	70	161.7	62.1	0.31	0.69
LU185	Pockmark	G008996	100	337.4	133.8	0.29	0.65
LU185	Pockmark	G008997	130	374.0	141.7	0.29	0.68
LU185	Pockmark	G008998	160	335.9	114.4	0.34	0.64
LU185	Pockmark	G008999	190	270.8	96.8	0.31	0.67

Table B.6: Data of Figure 3.8.

Core	Core Type	GFZ Sample Number	Depth cm	Σ Steranes	Σ Diasteranes	C_{29} R+S $\alpha\beta\beta/(\alpha\beta\beta+\alpha\alpha\alpha)$
LU 78	Reference	G008880	0	37.3	15.9	0.4
LU 78	Reference	G008882	20	106.8	52.3	0.37
LU 78	Reference	G008884	40	157.8	91.5	0.46
LU 78	Reference	G008886	70	200.2	110.4	0.31
LU 78	Reference	G008887	150	138	54.7	0.47
LU 78	Reference	G008889	230	220.4	89.3	0.39
LU88	Reference	G008910	0	31.3	13.7	0.42
LU88	Reference	G008912	20	51.4	31.2	0.41
LU88	Reference	G008914	40	90.0	46.3	0.49
LU88	Reference	G008915	110	117.8	65.0	0.41
LU88	Reference	G008917	150	92.1	27.4	0.38
LU88	Reference	G008919	230	143.1	53.1	0.41
LU 402	Pockmark	G009165	0	61.8	23.2	0.41
LU 402	Pockmark	G009166	10	108.8	69.6	0.4

continued on next page

Table B.6 – continued

Core	Core Type	GFZ Sample Number	Depth cm	Σ Steranes	Σ Diasteranes	$C_{29}R+S$ $\alpha\beta\beta/(\alpha\beta\beta+\alpha\alpha\alpha)$
LU 402	Pockmark	G009167	20	200.0	118.8	0.42
LU 402	Pockmark	G009168	30	261.1	185.1	0.39
LU 402	Pockmark	G009169	40	216.2	111.4	0.41
LU 402	Pockmark	G009170	60	62.6	39.8	0.33
LU 402	Pockmark	G009171	100	190.8	115.6	0.37
LU 402	Pockmark	G009172	140	152.8	41.3	0.44
LU 402	Pockmark	G009173	180	43.1	31.9	0.32
LU 402	Pockmark	G009174	210	248.1	87.1	0.42
LU450	Pockmark	G009195	0	36.2	12.2	0.41
LU450	Pockmark	G009196	10	131.0	81.8	0.28
LU450	Pockmark	G009197	20	72.9	34.5	
LU450	Pockmark	G009198	30	268.4	147.7	0.39
LU450	Pockmark	G009199	40	136.7	67.8	0.38
LU450	Pockmark	G009200	50	254.2	153.7	0.4
LU450	Pockmark	G009201	60	182.5	90.1	0.41

continued on next page

Table B.6 – continued

Core	**Core Type**	**GFZ Sample Number**	**Depth** cm	**Σ Steranes**	**Σ Diasteranes**	**$C_{29}R+S$ $\alpha\beta\beta/(\alpha\beta\beta+\alpha\alpha\alpha)$**
LU450	Pockmark	G009202	90	200.5	129.0	0.4
LU450	Pockmark	G009203	120	305.5	156.3	0.37
LU450	Pockmark	G009204	150	287.0	115.4	0.38
LU185	Pockmark	G008990	0	90.2	35.3	0.49
LU185	Pockmark	G008991	10	77.9	26.4	0.38
LU185	Pockmark	G008992	20	69.4	25.9	0.3
LU185	Pockmark	G008993	30	222.9	95.6	0.44
LU185	Pockmark	G008994	40	55.7	22.5	0.43
LU185	Pockmark	G008995	70	30.4	8.1	0.33
LU185	Pockmark	G008996	100	90.7	47.2	0.42
LU185	Pockmark	G008997	130	73.7	24.7	0.31
LU185	Pockmark	G008998	160	89.2	35.7	0.3
LU185	Pockmark	G008999	190	65.3	21.1	0.43

Table B.7: Data of Figure 4.4.

Core	Core Type	GFZ Sample Number	Depth	Relative Abundance				
				GDGT-0	GDGT-1	GDGT-2	GDGT-3	Crenarchaeol
			cm	%				
P1210 018	CC	G012457	Top	12.25	31.47	45.89	10.12	0.3
P1210 018	CC	G012458	Middle	15.76	37.16	41.73	5.26	0.1
P1210 018	CC	G012459	Bottom	14.87	36.46	42.24	6.29	0.1
P1210 020	CC core	G012396	2	48.25	6.95	7.07	2.85	34.9
P1210 020	CC core	G012398	6	41.63	8.92	13.66	5.15	30.6
P1210 020	CC core	G012402	16	26.26	16.59	29.89	11.40	15.9
LU 450	PM core	G009196	10	64.16	4.13	1.26	0.64	29.8
LU 450	PM core	G009201	60	57.96	4.49	1.91	0.93	34.7
LU 450	PM core	G009204	150	57.96	4.36	1.90	0.78	35.0

Table B.8: Data of Figure 4.5.

Core	Core Type	GFZ Sample Number	Depth cm	Archaeol ng/gSed	OH-Archaeol ng/gSed	di-OH-Archaeol ng/gSed	PMI ng/gSed	Crocetane ng/gSed
P1210 020	CC core	G012395	0	158.55	193.06	0.00	34.84	76.10
P1210 020	CC core	G012396	2	144.85	433.31	122.60	30.61	42.38
P1210 020	CC core	G012397	4	280.28	1203.68	271.80	52.42	59.32
P1210 020	CC core	G012398	6	376.08	1543.77	292.79	42.51	70.72
P1210 020	CC core	G012399	8	161.06	580.69	63.34	32.92	78.12
P1210 020	CC core	G012400	10	106.64	374.51	0.00	37.91	81.50
P1210 020	CC core	G012401	13	107.84	289.49	0.00	38.07	65.66
P1210 020	CC core	G012402	16	123.65	208.62	0.00	50.28	72.60
LU 450	PM core	G009195	0				2.40	
LU 450	PM core	G009196	10				21.13	
LU 450	PM core	G009197	20				8.25	
LU 450	PM core	G009198	30				18.77	
LU 450	PM core	G009199	40				9.33	
LU 450	PM core	G009200	50				14.92	
LU 450	PM core	G009201	60				10.32	
LU 450	PM core	G009202	90				16.83	
LU 450	PM core	G009203	120				10.32	
LU 450	PM core	G009204	150				6.28	

Table B.9: Data of Figure 4.6.

Core	Core Type	GFZ Sample Number	Depth cm	GDGT-0 ng/gSed	GDGT-1 ng/gSed	GDGT-2 ng/gSed	GDGT-3 ng/gSed	Chrenarchaeol ng/gSed
P1210 020	CC core	G012395	0	124.14	12.78	10.35	4.24	81.69
P1210 020	CC core	G012396	2	102.36	14.74	14.99	6.04	74.03
P1210 020	CC core	G012397	4	101.76	20.55	30.54	11.47	67.69
P1210 020	CC core	G012398	6	107.34	22.99	35.22	13.28	79.02
P1210 020	CC core	G012399	8	69.44	15.30	28.41	11.05	49.63
P1210 020	CC core	G012400	10	72.80	25.78	46.71	19.92	50.93
P1210 020	CC core	G012401	13	87.52	39.08	70.51	23.12	61.08
P1210 020	CC core	G012402	16	98.14	62.02	111.71	42.61	59.29
LU 450	PM core	G009195	0	255.32	22.06	8.35	3.00	121.76
LU 450	PM core	G009196	10	87.84	5.65	1.72	0.87	40.82
LU 450	PM core	G009197	20	92.65	6.99	1.81	0.86	46.38
LU 450	PM core	G009198	30	123.31	8.77	2.68	1.43	68.19
LU 450	PM core	G009199	40	36.71	2.65	0.79	0.45	18.69
LU 450	PM core	G009200	50	31.76	2.35	0.92	0.42	19.05
LU 450	PM core	G009201	60	21.84	1.69	0.72	0.35	13.08
LU 450	PM core	G009202	90	33.69	2.33	0.94	0.52	19.81

continued on next page

Table B.9 – continued

Core	**Core Type**	**GFZ Sample Number**	**Depth** cm	**GDGT-0** ng/gSed	**GDGT-1** ng/gSed	**GDGT-2** ng/gSed	**GDGT-3** ng/gSed	**Chrenarchaeol** ng/gSed
LU 450	PM core	G009203	120	23.47	1.57	0.61	0.31	15.01
LU 450	PM core	G009204	150	103.44	7.78	3.39	1.40	62.45

Table B.10: Data of Figure 4.8.

Core	Core Type	GFZ Sample Number	Depth	ΣPLFAs	ai 15:0	iso 15:0	iso 16:1 ω 5 cis+trans	20:5	22:5
			cm	ng/gSed	ng/gSed	ng/gSed	ng/gSed	ng/gSed	ng/gSed
P1210 020	CC core	G012395	0	17938.10	214.83	137.84	688.08	1303.23	231.55
P1210 020	CC core	G012396	2	10320.20	208.41	88.77	554.83	1155.27	231.12
P1210 020	CC core	G012397	4	12028.40	264.68	128.74	633.83	1421.91	373.59
P1210 020	CC core	G012398	6	10028.40	250.12	129.24	560.69	1028.34	298.41
P1210 020	CC core	G012399	8	2315.29	138.43	63.38	212.42	86.14	0.00
P1210 020	CC core	G012400	10	616.93	68.13	23.81	75.11	0.00	0.00
P1210 020	CC core	G012401	13	543.92	50.45	18.40	48.49	0.00	0.00
P1210 020	CC core	G012402	16	503.48	50.76	17.62	39.26	0.00	0.00
LU 450	PM core	G009195	0	157.27	7.14	19.11			
LU 450	PM core	G009197	20	104.21	1.95	3.23			
LU 450	PM core	G009199	40	61.47	1.99	3.76			
LU 450	PM core	G009201	60	82.65	2.34	3.84			
LU 450	PM core	G009203	120	67.94	2.42	4.35			
LU 450	PM core	G009204	150	93.71	1.71	2.71			

Appendix C

Supplemental Data

Data from samples of the 2011 cruise. Spreadsheets can be found on the enclosed data disc in Appendix D.

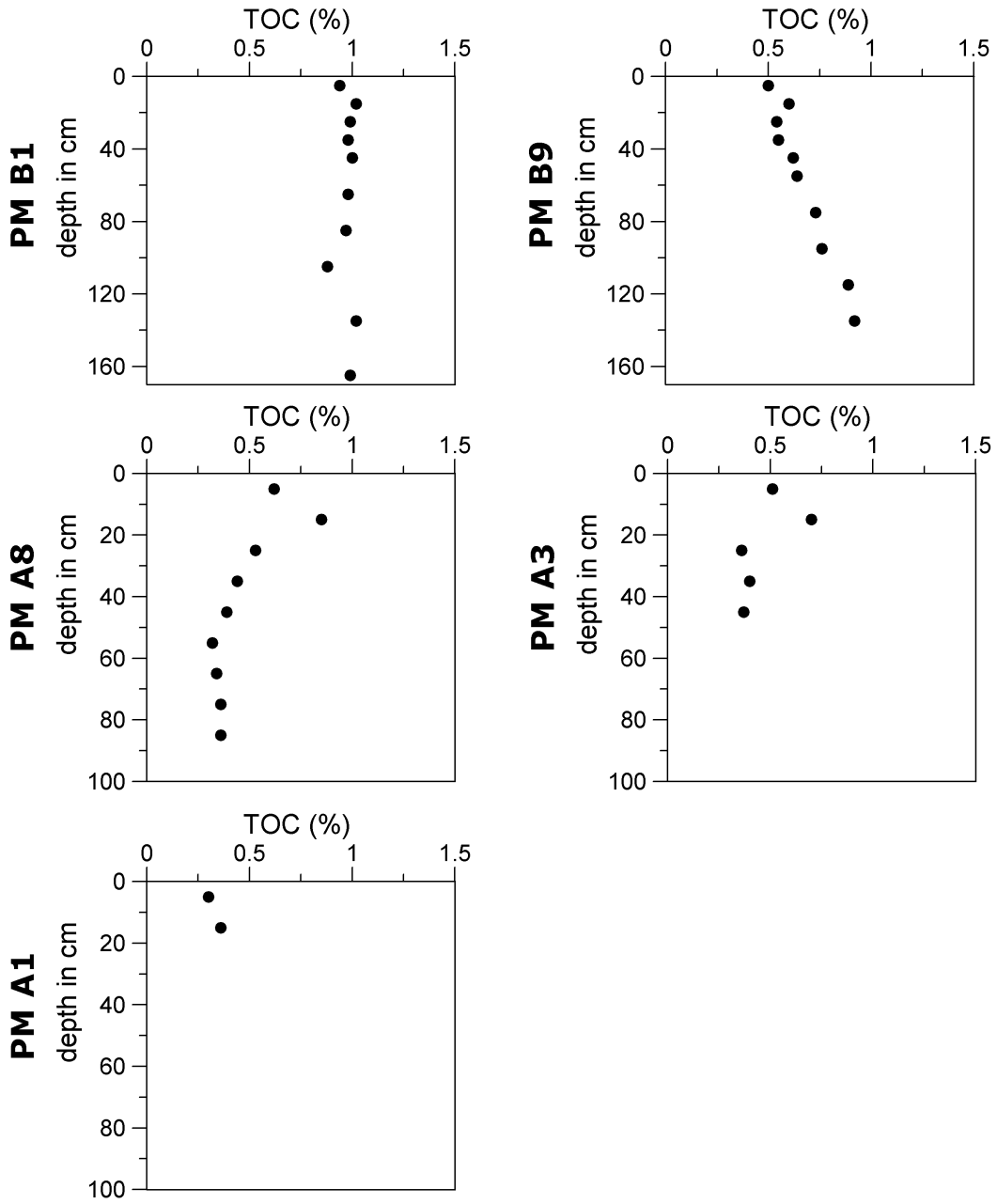

Figure C.1: Total organic carbon (TOC)

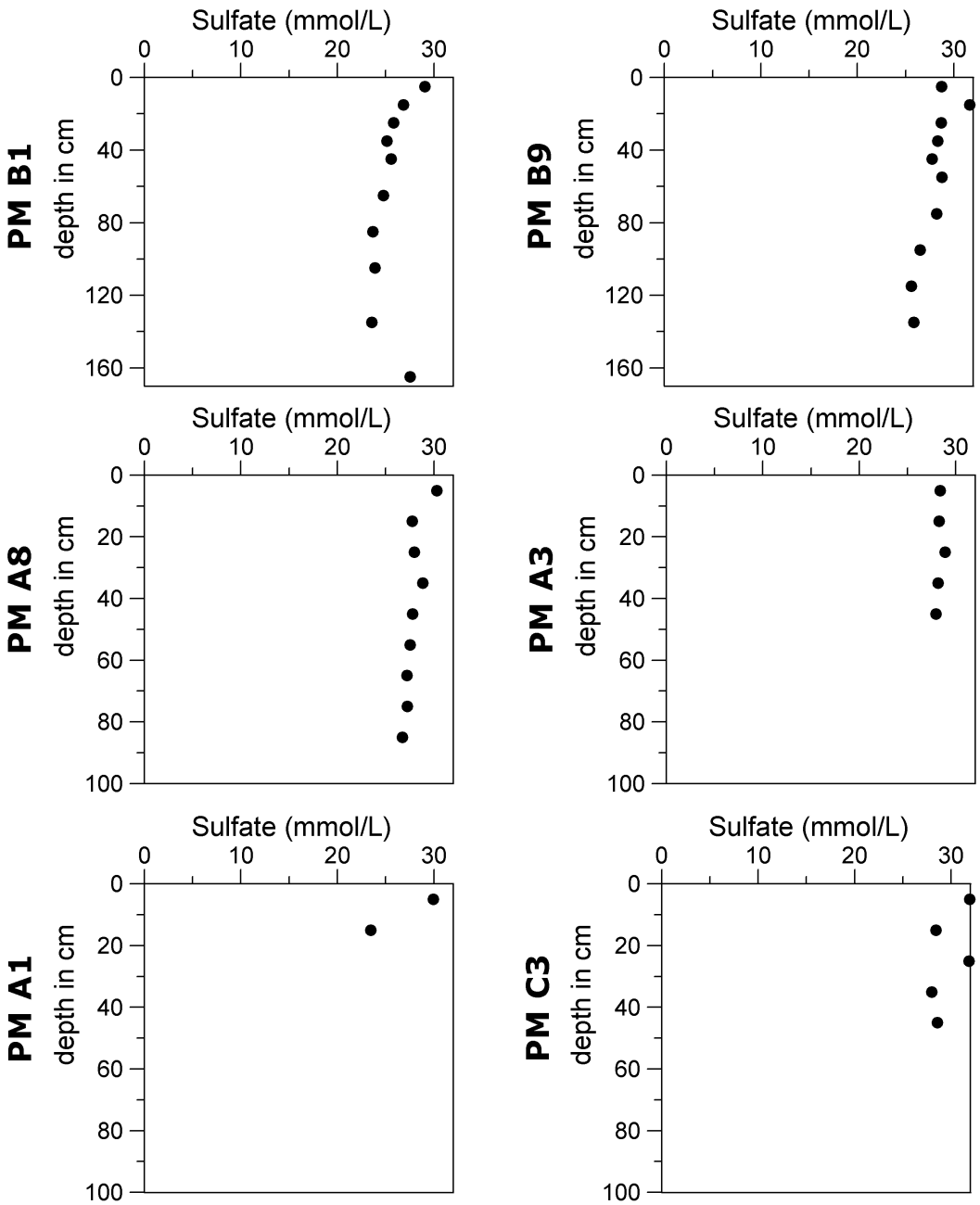

Figure C.2: Sulfate concentration

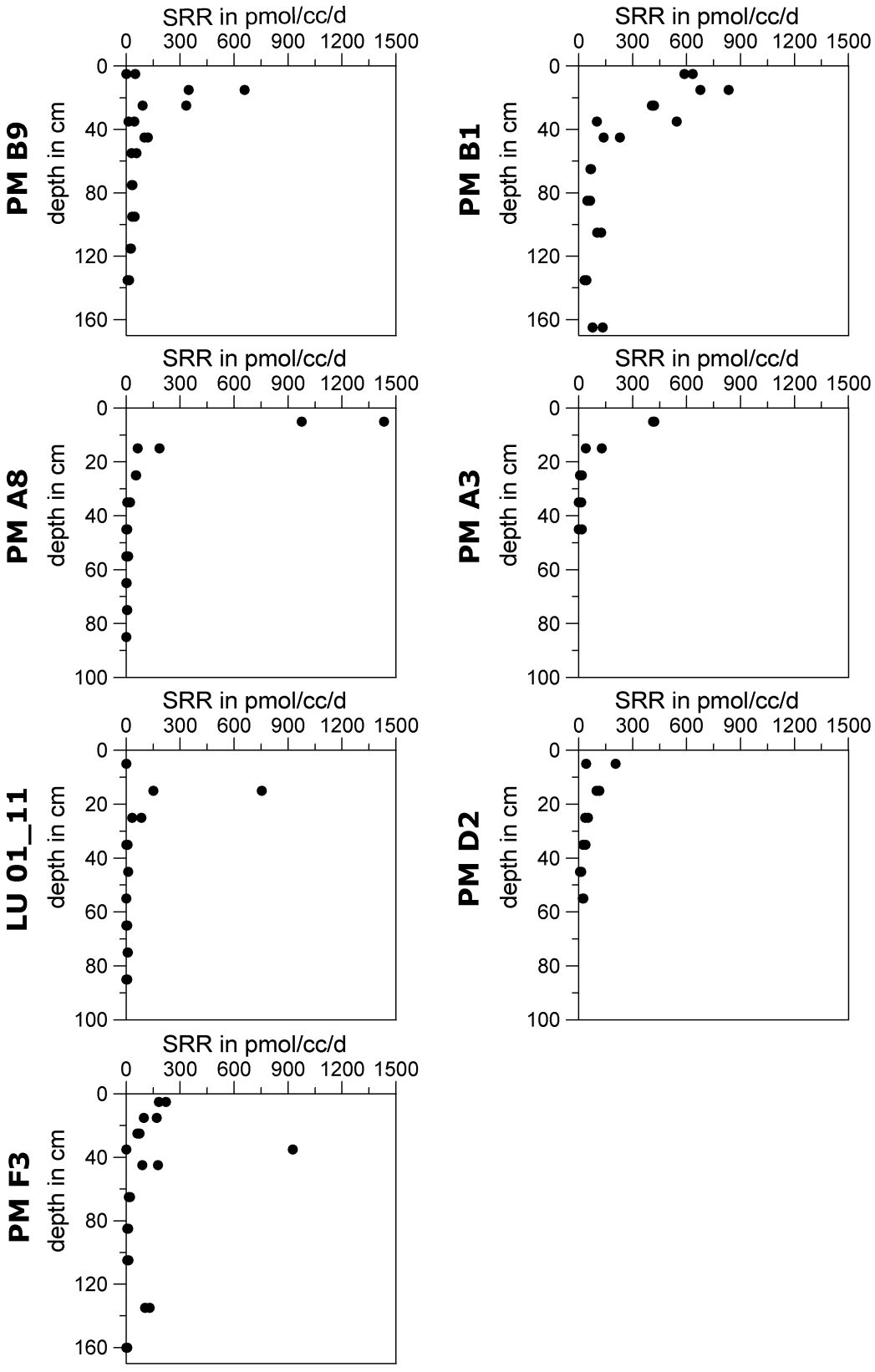

Figure C.3: Sulfate reduction rates (SRR)

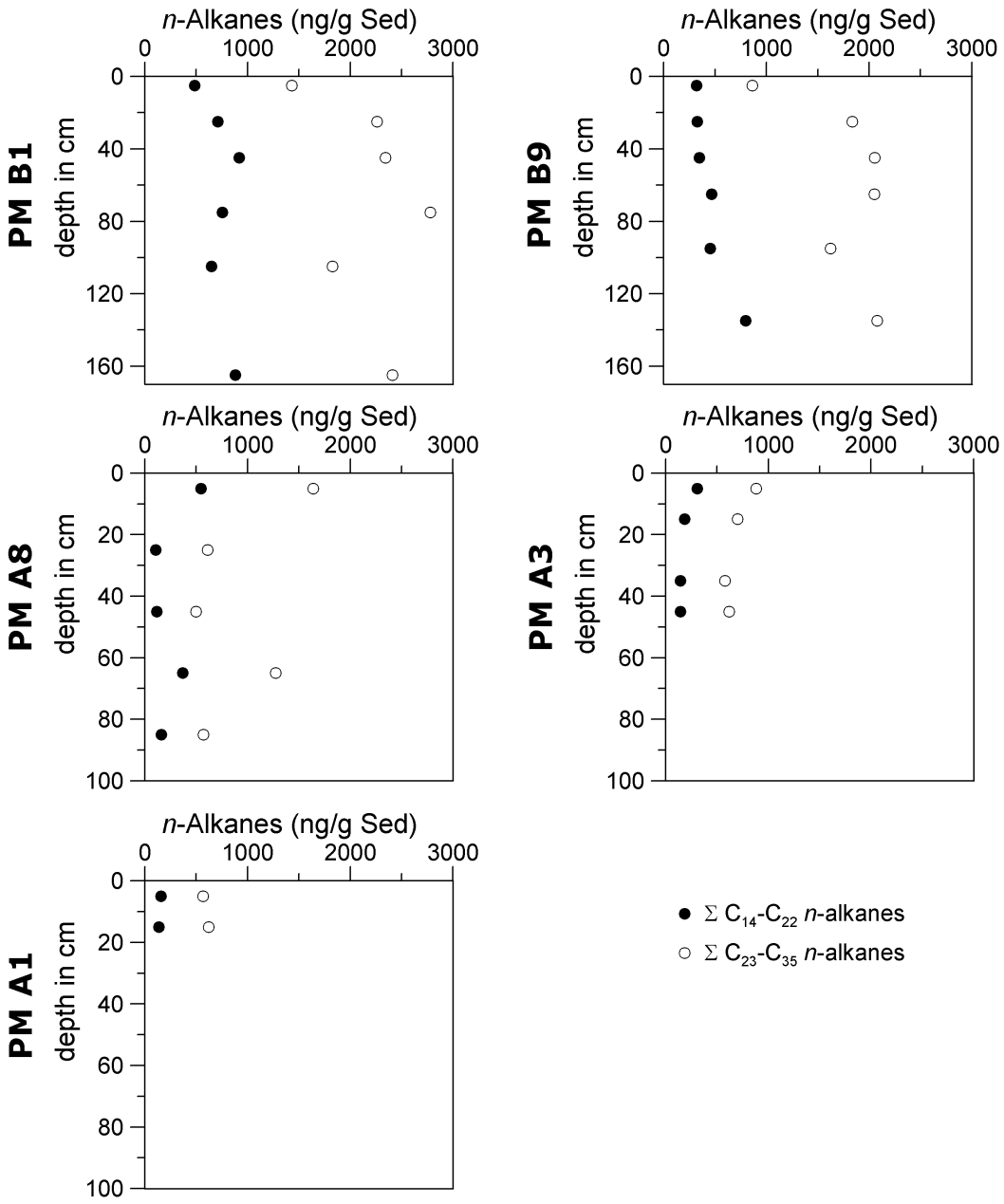

Figure C.4: Sum of shorter and longer chain *n*-alkanes

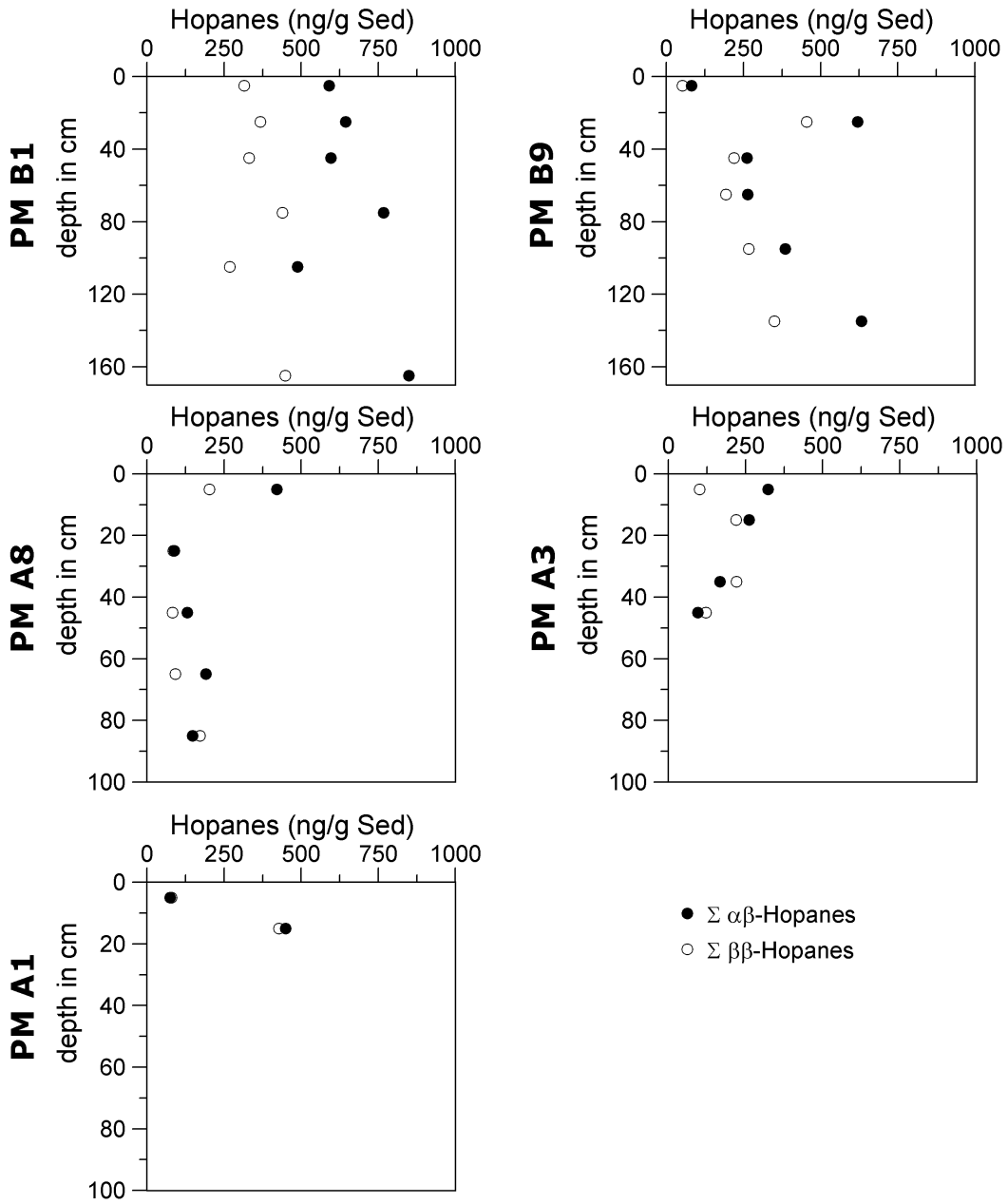

Figure C.5: Sum of $\alpha\beta$- and $\beta\beta$-hopanes

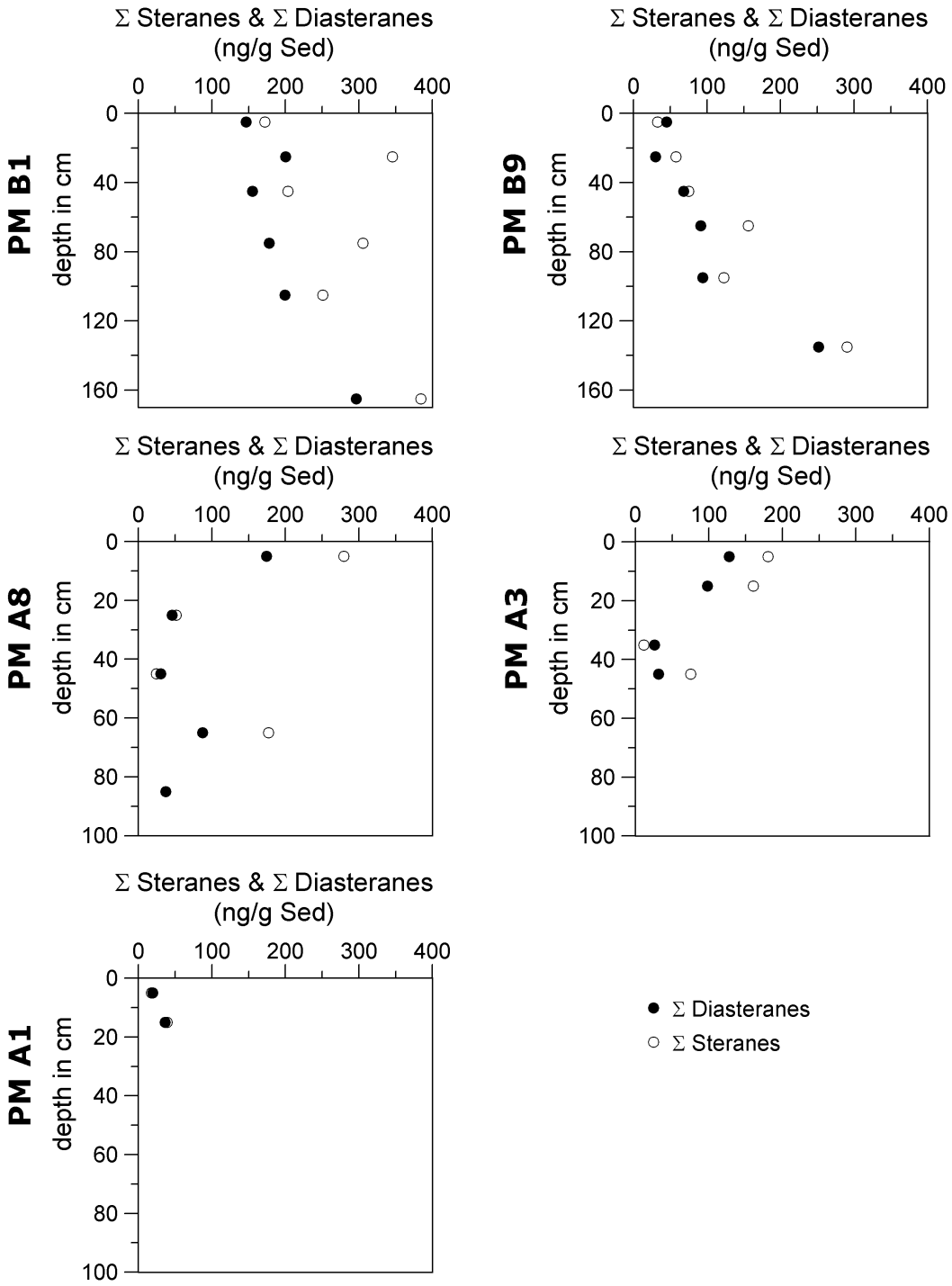

Figure C.6: Sum of steranes and diasteranes

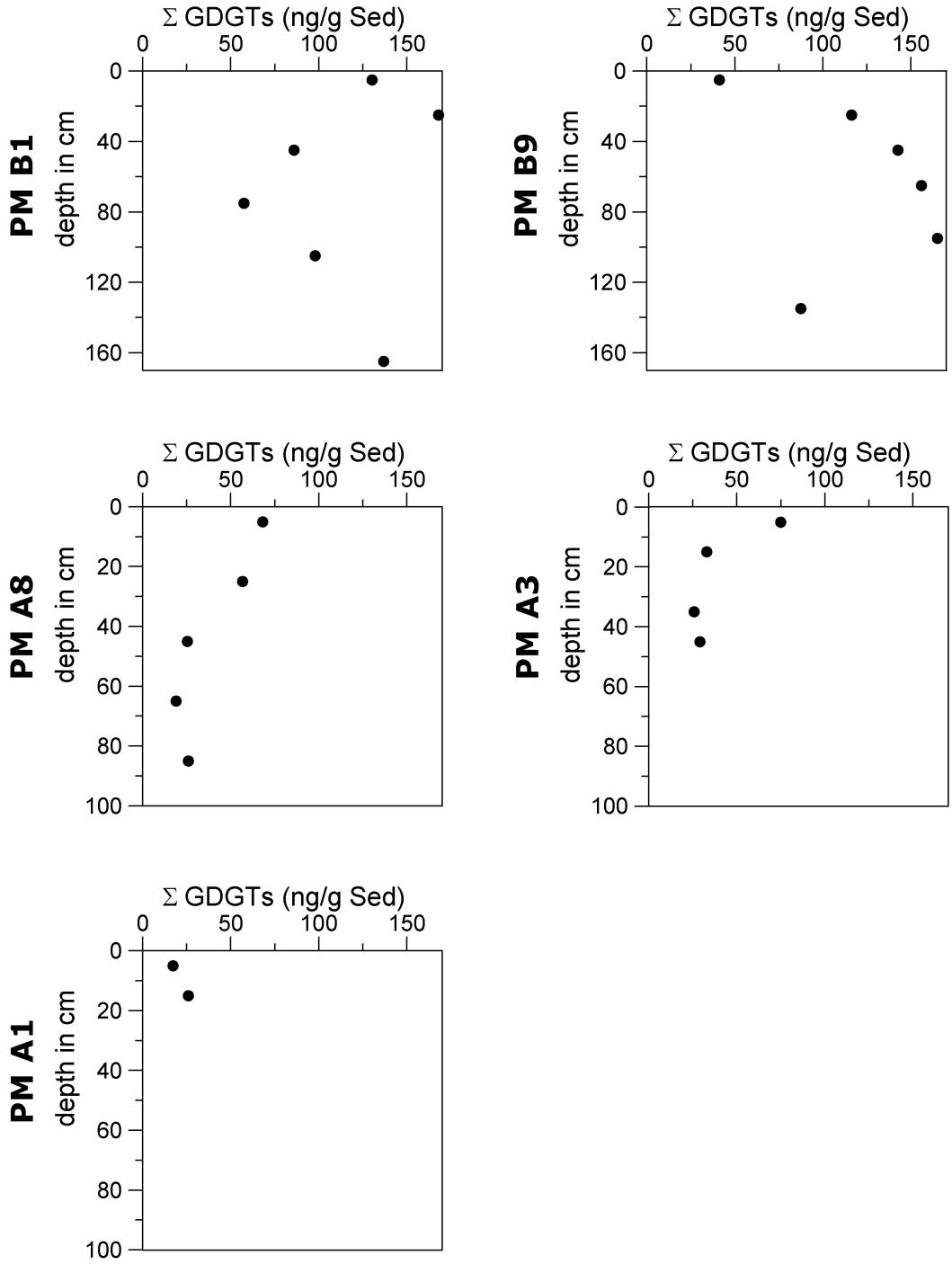

Figure C.7: Sum of glycerol dialkyl glycerol tetraethers (GDGTs)

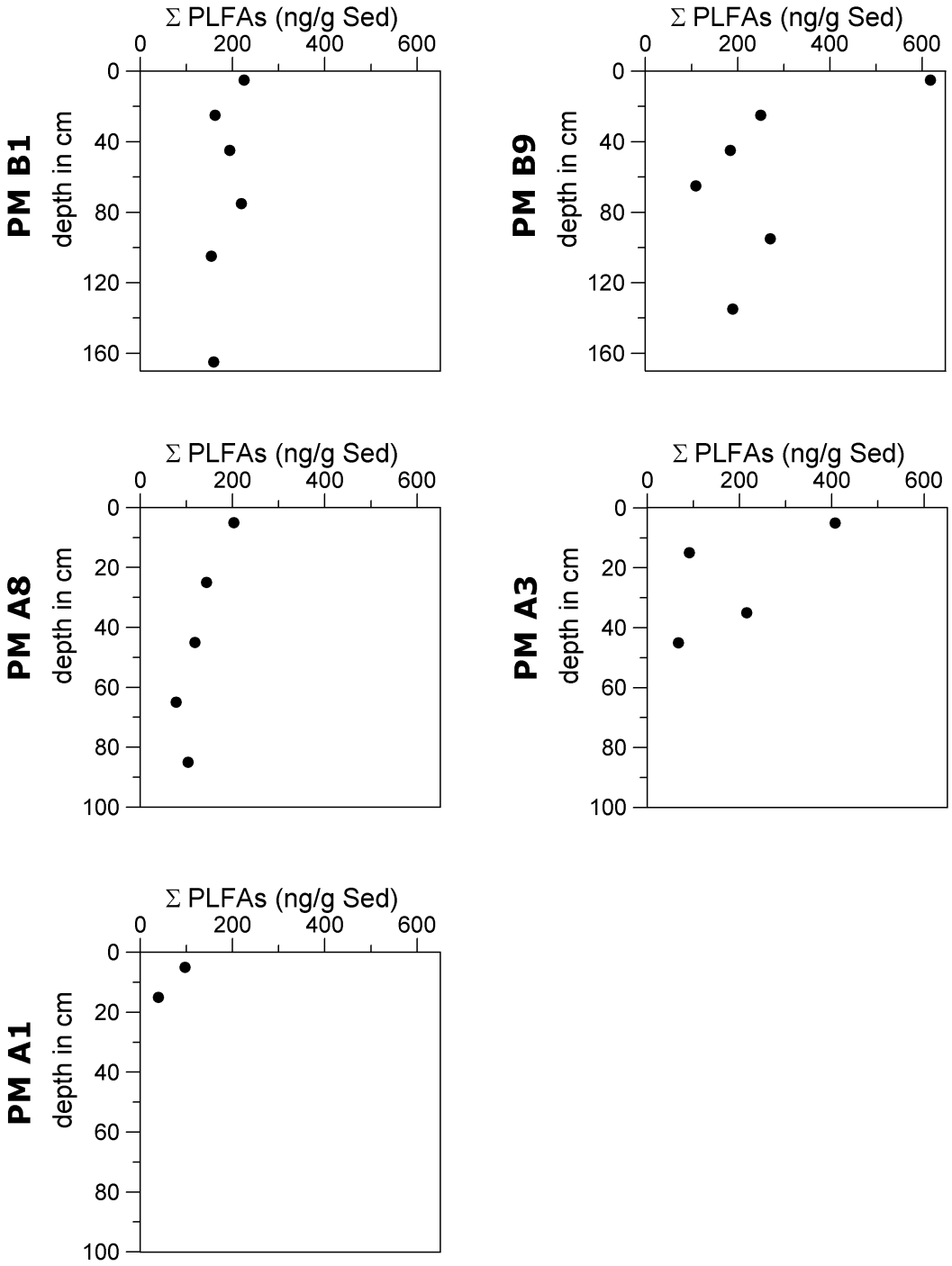

Figure C.8: Sum of phospholipid fatty acids (PLFAs)

Appendix D

Data Disc

The enclosed data disc includes a digital copy of the document at hand and selected data from organic geochemical, biogechemical and geomicrobiological measurements which has been generated during this study.